

AD A 050700

AD NO. 100
FILE COPY

12

AD-E300093

DNA 4278F-1

STRUCTURAL RESPONSE TO SIMULATED NUCLEAR OVERPRESSURE (STRESNO): A TEST PROGRAM ESTABLISHING A DATA BASE FOR EVALUATING PRESENT AND FUTURE ANALYTICAL TECHNIQUES

Volume I--Program Description and Results

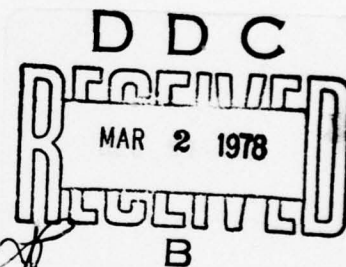
Boeing Wichita Company
3801 South Oliver
Wichita, Kansas 67210

March 1977

Final Report for Period 3 November 1975--28 February 1977

CONTRACT No. DNA 001-76-C-0084

APPROVED FOR PUBLIC RELEASE;
DISTRIBUTION UNLIMITED.



THIS WORK SPONSORED BY THE DEFENSE NUCLEAR AGENCY
UNDER RDT&E RMSS CODE B342076464 N99QAXAE51013 H2590D.

Prepared for

Director

DEFENSE NUCLEAR AGENCY

Washington, D. C. 20305

UNCLASSIFIED

SECURITY CLASSIFICATION OF THIS PAGE (When Data Entered)

REPORT DOCUMENTATION PAGE		READ INSTRUCTIONS BEFORE COMPLETING FORM
1. REPORT NUMBER DNA 4278F-1	2. GOVT ACCESSION NO. DNA 4278F-1 AD-E 366 493	3. RECIPIENT'S CATALOG NUMBER
4. TITLE (and Subtitle) STRUCTURAL RESPONSE TO SIMULATED NUCLEAR OVERPRESSURE (STRESNO): A TEST PROGRAM ESTABLISHING A DATA BASE FOR EVALUATING PRESENT AND FUTURE ANALYTICAL TECHNIQUES. Volume I. Program Description and Results.		5. TYPE OF REPORT & PERIOD COVERED Final Report, for Period 3 Nov 75-28 Feb 77,
7. AUTHOR(s) Roger P. Syring W. Dale Pierson		6. PERFORMING ORG. REPORT NUMBER D3-9788-5-VOL-1
9. PERFORMING ORGANIZATION NAME AND ADDRESS Boeing Wichita Company 3801 South Oliver Wichita, Kansas 67210		8. CONTRACT OR GRANT NUMBER(s) DNA 001-76-C-0084
11. CONTROLLING OFFICE NAME AND ADDRESS Director Defense Nuclear Agency Washington, D.C. 20305		10. PROGRAM ELEMENT, PROJECT, TASK AREA & WORK UNIT NUMBERS NWED Subtask N99QAXAE510-13
14. MONITORING AGENCY NAME & ADDRESS (if different from Controlling Office)		12. REPORT DATE March 1977
		13. NUMBER OF PAGES 204
		15. SECURITY CLASS (of this report) UNCLASSIFIED
16. DISTRIBUTION STATEMENT (of this Report) Approved for public release; distribution unlimited.		
17. DISTRIBUTION STATEMENT (of the abstract entered in Block 20, if different from Report)		
18. SUPPLEMENTARY NOTES This work sponsored by the Defense Nuclear Agency under RDT&E RMSS Code B342076464 N99QAXAE51013 H2590D.		
19. KEY WORDS (Continue on reverse side if necessary and identify by block number) Static Test Shock Load Test Shock Tube Nuclear Overpressure Structural Response Analysis NOVA-2 Basic Structural Elements Aircraft Vulnerability		
20. ABSTRACT (Continue on reverse side if necessary and identify by block number) This document reports on the following: (1) Experimental determination of the ability of 17 basic structural elements to withstand simulated nuclear overpressure loads (utilizing Sandia Corporation's THUNDERPIPE Shock Tube) and uniform static pressure loads; (2) Analytical determination of the ability of these structural elements to withstand nuclear overpressure loads and uniform static pressure loads (utilizing the NOVA-2 computer program developed by Kaman AviDyne for the Air Force Weapons Laboratory, Finite element techniques, and classical strength analysis techniques); (3) Identification and evaluation of		

DD FORM 1 JAN 73 1473

EDITION OF 1 NOV 65 IS OBSOLETE

UNCLASSIFIED

SECURITY CLASSIFICATION OF THIS PAGE (When Data Entered)

059650

next
page
Jell

UNCLASSIFIED

SECURITY CLASSIFICATION OF THIS PAGE(When Data Entered)

20. ABSTRACT (Continued)

cont. → differences between test results and analysis results; (4) Identification of suggested changes to NOVA-2 to upgrade its capabilities; (5) Analytical determination of the sensitivity of structural response to selected structural properties; and (6) Application of study results to future nuclear hardness assessments.

↖

ACCESSION for	
NTIS	White Section <input checked="" type="checkbox"/>
DDC	Buff Section <input type="checkbox"/>
UNANNOUNCED	
JUSTIFICATION	
BY	
DISTRIBUTION/AVAILABILITY	
NOTES	
CIAL	
A	

UNCLASSIFIED

SECURITY CLASSIFICATION OF THIS PAGE(When Data Entered)

Conversion Boeing factors for U.S. customary to metric (SI) units of measurement.

To Convert From	To	Multiply By
degree (angle)	radian (rad)	1.745 329 X E -2
foot	meter (m)	3.048 000 X E -1
foot-pound-force	joule (J)	1.355 818
inch	meter (m)	2.540 000 X E -2
kip (1000 lbf)	newton (N)	4.448 222 X E +3
kip/inch ² (ksi)	kilo pascal (kPa)	6.894 757 X E +3
mil	meter (m)	2.540 000 X E -5
pound-force (lbf avoirdupois)	newton (N)	4.448 222
pound-force inch	newton-meter (N·m)	1.129 848 X E -1
pound-force/inch	newton/meter (N/m)	1.751 268 X E +2
pound-force/foot ²	kilo pascal (kPa)	4.788 026 X E -2
pound-force/inch ²	kilo pascal (kPa)	6.894 757
pound-mass (lbm avoirdupois)	kilogram (kg)	4.535 924 X E -1
pound-mass-foot ² (moment of inertia)	kilogram-meter ² (kg·m ²)	4.214 011 X E -2
pound-mass/foot ³	kilogram/meter ³ (kg/m ³)	1.601 846 X E +1

TABLE OF CONTENTS (VOLUME 1)

	<u>PAGE</u>
LIST OF FIGURES -----	6
LIST OF TABLES -----	11
NOMENCLATURE -----	12
1.0 INTRODUCTION -----	15
2.0 TEST FACILITIES -----	16
3.0 TEST SPECIMENS -----	18
4.0 TEST FIXTURES -----	23
5.0 INSTRUMENTATION -----	25
6.0 TEST PROCEDURES -----	38
6.1 Static Test -----	38
6.2 Shock Load Test -----	38
7.0 ANALYSIS PROCEDURES -----	40
7.1 General Discussion -----	40
7.2 Static Analysis -----	40
7.2.1 Classical Techniques -----	40
7.2.2 Finite Element Techniques -----	41
7.2.3 NOVA-2 -----	42
8.0 RESULTS -----	43
8.1 General Discussion -----	43
8.2 Static Load Test/Analysis -----	43
8.2.1 Test Specimen No. 1 -----	44
8.2.2 Test Specimen No. 2 -----	47
8.2.3 Test Specimen No. 3 -----	47
8.2.4 Test Specimen No. 4 -----	47
8.2.5 Test Specimen No. 5 -----	47
8.2.6 Test Specimen No. 6 -----	57
8.2.7 Test Specimen No. 7 -----	57
8.2.8 Test Specimen No. 8 -----	57
8.2.9 Test Specimen No. 9 -----	64
8.2.10 Test Specimen No. 10 -----	64
8.2.11 Test Specimen No. 11 -----	64
8.2.12 Test Specimen No. 12 -----	71
8.2.13 Test Specimen No. 13 -----	71
8.2.14 Test Specimen No. 14 - 17 -----	77

		<u>PAGE</u>
8.0	(continued)	
8.3	Shock Load Test/Analysis Results -----	82
8.3.1	Test Specimen No. 1 -----	85
8.3.2	Test Specimen No. 2 -----	88
8.3.3	Test Specimen No. 3 -----	93
8.3.4	Test Specimen No. 4 -----	93
8.3.5	Test Specimen No. 5 -----	103
8.3.6	Test Specimen No. 6 -----	113
8.3.7	Test Specimen No. 7 -----	121
8.3.8	Test Specimen No. 8 -----	121
8.3.9	Test Specimen No. 9 -----	126
8.3.10	Test Specimen No. 10 -----	133
8.3.11	Test Specimen No. 11 -----	138
8.3.12	Test Specimen No. 12 -----	138
8.3.13	Test Specimen No. 13 -----	150
8.3.14	Test Specimen No. 14 - 17 -----	170
8.4	Summary of Static Load Test/Analysis Results -----	174
8.5	Summary of Shock Load Test/Analysis Results -----	178
8.6	Static Test Results Vs Dynamic Test Results -----	180
8.7	Sensitivity Analysis -----	180
9.0	OBSERVATIONS AND CONCLUSIONS -----	188
10.0	APPLICATION OF TEST/ANALYSIS RESULTS -----	196
10.1	General Discussion -----	196
10.2	Impact on Future Nuclear Hardness Studies -----	196
	REFERENCES -----	199
	ACTIVE SHEET RECORD -----	200

TABLE OF CONTENTS -- VOLUME II
(NUMBERS IN BLOCKS ARE PAGE NUMBERS)

Spec No.	Description and Instru.	Spec Drawing	Static Test Photos	Static Analyses Models	Static Test Results	Shock Test Photos	Shock Analyses Models	Shock Test Results
1	11	12	13-15	16	17	18	19	20-51
2	53	54	55	56	57	58-60	61	62-82
3	84	85	86-87	88	89	90-91	92	93-117
4	119	120	121	122	123	124-127	128	129-215
5	217	218	219-220	221	222	223	224	225-285
6	287	288	289-290	291	292	293-297	298-299	300-346
7	348	349	350-351	353	363	365	366	369-391
8	348	349	352	354	364	367	368	392-416
9	418-419	420	421-422	426-427	430	432-435	436-437	443-465
10	418-419	420	423-425	428-429	431	438-440	441-442	465-496
11	498	499	500-501	502	503	504-509	510	511-538
12	540-541	542	543-546	549	551	553-559	560	569-603
13	540-541	542	547-548	550	552	561-567	568	604-638
14-17	640	641	642-645	646-654	655	656-657	658	659-699

LIST OF FIGURES

<u>Figure No.</u>	<u>Title</u>	<u>PAGE</u>
1	Thunderpipe Shock Tube -----	17
2	Test Hardware -----	23
3	Instrumentation Locations - Specimens 1, 4 & 5 -----	26
4	Instrumentation Locations - Specimen 2 -----	27
5	Instrumentation Locations - Specimen 3 -----	28
6	Instrumentation Locations - Specimen 6 -----	29
7	Instrumentation Locations - Specimens 7 & 8 -----	30
8	Instrumentation Locations - Specimens 9 & 10 -----	31
9	Instrumentation Locations - Specimen 11 -----	32
10	Instrumentation Locations - Specimens 12 & 13 -----	33
11	Instrumentation Locations - Specimens 14,15,16 & 17 -----	34
12	Instrumentation Locations - Fixtures -----	35
13	Bar-Mass-Representation-of-a-Beam-----	46
14	NOVA-2-Cross-Section-Idealization-----	47 Deleted
15	Idealized-Stress-Strain-Curve-----	48
16	Schematic-of-Mechanical-Sublayer-Stress-Strain-Model-----	55
17	Cyclic-Stress-Strain-Load-Paths-----	56
18	Coordinate-Surface-for-Cylindrical-Panel-----	60
19	Stress Vs Pressure - Gauge S1-3 - Specimen No. 1 -----	45
20	Deflection Vs Pressure - Specimen No. 1 -----	46
21	Stress Vs Pressure - Gauge S2-2 - Specimen No. 2 -----	48
22	Deflection Vs Pressure - Specimen No. 2 -----	49
23	Stress Vs Pressure - Gauge S3-4 - Specimen No. 3 -----	50
24	Deflection Vs Pressure - Specimen No. 3 -----	51
25	Stress Vs Pressure - Gauge S4-3 - Specimen No. 4 -----	52
26	Deflection Vs Pressure - Specimen No. 4 -----	53
27	Stress Vs Pressure - Gauge S5-5 - Specimen No. 5 -----	54
28	Deflection Vs Pressure - Specimen No. 5 -----	55
29	Stress Vs Pressure - Gauge S5-2 - Specimen No. 5 -----	56
30	Stress Vs Pressure - Gauge S6-1 - Specimen No. 6 -----	58

LIST OF FIGURES (Cont'd)

<u>Figure No.</u>	<u>Title</u>	<u>PAGE</u>
31	Stress Vs Pressure - Gauge S6-1 - Specimen No. 6 -----	59
32	Stress Vs Pressure - Gauge S7-2 - Specimen No. 7 -----	60
33	Deflection Vs Pressure - Specimen No. 7 -----	61
34	Stress Vs Pressure - Gauge S8-2 - Specimen No. 8-----	62
35	Deflection Vs Pressure - Specimen No. 8 -----	63
36	Stress Vs Pressure - Gauge S9-5 - Specimen No. 9 -----	65
37	Stress Vs Pressure - Gauge S9-7 - Specimen No. 9 -----	66
38	Deflection Vs Pressure - Specimen No. 9 -----	67
39	Stress Vs Pressure - Gauge S10-6 - Specimen No. 10 -----	68
40	Deflection Vs Pressure - Specimen No. 10 -----	69
41	Stress Vs Pressure - Gauge S11-5 - Specimen No. 11 -----	70
42	Stress Vs Pressure - Gauge S12-2 - Specimen No. 12 -----	72
43	Stress Vs Pressure - Gauge S12-14 - Specimen No. 12 -----	73
44	Stress Vs Pressure - Gauge S13-2 - Specimen No. 13 -----	74
45	Stress Vs Pressure - Gauge S13-9 - Specimen No. 13 -----	75
46	Stress Vs Pressure - Gauge S13-14 - Specimen No. 13 -----	76
47	Stress Vs Pressure - Gauge S17-1 - Specimen No. 17 -----	78
48	Stress Vs Pressure - Gauge S17-2 - Specimen No. 17 -----	79
49	Displacement Vs Pressure - Specimen No. 17 -----	80
50	Stress Vs Displacement - Specimen No. 17 -----	81
51	Typical Free Field Pressure Pulse -----	84
52	Stress Vs Free Field Overpressure - Specimen 1 -----	86
53	Displacement Vs Free Field Overpressure - Specimen 1 -----	87
54	Stress Time History - Specimen 1 -----	89
55	Stress Vs Free Field Overpressure - Specimen 2 -----	90
56	Displacement Vs Free Field Overpressure - Specimen 2 -----	91
57	Stress Time History - Specimen 2 -----	92
58	Stress Vs Free Field Overpressure - Specimen 3 -----	94
59	Displacement Vs Free Field Overpressure - Specimen 3 -----	95
60	Stress Time History - Specimen 3 -----	96
61	Stress Vs Free Field Overpressure - Specimen 4 -----	97

LIST OF FIGURES (Cont'd)

<u>Figure No.</u>	<u>Title</u>	<u>PAGE</u>
62	Stress Vs Free Field Overpressure - Specimen 4 -----	98
63	Stress Vs Free Field Overpressure - Specimen 4 -----	99
64	Displacement Vs Free Field Overpressure - Specimen 4 -----	100
65	Displacement Vs Free Field Overpressure - Specimen 4 -----	101
66	Displacement Vs Free Field Overpressure - Specimen 4 -----	102
67	Shock Reflection Factor Vs Free Field Overpressure - Specimen 4 -----	104
68	Shock Reflection Factor Vs Incidence Angle - Specimen 4 ----	105
69	Stress Time History Specimen 4 -----	106
70	Stress Vs Free Field Overpressure - Specimen 5 -----	107
71	Stress Vs Free Field Overpressure - Specimen 5 -----	108
72	Stress Vs Free Field Overpressure - Specimen 5 -----	109
73	Displacement Vs Free Field Overpressure - Specimen 5 -----	110
74	Displacement Vs Free Field Overpressure - Specimen 5 -----	111
75	Displacement Vs Free Field Overpressure - Specimen 5 -----	112
76	Stress Time History - Specimen 5 -----	114
77	Stress Vs Free Field Overpressure - Specimen 6 -----	115
78	Stress Vs Free Field Overpressure - Specimen 6 -----	116
79	Stress Vs Free Field Overpressure - Specimen 6 -----	117
80	Stress Vs Free Field Overpressure - Specimen 6 -----	118
81	Stress Vs Free Field Overpressure - Specimen 6 -----	119
82	Stress Vs Free Field Overpressure - Specimen 6 -----	120
83	Stress Time History - Specimen 6 -----	122
84	Stress Vs Free Field Overpressure - Specimen 7 -----	123
85	Displacement Vs Free Field Overpressure - Specimen 7 -----	124
86	Stress Time History - Specimen 7 -----	125
87	Stress Vs Free Field Overpressure - Specimen 8 -----	127
88	Displacement Vs Free Field Overpressure - Specimen 8 -----	128
89	Stress Time History - Specimen 8 -----	129
90	Stress Vs Free Field Overpressure - Specimen 9 -----	130
91	Displacement Vs Free Field Overpressure - Specimen 9 -----	131
92	Stress Time History - Specimen 9 -----	132
93	Pressure Time History Inside the Specimen 9/Holding Fixture Cavity -----	134

LIST OF FIGURES (Cont'd)

<u>Figure No.</u>	<u>Title</u>	<u>PAGE</u>
94	Stress Vs Free Field Overpressure - Specimen 10 -----	135
95	Displacement Vs Free Field Overpressure - Specimen 10 -----	136
96	Stress Time History - Specimen 10 -----	137
97	Stress Vs Free Field Overpressure - Specimen 11 -----	139
98	Stress Vs Free Field Overpressure - Specimen 11 -----	140
99	Stress Time History - Specimen 11 -----	141
100	Compressive Stress Vs Free Field Overpressure - Specimen 12 -	142
101	Tensile Stress Vs Free Field Overpressure - Specimen 12 -----	143
102	Compressive Stress Vs Free Field Overpressure - Specimen 12 -	144
103	Tensile Stress Vs Free Field Overpressure - Specimen 12 -----	145
104	Compressive Stress Vs Free Field Overpressure - Specimen 12 -	146
105	Tensile Stress Vs Free Field Overpressure - Specimen 12 -----	147
106	Compressive Stress Vs Free Field Overpressure - Specimen 12 -	148
107	Tensile Stress Vs Free Field Overpressure - Specimen 12 -----	149
108	Stress Time History - Specimen 12 -----	151
109	Stress Time History - Specimen 12 -----	152
110	Compressive Stress Vs Free Field Overpressure - Specimen 13 -	155
111	Tensile Stress Vs Free Field Overpressure - Specimen 13 -----	156
112	Compressive Stress Vs Free Field Overpressure - Specimen 13 -	157
113	Tensile Stress Vs Free Field Overpressure - Specimen 13 -----	158
114	Compressive Stress Vs Free Field Overpressure - Specimen 13 -	159
115	Tensile Stress Vs Free Field Overpressure - Specimen 13 -----	160
116	Compressive Stress Vs Free Field Overpressure - Specimen 13 -	161
117	Tensile Stress Vs Free Field Overpressure - Specimen 13 -----	162
118	Stress Time History - Specimen 13 -----	163
119	The Effect of Internal Pressure and Shock Incidence Angle on Response of Specimen 13 -----	164
120	The Effect of Internal Pressure and Shock Incidence Angle on Response of Specimen 13 -----	165
121	The Effect of Internal Pressure and Shock Incidence Angle on Response of Specimen 13 -----	166
122	The Effect of Internal Pressure and Shock Incidence Angle on Response of Specimen 13 -----	167
123	The Effect of Internal Pressure and Shock Incidence Angle on Response of Specimen 13 -----	168

LIST OF FIGURES (Cont'd)

<u>Figure No.</u>	<u>Title</u>	<u>PAGE</u>
124	The Effect of Internal Pressure and Shock Incidence Angle on Response of Specimen 13 -----	169
125	Box Holding Fixture -----	171
126	Column Loading Device -----	172
127	Stress Vs Free Field Overpressure - Specimens 14-17 -----	173
128	Stress Time History - Specimen 16 -----	175
129	Static Test and Analysis Ratio Vs Specimen No. -----	177
130	Shock Load Analysis and Test Ratio Vs Specimen No -----	179
131	Comparison of ΔP_{ff} and ΔP_s from Test Resulting in the Same Structural Response Vs Specimen No. -----	181
132	Effect of Panel Thickness on ΔP_{ff} (Critical) -----	183
133	Effect of Panel Length (Width) on ΔP_{ff} (Critical) -----	184
134	Effect of Modulus of Elasticity on ΔP_{ff} (Critical) -----	186
135	Effect of Beam Length on ΔP_{ff} (Critical) -----	187

LIST OF TABLES

<u>Table No.</u>	<u>Title</u>	<u>PAGE</u>
I	SPECIMEN DESCRIPTION -----	19
II	MECHANICAL PROPERTIES -----	20
III	STIFFENER GEOMETRY -----	21
IV	SPECIMEN PART NUMBERS -----	22
V	FIXTURE PART NUMBERS -----	24
VI	FIXTURE/SPECIMEN RELATIONSHIPS -----	24
VII	INSTRUMENTATION -----	25
VIII	RETENTION SET CONFIGURATION -----	43
IX	CONVERGENCE STUDY RESULTS - STRESS/DISPLACEMENT -----	44
X	CONVERGENCE STUDY RESULTS - RETENTION SET DIFFERENCES -----	44
XI	EFFECTS OF COLUMN INITIAL IMPERFECTIONS -----	82
XII	SPECIMEN 13 SHOCK LOAD TEST CONDITIONS -----	154
XIII	ANALYSIS STRESS TIME HISTORY FOR CENTER OF SPECIMEN 14-17 FOR TEST SHOT 5 (INITIAL IMP = 0.01") -----	176
XIV	TEST AND ANALYSIS RESULTS IN THE PLASTIC REGION -----	178
XV	SENSITIVITY STUDY VARIATIONS -----	182
XVI	TEST AND ANALYSIS STRUCTURAL RESPONSE FREQUENCIES -----	190
XVII	SUMMARY OF ELASTIC/PLASTIC TEST RESULTS -----	192
XVIII	MATHEMATICAL MODEL DATA FOR HOMOGENEOUS FLAT PANELS -----	193
XIX	MATHEMATICAL MODEL DATA FOR STRAIGHT BEAMS -----	194
XX	TYPICAL NOVA-2 RUN TIMES ON CDC 7600 COMPUTER -----	198

NOMENCLATURE

A	Area
AFWL	Air Force Weapons Laboratory
b	Width of layer in beam model
c	Distance from neutral axis to extreme fiber
CPS	Cycles per second
d	Spacing between flanges in a layer of a beam model
\bar{d}	Displacement vector
E	Modulus of elasticity
EMP	Electromagnetic pulse
\bar{F}	Surface force vector
F _y	External force per unit length in the y-direction
F _z	External force per unit length in the z-direction
f _{t_y}	Tensile yield stress
h	Depth of layer in beam model
Hz	Hertz
in	Inches
[K]	Stiffness matrix
KT	Kiloton
l	Length
M	Internal moment
MB	Number of modes in the beta direction of a panel model
MG	Number of modes in the gamma direction of a panel model
[M]	Mass matrix

N	Internal axial force Number of mass points
n	Number of flanges in a layer of a beam model
psi	Pounds per square inch
Q	Internal shear force
R	Radius
T	Kinetic energy
t	Time
TREES	Transient radiation effects on electronic systems
V	Volume
v	Position in the y-direction
w	Position in the Z-direction
$\overset{\circ}{W}$	Initial radial imperfection
x	Displacement
\dot{x}	Velocity
\ddot{x}	Acceleration
x_{cg}	Location of centroidal axis
δ	Initial imperfection in a column Permanent deformation
$\delta u, \delta v, \delta w$	Virtual displacements
ΔP_{ff}	Free field (incident) overpressure
ΔP_s	Static overpressure
Δt	Time increment
ϵ	Strain
λ	Eigenvalue
μ	Poisson's ratio
ρ	Density

σ	Stress
θ	Angular Measurement
ω	Frequency

The ability of a weapon system to survive in a nuclear environment is a function of many variables, particularly the nuclear hardness of the system. Determination of the nuclear hardness of a system typically requires a detailed study of the interaction of the system elements (e.g., crew, avionics, control system, airframe) with the nuclear environments (e.g., nuclear radiation, thermal radiation, blast effects, EMP, TREES).

The ability of an airframe to resist nuclear blast effects (gust and overpressure) and thermal radiation is a primary concern in a nuclear hardness assessment. Because of the nature of blast loading, gust effects are generally considered when determining the dynamic response of low-frequency, primary structural components, such as an aircraft wing, fuselage or empennage. Conversely, overpressure loading is the significant blast effect when determining the response of high-frequency structural components, such as aircraft skin panels, stringers, frames and radomes.

As a result of the moratorium on nuclear weapons effects tests in the atmosphere, response of systems to nuclear environments is usually determined analytically, supported by laboratory experiments. Techniques such as NOVA-2 (Reference 1) are frequently used for determining structural response to nuclear overpressure and are supplemented with experimental data obtained from tests conducted in nuclear overpressure simulation facilities similar to those described in Reference 2. However, experimental data describing the response of basic structural elements (e.g., skin panels, stringers, frames, columns) to nuclear overpressure has been found to be extremely limited. To help alleviate this deficiency in this critical area of technology, a program was conducted (including analysis and experiment) to determine the response of 17 basic structural elements to simulated nuclear overpressure loading.

These structural elements were designed and manufactured specifically for this program and are representative of structural elements found in aircraft. This report describes the results of the program.

The major tasks that were accomplished in this program and are discussed in this report are: (1) experimental determination of the ability of 17 basic structural elements to withstand simulated nuclear overpressure loads (utilizing Sandia Corporation's THUNDERPIPE Shock Tube) and uniform static pressure loads; (2) analytical determination of the ability of these structural elements to withstand nuclear overpressure loads and uniform static pressure loads (utilizing NOVA-2, finite element techniques, and classical strength analysis techniques); (3) identification and evaluation of differences between test results and analysis results; (4) identification of suggested changes to NOVA-2 to upgrade its capabilities; (5) analytical determination of the sensitivity of structural response to selected structural properties; and (6) application of program results to future nuclear hardness assessments.

2.0

TEST FACILITIES

The simulated nuclear overpressure testing was conducted at Sandia Corporation's THUNDERPIPE shock tube in Albuquerque, New Mexico. As illustrated in Figure 1, this shock tube consists of a 200-foot long, constant diameter (six feet) driver chamber, a 40-foot long, conical section which provides a transition from the driver chamber to the test section, and a 66-foot long, constant diameter (19 feet) test section. A portion of the driver chamber wall is constructed of three-inch thick, mild steel, whereas the remainder of the tunnel wall is constructed of one-inch thick, mild steel. In addition, the 19-foot diameter test section is reinforced with circumferential stiffeners at approximately 10-foot intervals as shown in Figure 1.

Blast waves, simulating a nuclear overpressure pulse, were generated by igniting PETN primacord explosive charges (up to 183 feet long). The primacord was positioned in the centerline of the driver chamber by a series of expendable nylon cords. Use of the long explosive charges resulted in the desired positive phase duration of the pressure pulse (approximately 100 milliseconds). Peak intensity of the free field pressure pulse was controlled by the longitudinal position of the test specimen within the tunnel as well as the density of the explosive charge, i.e., the number of grains of explosive per lineal foot of cord. For example, use of approximately ten pounds of explosive resulted in a free field overpressure peak intensity of approximately four psi at a location approximately 45 feet upstream from the muzzle end.

The inside wall of the test section was instrumented with seven pressure transducers to measure free field (incident) overpressure and four transducers to measure reflected overpressure. These transducers were positioned in the wall of the test section in such a manner that an accurate definition of the free field overpressure time histories at the test specimen location was available.

Sandia Laboratories provided all signal conditioning and recording equipment and associated personnel. They also provided ordinance personnel, mechanics and equipment operators. Sandia Laboratories was also responsible for transposing data from the recording analog tapes to digital tapes suitable for computer plotting and providing all plots of strain, pressure, displacement, temperature, and acceleration. (It should be noted here that the Air Force Weapons Laboratory, Kirtland Air Force Base, provided Gould plots of converted strain-to-stress and acceleration-to-displacement data.)

In addition to the simulated nuclear overpressure testing, static testing was accomplished for all test specimens to determine their respective response characteristics to spatially uniform, statically applied external pressure and to checkout selected instrumentation. This testing was accomplished in the Structural Test Laboratories of The Boeing Company, Wichita, Kansas.

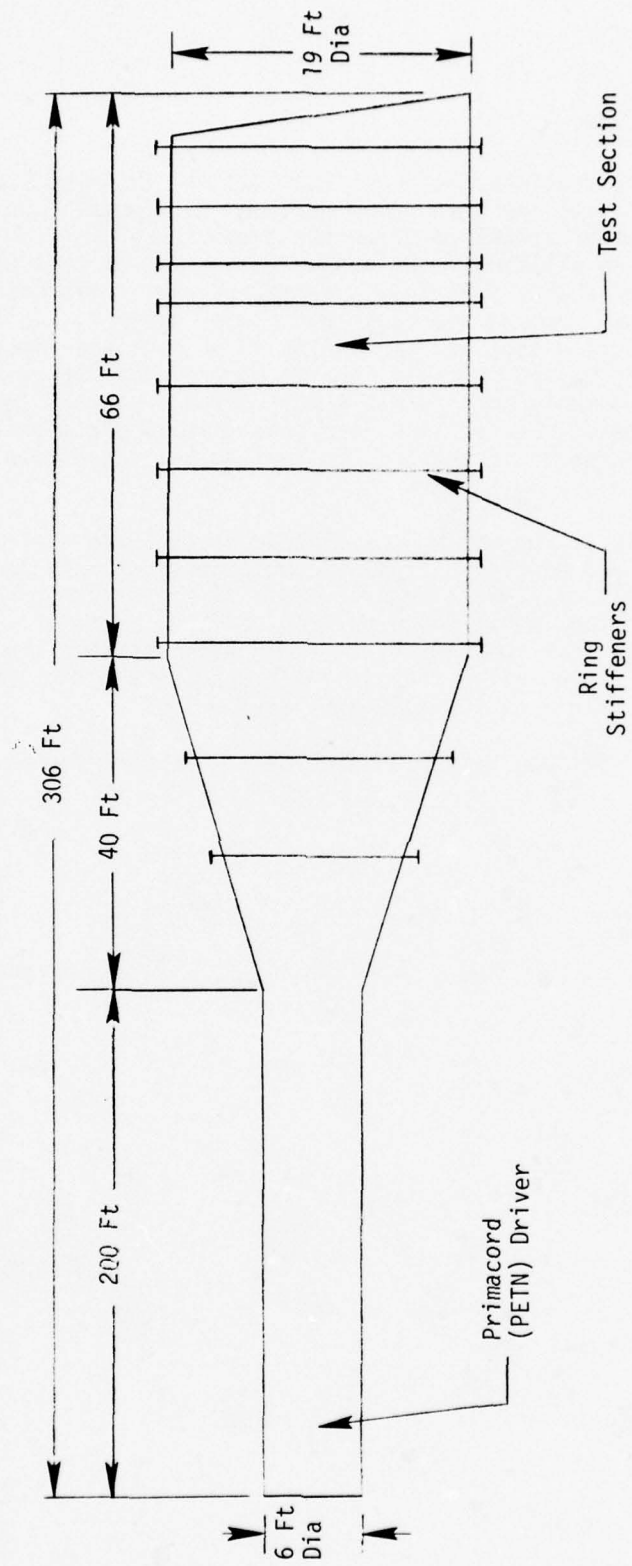


FIGURE 1. THUNDERPIPE SHOCK TUBE

3.0 TEST SPECIMENS

Seventeen aluminum test specimens were designed and manufactured specifically for this study. These test specimens were designed to simulate basic structural elements representative of structure primarily found in aircraft. The guidelines that were utilized in selecting this group of test specimens were: (1) inclusion of a wide variety of parameters that influence structural response characteristics such as boundary conditions, geometry, failure mechanism, and construction type and (2) inclusion of test specimens that the NOVA-2 computer program was potentially capable of properly analyzing. That is, the test specimens were designed to exhibit well-defined primary load paths. In addition, these specimens were sized such that initial yielding (threshold of permanent damage) occurred in the one psi to five psi free field overpressure range.

As illustrated in Table I, the set of test specimens included flat and curved stiffened and unstiffened panels, flat honeycomb panels, skin/frame circular cylinders, and buckling sensitive columns. Table II describes the material properties of the test specimens, which were established by tensile coupon tests of material taken from the same stock from which the specimen was made. In addition, Table III illustrates the stiffener spacing and the geometry of the stiffener cross sections for test specimens 9-13.

The test specimens are defined by Boeing drawings. The part numbers are shown in Table IV.

SPECIMEN NUMBER	DESCRIPTION	LENGTH (IN)	WIDTH (IN)	THICKNESS (IN)	BOUNDARY CONDITIONS
1	Flat Panel	22.0	22.0	.191	4 Sides Clamped
2	Flat Panel	22.0	22.0	.191	4 Sides Pinned
3	Flat Panel	22.0	22.0	.193	2 Sides Clamped 2 Sides Pinned
4	Flat Panel	22.0	22.0	.316	4 Sides Clamped
5	Flat Panel	22.0	22.0	.020	4 Sides Clamped
6	Curved Panel	36.0	1	.08	4 Sides Clamped
7	Flat Honeycomb Panel	22.0	22.0	2	4 Sides Pinned
8	Flat Honeycomb Panel	22.0	22.0	3	4 Sides Pinned
9	Flat Stiffened Panel	36.0	36.0	4 .0625 Skin	Stiffener Ends Clamped
10	Flat Stiffened Panel	36.0	36.0	4 .0625 Skin	Stiffener Ends Pinned
11	Curved Stiffened Panel	36.0	1	4 .020 Skin	Stiffener Ends Clamped
12	Skin/Frame Cylinder	36.0	24" Radius	4 .020 Skin	Stiffener Ends Clamped (0° & 180°)
13	Skin/Frame Cylinder	36.0	24" Radius	4 .020 Skin	Stiffener Ends Clamped (0° & 180°)
14-17	Columns	10.0	5.0	.031	Clamped Ends





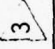
TABLE I. SPECIMEN DESCRIPTION

- 1 24.0" Radius; 54.56° Subtended Angle
2 .013" Face Sheets; Core Depth = .3065" ; Cell Size = .375"
3 .013" Face Sheets; Core Depth = .292" ; Cell Size = .125"
4 For Stiffener Geometry See Table III

SPECIMEN NUMBER	ALUMINUM MATERIAL	YIELD STRESS (psi)	ULTIMATE STRESS (psi)	% ELONGATION	MODULUS of ELASTICITY (psi) x 10 ⁻⁶
1	6061-T6	40,350	44,820	14.5	11.0
2	6061-T42	18,410	36,090	25.5	10.4
3	6061-T6	40,500	45,200	15.0	10.9
4	6061-T42	19,380	37,810	26.8	10.6
5	6061-T6	41,180	46,760	12.0	10.1
6	6061-T6	40,500	45,200	15.0	10.9
7 & 8 (Skin)	5052-0	13,270	30,300	21.0	12.3
9 (Stiffener)	2024-T3511	52,230	66,320	22.0	10.6
9 (Skin)	2024-T3	53,230	69,800	18.0	10.0
10 (Stiffener)	2024-T3511	52,710	67,310	18.0	10.8
10 (Skin)	2024-T3	54,620	70,200	15.0	9.8
11 (Stiffener)	6061-T42	19,670	36,600	27.0	10.5
12 (Stiffener)	6061-T42	19,460	37,900	25.0	10.3
13 (Stiffener)	6061-T42	20,800	36,690	25.5	10.6
14-17	7075-T6	70,500	83,000	8.0	10.5

TABLE II. MECHANICAL PROPERTIES

1 See Reference 3.

SPECIMEN NUMBER	STIFFENER SPACING (in)	CROSS SECTION	DIMENSIONS (in)					
			A	B	C	D	E	F
9	9.0		.998	.101	.705	.098	2.112	2.202
10	9.0		1.005	.103	.724	.098	2.118	2.202
11	9.0		.710	.101	.461	.104	1.895	2.0
12	9.0		.706	.103	.457	.105	1.90	2.005
13	9.0		.706	.148	.106	.602	--	--

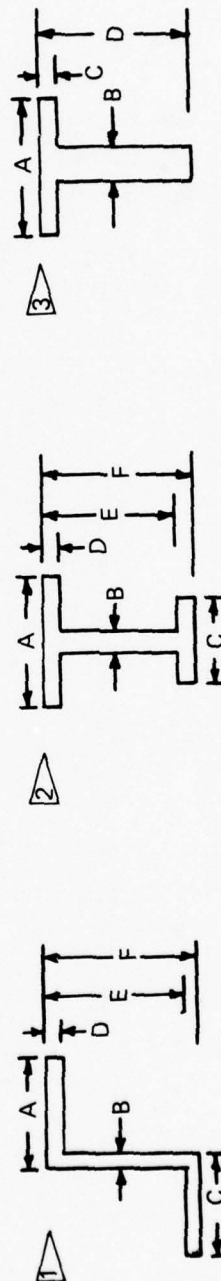


TABLE III. GEOMETRY

TABLE IV

SPECIMEN	PART NUMBERS
1	EX3027-1
2	EX3027-2
3	EX3027-3
4	EX3027-4
5	EX3027-5
6	EX3028-6
7	EX3027-7
8	EX3027-8
9	EX3029-9
10	EX3029-10
11	EX3030-11
12	EX3030-12
13	EX3030-13
14-17	EX3031-14

4.0

TEST FIXTURES

The test holding fixtures were expressly designed for the specimens being tested; however, versatility, interchangeability, and adaptability to a variety of specimens was stressed. These fixtures consisted of: (1) a master frame which bolted to two longitudinal rails that were welded to the shock tube floor, (2) a rectangular box holding fixture which attached to the master frame and to which was mounted all flat test specimens, (3) a partial cylinder fixture which attached to the master frame and to which was mounted the two curved panel specimens, and (4) a pair of circular end plates that served as the interface between the master frame and the skin/frame cylinders. Figure 2 illustrates the installation of the master frame and fixtures in the shock tube.

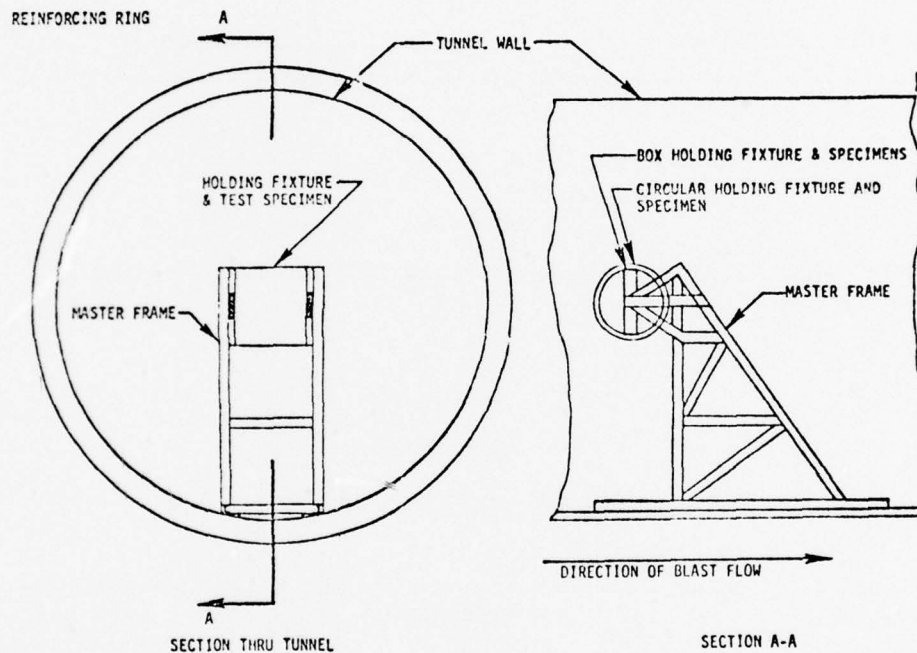


FIGURE 2. TEST HARDWARE

The fixtures are defined by Boeing drawings. A list of the fixtures and their respective part numbers is shown in Table V.

TABLE V
FIXTURE PART NUMBERS

FIXTURE	BOEING PART NO.
Box Holding Fixture	EX3032-21
Small Panel Adapter Plate	EX3032-26
End Plates (2)	EX3032-30
Partial Cylinder Adapter	EX3032-33
Frame Assemblies	EX3032-35, 36

In addition, Table VI illustrates the various test specimens that were mounted to the test fixtures.

TABLE VI
FIXTURE/SPECIMEN RELATIONSHIPS

FIXTURE	SPECIMEN NO.													
	1	2	3	4	5	6	7	8	9	10	11	12	13	14-17
Box Holding Fixture	X	X	X	X	X		X	X	X	X				X
Small Panel Adapter Plate	X	X	X	X	X		X	X						
End Plates						X					X	X	X	
Partial Cylinder Adapter						X					X			
Frame Assemblies						X					X	X	X	

5.0

INSTRUMENTATION

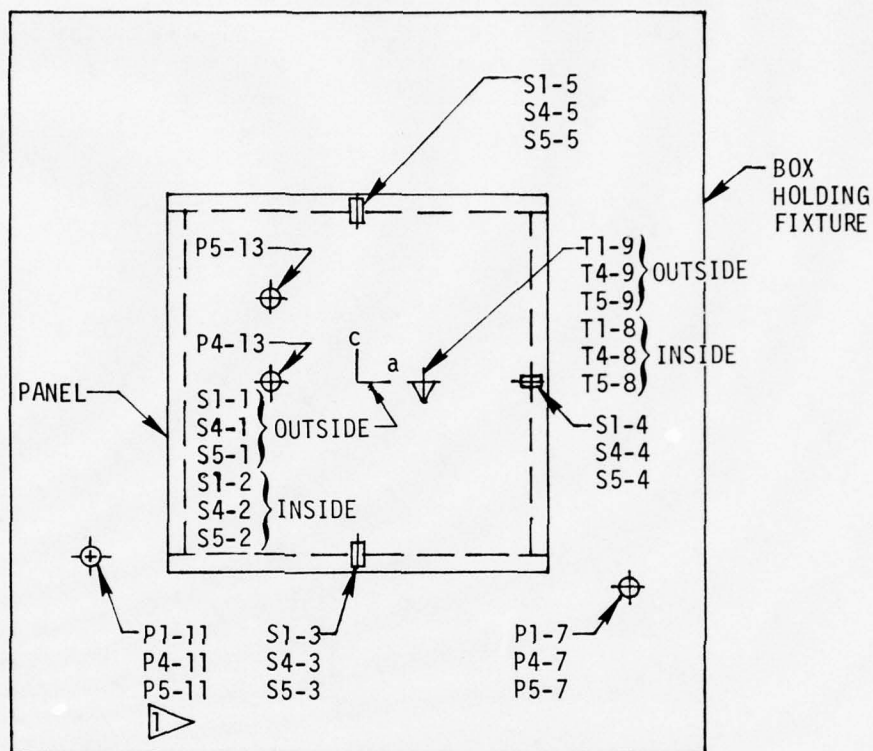
In addition to the pressure transducers that were mounted in the wall of the shock tube test section, various instrumentation was mounted on the test specimens and holding fixtures as well as inside the test fixture/specimen cavities. During the shock load testing, fourteen different test set-ups were required, utilizing equipment that is illustrated in Table VII.

TABLE VII
INSTRUMENTATION

PARAMETER	SENSOR DESCRIPTION
Pressure	KULITE XCQL-12-152-25S
Strain	MM EA-13-125RA-120W Rosette MM EA-13-125BT-120 Axial
Deflection	KD-2300-10CU Proximity Gauge
Acceleration	KULITE GYN-155-250 ENDEVCO 2261 M6
Temperature	MM-ETG-50

The Sandia Laboratories instrumentation equipment consisted of bridge conditioning, ENDEVCO signal conditioning, RED COR differential amplification, EMR voltage controlled oscillators, and CEC VR 3300 analog tape recorders.

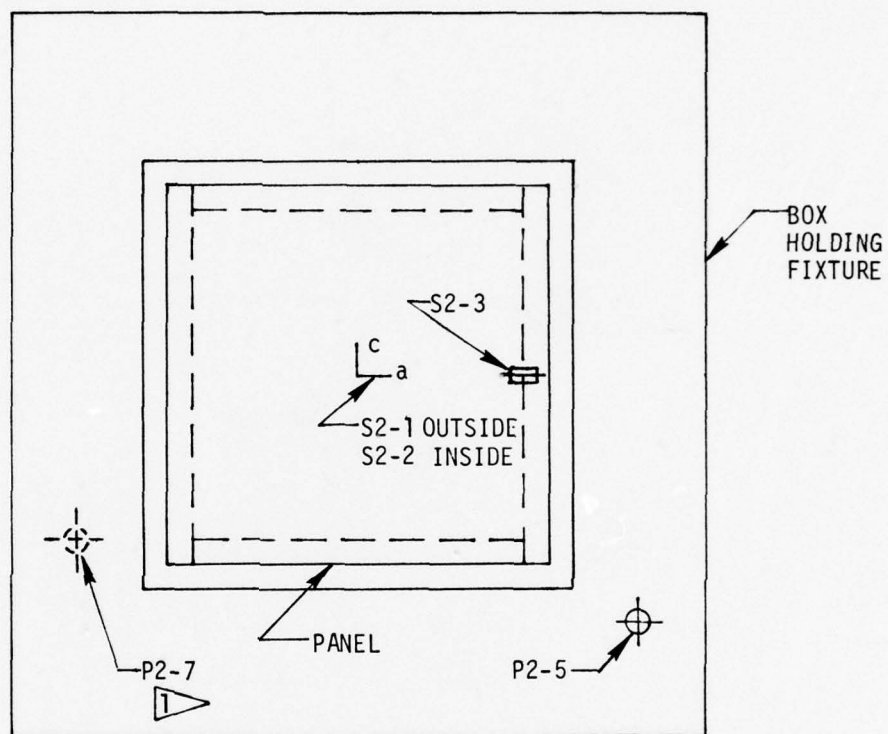
Strain gauge locations were selected to be in the areas of maximum strain as determined by analysis. Axial gauges were utilized in both uniaxial and bi-axial stress fields. Single gauges were utilized in uniaxial stress fields. Two gauges per location (rotated 90° with respect to each other) were utilized in bi-axial stress fields where the principal stress direction was known. In addition, 45° rosettes were utilized in bi-axial stress fields where principal stress directions were not known. A detailed illustration of all instrumentation locations is shown in Figures 3-12. The letters P,S,D,A & Y represent pressure, strain, deflection, acceleration and temperature, respectively. The digit adjacent to the letter is the specimen number and the dash number is simply the serial number of the transducer associated with that specimen.



SPECIMEN NOS. 1, 4 & 5


FIGURE 3. INSTRUMENTATION LOCATIONS

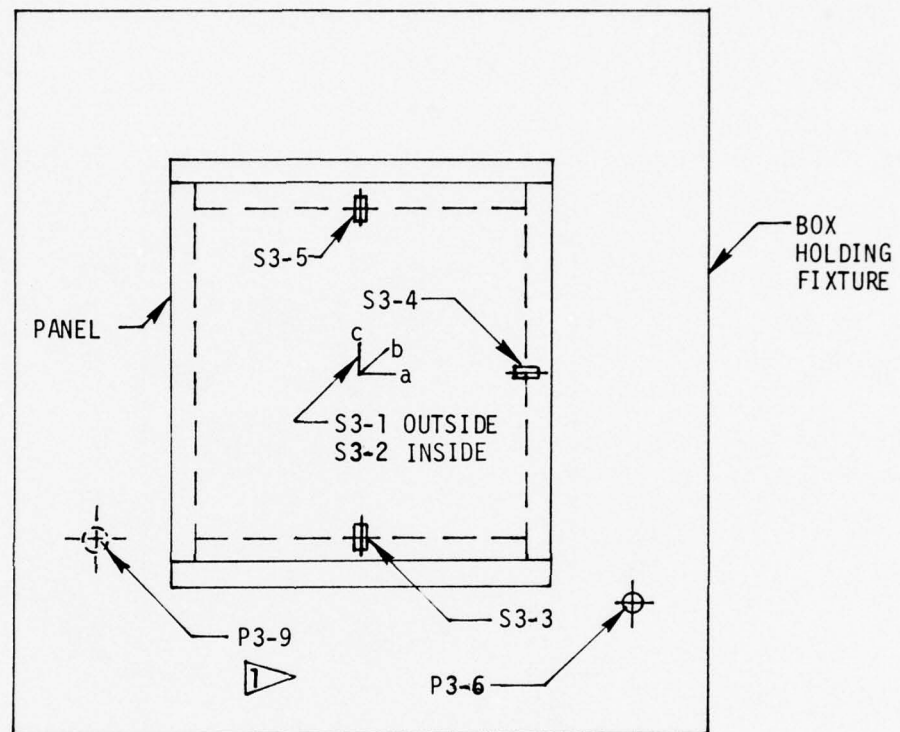
1 ON BACK SIDE ON BOX HOLDING FIXTURE ONLY



SPECIMEN NO. 2

FIGURE 4. INSTRUMENTATION LOCATIONS

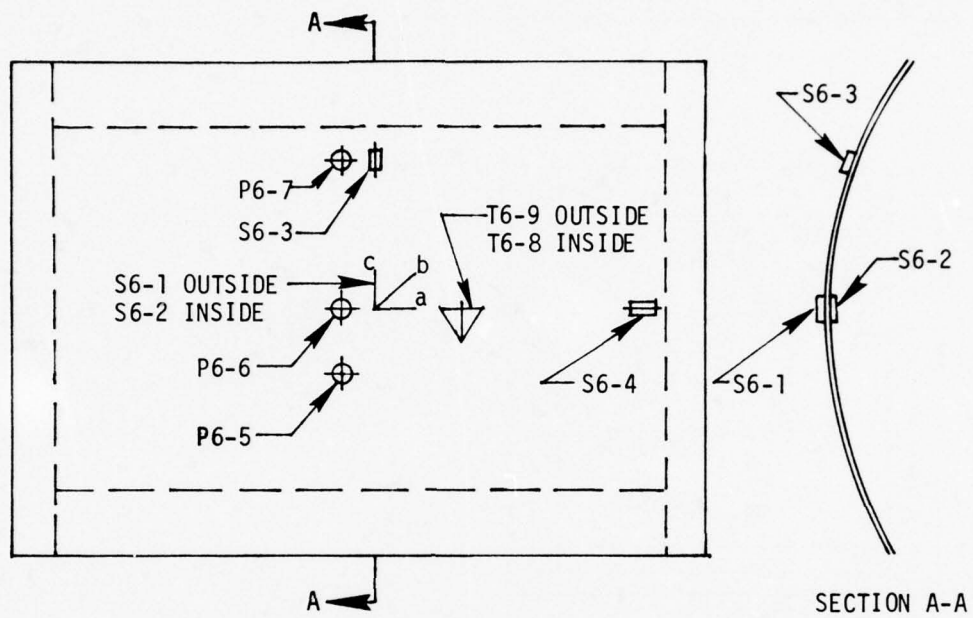
 ON BACK SIDE ON BOX HOLDING FIXTURE ONLY



SPECIMEN NO. 3

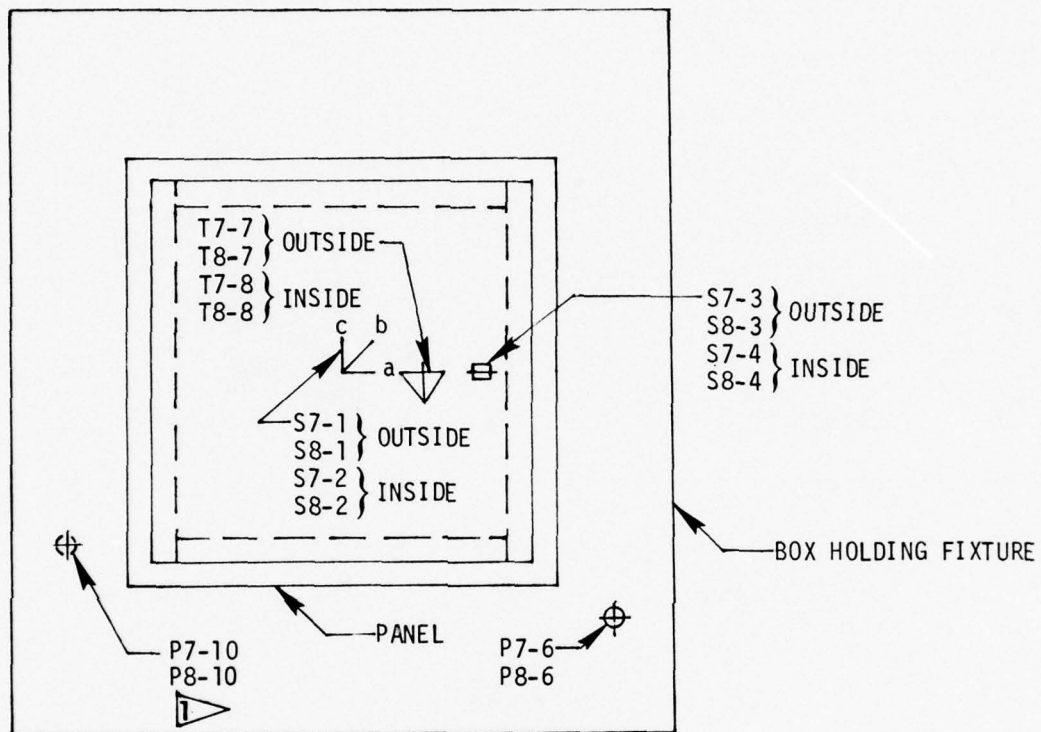
FIGURE 5. INSTRUMENTATION LOCATIONS

1 ON BACK SIDE ON BOX HOLDING FIXTURE ONLY



SPECIMEN NO. 6

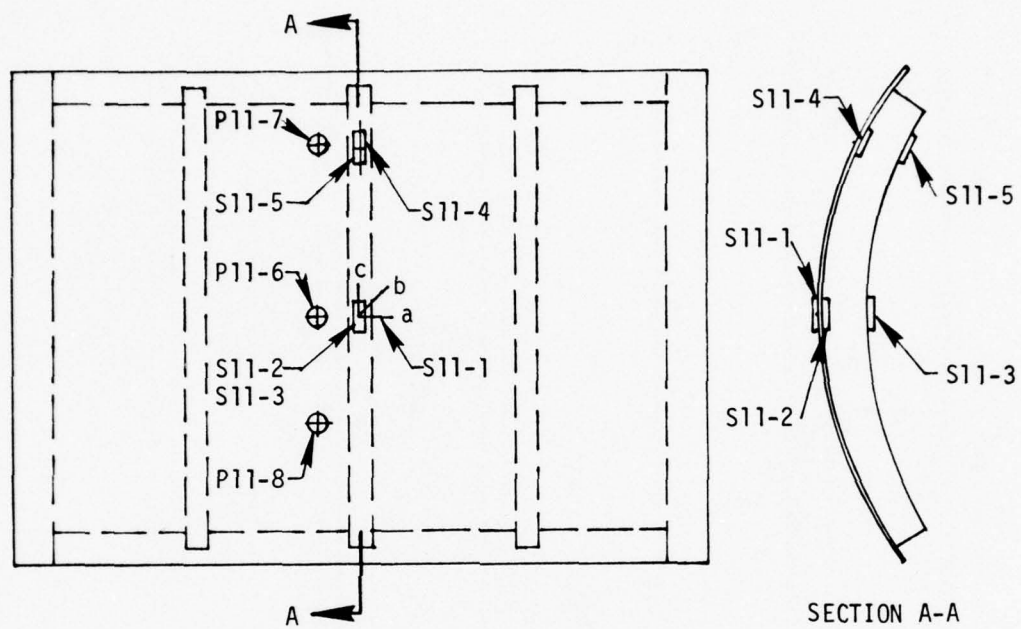
FIGURE 6. INSTRUMENTATION LOCATIONS



SPECIMEN NOS. 7 & 8

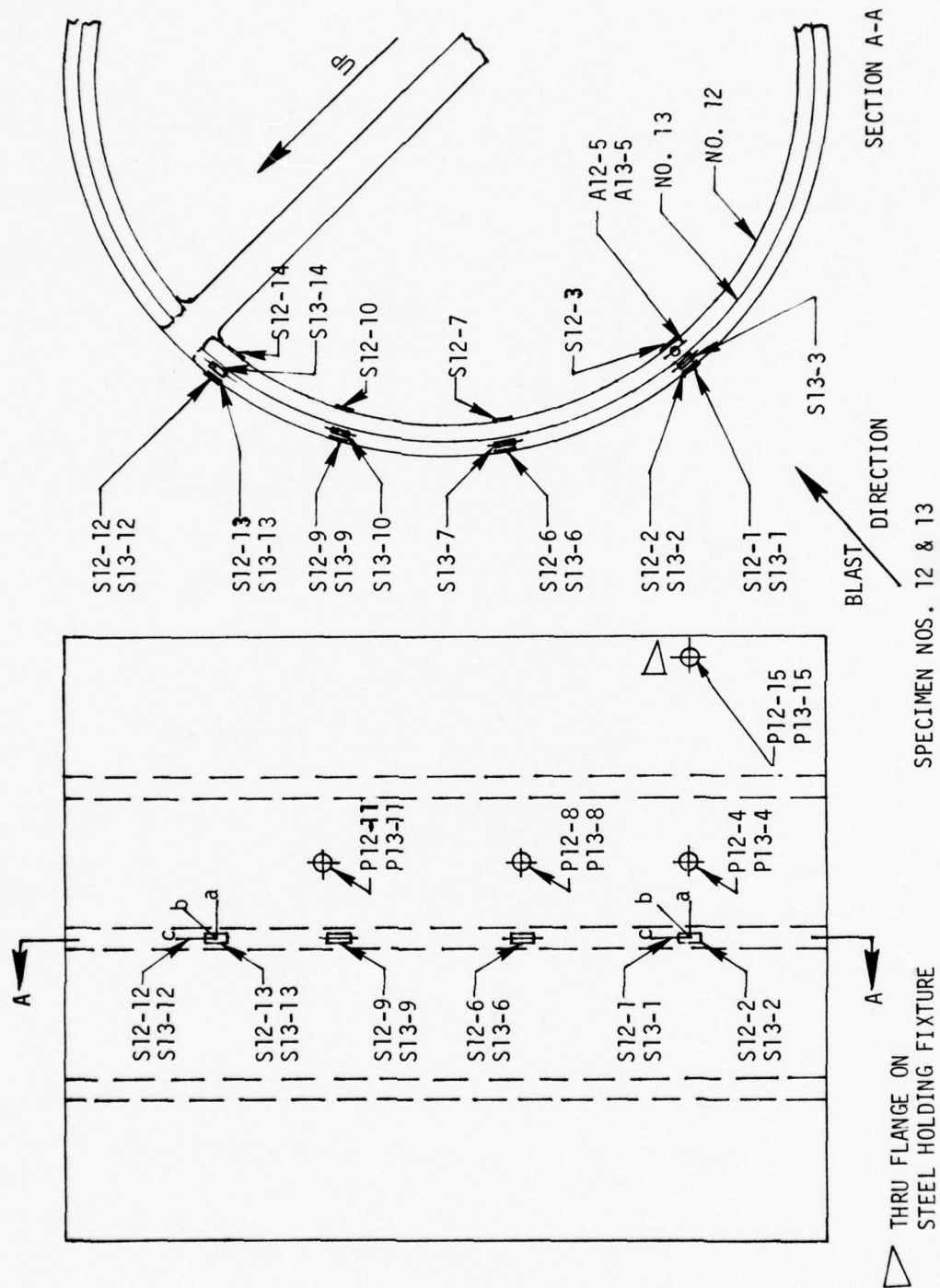
FIGURE 7. INSTRUMENTATION LOCATIONS

△ ON BACK SIDE ON BOX HOLDING FIXTURE ONLY



SPECIMEN NO. 11

FIGURE 9. INSTRUMENTATION LOCATIONS



SPECIMEN NOS. 12 & 13
FIGURE 10. INSTRUMENTATION LOCATIONS

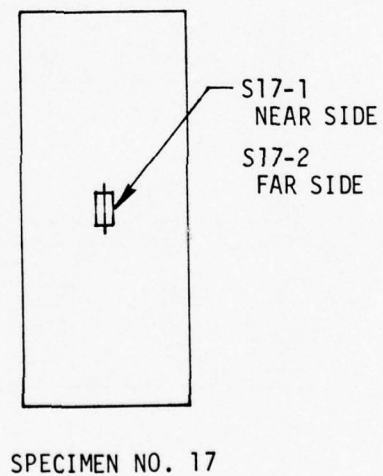
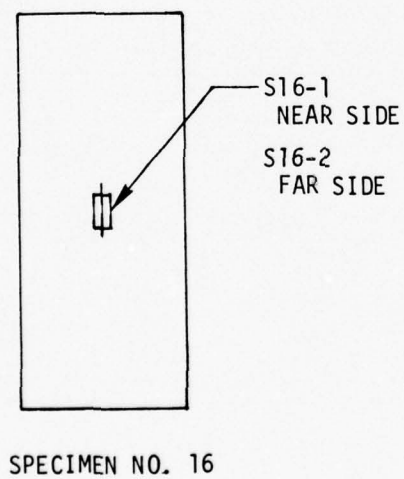
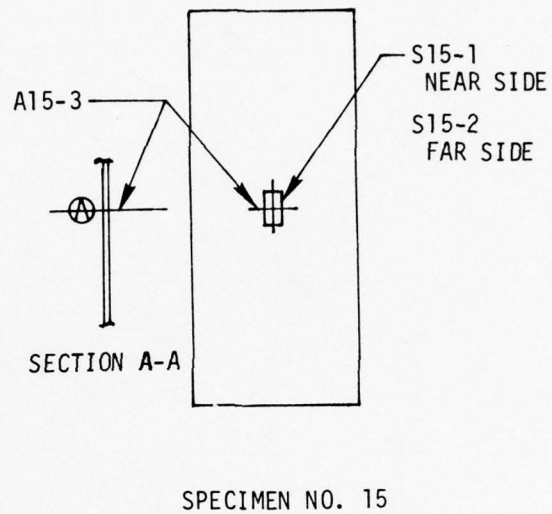
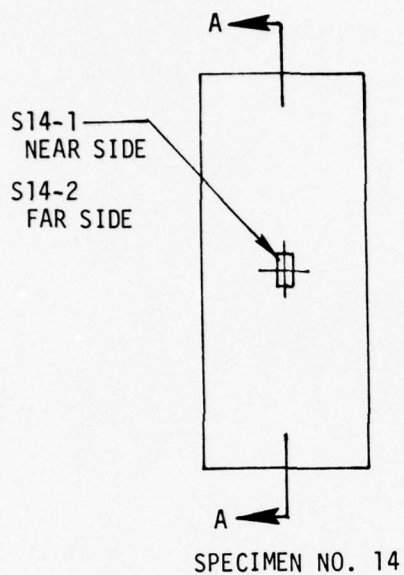
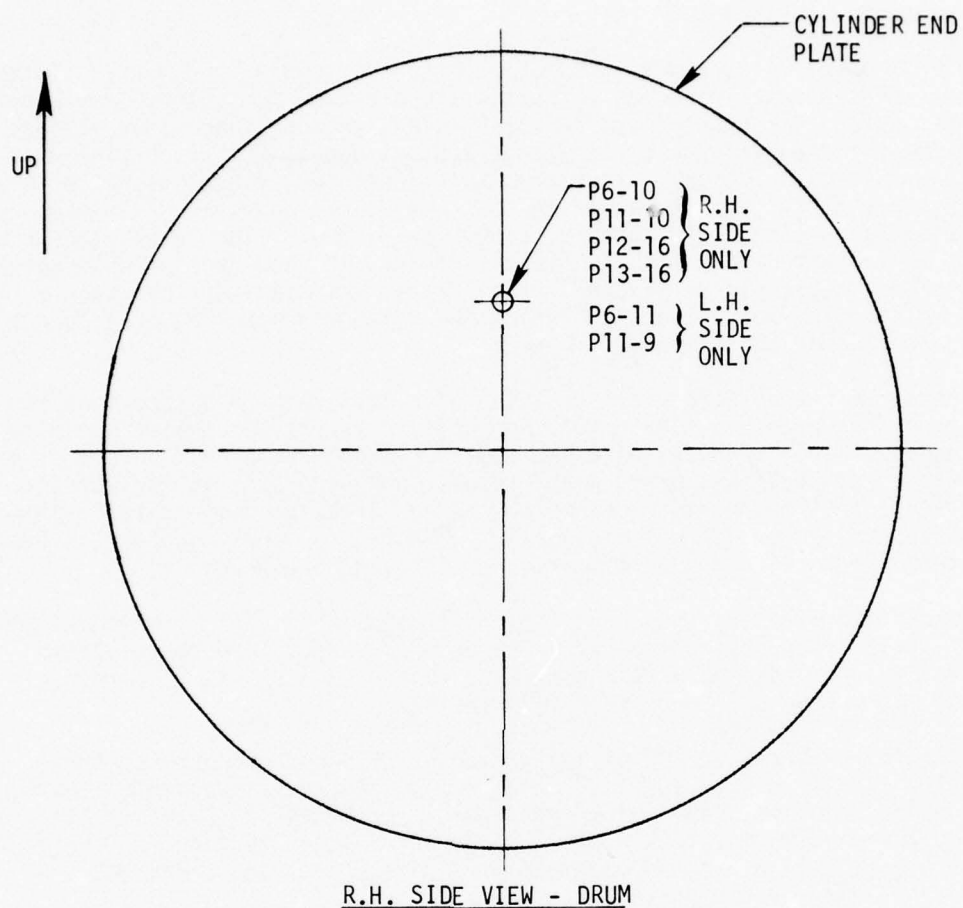
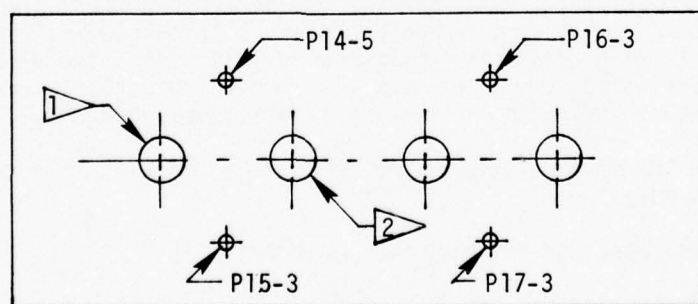


FIGURE 11. INSTRUMENTATION LOCATIONS



R.H. SIDE VIEW - DRUM



EX3032-69 FACE PLATE

- 2 A15-4
 1 A14-4
- } LOCATED ON PISTON

FIGURE 12. INSTRUMENTATION LOCATIONS

The strain channel circuits consisted of a three leadwire system from the strain gauge to a bridge completion unit. The bridge completion units consisted of a precision certified compensating gauge plus half bridge. By connecting a shunt calibration resistor across the compensating gauge, system check-out and system calibration was performed one time per channel per specimen. When using this type of system calibration, knowing the bridge voltage, leadwire resistance, and cable resistance was not necessary for obtaining accurate system calibration. Since the instrumentation system was not of the null balance variety, an unknown bridge voltage change between calibration and testing was a potential source of significant error. Therefore, the bridge voltages were checked prior to each test shot and, if required, were adjusted to the bridge voltage value present during system calibration. Balancing, setting calibration output, and adjusting the voltage controlled oscillators were also performed at this time.

The temperature channel circuits consisted of a two leadwire system from the temperature sensor to a bridge completion unit. The bridge completion units consisted of a linearizing network (MM LST-100F-120B) and a half bridge. The system shunt calibration procedure and results were the same as for strain gauges except that temperature channels were not leadwire compensated. Since the temperature sensors have a high output compared to strain gauges, analysis showed that leadwire errors were small and therefore neglected.

The pressure and acceleration channel circuits consisted of full bridge transducers. These transducers were certified prior to shock load testing, and output voltage per test parameter per input voltage was known. The instrumentation was set up utilizing this information.

The deflection system's specification stated a frequency response that was essentially flat from 0 to 2000 Hz. However, a frequency response evaluation was conducted prior to usage which verified its operational characteristics in the frequency range of interest (0-200Hz). Prior to selected test shots, the deflection system was calibrated statically by displacing the sensor and monitoring voltage output versus displacement.

Static load testing also required the use of the fourteen test setups which utilized the strain gauges and deflection gauge illustrated in Table IV. In addition, the following certified equipment was utilized: two BLH Model 225 switch and balance units, one BLH Model 120 strain indicator, one Wallace and Tiernam pressure indicator, and two deflection measuring, dial indicators.

Strain data from the strain gauges were reduced to stresses in accordance with the following formulas:

Uni-directional stress - no constraints

$$\sigma = E \epsilon$$

Uni-directional stress - restrained transverse strain

$$\sigma = \frac{E \epsilon}{1 - \mu^2}$$

Bi-axial stress - direction known

$$\sigma_a = \frac{E}{1-\mu^2} (\epsilon_a + \mu \epsilon_c)$$

$$\sigma_c = \frac{E}{1-\mu^2} (\epsilon_c + \mu \epsilon_a)$$

Bi-axial stress - direction unknown

$$\sigma_{MAX} = E \left\{ \frac{\epsilon_a + \epsilon_c}{2(1-\mu)} + \frac{\sqrt{2[(\epsilon_a - \epsilon_b)^2 + (\epsilon_b - \epsilon_c)^2]}}{2(1+\mu)} \right\}$$

$$\sigma_{MIN} = E \left\{ \frac{\epsilon_a + \epsilon_c}{2(1-\mu)} - \frac{\sqrt{2[(\epsilon_a - \epsilon_b)^2 + (\epsilon_b - \epsilon_c)^2]}}{2(1+\mu)} \right\}$$

Where:

σ = Stress

E = Modulus of Elasticity (Young's Modulus)

ϵ = Strain

μ = Poisson's Ratio

$\left. \begin{matrix} a \\ b \\ c \end{matrix} \right\}$ = Subscripts referencing
each leg of bi-axial or
45 degree shear rosette strain gauges

6.0 TEST PROCEDURES

6.1 Static Test

Prior to the shock load testing, static overpressure load testing was accomplished for all test specimens. The objectives of the static testing were: (1) to provide experimental data on the structural response of the test specimens to spatially uniform, statically applied overpressure for comparison with static analysis results and subsequent shock test results and (2) to provide a checkout of the strain gauges and deflection measuring system. Since these test specimens were to be shock tested subsequent to the static tests, the static test of each specimen was stopped prior to initiation of yielding. The procedures that were followed during static testing were as delineated below:

- (1) The instrumented specimen was loaded into the appropriate test fixture and instrumentation wiring was connected.
- (2) Photographs were taken.
- (3) Zero load readings were recorded.
- (4) The test fixture was sealed against significant air leaks.
- (5) Except for the column specimens, air was evacuated from within the test fixture/specimen cavity causing an externally applied, uniformly distributed, differential pressure on the specimen. The column specimens were loaded by gradually applying dead weight to a driver piston which was connected to the column.
- (6) Instrumentation readings were recorded at each load increment and evaluated to determine whether the specimen was capable of withstanding the next load increment without yielding.
- (7) After reaching the maximum load established by the test engineer, the load was released and zero load readings were recorded.

6.2 Shock Load Test

The objective of the shock load testing was to expose the test specimens individually (however, the four column specimens were tested simultaneously) to a series of simulated nuclear overpressure pulses to determine: (1) the response characteristics of the specimens in the elastic range, (2) the level of free field overpressure defining the threshold of damage (yielding), which will be referred to as the critical free field overpressure, and (3) the degree of permanent deformation resulting from one test shot per specimen at a pressure intensity significantly greater than the respective critical overpressures.

To accomplish the objectives stated above, the flat test specimens were oriented in the shock tube such that the shock propagation vector was perpendicular to the plane of the specimen, whereas the curved specimens were oriented such that the shock propagation vector was perpendicular to the longitudinal axis of the cylinder formed by the specimen/fixture. The columns were oriented such that the simulated nuclear overpressure produced an axial load environment.

The procedures that were followed during shock load testing were detailed in advance by Reference 3 and were as delineated below:

- (1) The instrumented test specimen was mounted to the appropriate test fixture.
- (2) The test fixture, complete with specimen, was mounted to the master frame.
- (3) The master frame/fixture/specimen was installed in the shock tube at the pre-selected test station.
- (4) Instrumentation wiring was connected to appropriate cables, and calibration was completed.
- (5) Photographs were taken.
- (6) Based on the requested free field shock intensity, an appropriate amount of primacord was loaded into the driver chamber.
- (7) Immediately after firing, visicorder copies of twelve channels of data were available for examination. In addition, visual inspection of the test setup was conducted after most test shots.
- (8) Based on examination of the structural response data, the next pressure intensity was chosen.
- (9) Steps 5-8 were repeated until yielding occurred (usually four shots per specimen were required).
- (10) A final pressure intensity was chosen such that significant permanent deformation occurred.
- (11) Photographs were taken.
- (12) All instrumentation wiring was disconnected and the specimen/fixture disassembled after each test series.
- (13) The specimen was examined for failure and the nature of the failure recorded.

A total of 87 test shots were conducted in the study. For selected test shots, high speed (1000 frames/second) motion pictures were taken.

7.0 ANALYSIS PROCEDURES

7.1 General Discussion

A variety of analysis techniques were employed in accomplishing this study. For the static load analysis, these techniques included classical strength analysis techniques such as those described in References 8 & 9, finite element techniques such as NASTRAN (References 4-7), and the NOVA-2 computer code. For the nuclear overpressure dynamic analysis, NOVA-2 was utilized exclusively.

7.2 Static Load Analysis

Analyses were accomplished for all test specimens to determine their respective response to uniform externally applied static load. These analyses were conducted to: 1) support test specimen sizing for desired strength properties and associated failure mechanisms; 2) to check out static response analysis techniques contained in NOVA-2; and 3) to indicate response characteristics of the test specimens as a function of load level, i.e., not simply to determine the critical static load level.

The analysis tools that were utilized in accomplishing the static analysis included classical strength analysis techniques, finite element techniques, and NOVA 2. These techniques will be discussed in more detail in subsequent sections of this report.

7.2.1 Classical Techniques

Classical stress analysis techniques were utilized where possible to size the test specimens. This sizing was accomplished to provide specimen strengths in the desired range. When classical techniques were not applicable, finite element techniques (discussed in Paragraph 7.2.2) or adaptations of classical techniques were employed. Classical techniques are defined as those techniques commonly found in recognized texts or handbooks on the subject of stress analysis and by such well-known authors as Roark and Sechler & Dunn. (See References 8 & 9).

For specimens one, two, and four, flat plate analytical methods from Roark (Reference 8) were utilized. For the boundary conditions of specimen three, no classical approach is known (see Paragraph 7.2.2). Specimen five was analyzed using the membrane analysis found in Sechler & Dunn (Reference 9). Specimen six was analyzed using the curved panel analysis found in Roark (Reference 8), although this analysis was only approximate because the true boundary conditions are not exemplified therein. Specimens seven and eight were originally sized using the standard approach of reducing the sandwich panels to a single-layered panel of equivalent thickness and analyzing as a thin plate using the Roark technique. However, this method was found to be inaccurate when compared to test results. Therefore, a special analysis was derived (see Volume II, page 355) which agreed very well with test results.

Specimens nine and ten behaved in accordance with classic beam analysis results. Specimens 11 and 12 were analyzed as rings in hoop compression, but these specimens did not entirely behave as such due to peculiarities in the boundary constraints. Specimen 13 was analyzed as a buckling - critical ring using the Roark technique. Specimens 14 through 17 required special analysis for yielding failure, since columns are usually considered to have failed at the onset of buckling, i.e., prior to yielding. However, the classic Euler formula for column buckling was found to be accurate for this mode of failure. See Volume II, page 646, for a more detailed description of column analysis for yielding failure.

A discussion of all specimen analyses and static tests results is given in more detail in Section 8.2.

7.2.2 Finite Element Techniques

The NASTRAN computer code was utilized in the static stress analysis of test specimens 11, 12 and 13 which are curved beam specimens. In addition to the static stress analysis, a buckling analysis of test specimen 13 and a vibration analysis of test specimen 11 were accomplished.

NASTRAN is documented extensively in References 4 through 7, and no attempt will be made here to reproduce these documents. Instead, what follows is a brief description of the NASTRAN computer code, highlighting some of its many capabilities.

NASTRAN (NAsa STRuctural ANalyzer) is a general purpose digital computer code designed to analyze the behavior of elastic structures under a range of loading conditions using a finite element displacement method approach.

The code is applicable to almost any type of linear and some nonlinear structures that can be represented by combinations of elements contained in the NASTRAN library, such as beams, rods, shear and twist panels, triangular and quadrilateral plates, conical and toroidal shells, solids of revolution, scalar elements, general elements, and constraint elements.

A wide range of analysis capability has been built into NASTRAN including static response to concentrated and distributed loads, to thermal expansion, and to enforced deformation; dynamic response to transient loads, to steady state sinusoidal loads, and to random excitation; determination of real and complex eigenvalues for use in vibration analysis, dynamic stability analysis, and elastic stability analysis. In addition, there is a limited capability for solving nonlinear problems including piecewise linear analysis of non-linear static response and transient analysis of nonlinear dynamic response.

7.2.3 NOVA-2

NOVA-2 (Reference 1) is a digital computer program that performs a complex analysis of structural elements subjected to nuclear overpressure effects. This code was developed by Kaman Avidyne, a division of Kaman Sciences Corporation, for the Analysis Branch of the Air Force Weapons Laboratory. This computer code is documented in detail in Reference 1, and no attempt will be made to reproduce that document in this report. Rather, the analysis techniques contained in the computer code and the capabilities of the computer code that are applicable to this study have been extracted directly from Reference 1 and summarized in this report.

The NOVA-2 code provides a technique for predicting the elastic and inelastic response of structural elements to the transient pressure loads associated with the blast wave from a nuclear explosion as well as uniform static preblast pressure loads. The high intensity blast pressure loads are associated with the initial reflected pressure which occurs during diffraction of the blast wave around the structure. Because the pressures exist for such a short time, they excite high frequency, secondary structure such as skin panels, stringers, longerons, frames, ribs, canopies, and radomes.

A single element dynamic analysis technique, which considers both linear elastic and inelastic deformations and assumes that the element does not interact with adjacent elements, reduces the complexity of the modeling and analysis, and thus provides a solution more rapidly than a finite element analysis. A 1 KT nuclear standard, based on data obtained from the AFWL SPUTTER and SAP fluid dynamics programs, provides the time dependent free-air blast characteristics for the BLAST routines. The program consists of three distinct routines, NOVA, DEPROB (Dynamic Elastic Plastic Response of Beams), and DEPROP (Dynamic Elastic Plastic Response of Panels), written in Fortran IV. The NOVA routine is the master routine which controls the logic of the overall program. It contains the subroutines for predicting the blast pressure environment.

8.0 RESULTS

8.1 General Discussion

Results from this study fall into four general categories: static test, static analysis, shock load test, and shock load analysis. Test results are compared to analysis results in Sections 8.2 - 8.5. Results from the static test and the shock load test are compared in Section 8.6. In addition, shock load analysis results associated with a sensitivity study are presented in Section 8.7. Only data from critical locations are shown in the figures in this section.

8.2 Static Load Test/Analysis

In reviewing the following results, the reader should bear in mind that all static loads were applied as a uniform pressure differential acting from outward to inward on the test fixture except, of course, the column specimens. As mentioned in paragraph 6.1, the column specimens were loaded by lead shot. All loads were applied gradually in increments, and data were recorded at each increment. All specimens, except the columns, were analyzed for stress and deflection under load using the NOVA-2 computer code and either a classical method of analysis or a finite element method of analysis. NOVA-2 is not designed to analyze columns for stress or deflection under static load. Comparisons of significant test and analysis results are shown in the accompanying figures for each specimen. Static test photographs and static test recorded data are shown in Volume II.

All analyses were conducted utilizing the modulus of elasticity and yield strength established by coupon tests of the material from which the specimen was made - except the column specimens, which were expected to conform to MIL-HDBK-5 (Reference 12) values for 7075-T6 aluminum alloy. The analyses also utilized actual specimen measured geometry (thickness, area, etc.) to establish the correct section properties.

To determine the effect of modal retention set on the structural responses of the panel test specimens under static load, a limited convergence study was conducted utilizing the NOVA-2 computer program. The retention sets studied are shown in Table VIII, and the results of the convergence study are illustrated in Tables IX and X.

TABLE VIII
RETENTION SET CONFIGURATION

Retention Set	MG	MB	Modes Deleted	Modes Retained
1	3	3	None	9
2	4	4	None	16
3	5	5	10	15
4	6	6	17	19

TABLE IX
CONVERGENCE STUDY RESULTS - STRESS/DISPLACEMENT

Retention Set	Maximum Stress (psi)	Maximum Displacement (in)
1	7635	.0845
2	7847	.0841
3	7992	.0843
4	8060	.0842

TABLE X
CONVERGENCE STUDY RESULTS - RETENTION SET DIFFERENCES

From Retention Set	To Retention Set	% Change In Maximum Stress
1	2	2.8
2	3	1.9
3	4	0.9

Based on the convergence study results, modal retention set 3 was utilized for all panels (except test specimens 5 and 6) in conducting the NOVA-2 static analysis. Due to the large stress gradients that occur at the boundaries of test specimen 5 because of its thin gauge and due to the curvature of test specimen 6, a larger modal retention set was required. This is discussed more fully in subsequent sections of this report.

8.2.1 Test Specimen Number One

Specimen number 1 is categorized as a thin plate (span/thickness = 115) with fixed edges. With regard to stress, test and analytical results agree very well as shown in Figure 19. The results predict static failure at approximately 14 psi. A small discrepancy (approximately 11 percent) exists between test and analysis with regard to deflection as shown in Figure 20. This discrepancy can be explained by the fact that a pure "thin plate" does not exist. Thin plates are simply transitions between membranes and thick plates or vice versa. In this case, the results simply indicate that the panel was deflecting somewhat more like a "thick plate" than the analysis, using Reference 8 methods, was able to predict.

STRESS VS. PRESSURE GAUGE S1-3, SPECIMEN NO. 1

○ TEST DATA

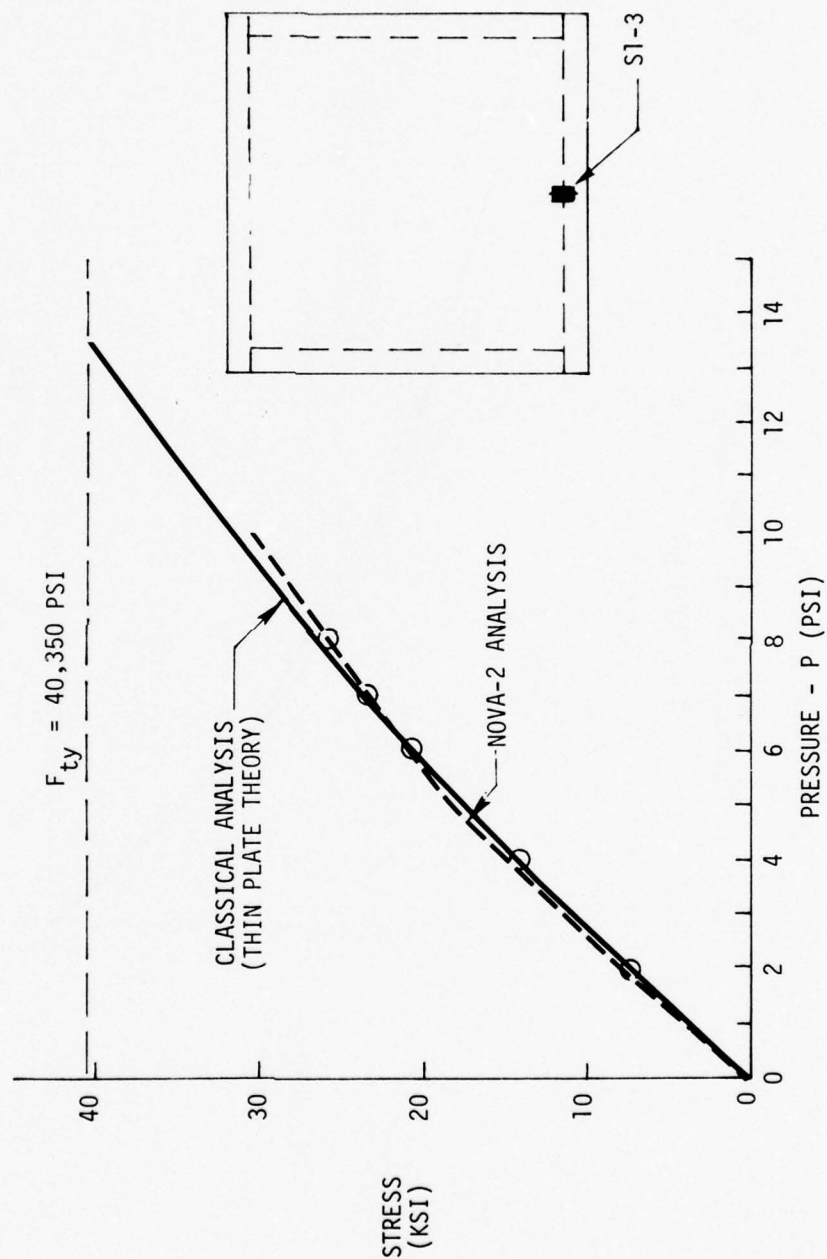


FIGURE 19.

DEFLECTION VS. PRESSURE

SPECIMEN NO. 1

○ TEST DATA

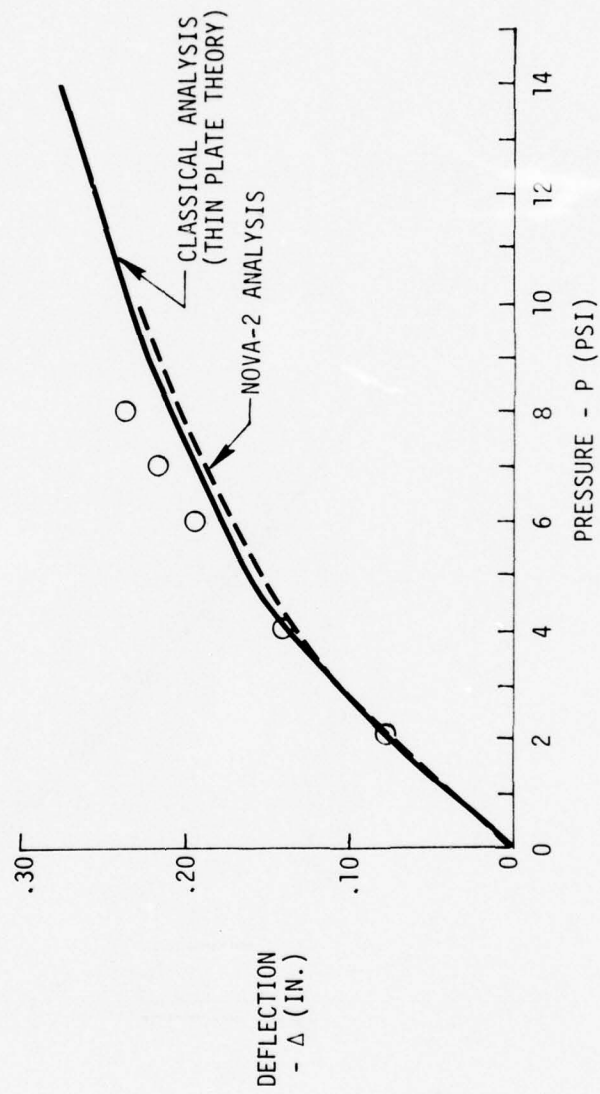


FIGURE 20.

8.2.2 Test Specimen Number Two

Specimen number 2 is categorized as a thin plate with pinned edges. Test and analytical results agree very well with regard to stress. The rationale used for specimen number 1 with regard to deflection applies here, also. However, the nature of the hinge configuration affects the displacement at the panel center. The offset (approximately 0.25 inches) between the hinge centerline and the panel elastic axis allows the panel edges to move toward the panel center, allowing the panel center to displace more in a direction perpendicular to its plane. Figures 21 and 22 indicate that NOVA-2 and classical analysis results are in good agreement with each other.

8.2.3 Test Specimen Number Three

Specimen number 3 is also categorized as a thin plate; however, the boundary conditions here are two opposing sides pinned and the other two opposing sides fixed. These boundary conditions cannot be analyzed using classical methods, and were, therefore, analyzed using a finite element computer program. The finite element method was very conservative in its prediction of stress vs. pressure and did reasonably well in its prediction of deflection vs. pressure. The rationale discussed above in Section 8.2.2 regarding the effect of the hinge offset from the elastic axis applies here also but to a lesser degree since only two sides are pinned. Figures 23 and 24 indicate that NOVA-2 predicted stress more accurately than displacement.

8.2.4 Test Specimen Number Four

Specimen Number 4 is a thick plate (span/thickness = 71) with fixed edges. This panel responded to load in a linear fashion as was predicted. A small discrepancy (approximately 9 percent) exists between test and analytical results with respect to stress. This plate is borderline between thick plate and thin plate - a fact that is assumed to account for the discrepancy between test and analytical results with respect to deflection. As shown in Figures 25 and 26, NOVA-2 and classical analysis methods agree very well with regard to both stress and deflection.

8.2.5 Test Specimen Number Five

Specimen number 5 is a membrane (span/thickness = 1100) with fixed edges. Test stresses at the center of the fixed edges were considerably higher than were predicted. This phenomenon is commonplace in membrane structures because of the substantial bending of the material over the supports that takes place. This phenomenon has little effect on the panel overall strength since, once the local yielding has occurred, the panel will behave as a membrane. It should be noted that neither the classical analysis nor the NOVA-2 analysis accurately predicted the stresses at the fixed edges as shown in Figures 27 and 28. Some improvement was noted in the NOVA-2 analysis results when 25 modes were retained instead of 15 modes. However, additional analysis of this specimen with more than 25 modes retained did not alter the response data significantly. Stress and displacement at the center of the panel were predicted quite accurately as shown in Figures 28 and 29.

STRESS VS. PRESSURE
GAUGE S2-2, SPECIMEN NO. 2
○ TEST DATA

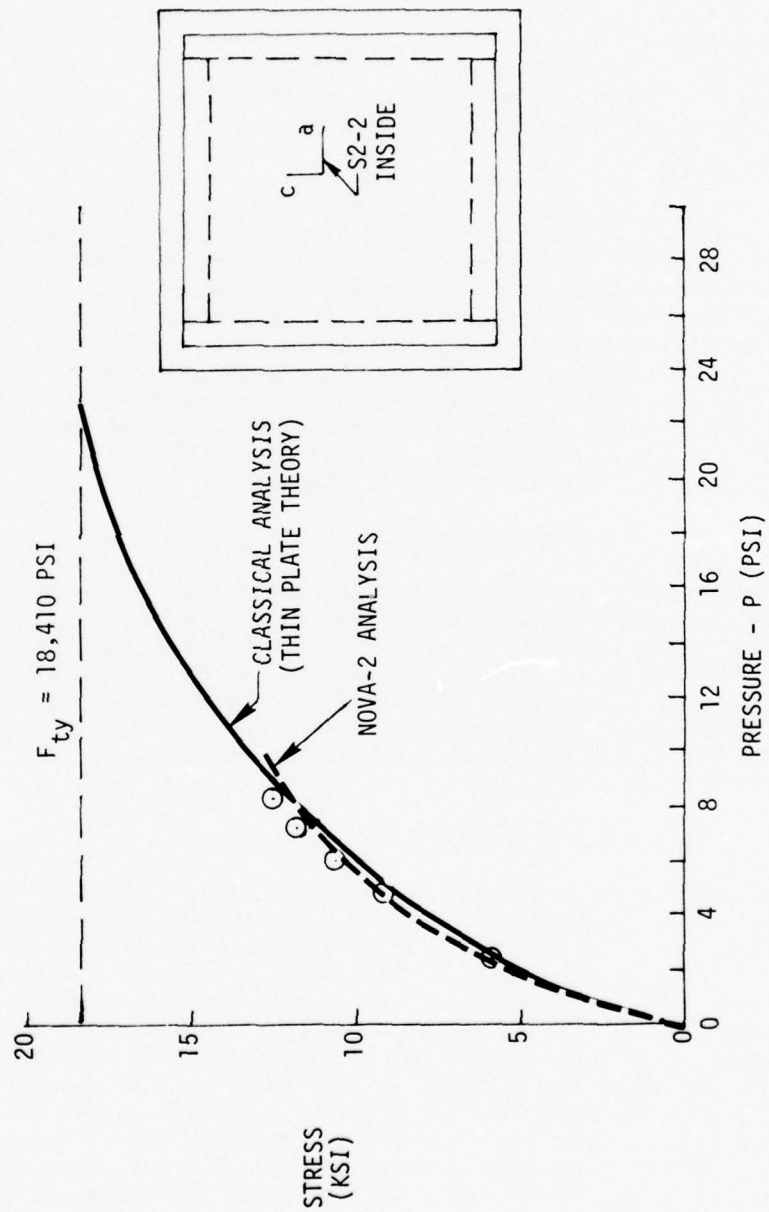


FIGURE 21.

DEFLECTION VS. PRESSURE

SPECIMEN NO. 2

○ TEST DATA

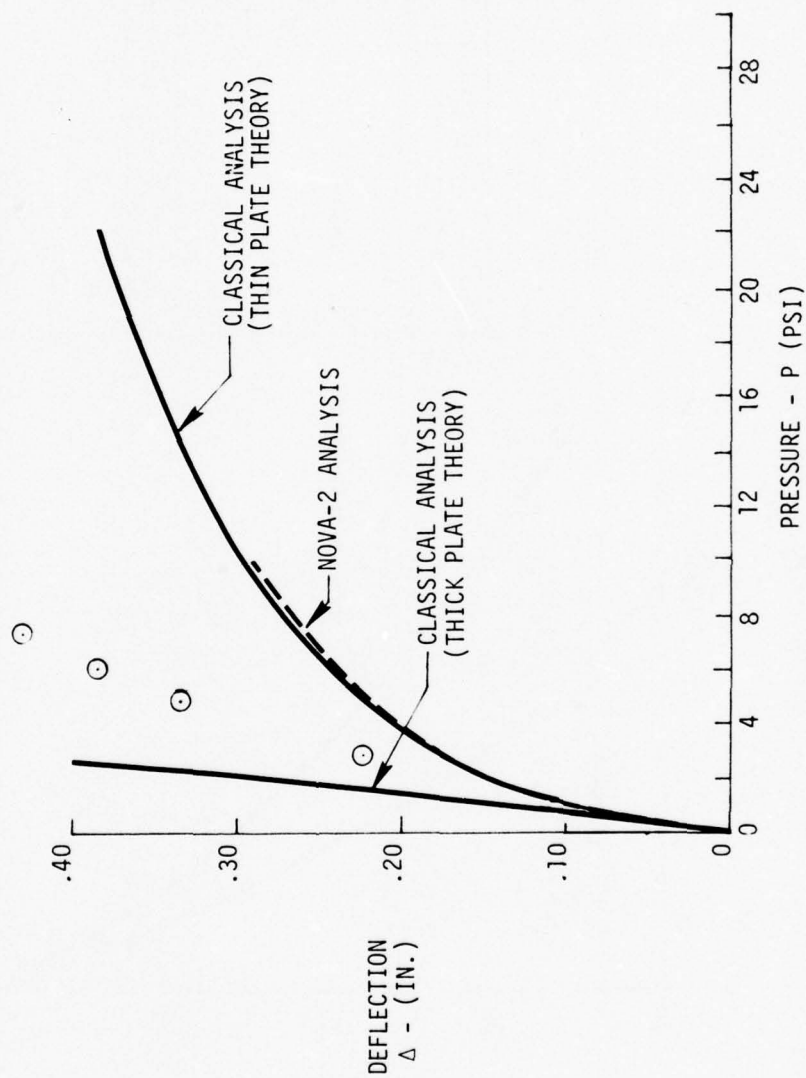


FIGURE 22.

STRESS VS. PRESSURE GAUGE S3-4 SPECIMEN NO. 3

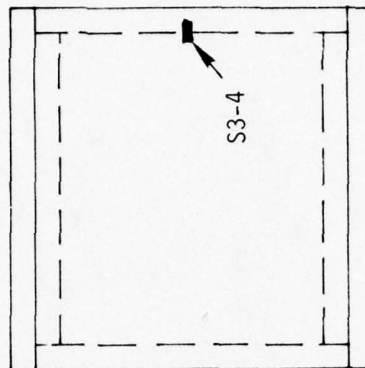
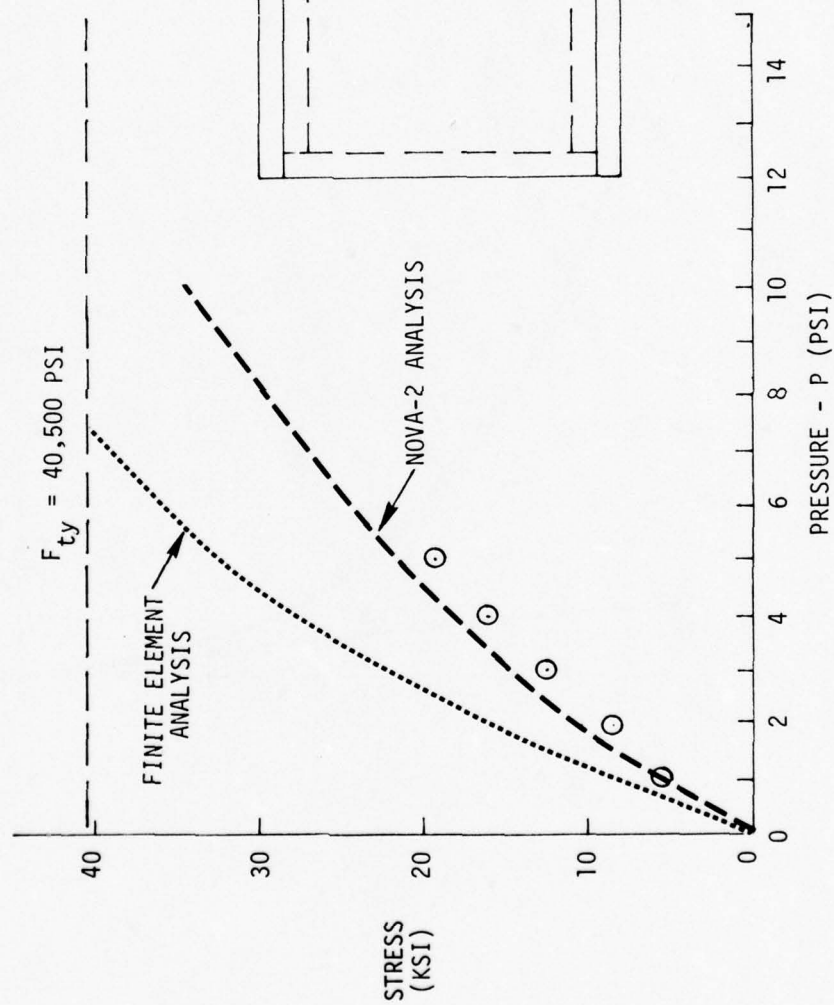


FIGURE 23.

DEFLECTION VS. PRESSURE SPECIMEN NO. 3

○ TEST DATA

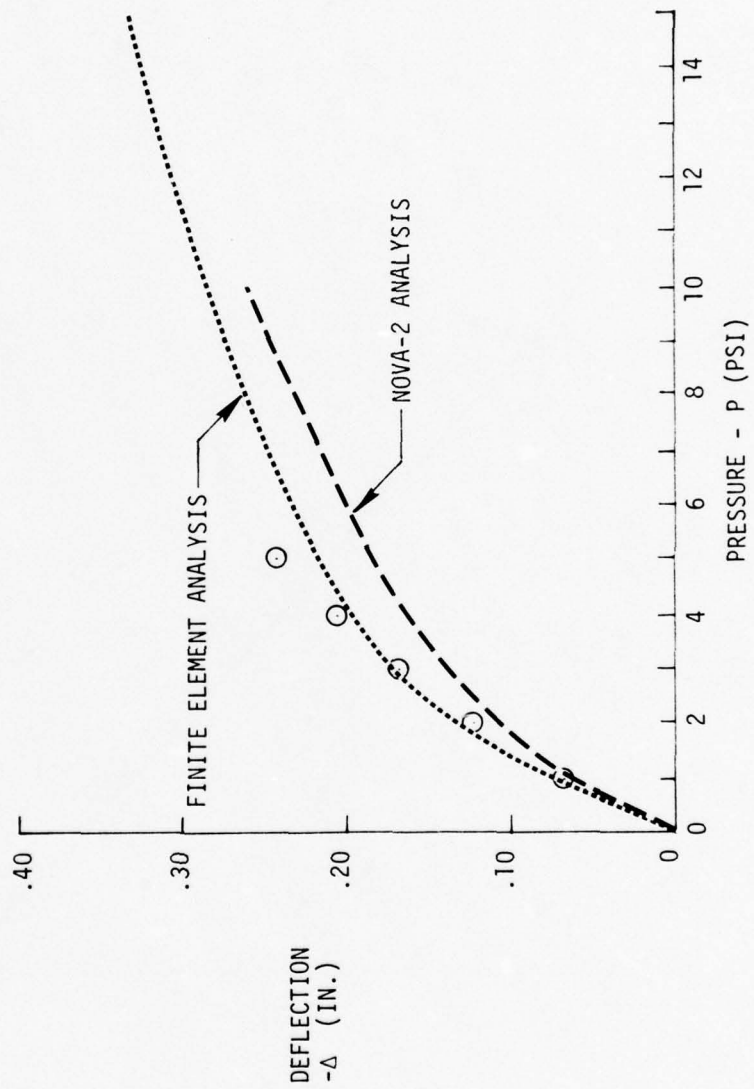


FIGURE 24.

STRESS VS. PRESSURE
GAUGE S4-3 SPECIMEN NO. 4
○ TEST DATA

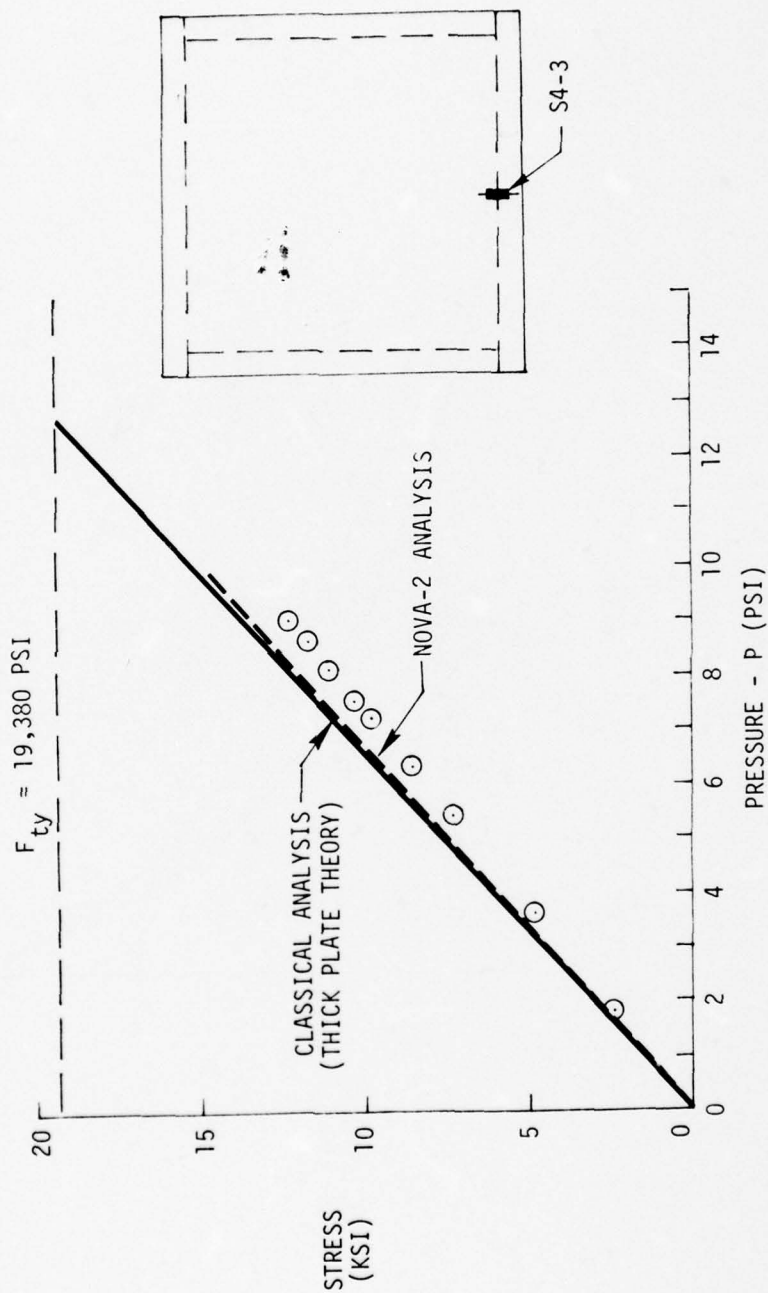


FIGURE 25

DEFLECTION VS. PRESSURE

SPECIMEN NO. 4

○ TEST DATA

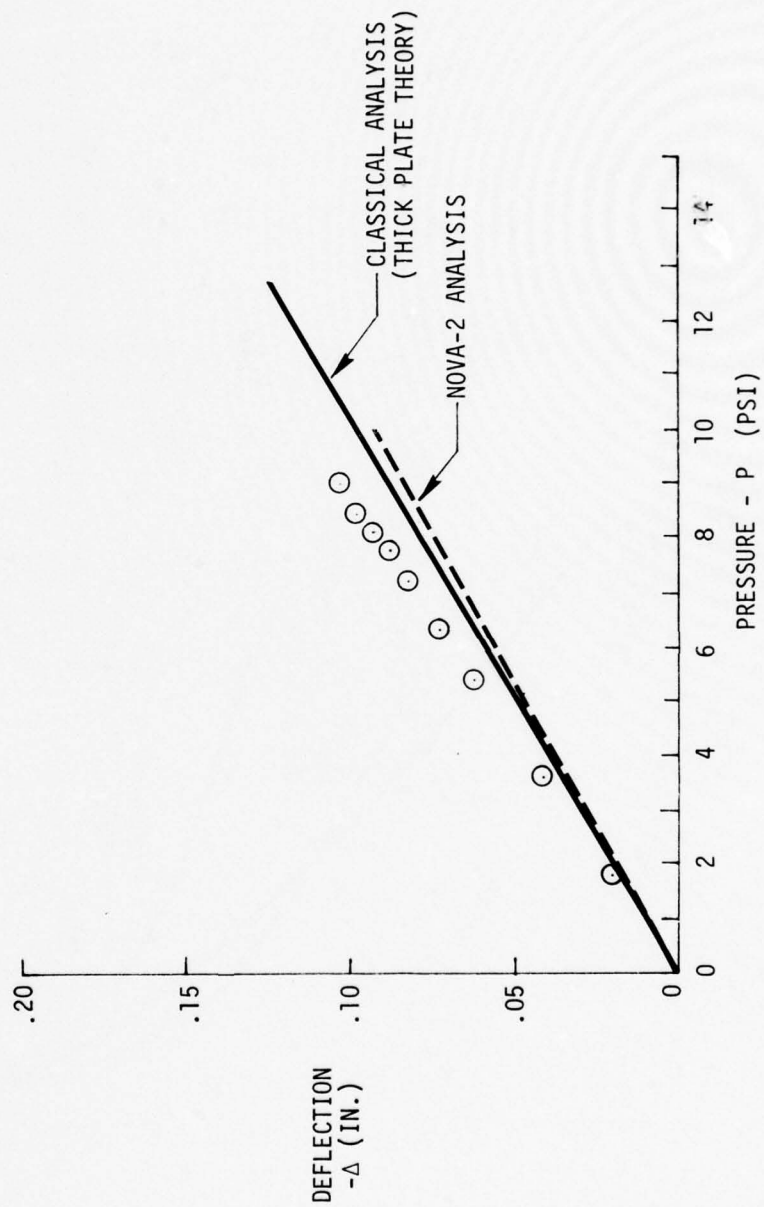


FIGURE 26

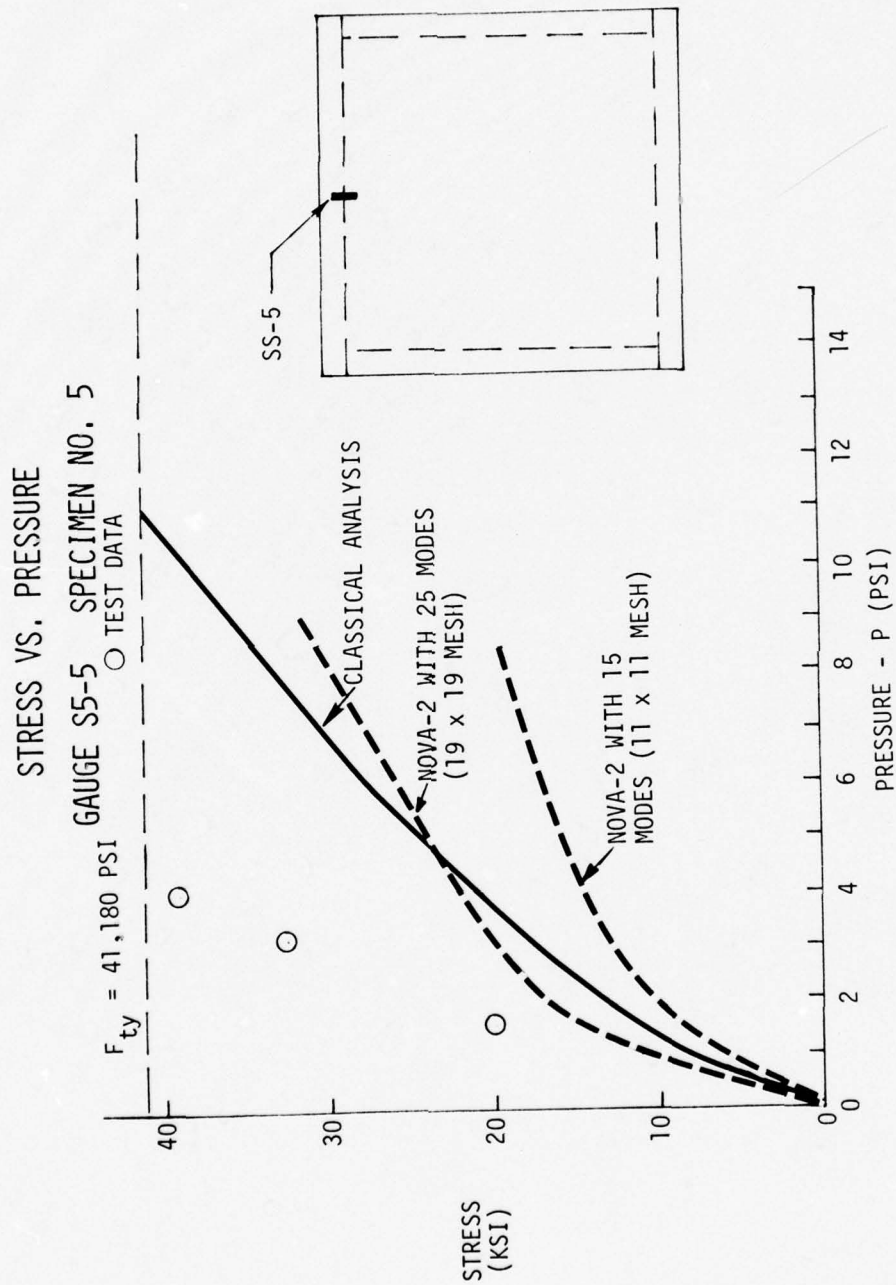


FIGURE 27

DEFLECTION VS. PRESSURE
SPECIMEN NO. 5

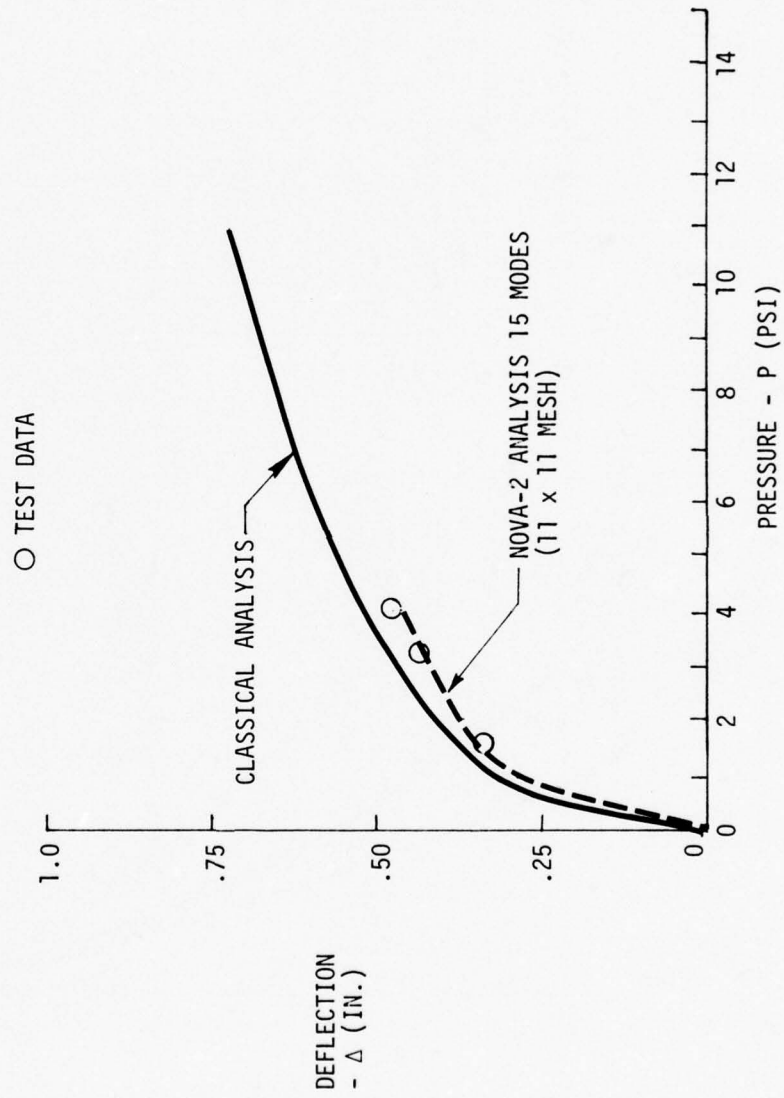


FIGURE 28

STRESS VS. PRESSURE GAUGE S5-2 SPECIMEN NO. 5

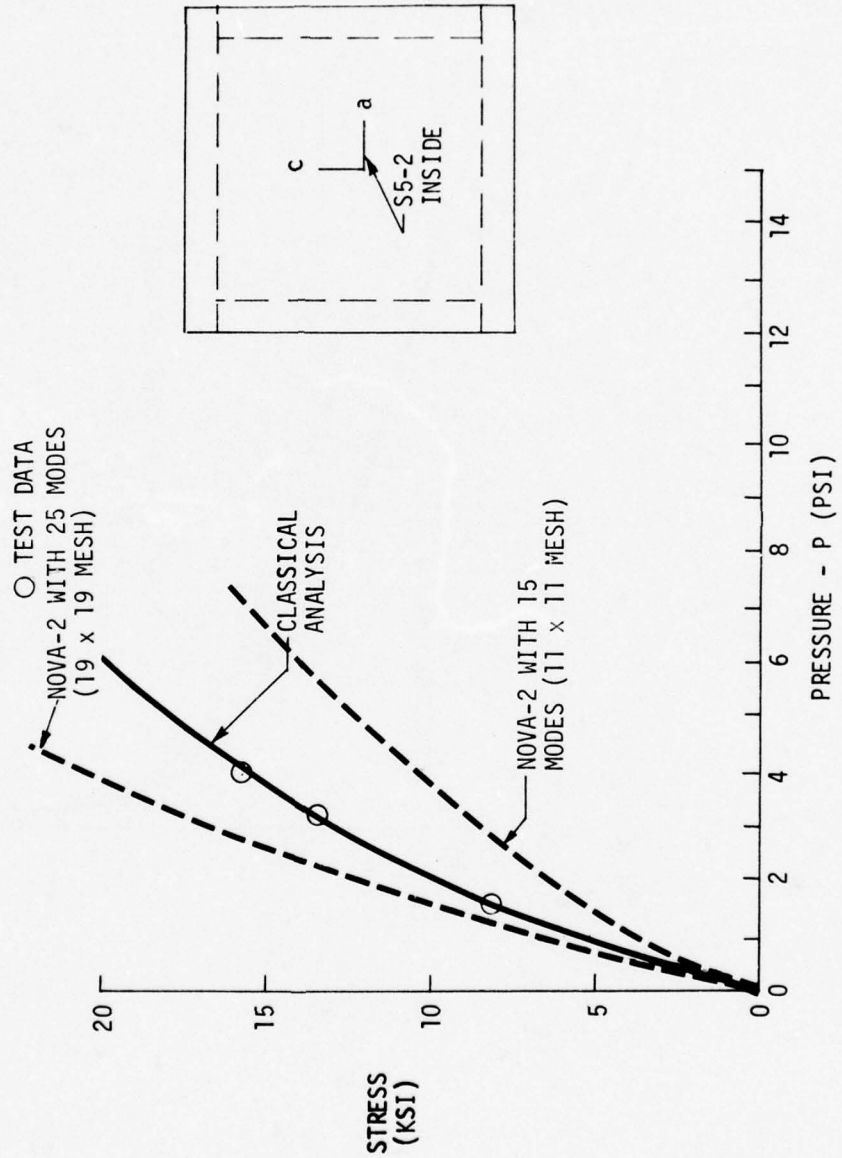


FIGURE 29

8.2.6 Test Specimen Number Six

Specimen six is a homogeneous cylindrical panel subtending an arc of 54.56 degrees. With the panel subjected to a uniform external pressure, the critical principal stress was recorded at the center of the panel. This stress increased considerably faster than was predicted by analysis as shown in Figure 30. The analysis results were obtained by including 15 modes in the analysis model and assuming that initial imperfections were not present in the specimen. Subsequent to the static test, Kaman AviDyne performed a sensitivity study regarding test specimen six. The results of this study are shown in Figure 31. These data were obtained by including 32 modes in the NOVA-2 model (from an 8 x 8 modal matrix. In addition, initial radial imperfections as shown were included in the analysis. Since no measurements were made of initial imperfections prior to static testing, it is difficult to say whether the initial imperfections included in the model accurately describe the actual specimen. As noted in Figure 31, however, there is excellent agreement between the revised analysis results and the test result.

8.2.7 Test Specimen Number Seven

Specimen number 7 is a honeycomb sandwich panel consisting of two - .0135 in. thick 5052-0 skins bonded to a MIL-C-7438 6.5-3/8-50 5052-0 aluminum honeycomb core that is .306 inches thick.

The NOVA-2 analysis treated this specimen as a multilayered panel. The results illustrated in Figures 32 and 33 show the excellent agreement between the test data and the NOVA-2 analysis data.

In addition to the NOVA-2 analysis, specimen 7 was also analyzed by classical methods. Initially, specimen seven was treated as a homogeneous thin plate of some equivalent thickness in accordance with the classical approach. When the test stresses were observed to be much higher than were predicted (see Figure 32), the panel was re-analyzed and modeled as a thick plate influenced by two membranes, i.e., the face sheets. This analysis approach results in stresses that agree very well with the test data and the NOVA-2 data.

8.2.8 Test Specimen Number Eight

Specimen number 8 is also a honeycomb sandwich panel very similar to specimen number 7. The fundamental difference between them is the core cell size. Specimen number 7 has a 3/8 inch cell size and specimen number 8 has a 1/8 inch cell size. These cell sizes were selected in order to evaluate the difference in panel strength as affected by the core and to determine if intra-cell buckling could be manifested with a corresponding relative effect on panel strength. The core for this specimen is a MIL-C-7438 8.1-1/8-20 5052-0 aluminum core that is .292 inches thick. The inner skin was .014 inches thick, and the outer skin was .013 inches thick.

No intra-cell buckling was evident on either specimen 7 or 8. As shown in Figures 34 and 35, specimen 8 exhibited somewhat lower response than specimen 7, which fact could be attributed to its more dense core.

STRESS VS. PRESSURE
GAUGE S6-1 SPECIMEN NO. 6

○ TEST DATA

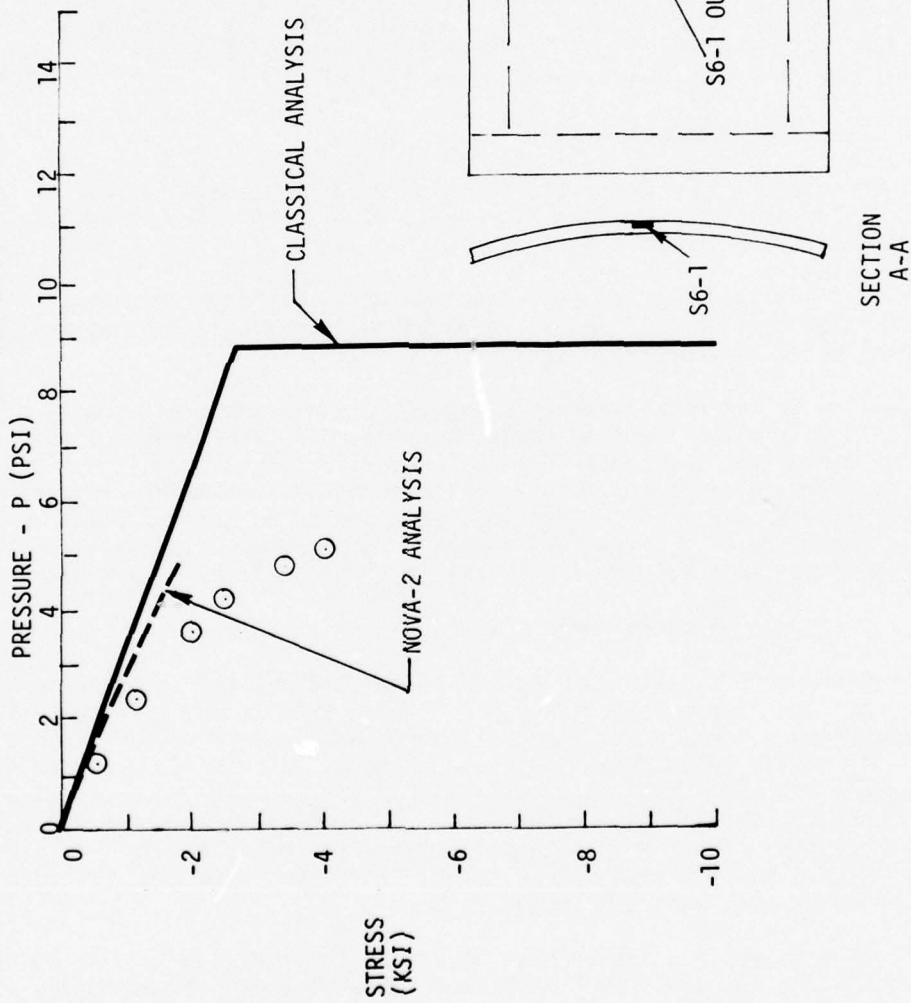


FIGURE 30

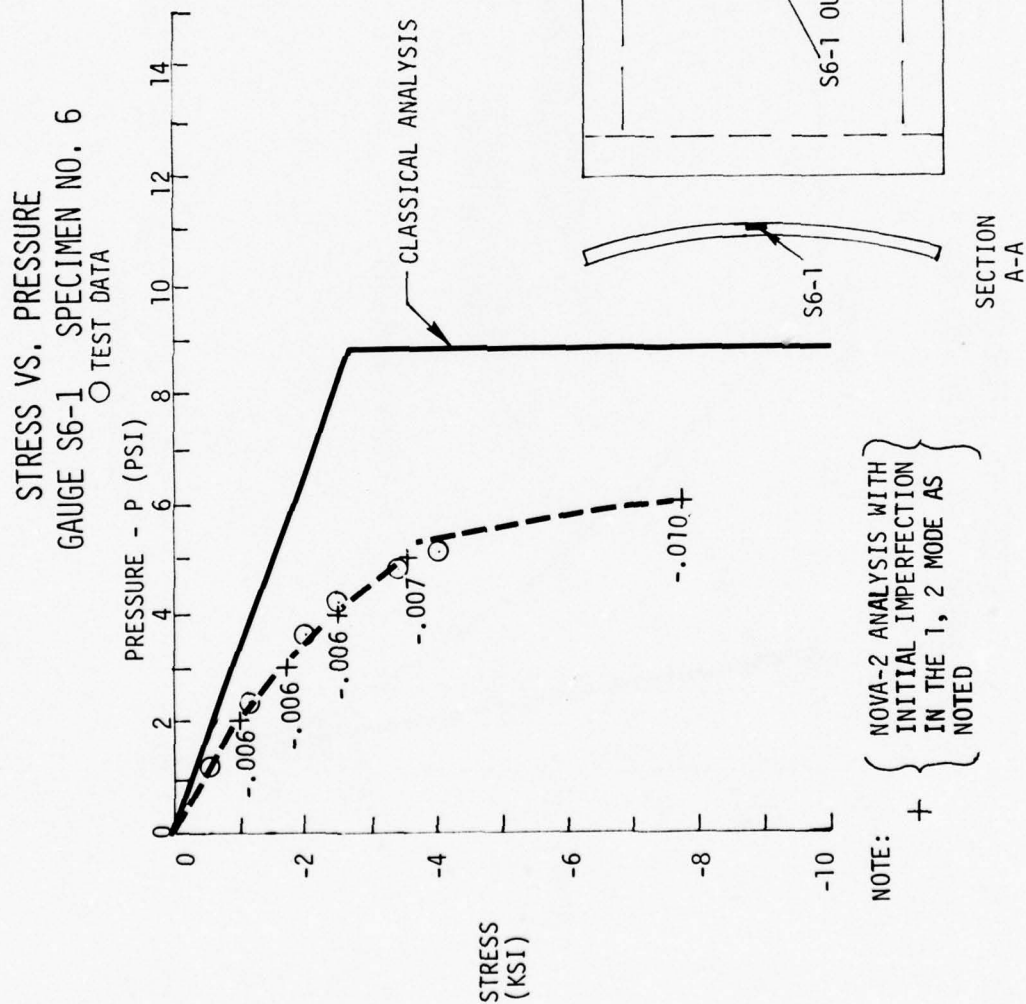


FIGURE 31

STRESS VS. PRESSURE
GAUGE S7-2 SPECIMEN NO. 7
○ TEST DATA

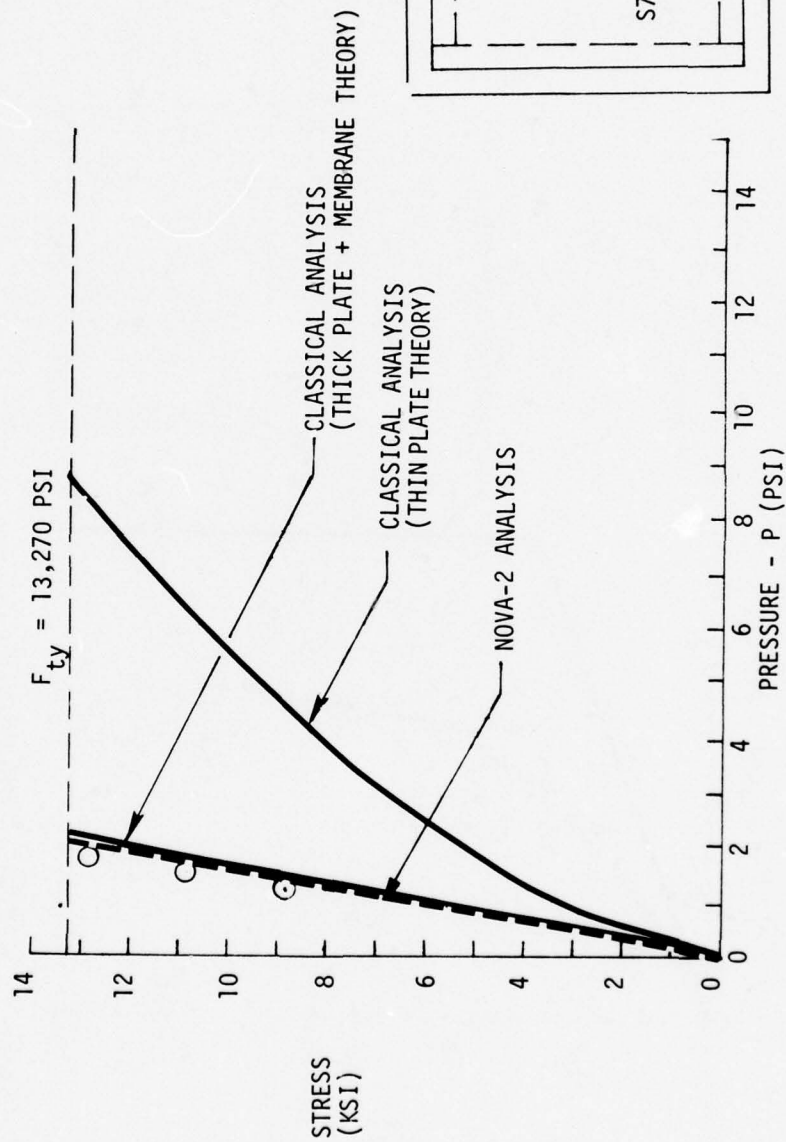


FIGURE 32

DEFLECTION VS. PRESSURE
SPECIMEN NO. 7
○ TEST DATA

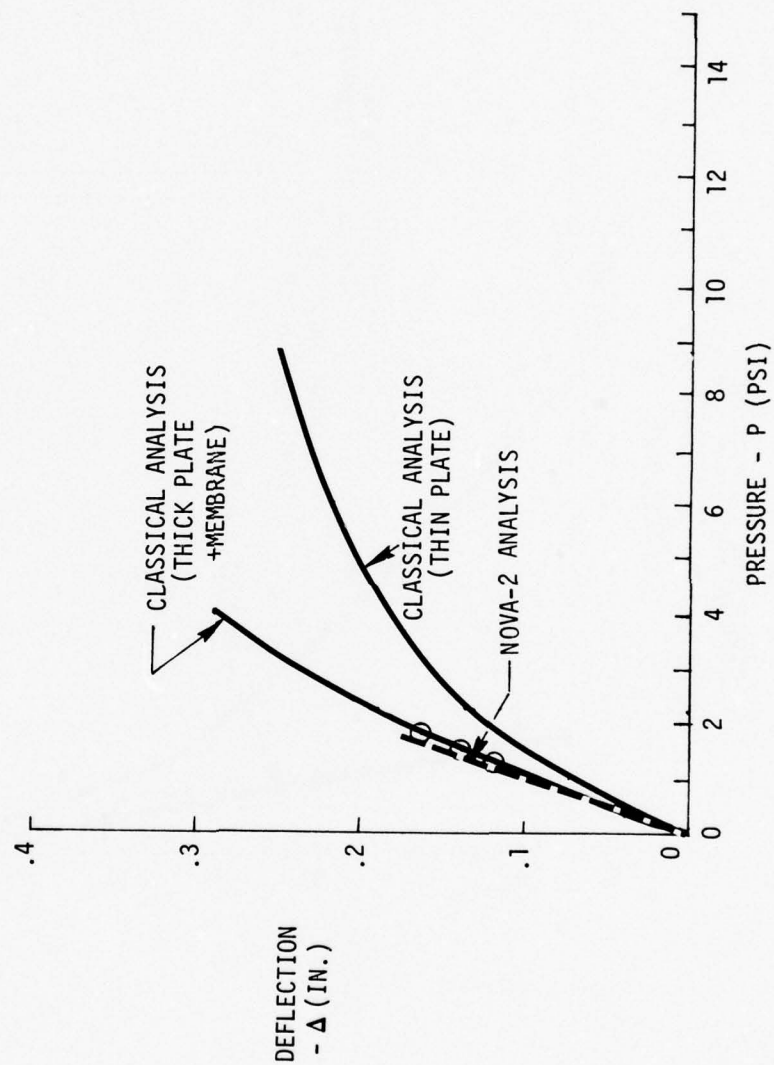


FIGURE 33

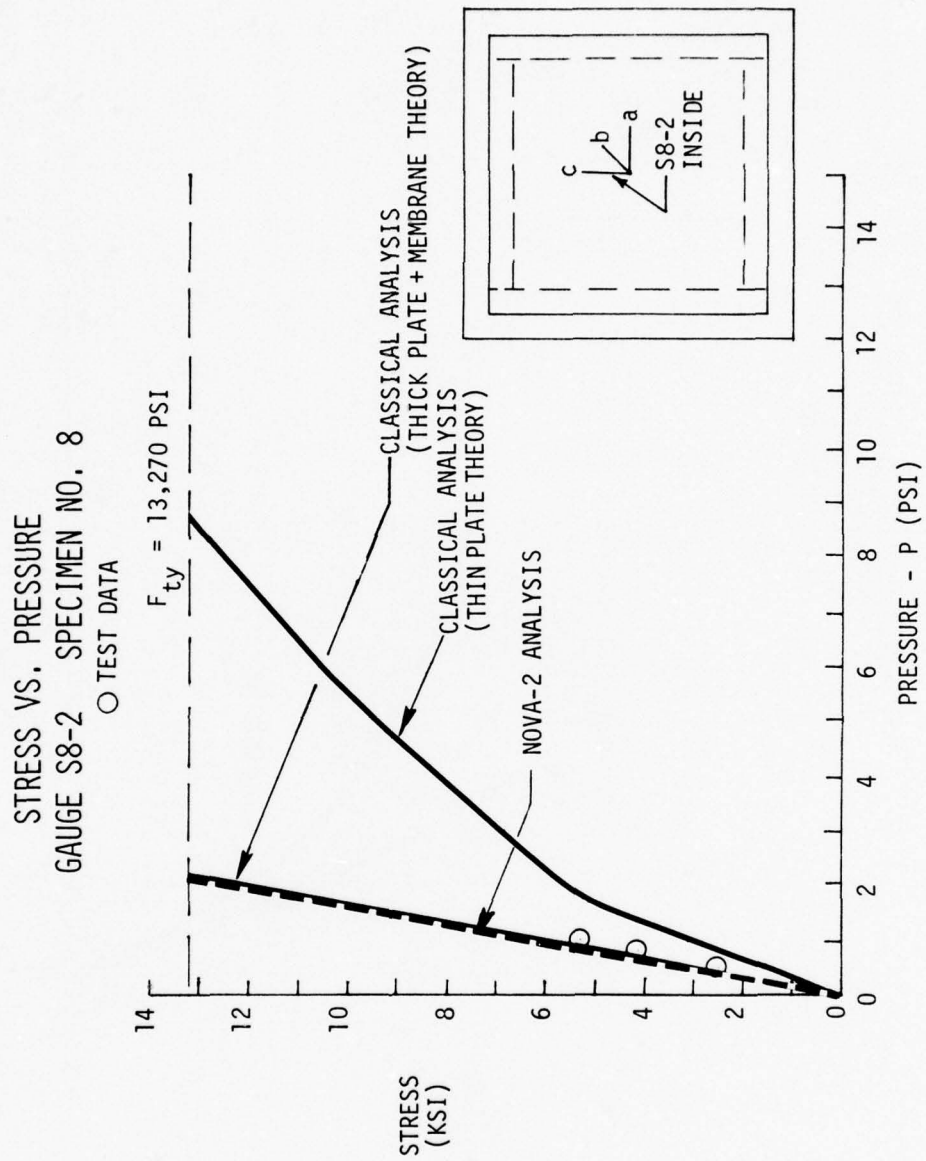


FIGURE 34

DEFLECTION VS. PRESSURE
SPECIMEN NO. 8

○ TEST DATA

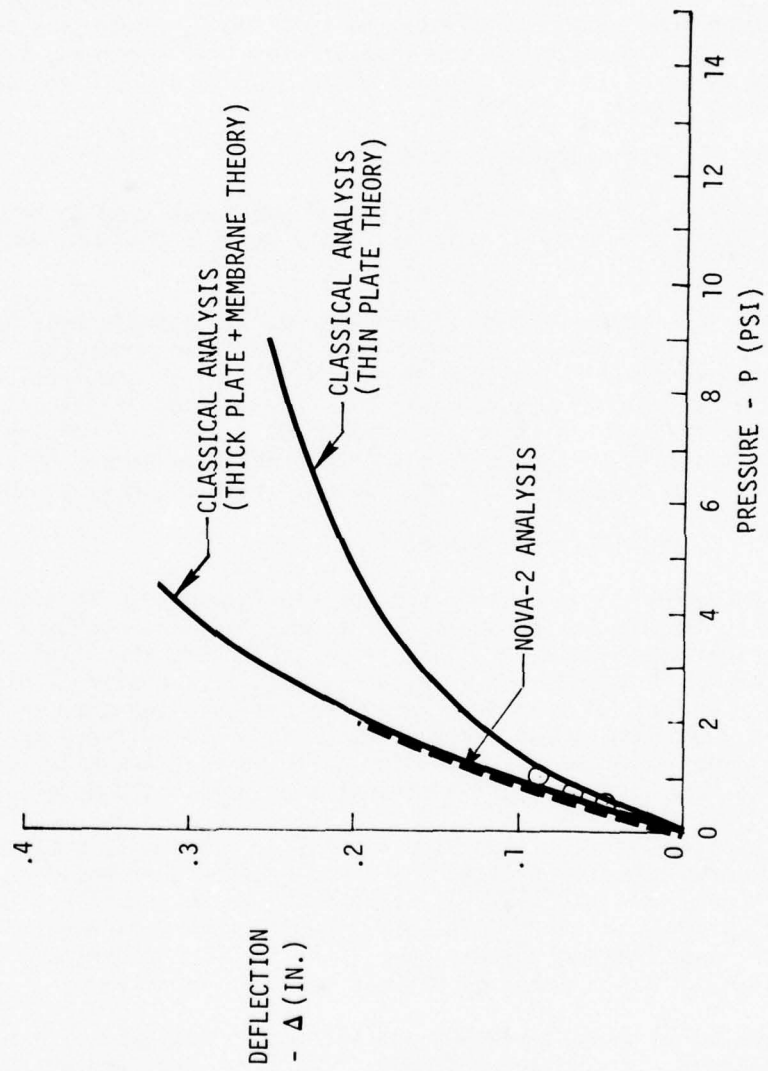


FIGURE 35

8.2.9 Test Specimen Number 9

This specimen is a flat, stiffened panel. The stiffeners are extruded aluminum zee-sections machined to the desired dimensions. Although the specimen is a panel, the skin exists for the sole purpose of distributing the applied pressure load to the stiffeners which were evaluated as simple beams with fixed ends. Figures 36 and 37 illustrate the excellent agreement between test and analysis stresses. The differences between test and analysis displacements shown in Figure 38 is attributed to lack of an absolutely rigid foundation. This has a more pronounced effect on displacement of the specimen than on stress. Subsequent to the completion of the analysis for this specimen, Kaman AviDyne discovered an error in NOVA-2 for beams at high strains. The result of the program revision is shown in Figure 36.

8.2.10 Test Specimen Number 10

This specimen is also a flat, stiffened panel designed to permit evaluation of the stiffeners as beams. However, these beams are pinned at the ends rather than fixed.

As shown in Figure 39, some discrepancy exists between test and analysis stresses. Since the test stresses are lower than predicted, it is concluded that the amount of skin assumed to be effective in compression may have been inaccurate. This is understandable as the methods of selecting this amount of effective skin are designed, and expected, to be conservative. Also, some imperfections in the boundary conditions may have served to reduce the stresses, i.e., the boundary condition may not have been a purely pinned condition.

8.2.11 Test Specimen Number 11

Specimen number 11 is a stiffened, partial cylinder. To avoid the effects of eccentric loading on the beams/stiffeners, they are machined I-sections of symmetrical cross-section. These beam/stiffeners are fixed on the ends. As on specimens 9 and 10, the skin serves only as a device to distribute the pressure to the stiffeners. The stiffeners have the same cross-section as those on specimen number twelve, which is a full cylinder specimen of the same radius (24 inches). This similarity in configuration was deliberate in order to compare the relative strengths of full and partial cylinders.

The classical method of analysis assumes no bending of a circular arch under uniform pressure and analyzes the structure for pure hoop compression. As can be seen in Figure 41, this is somewhat unconservative. Hard mounting or fixing the ends of the stiffness does not permit uniform displacement, and as a result some bending takes place. This bending is contrary to the assumption resulting in the discrepancy between test and the classical analysis results.

Computer codes such as NASTRAN and NOVA-2 can evaluate effects of non-uniform displacements on stresses and were, therefore, employed in the analysis. The results of these analyses are conservative as can also be seen in Figure 41. It should be noted that the NASTRAN and NOVA-2 results agree reasonably well. Since the skins were bonded to the frames with a correspondingly low shear transfer (rather than riveted), the results of analyses assuming both effective and non-effective skins are presented in the chart for comparison.

STRESS VS. PRESSURE
GAUGE S9-5 SPECIMEN NO. 9
○ TEST DATA

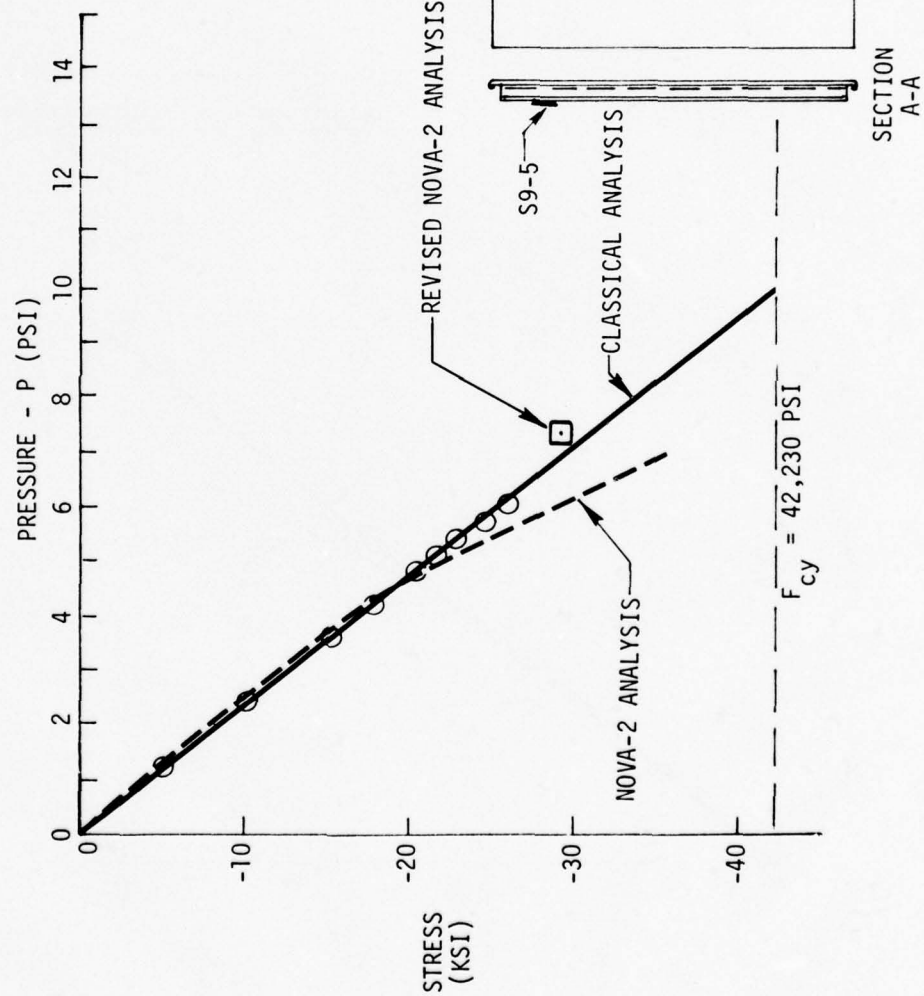


FIGURE 36

STRESS VS. PRESSURE
GAUGE S9-7 SPECIMEN NO. 9
○ TEST DATA

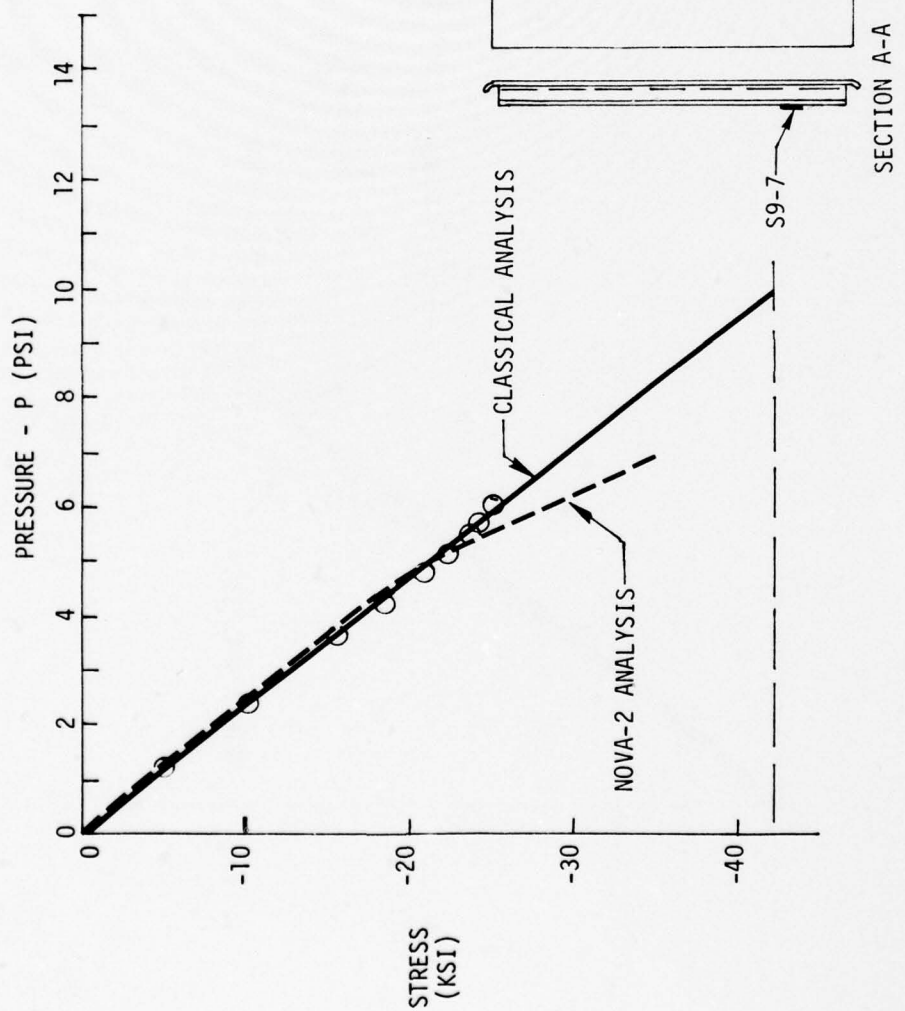
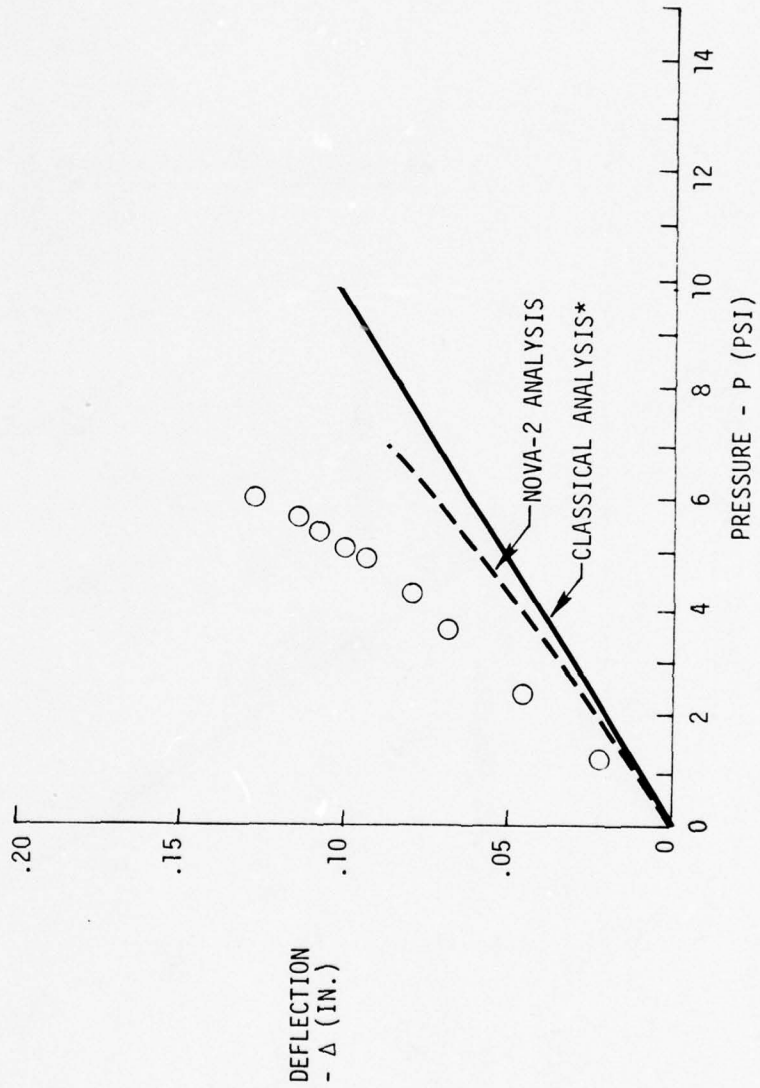


FIGURE 37

DEFLECTION VS. PRESSURE
SPECIMEN NO. 9

○ TEST DATA



*ASSUMES AN ABSOLUTELY RIGID FOUNDATION

FIGURE 38

STRESS VS. PRESSURE
GAUGE S10-6 SPECIMEN NO. 10

○ TEST DATA

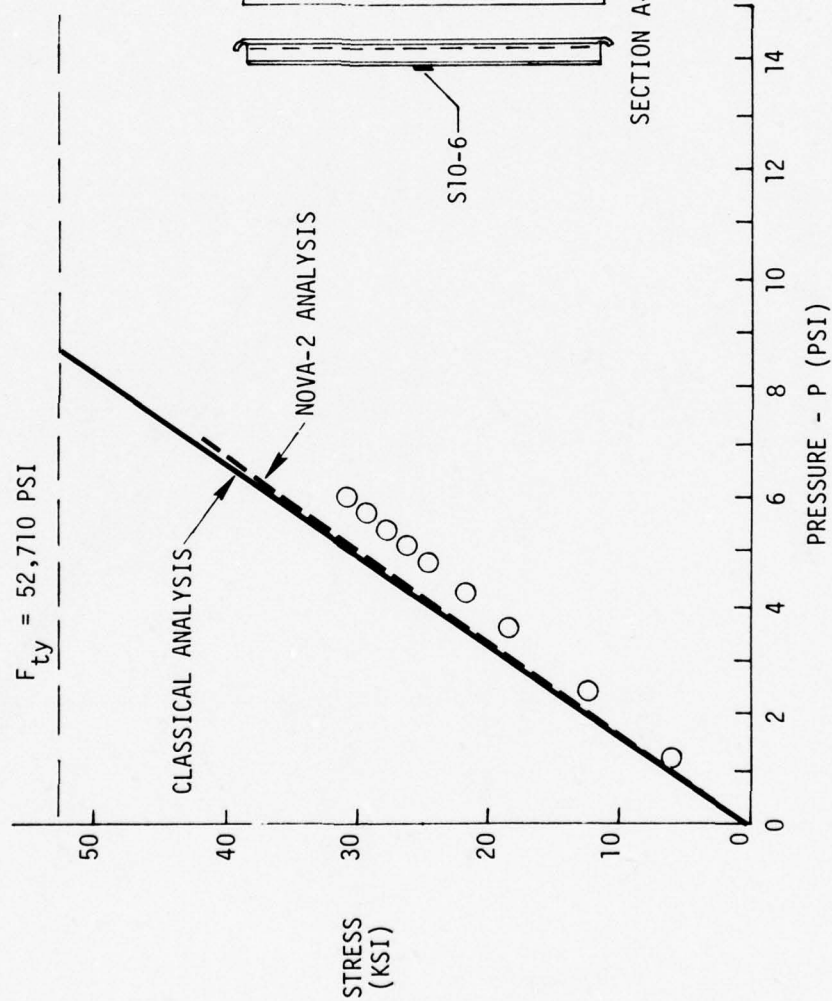


FIGURE 39

DEFLECTION VS. PRESSURE SPECIMEN NO. 10

○ TEST DATA

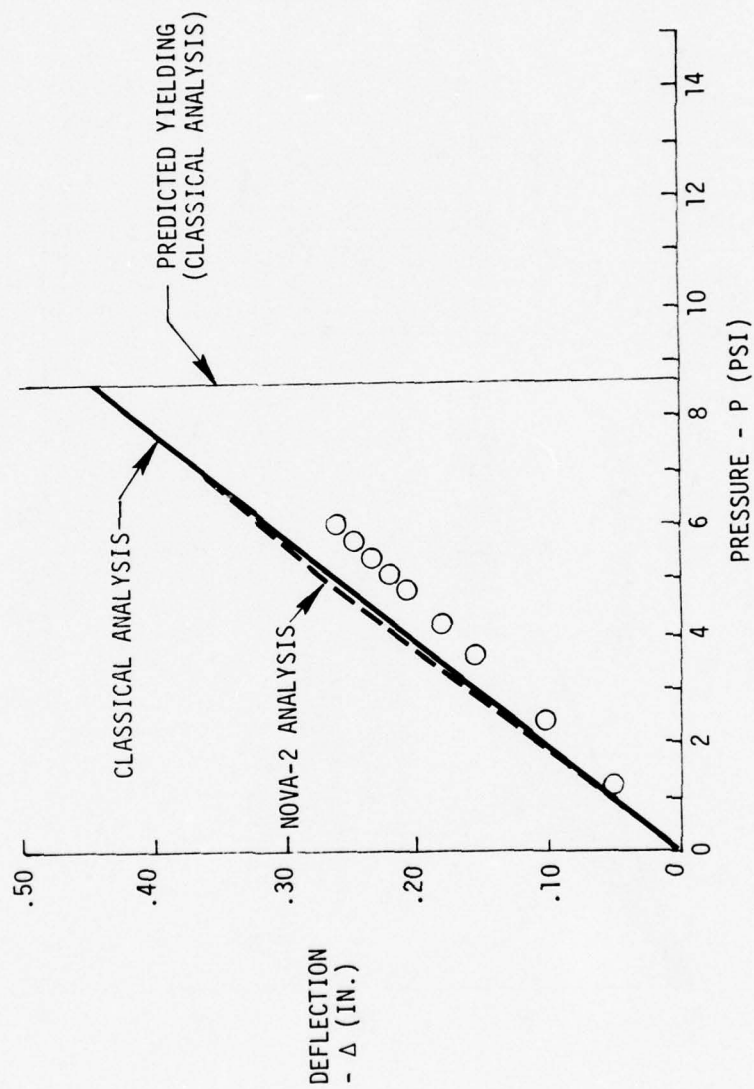


FIGURE 40

STRESS VS. PRESSURE
GAUGE S11-5 SPECIMEN NO. 11
○ TEST DATA

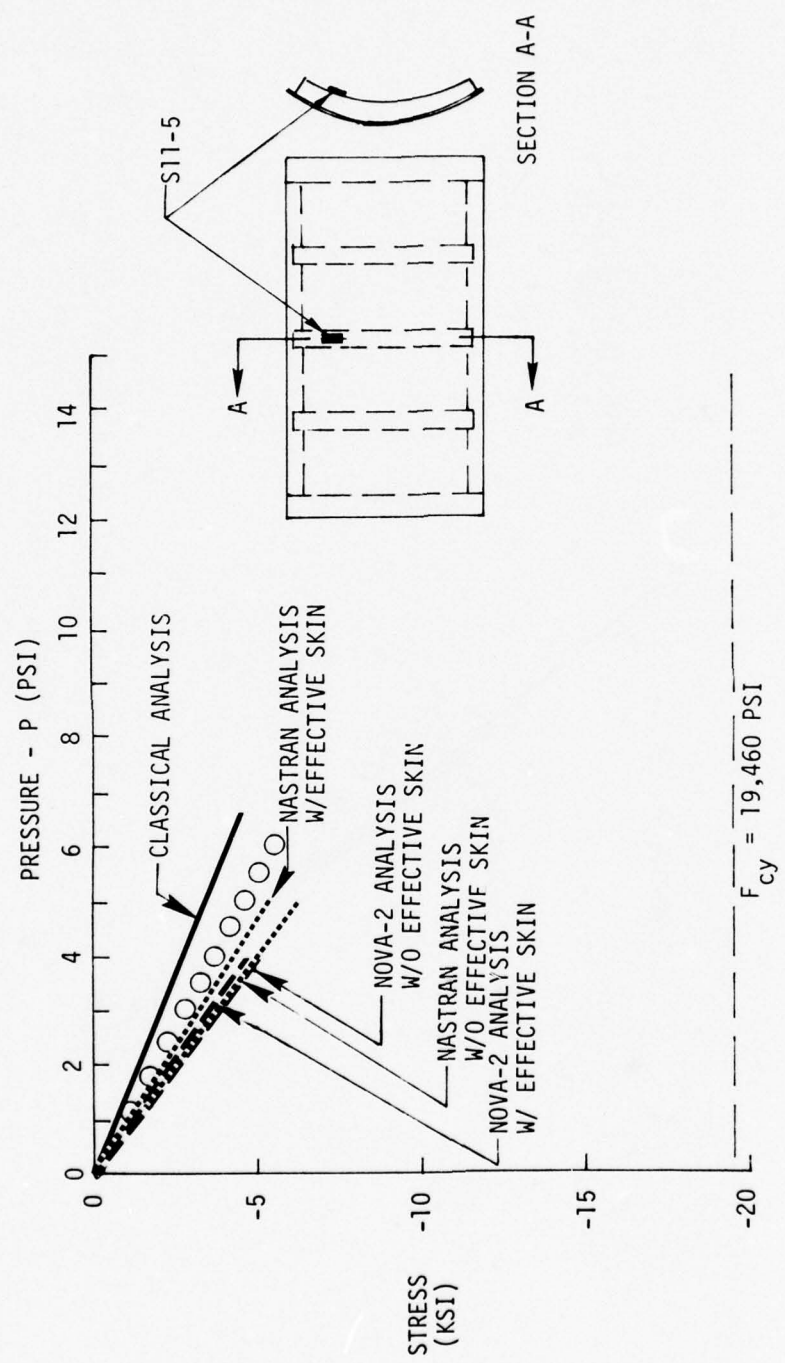


FIGURE 41

8.2.12 Test Specimen Number 12

As mentioned in Section 8.2.11, this specimen is a stiffened, full cylinder with stiffeners/frames that have the same symmetrical cross-section as those of specimen 11. The frames, in addition to being full cylindrical rings, incorporate a relatively stiff, integral bar that bisects the cylinder at the diameter and spans from side to side. This configuration simulates the ring frame of a circular fuselage fixed to the floor beam. In addition, incorporation of this bar permits utilization of NOVA-2 as an analysis tool, since it does not analyze a full 360 degree multi-layered structure such as this frame.

As for specimen number 11, the classical method of analysis assumes no bending of a circular ring under uniform pressure and analyzes the structure for pure hoop compression. As can be seen in Figures 42 and 43, this yields very unconservative results.

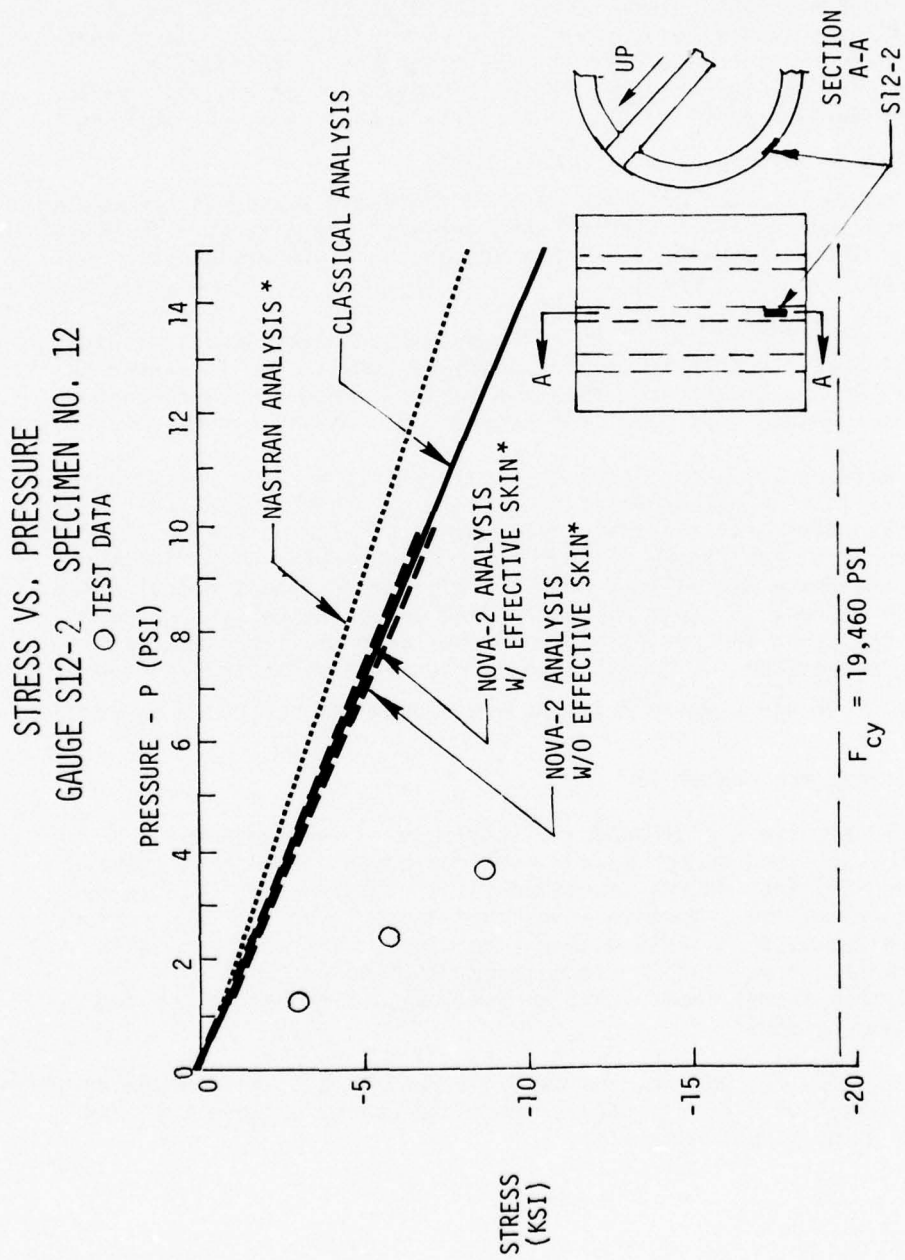
In this case, the use of NASTRAN and NOVA-2 also yielded very unconservative results, although NOVA-2 and the classical analysis results are in very good agreement. This agreement exists because the computed bending moments were insignificant, as both analyses predicted behavior basically in hoop compression.

The discrepancy between test and analysis results exists because the structure actually displaced in a higher order of complexity due to the 'waffled' loading pattern of the skins acting as thin membranes. (The skins were deliberately made thin and bonded to the frames in order to preclude their significantly contributing to the frame overall strength.) This complex loading caused the frames to bend in and out of their circular shape in an unusually excessive number of modes resulting in bending of the frames over smaller radii of curvature. This phenomenon, of course, caused higher stresses in accordance with the formula $\sigma = \frac{Ec}{R}$, where R is the aforementioned radius of curvature.

8.2.13 Test Specimen Number 13

Specimen number 13 is also a stiffened, full cylinder. The fundamental difference between specimen number 13 and specimen number 12 is that specimen 13 is buckling critical whereas specimen 12 is yielding critical. Like specimen 12, the frames are symmetrical in cross-section for the same reason; however, they are tee-sections rather than I-sections. This shape reduces the moment of inertia, resulting in the desired buckling criticality. Also, like specimen 12, the frames incorporate an integral, stiff bar across the center for the same reasons.

As shown in Figures 44, 45, and 46, the analysis results are again unconservative. The discussion in Section 8.2.12 regarding the discrepancy between test and analysis results is pertinent here also.



*EXTREME FIBER

FIGURE 42

STRESS VS. PRESSURE
GAUGE S12-14 SPECIMEN NO. 12
○ TEST DATA

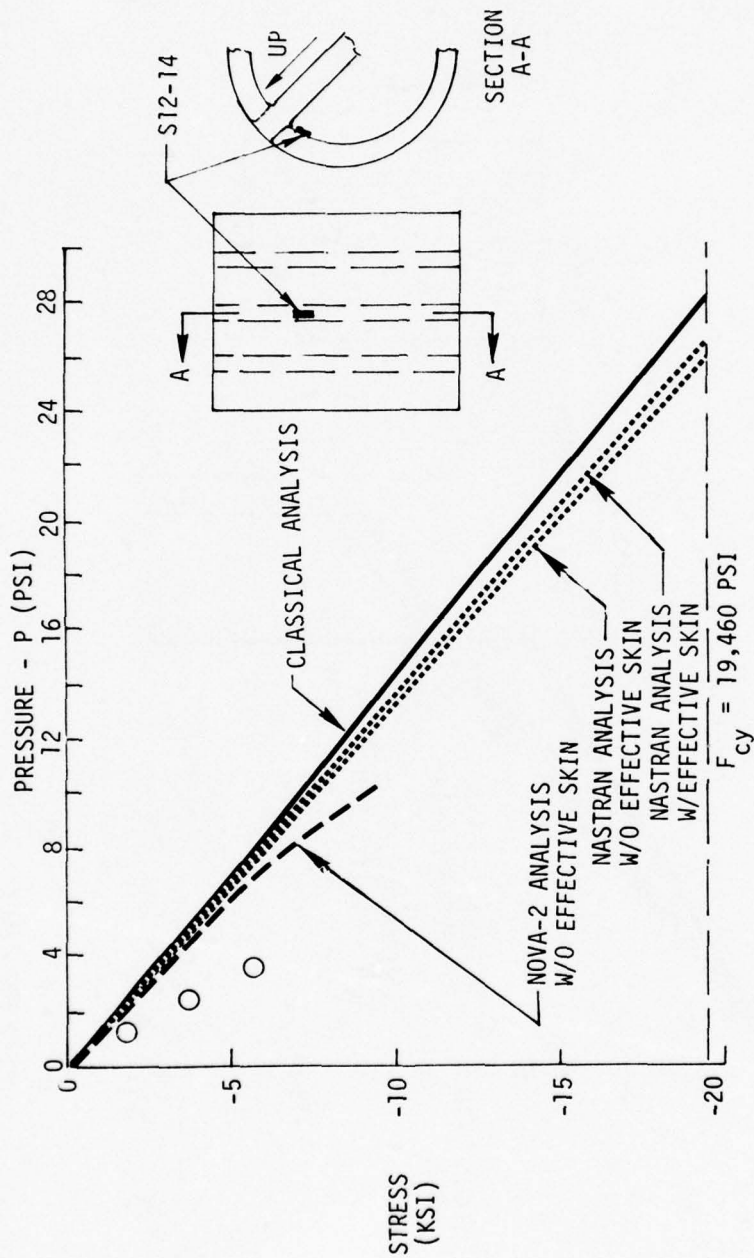
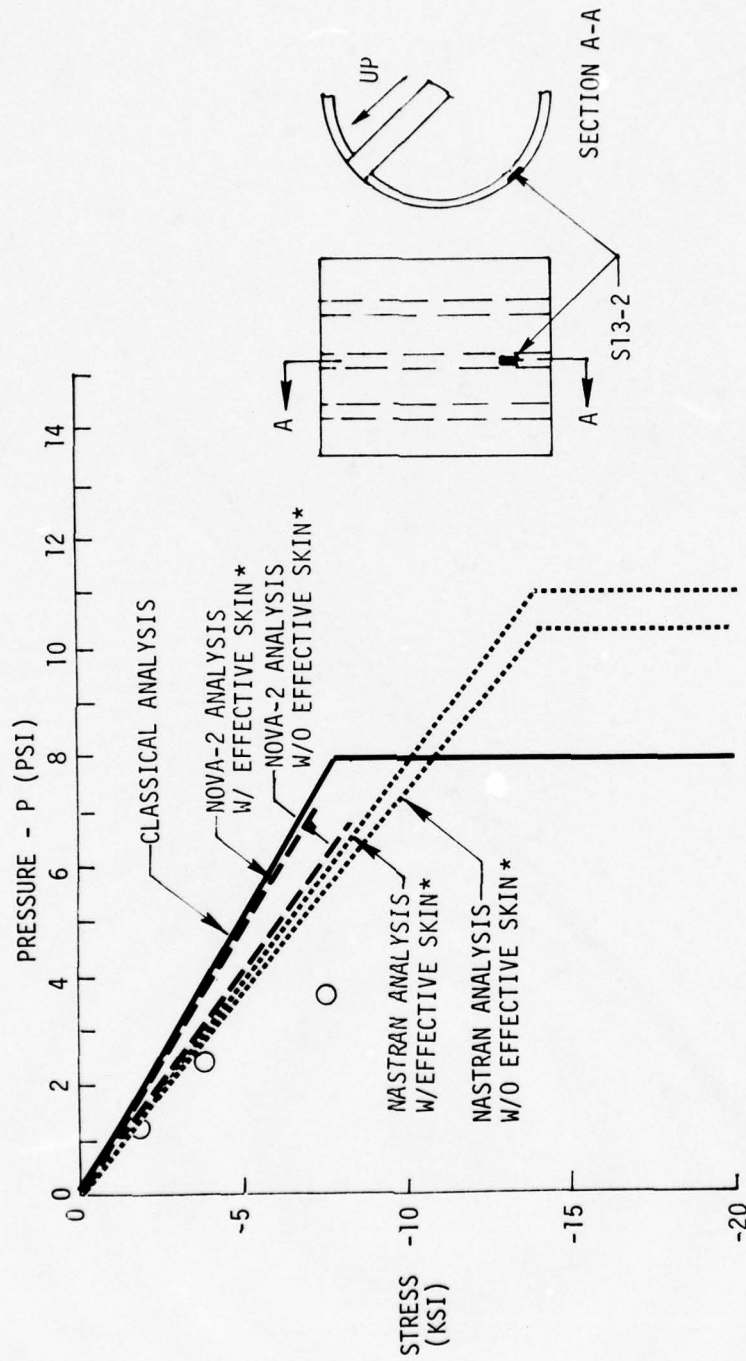


FIGURE 43

STRESS VS. PRESSURE GAUGE S13-2 SPECIMEN NO. 13

○ TEST DATA



*EXTREME FIBER

FIGURE 44

STRESS VS. PRESSURE GAUGE S13-9 SPECIMEN NO. 13 O TEST DATA

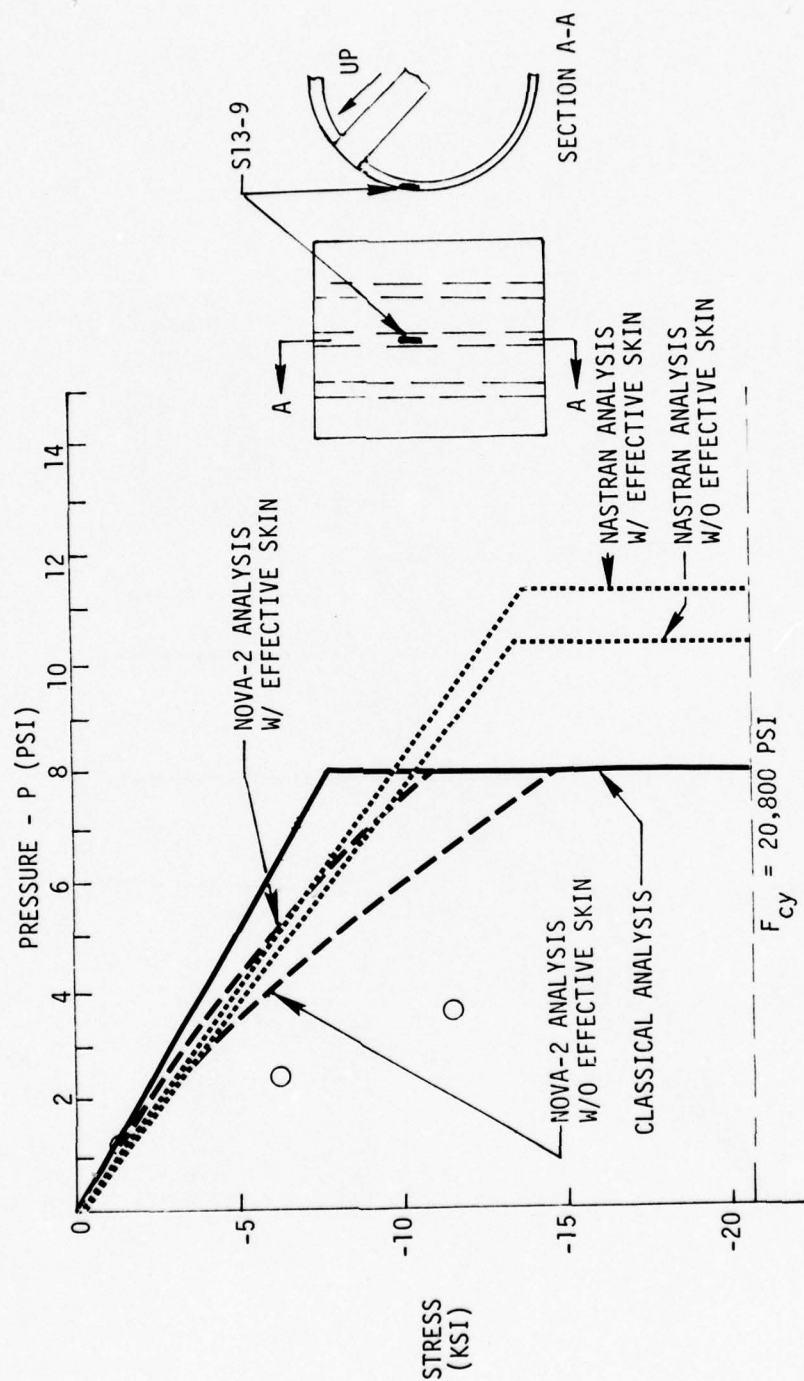


FIGURE 45

STRESS VS. PRESSURE
GAUGE S13-14 SPECIMEN NO. 13
○ TEST DATA

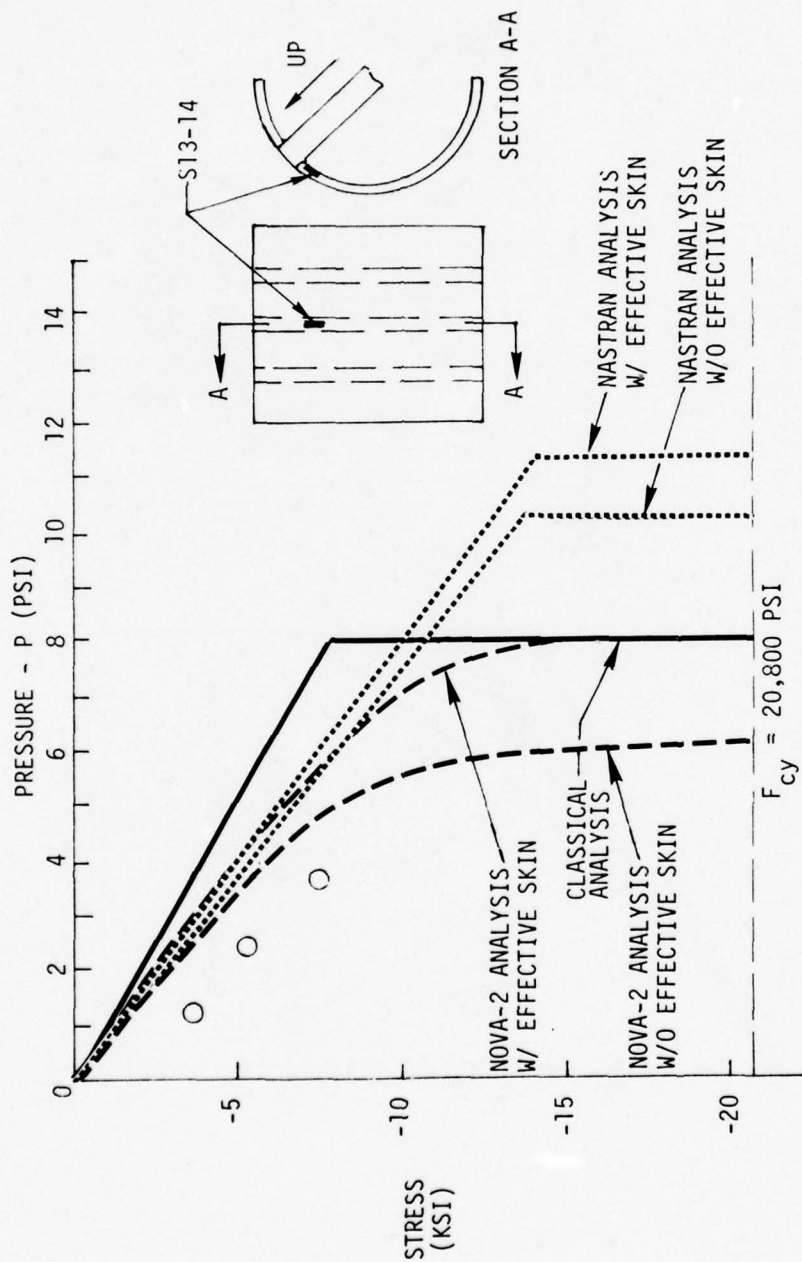


FIGURE 46

8.2.14 Test Specimen Number 14 through 17

These four specimens are all like columns and are, therefore, discussed here together. These columns are simple flat plates .031 inches thick and five inches wide with a clear span of ten inches. The columns were fixed at the ends. The columns contained the following initial imperfections at their respective mid-spans: specimen 14 (0.0 inches), specimen 15 (0.01 inches), specimen 16 (0.0 inches), and specimen 17 (0.03 inches).

The configuration of the columns was designed to result in relatively high L/P ratios so that the Euler long-column theory would be applicable. Traditionally, columns are considered to have failed at the point at which they buckle. However, since it was known that these columns would undergo dynamic (shock) testing where load duration is a critical factor, it was desired to examine their residual strength after buckling under static load, up to the point of yielding.

Figures 47 through 50 illustrate that this residual strength does exist and exceeds the buckling strength. These figures also show excellent agreement between test and analysis. The lack of an abrupt change in stress at the onset of buckling is attributed to the fixed-end nature of the columns. This abrupt change, or "snap-through" buckling, would more likely be evident in a pin-ended column configuration.

Analyses of long columns beyond the buckling mode are rare; so an analysis method was derived based on the assumption that fixed-end columns displace to a sine-wave shape. This assumption was verified by the test as shown in the excellent correlation between test and analysis with regard to deflection as shown in Figures 49 and 50. This analysis method is discussed in detail in Volume II. NOVA-2 does not predict the behavior of columns under static load and, therefore, could not be used here.

The effect of initial imperfection on the response of the columns is illustrated in Table XI. With the exception of several data points, the static test results indicated that as the initial imperfection increased, response for a given load level also increased. As shown, the amount of initial imperfection influenced the load level at which the column buckled as well as the response prior to buckling. However, it appeared that all four columns would have yielded at approximately the same load level.

STRESS VS. PRESSURE
GAUGE S17-1 SPECIMEN NO. 17

○ TEST DATA

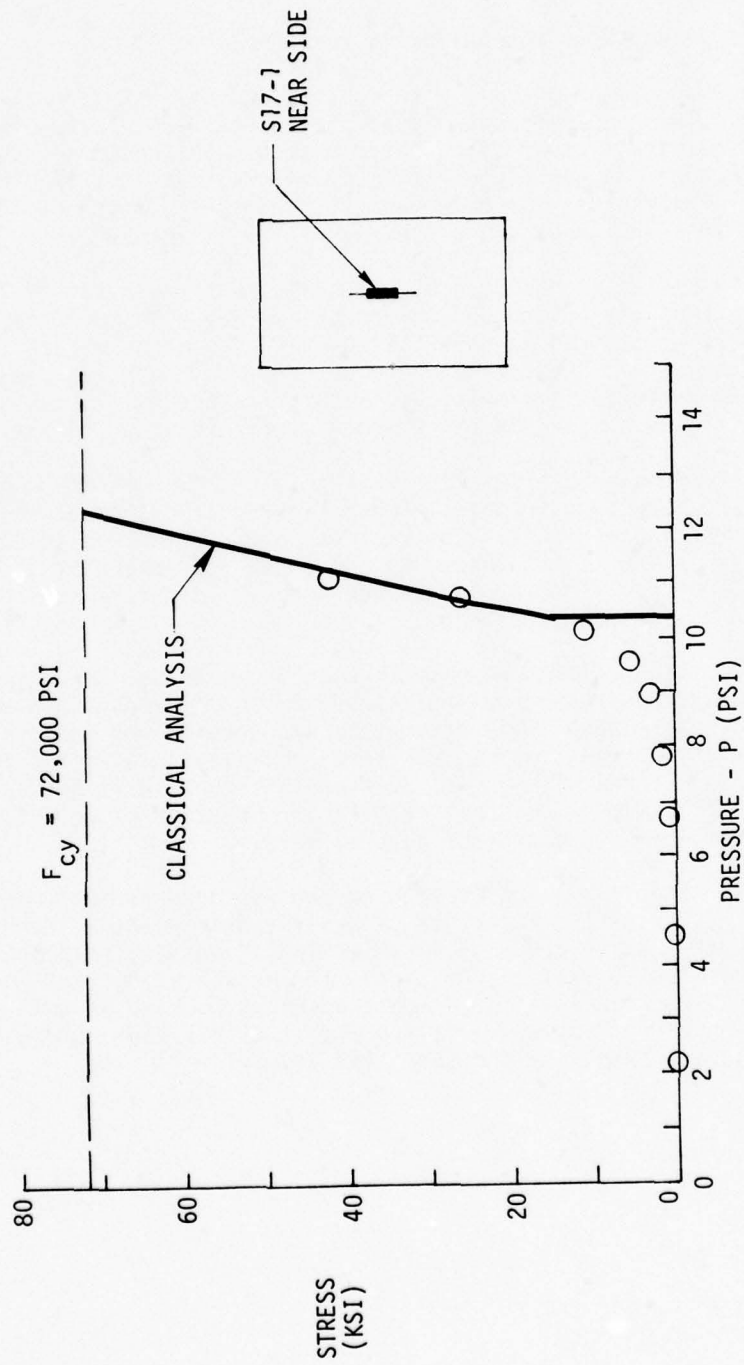


FIGURE 47

STRESS VS. PRESSURE
GAUGE S17-2 SPECIMEN NO. 17
○ TEST DATA

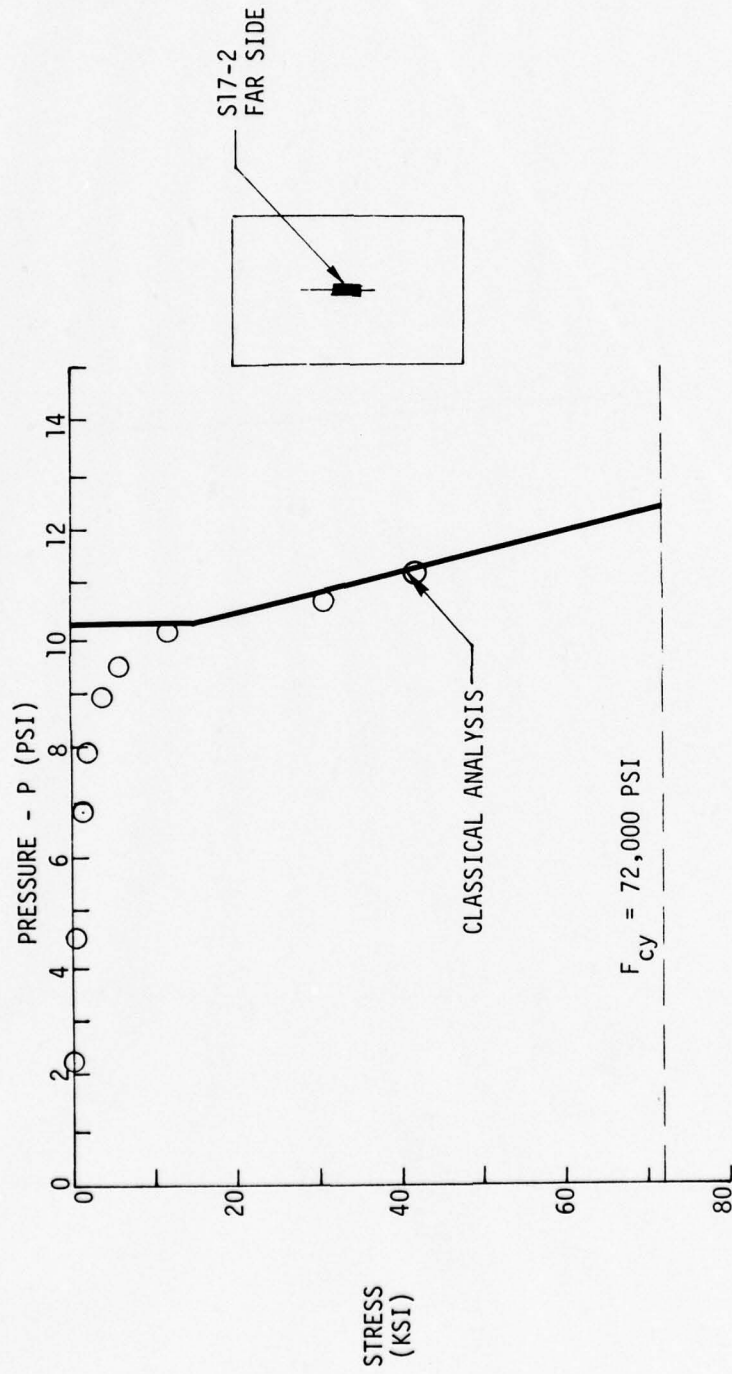


FIGURE 48

PRESSURE VS. DISPLACEMENT
SPECIMEN NO. 17

○ TEST DATA

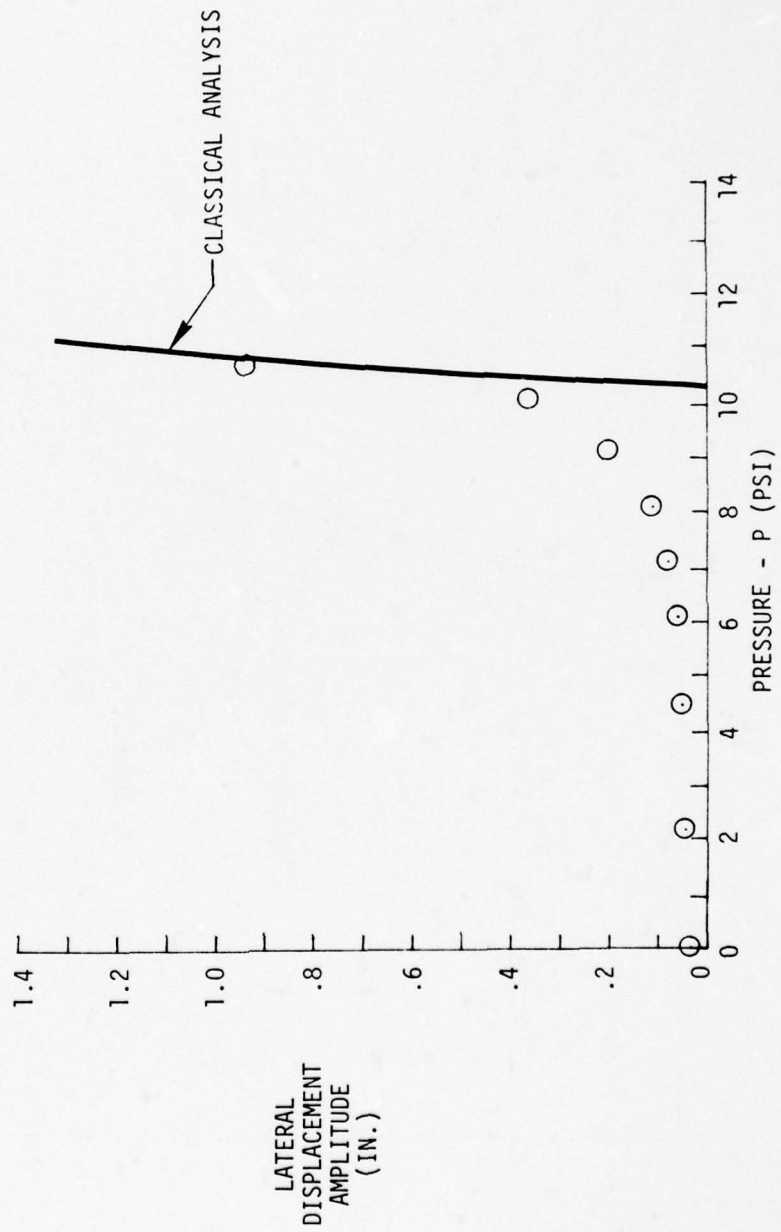


FIGURE 49

STRESS VS. DISPLACEMENT
SPECIMEN NO. 17

○ TEST DATA

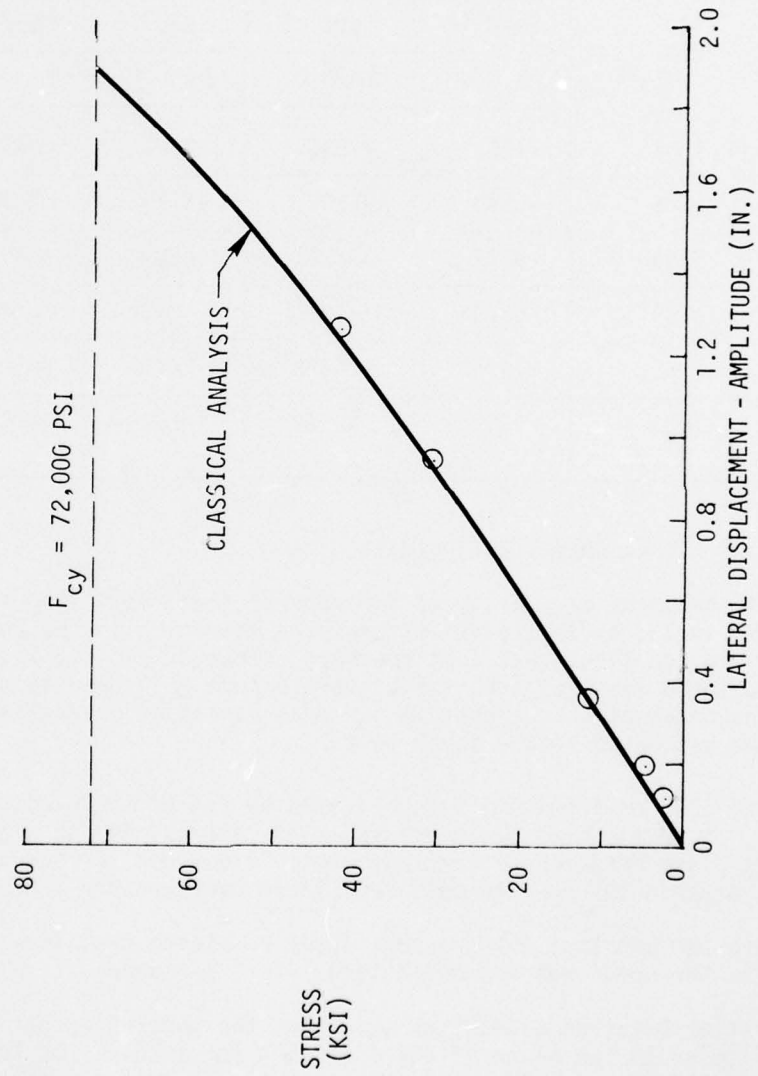


FIGURE 50

TABLE XI
EFFECTS OF COLUMN INITIAL IMPERFECTIONS

ΔP	Stress at Center of Columns (PSI)			
	Spec 14	Spec 15	Spec 16	Spec 17
	$\delta = 0.0$	$\delta = 0.01$	$\delta = 0.0$	$\delta = 0.03$
7.84	-1761	-4635.	-2194	-2256.
8.96	-2843	-5603.	-3193	-4038.
9.53	-4017	-6520.	-4089	-6283.
10.08	-6695	-8127.	-4893	-11649
10.65	-14750	-14286	-20755	-32157
11.20	-28521	-40469	-35123	-42436

8.3 Shock Load Test/Analysis

All test specimens were analyzed for several free field shocks intensities up to and including that level of pressure resulting in the onset of permanent damage. In addition, each test specimen except 6, 11, 14, 15, 16, and 17 were analyzed for a level of free field overpressure resulting in significant permanent deformation. These latter peak levels of overpressure were those that were generated in the shock test.

The shock load environments were obtained by use of the blast routines within NOVA-2. To obtain free field pressures of interest and to closely match the positive phase duration of the test pressure pulses, various slant ranges were used to provide the desired peak free field overpressure intensities.

To negate the preblast overpressure loads resulting from forward speed of the aircraft, the speed was set equal to 0.1 feet per second.

The burst orientation was chosen such that the shock propagation vector was perpendicular to the plane of the flat test specimens. For the curved test specimens, the burst orientation was chosen such that a symmetric loading pattern was imposed on the specimen.

In addition to the analysis described above, the test specimens were also analyzed utilizing the measured reflected pressure time histories as input. This was accomplished because of differences that were noted between the measured and predicted reflected pressure time histories. For certain test specimens, it was noted that a time varying pressure buildup occurred inside the specimen/fixture cavity due to deformation of the specimen. This internal pressure time history was included in the analysis by subtracting it from the external reflected pressure time history.

In addition to comparisons of test and analysis structural response data, subsequent sections of this report discuss test and analysis shock reflection factors and how they were found to vary with shock strength and orientation angle.

All analyses were conducted utilizing modulus of elasticity data and yield strength data established by coupon tests of the material from which the specimen was constructed. An exception to this was the column specimens, where MIL-HDB-5 (Reference 12) data was utilized for the 7075-T6 aluminum alloy. The analyses also utilized the actual specimen measured geometry (thickness, area, etc.) to establish the correct section properties.

Many of the results shown in subsequent sections of this report make reference to measured peak free field overpressure values. Due to the ragged nature of the incident (free field) pressure pulse, a smoothing process was utilized in order to describe the peak value. This is illustrated in Figure 51, which shows the results of the smoothing process. For this particular test shot, the peak value was defined to be 3.7 psi. Therefore, whenever reference is made to peak free field or incident overpressure, the reader must bear in mind that a smoothing process has been applied to the measured data.

As stated earlier in this report, the test specimens were initially analyzed using the pressure time history data generated by a blast environment module within the NOVA-2 computer program. Based on the differences that were observed between the predicted pressure time histories and the measured pressure time histories, Kaman Avidyne and the Air Force Weapons Laboratory modified the NOVA-2 program to allow the user to input the desired reflected pressure time history environment. This resulted in a revised analysis of all test specimens utilizing measured reflected pressure time history data. Subsequent to the completion of the revised analysis, it was discovered that the modifications made to NOVA-2 resulted in an analysis tool that was applicable only to flat specimens. The explanation of this is as follows. Consider a curved specimen such as 6, 11, 12 or 13. For the blast/structure incidence angles considered in this program, as the shock wave makes initial contact with the specimen, only the point of contact experiences an abrupt increase in pressure. As the shock wave travels over the specimen, additional points on the specimen experience an increase in pressure until eventually the entire structure is engulfed in the pressure field. However, not all points on the specimen experience the same magnitude of reflected pressure (due to differences

TEST SPECIMEN NO. 4
TEST SHOT NO. 4
INCIDENT PRESSURE AT GAUGE P-5

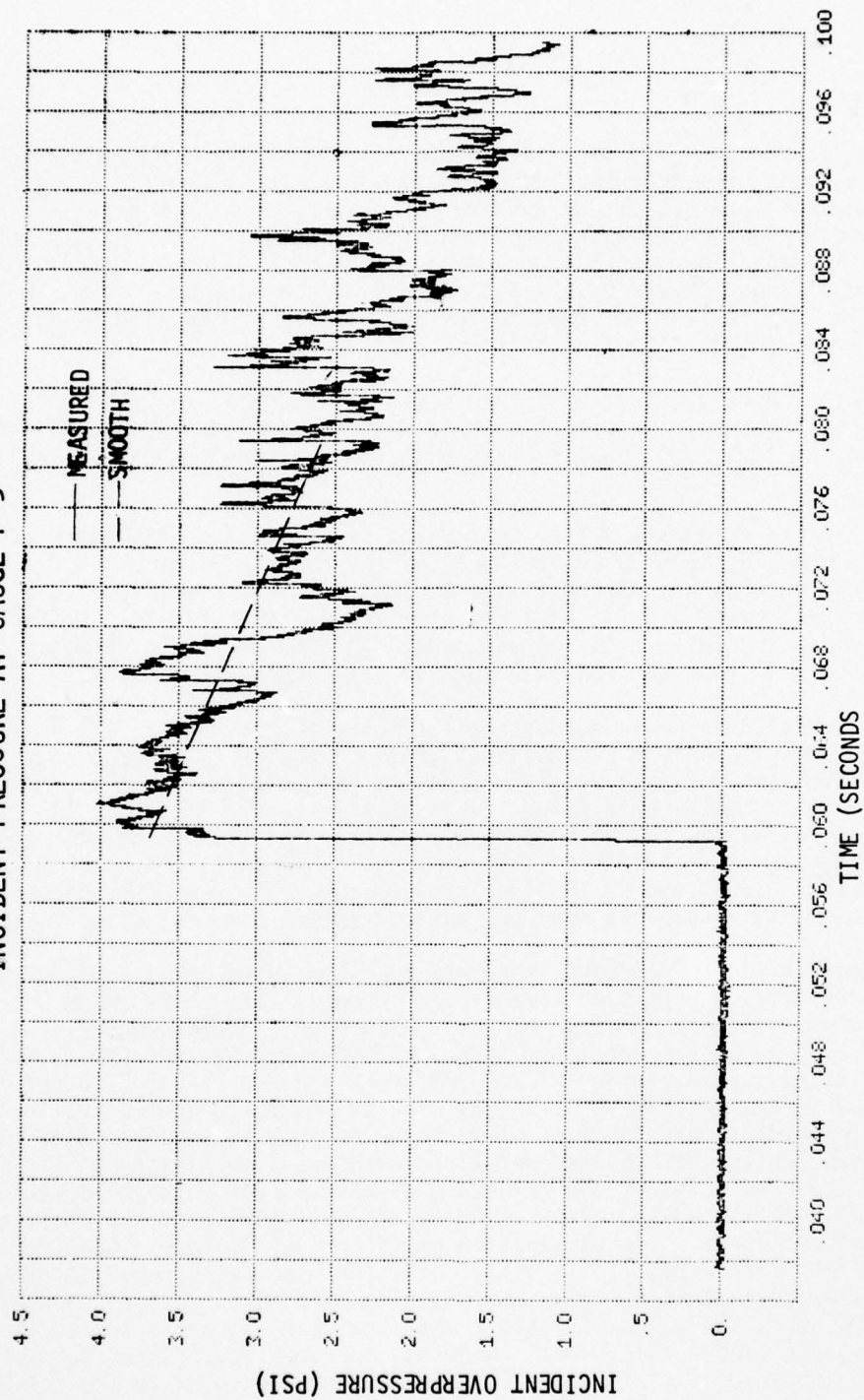


FIGURE 51. TYPICAL FREE FIELD PRESSURE PULSE

in the shock/structure incidence angles) nor do they experience pressure increases at the same instant of time (due to the finite amount of time required for the shock to engulf the specimen). Only for a flat specimen would all points on the specimen experience similar pressure time histories. Furthermore, even a flat specimen oriented at other than a 90° incidence angle would experience small differences in pressure as a function of spacial location since not all points on the panel would experience pressure increases simultaneously. The modifications to NOVA-2 resulted in all points on the test specimen experiencing the same reflected pressure at the same instant of time. In other words, the NOVA-2 program treated the reflected pressure as being uniform spacially and variable temporally.

The net result is that neither the original stress analysis results nor the revised stress analysis results can be compared directly with measured stress results from the shock load test except for the flat specimens oriented at 90° incidence angle. Two flat panel specimens (4 and 5) were tested at incidence angles of 60° and 30° as well as 90°. Due to the relatively small size of these specimens (22 inches by 22 inches), however, it is anticipated that stress results from the revised analysis can be compared directly to the test data without introducing significant errors.

It is difficult to make a meaningful comparison of predicted shock load stress data and measured shock load stress data for specimens 6, 11, 12 and 13 due to the curvature of these test specimens and the limitations of the current versions of NOVA-2 discussed earlier in this section. In subsequent sections of this report (sections 8.3.6, 8.3.11, 8.3.12 and 8.3.13), however, comparisons of predicted stress data and measured stress data are made. The results of this comparison should be interpreted as qualitative as opposed to quantitative. The reader is cautioned that the analysis results are in error due to the reasons described above.

As stated earlier, the primary objective of this program was to generate experimental data that could be utilized to evaluate current and future analysis tools. This objective has been accomplished. However, additional modifications will have to be made to NOVA-2 in order to evaluate its predictive capabilities regarding the curved test specimens in this program.

8.3.1 Test Specimen Number 1

Specimen 1 is a single layer homogeneous flat panel with all four edges fixed as described in Tables I and II. All analyses and tests for specimen 1 were conducted for a blast/structure incidence angle of 90 degrees.

Analysis results and test results are shown in Figures 52 and 53 which indicate maximum stress occurs at the center of the clamped edge and maximum displacement occurs at the center of the panel as expected. These figures illustrate very good agreement on maximum stresses. The test stresses shown here are an average of stresses at the centers of three edges. The level of agreement associated with displacement is not as good as that for stresses. It is anticipated that this is due to a very small amount of displacement of the walls of the box holding fixture and was also experienced in the static test.

TEST SPECIMEN NO. 1
STRESS AT CENTER OF CLAMPED EDGES
(GAUGES S1-3, 4, 5)

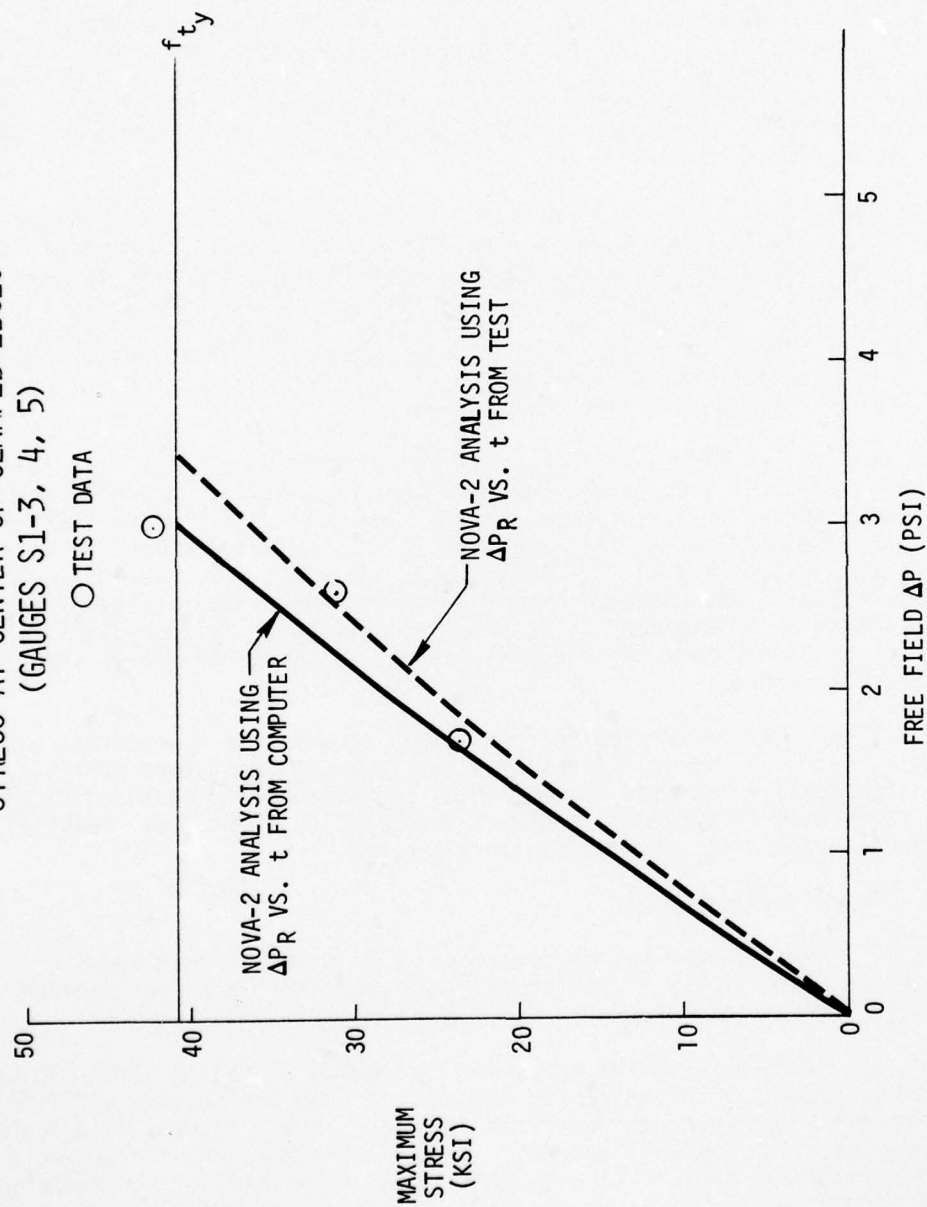


FIGURE 52. STRESS VS. FREE FIELD OVERPRESSURE - SPECIMEN 1

TEST SPECIMEN NO. 1
DISPLACEMENT AT PANEL CENTER
(GAUGE D1-10)

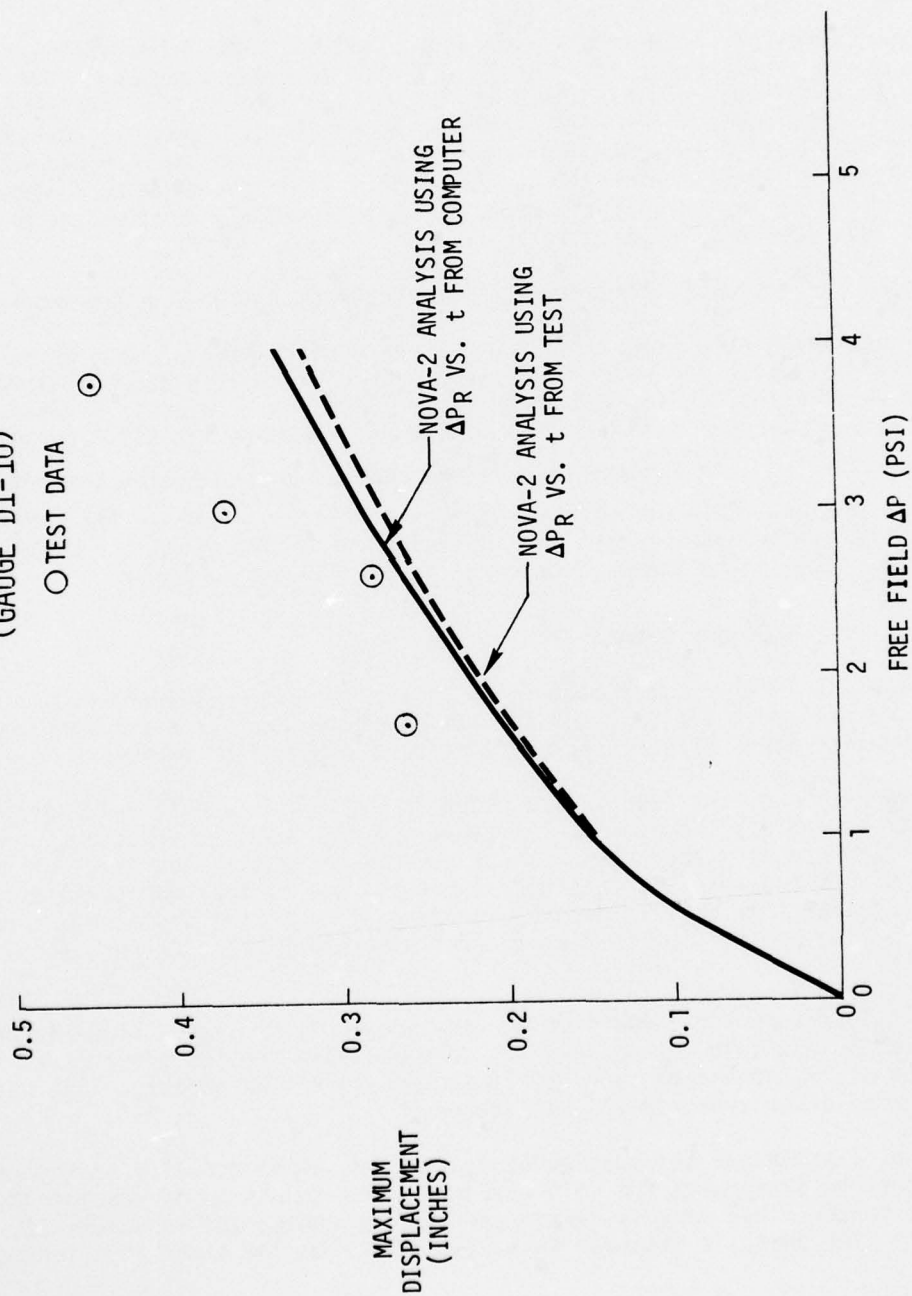


FIGURE 53. DISPLACEMENT VS. FREE FIELD OVERPRESSURE - SPECIMEN 1

Figure 54 illustrates the comparison of test and analysis stress time history for a selected test shot for specimen one. The analysis results shown were obtained by utilizing the measured reflected pressure time history. The test stress shown is at one of the three edges that was instrumented. Therefore, the peak value does not agree identically with the peak value shown in Figure 52. The analysis was terminated after approximately 11 milliseconds.

In addition, a permanent deformation of approximately 0.06 inches was measured manually at the panel center after the final shot for this specimen. The analysis response data resulting from the final shot indicated no permanent deformation. The maximum recorded strain (average of three gauges) associated with the final shot was 12700 micro-inches per inch, whereas the corresponding predicted strain was 8420 micro-inches per inch. It is possible that more modes are required in the analysis model to more accurately predict the behavior of this specimen in the plastic range.

As indicated in Figure 52, measured stress data greater than f_{ty} is shown.

This data point was obtained by scaling the appropriate strain value by E , where E is that value in the elastic range. Thus the stress shown is larger than that which actually occurred in the test. Scaling by elastic E was done to allow for proper interpolation of the test data to establish the ΔP_{FF} associated with f_{ty} . In essence this is the same as interpolating between strain data points. No other use was made of this stress data in the plastic region, since comparisons of test and analysis data in the plastic region were performed utilizing strain data directly as illustrated above.

8.3.2 Test Specimen Number 2

Specimen 2 was a single layer homogeneous flat panel with all four edges pinned as described in Tables I and II. All analyses and tests for specimen 2 were conducted for a blast/structure incidence angle of 90 degrees.

Analysis results and test results are shown in Figures 55 and 56 which indicate maximum stress and displacement at the center of the panel as expected. These figures illustrate very good agreement on maximum stresses. The level of agreement associated with displacement is not as good as that for stresses. It is anticipated that this is due to a very small amount of displacement of the walls of the box holding fixture and was also experienced during the static test.

Figure 57 illustrates the comparison of test and analysis stress time history for a selected test shot for specimen 2. The analysis results shown were obtained by utilizing the measured reflected pressure time history. The analysis was terminated after approximately 11 seconds.

In addition, a permanent deformation of 0.78 was measured manually at the panel center after the final shot for this specimen. The condition of specimen 2 subsequent to the final shot is illustrated in the photograph in Volume II, page 60. The analysis response data resulting from the final shot indicated

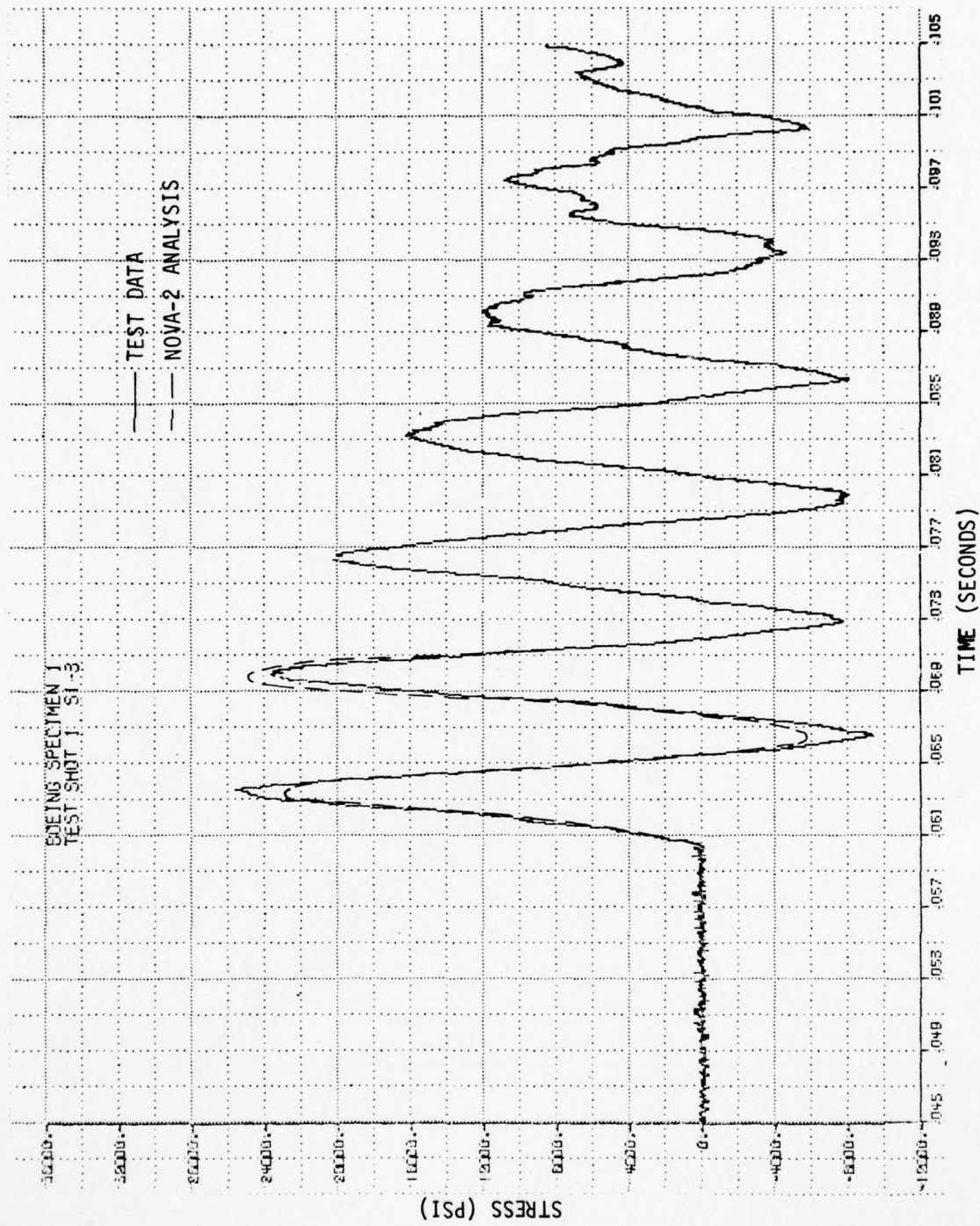


FIGURE 54. STRESS TIME HISTORY - SPECIMEN 1

TEST SPECIMEN NO. 2
STRESS AT CENTER OF PANEL
(GAUGE S2-2)

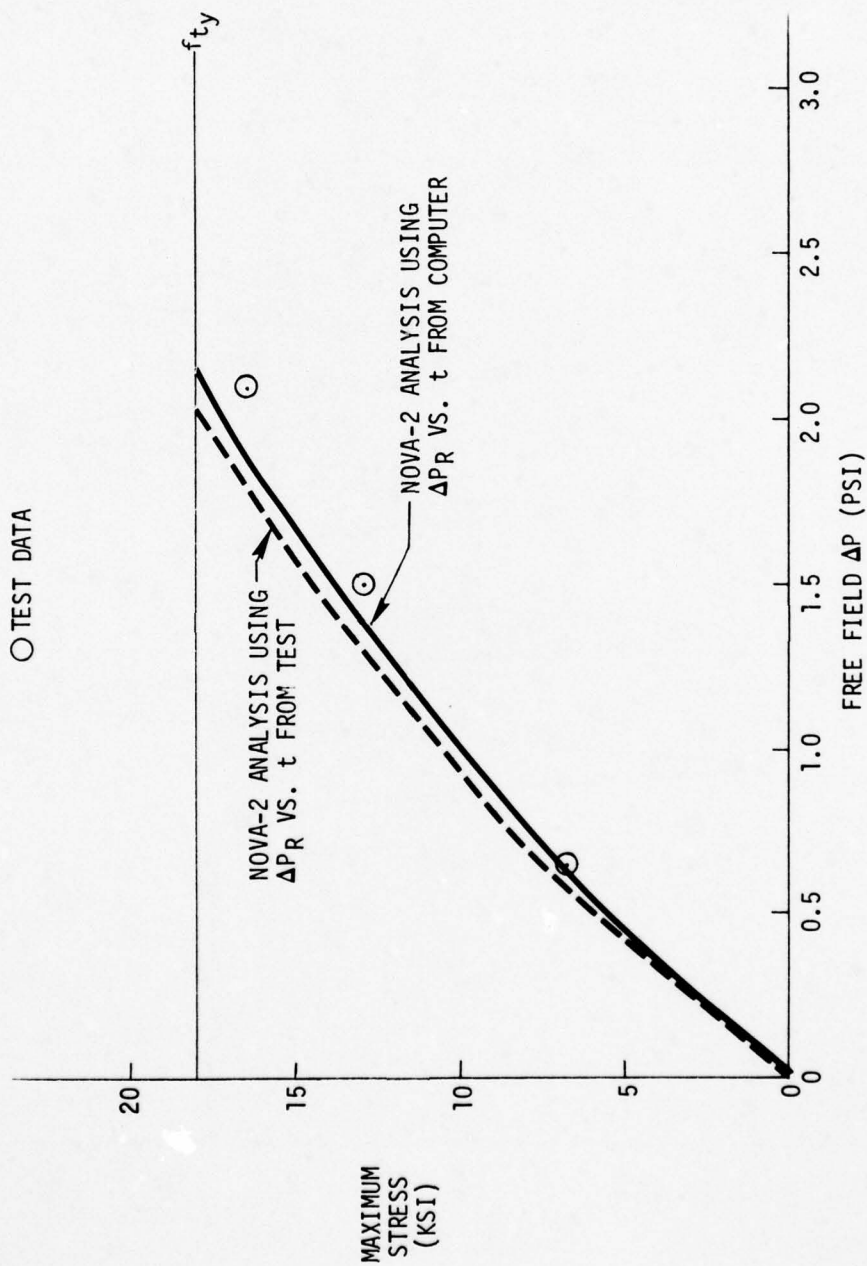


FIGURE 55. STRESS VS. FREE FIELD OVERPRESSURE - SPECIMEN 2

TEST SPECIMEN NO. 2
DISPLACEMENT AT PANEL CENTER
(GAUGE D2-6)

○ TEST DATA

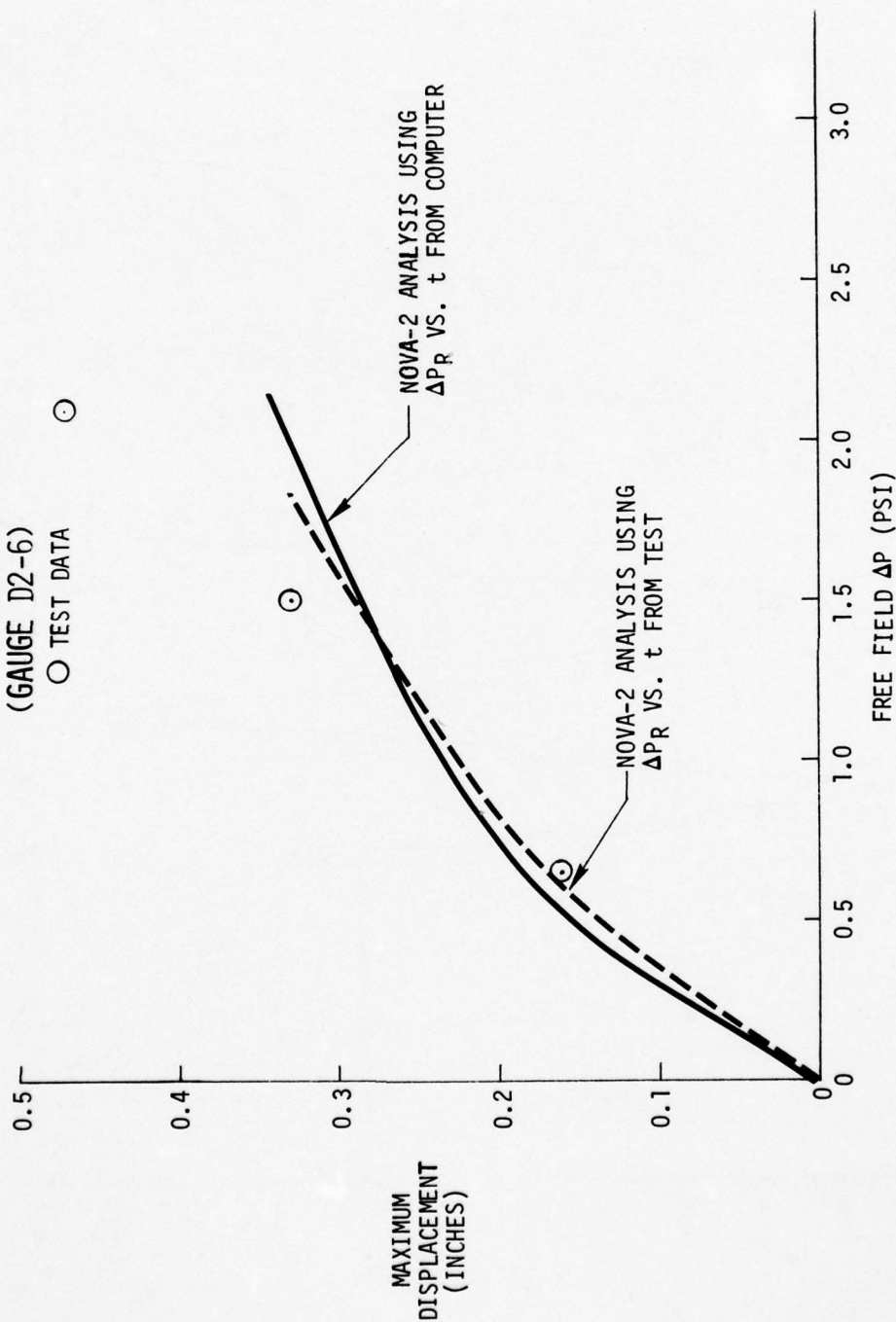


FIGURE 56. DISPLACEMENT VS. FREE FIELD OVERPRESSURE - SPECIMEN 2

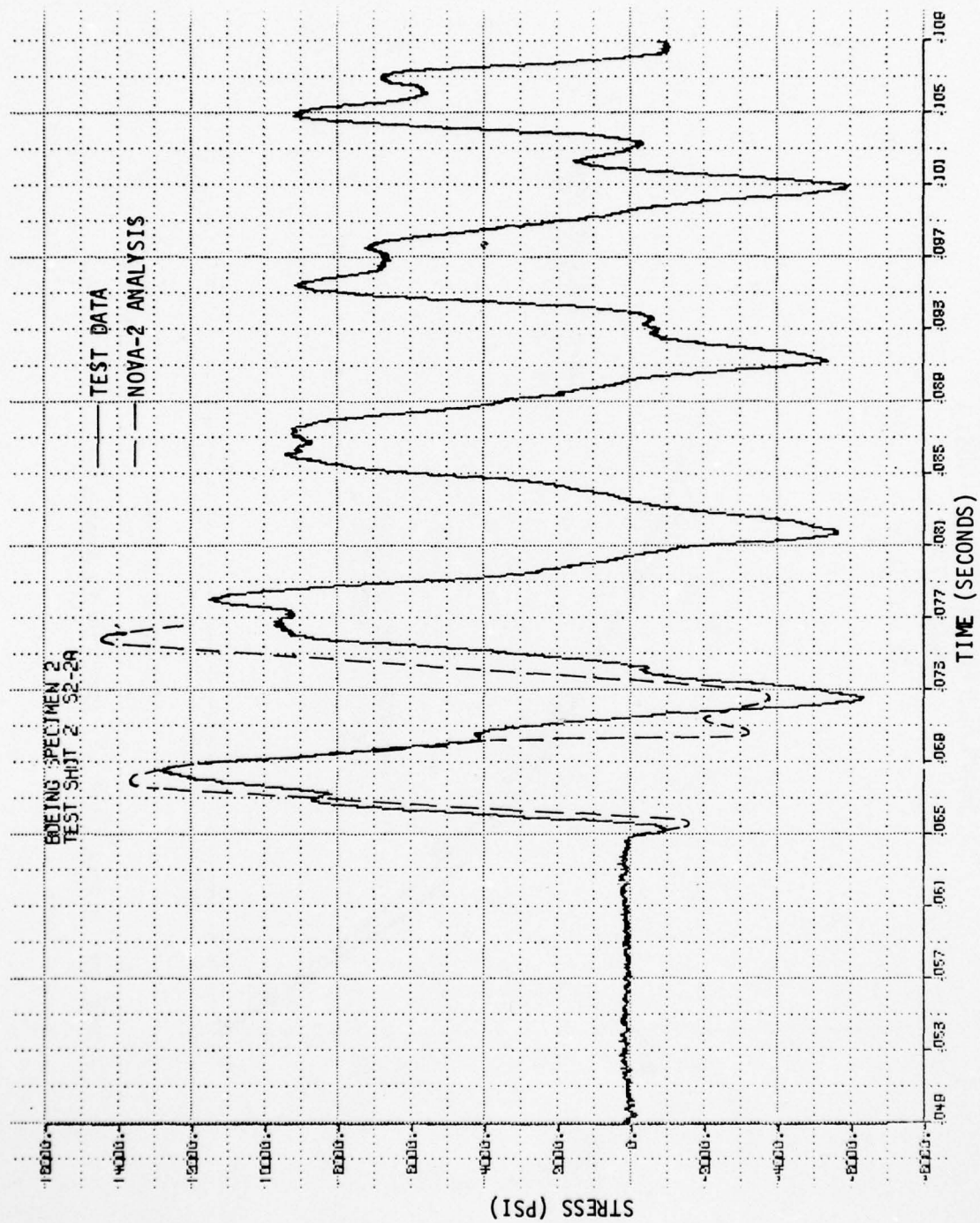


FIGURE 57. STRESS TIME HISTORY - SPECIMEN 2

approximately 0.2 inches permanent deformation. The maximum recorded strain associated with the final shot was 4100 micro-inches per inch along the "A" leg of the strain gauge and 4850 micro-inches per inch along the "C" leg of the strain gauge. For this condition, the analysis predicted 3230 micro-inches per inch in each direction. As in the case of specimen 1, more modes may be required to accurately predict the behavior of this specimen in the plastic range.

8.3.3 Test Specimen Number 3

Specimen 3 was a single layer homogeneous flat panel with two opposite sides fixed and the other two sides pinned as described in Tables I and II. All analyses and tests for specimen three were conducted for a blast/structure incidence angle of 90 degrees.

Analysis results and test results are shown in Figures 58 and 59 which indicate maximum stress at the center of a clamped edge and maximum displacement at the center of the panel as expected. Similar to specimens 1 and 2, the agreement between test and analysis is better for stress than for displacement. Comments in the previous two sections regarding this phenomenon apply here also.

Figure 60 illustrates the comparison of test and analysis stress time history for a selected test shot for specimen 3. The analysis results shown here were obtained by utilizing the measured reflected pressure time history. The analysis was terminated after approximately 10 seconds.

In addition, a permanent deformation of 0.14 inches was measured manually at the panel center after the final shot for this specimen. The condition of specimen 3 subsequent to the final test shot is illustrated in the photograph in Volume II, page 91. The analysis response data resulting from the final shot indicated approximately 0.13 inches permanent deformation. The maximum recorded strain associated with the final shot was 12000 micro-inches per inch at the center of the clamped edge. For this condition, the analysis predicted 10,850 micro-inches per inch.

8.3.4 Test Specimen Number 4

Specimen 4 was a single layer homogeneous flat panel with all four sides fixed as described in Tables I and II. Tests and analyses were conducted for this specimen using shock incidence angles of 90°, 60°, and 30°. The primary objective of testing at angles other than 90°, i.e., "head-on", was to generate data regarding shock enhancement as a function of incidence angle and shock strength.

Analysis results and test results are shown in Figures 61 - 66 which indicate maximum stress at the center of a clamped edge and maximum displacement at the center of the panel as expected. The stress data represents an average of gauges at the centers of three edges of the panel. For all three orientations, consistently good agreement between test and analysis exists for the maximum stress data. The agreement between test data and analysis data is also reasonably good regarding displacement at the center of the panel. In addition, the data is consistent with regard to response as a function of incidence angle, i.e., "head-on" gives rise to the highest responses whereas 30° results in the lowest responses.

TEST SPECIMEN NO. 3
STRESS AT CENTER OF CLAMPED EDGE
(GAGE S3-4)

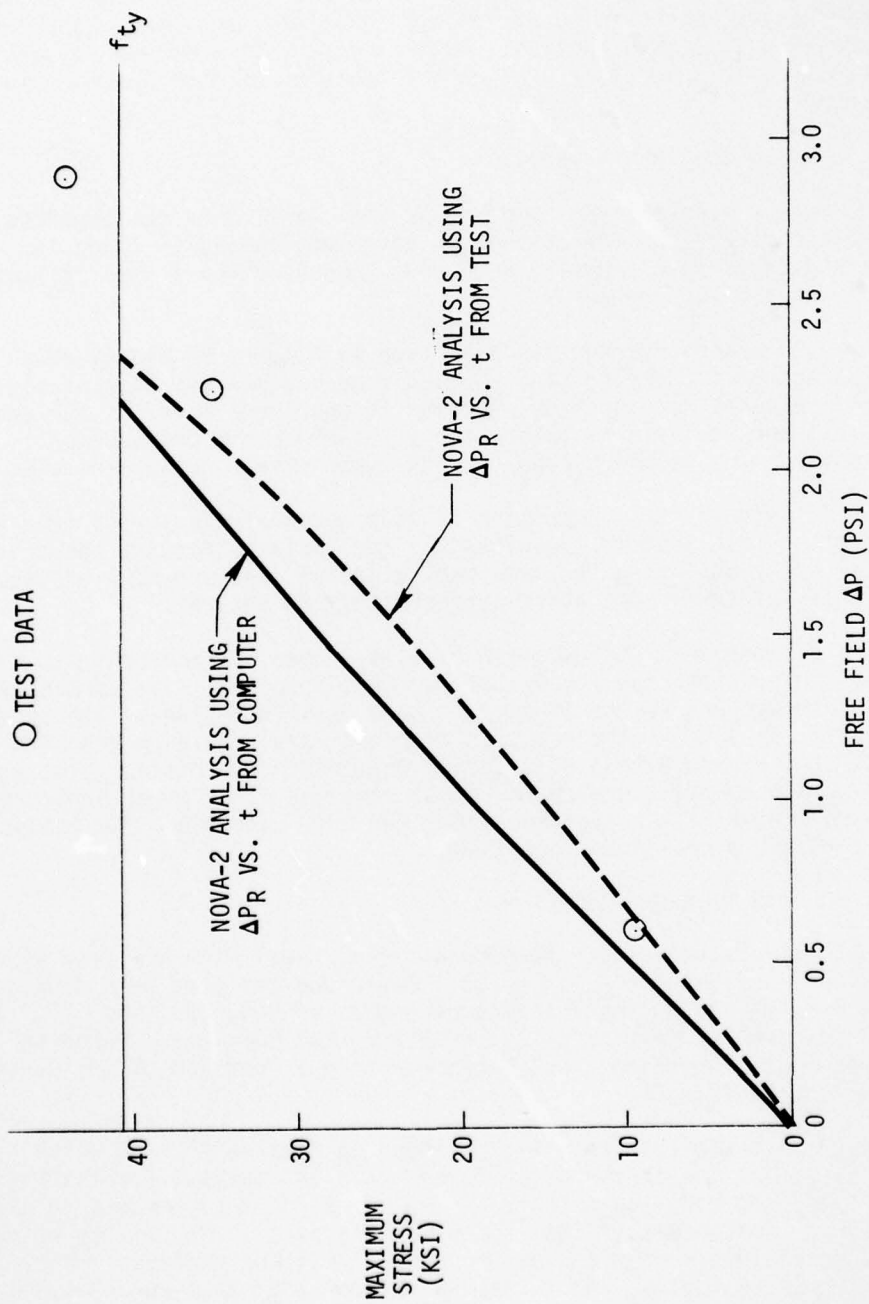


FIGURE 58. STRESS VS. FREE FIELD OVERPRESSURE - SPECIMEN 3

TEST SPECIMEN NO. 3
DISPLACEMENT AT PANEL CENTER
(GAUGE D3-8)

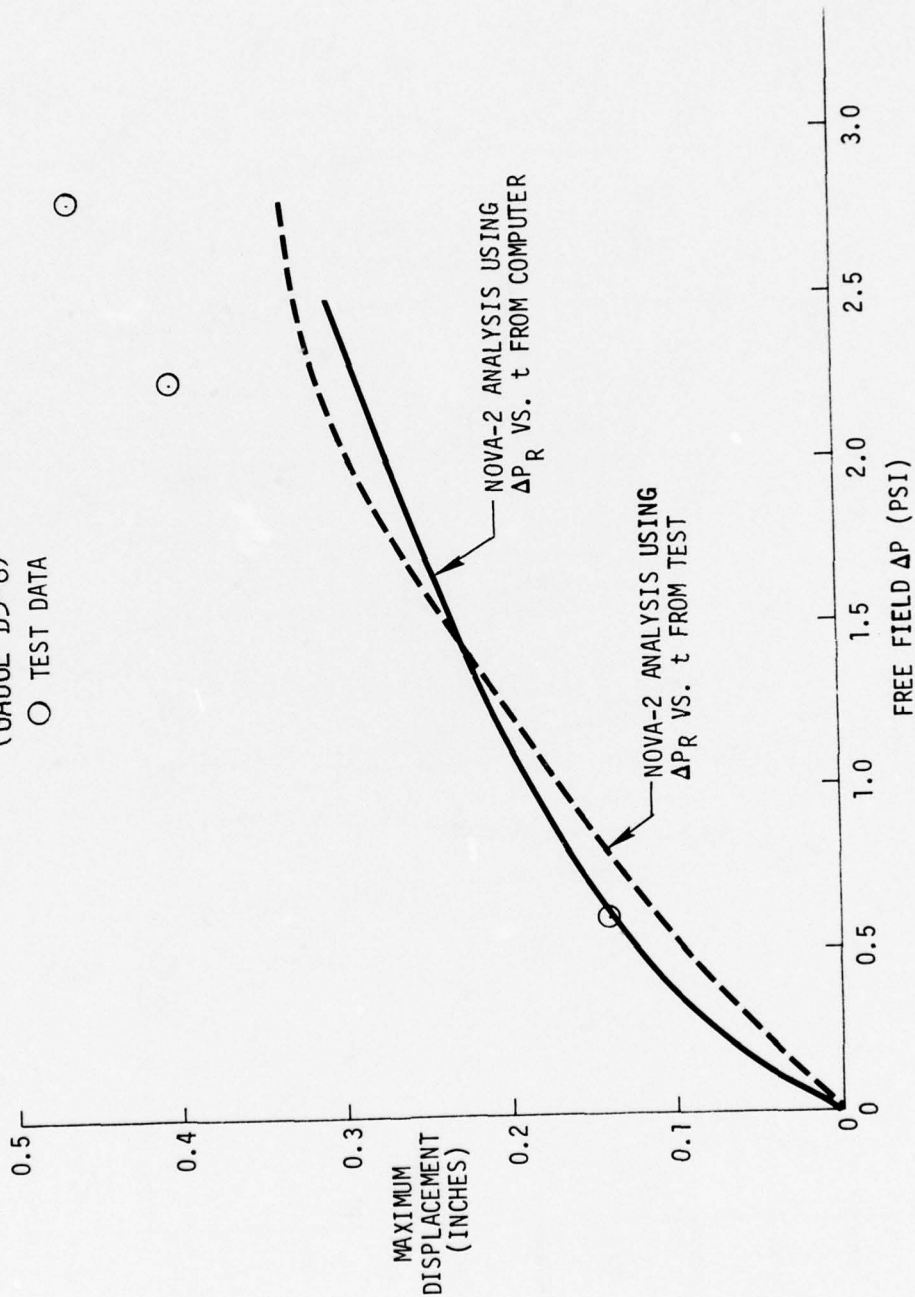


FIGURE 59. DISPLACEMENT VS. FREE FIELD OVERPRESSURE - SPECIMEN 3

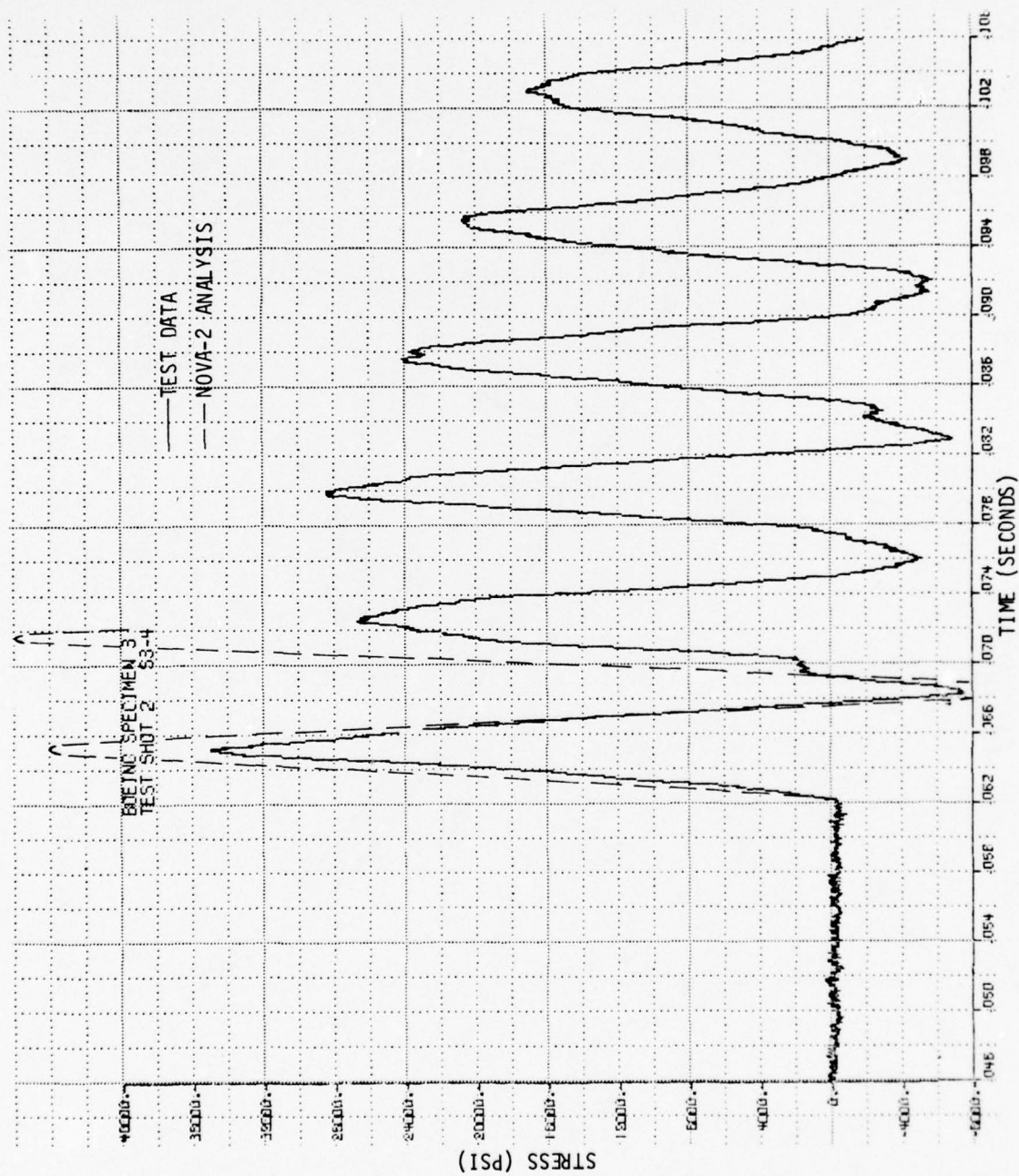


FIGURE 60. STRESS TIME HISTORY - SPECIMEN 3

TEST SPECIMEN NO. 4
STRESS AT CENTER OF EDGE
INCIDENCE ANGLE = 90°
(GAUGES S4-3, 4, 5)

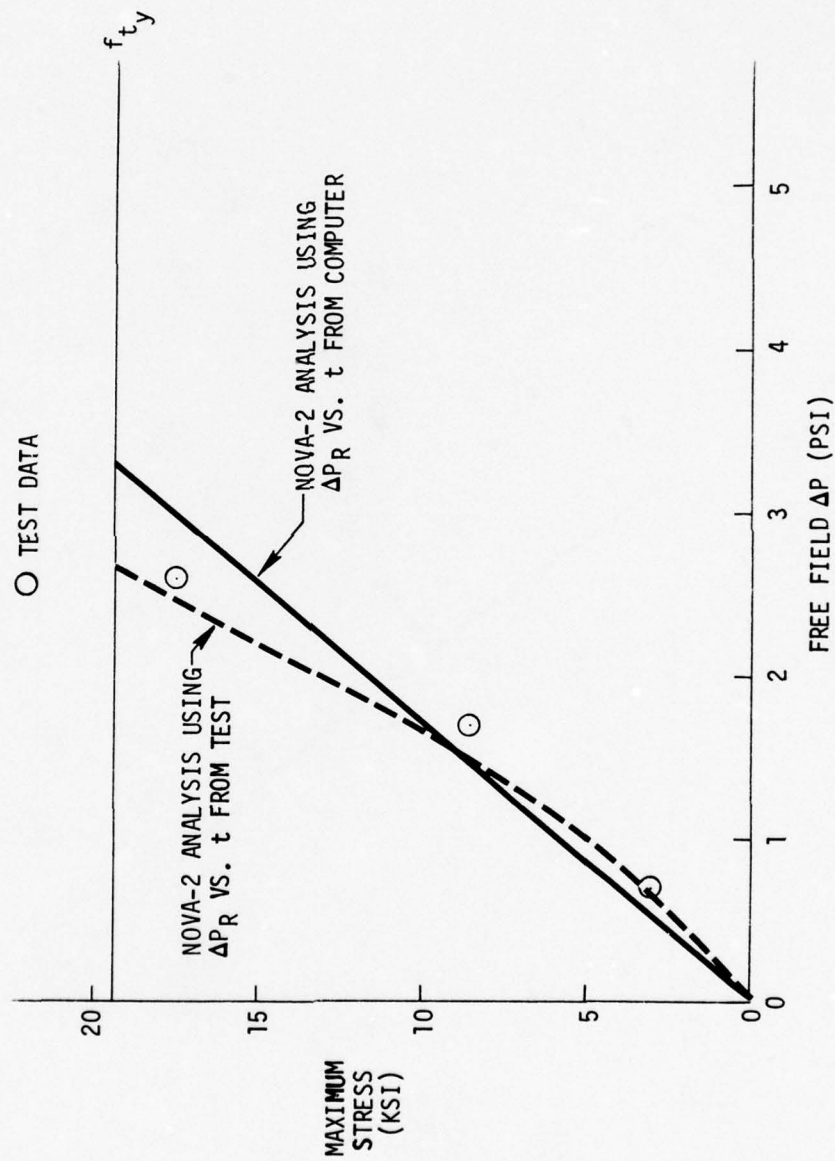


FIGURE 61. STRESS VS. FREE FIELD OVERPRESSURE - SPECIMEN 4

TEST SPECIMEN NO. 4
 STRESS AT CENTER OF EDGE
 INCIDENCE ANGLE = 60°
 (GAUGES S4-3, 4, 5)

○ TEST DATA

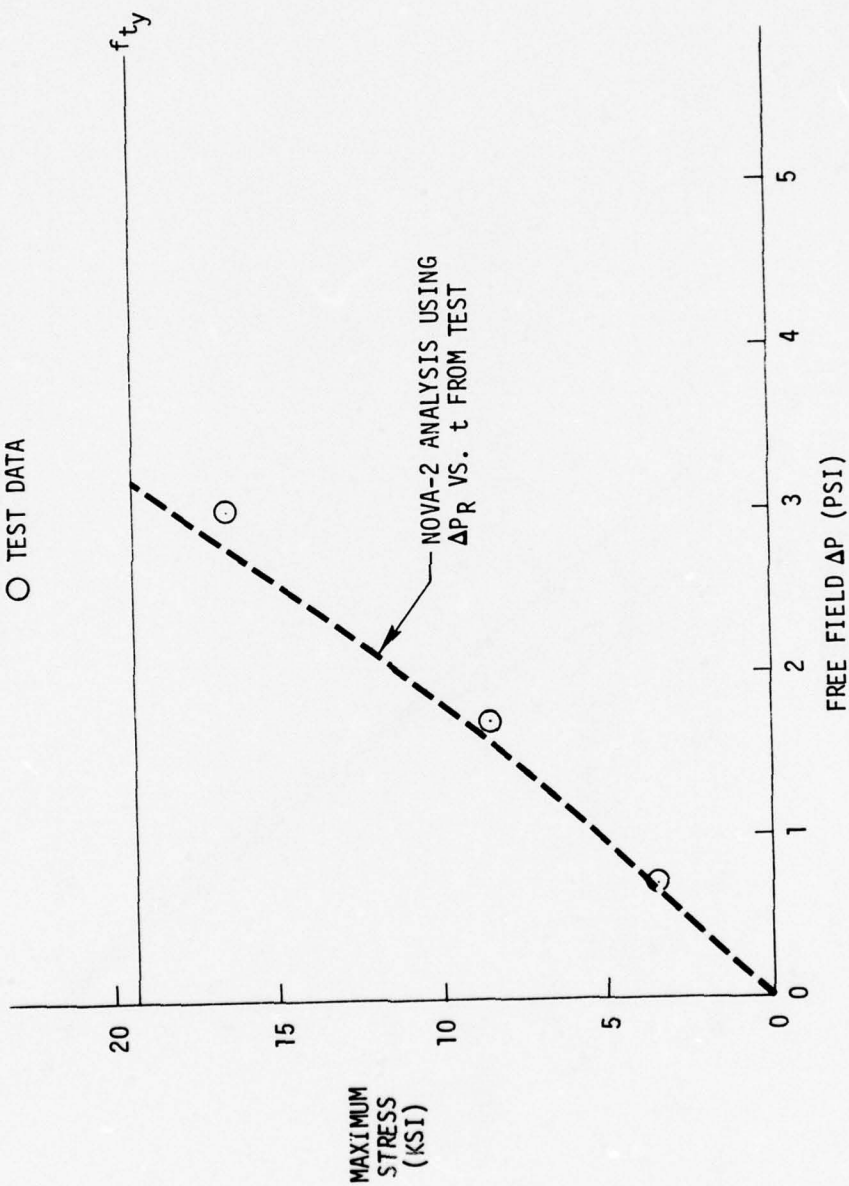


FIGURE 62. STRESS VS. FREE FIELD OVERPRESSURE - SPECIMEN 4

TEST SPECIMEN NO. 4
 STRESS AT CENTER OF EDGE
 INCIDENCE ANGLE = 30°
 (GAUGES S4-3, 4, 5)

○ TEST DATA

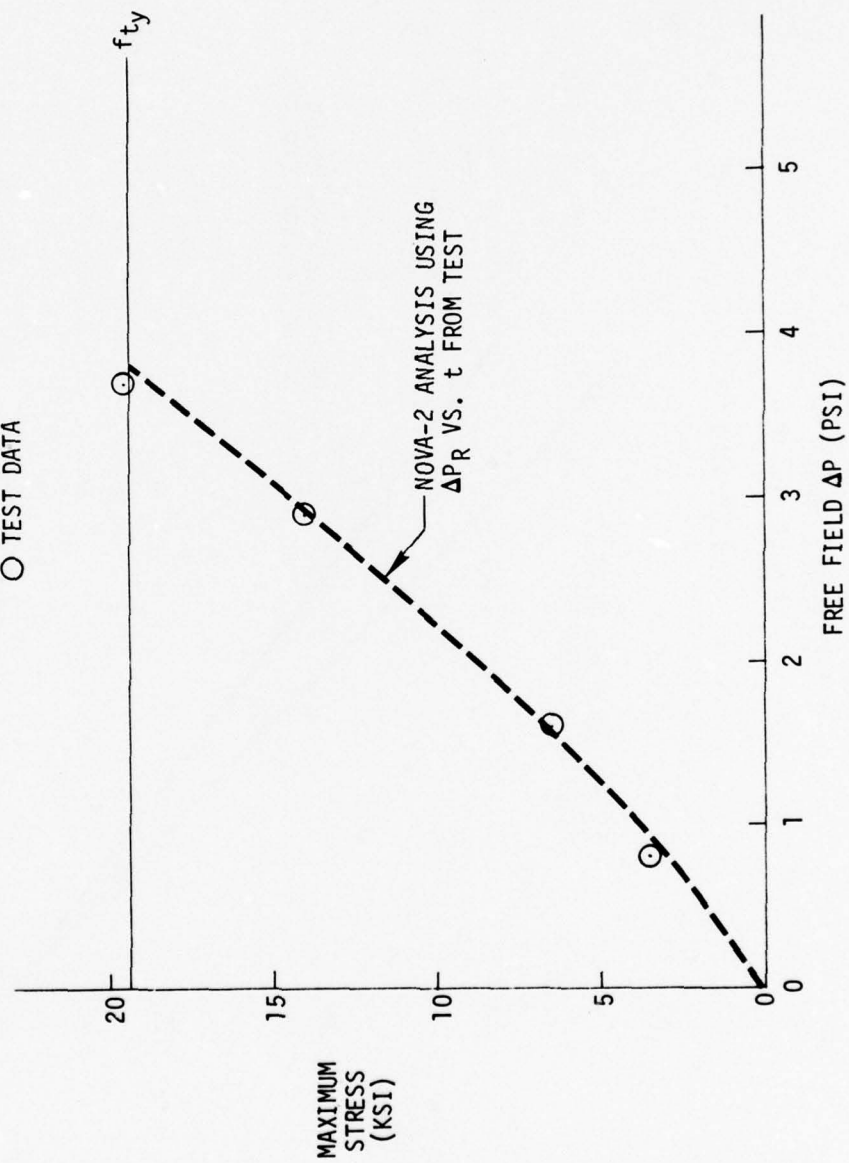


FIGURE 63. STRESS VS. FREE FIELD OVERPRESSURE - SPECIMEN 4

TEST SPECIMEN NO. 4
 DEFLECTION AT CENTER OF PANEL
 INCIDENCE ANGLE = 90°
 (GAUGE D4-10)

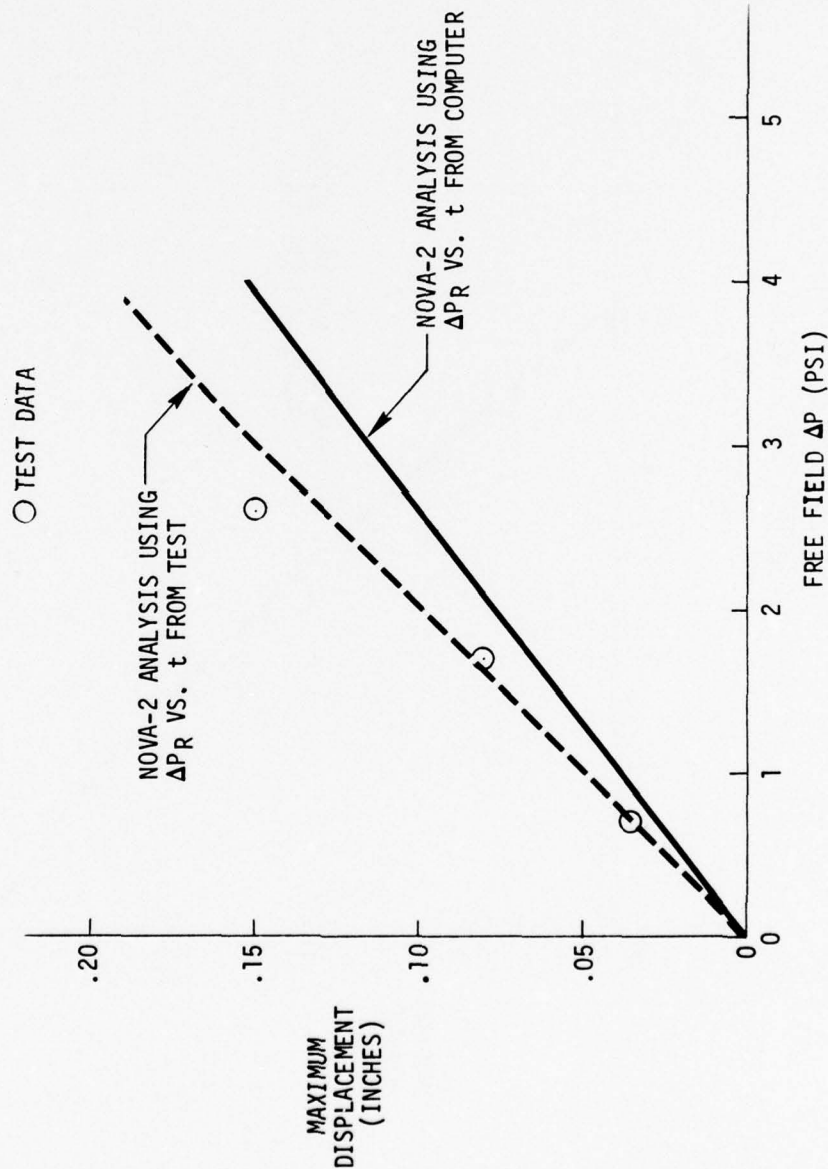


FIGURE 64. DISPLACEMENT VS FREE FIELD OVERPRESSURE - SPECIMEN 4

TEST SPECIMEN NO. 4
 DEFLECTION AT CENTER OF PANEL
 INCIDENCE ANGLE = 60°
 (GAUGE D4-10)
 ○ TEST DATA

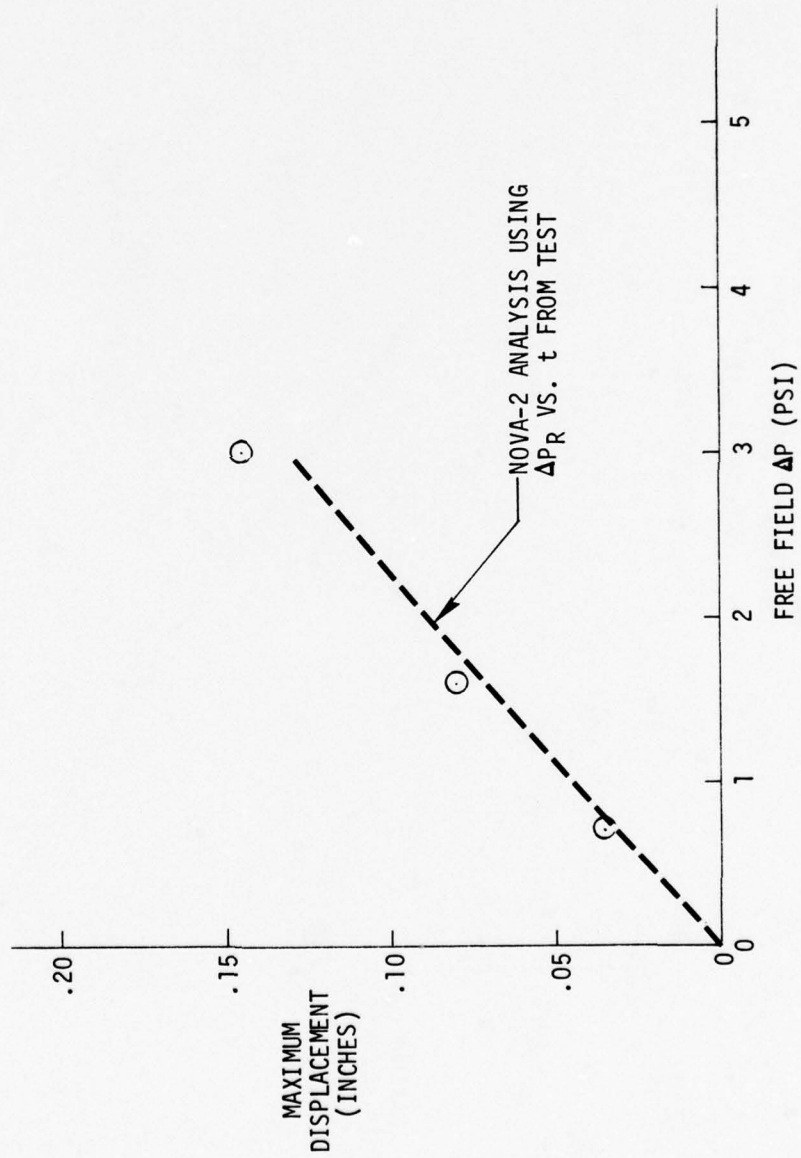


FIGURE 65. DISPLACEMENT VS. FREE FIELD OVERPRESSURE - SPECIMEN 4

TEST SPECIMEN NO. 4
 DEFLECTION AT CENTER OF PANEL
 INCIDENCE ANGLE = 30°
 (GAUGE D4-10)

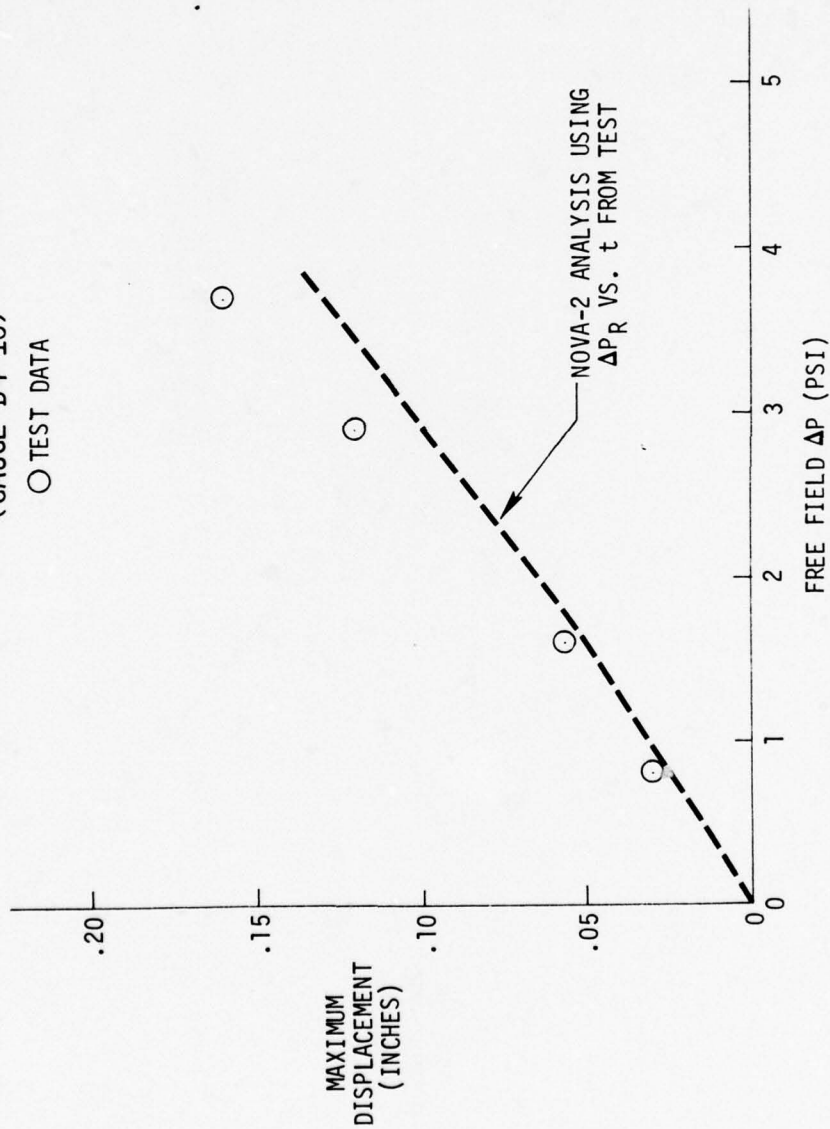


FIGURE 66. DISPLACEMENT VS. FREE FIELD OVERPRESSURE - SPECIMEN 4

Figure 67 illustrates measured reflection factor data as a function of shock strength for the three incidence angles. Reflection factor is defined as the peak reflected overpressure on the specimen divided by the peak free field overpressure measured at the wall of the test section at the test specimen location. As described earlier, free field overpressure data was obtained by smoothing the peaks and valleys of the ragged pressure pulse over the response time of interest (approximately 10-20 milliseconds). Also shown in Figure 67 are reflection factor data obtained from NOVA-2 for $\theta = 90^\circ$.

The data from Figure 67 were cross plotted and are illustrated in Figure 68 as a function of incidence angle. These data indicate that for free field overpressure levels between 1.0 psi and 3.0 psi, reflection factors are relatively constant for incidence angles of 60° and 90° , whereas the enhancement of the incident pressure pulse is somewhat less for 30° .

Figure 69 illustrates a comparison of test and analysis stress time history for test shot number ten involving specimen 4. The test stress data shown is at one of the three edges that was instrumented. Therefore, the peak value does not agree identically with the peak value shown in Figure 61. Both test and analysis indicate a response frequency of approximately 200 CPS. The analysis was terminated after approximately 10 milliseconds.

In addition, a permanent deformation of 0.16 inches was measured manually at the panel center after the final shot for this specimen. The condition of specimen 4 subsequent to the final test shot is illustrated in the photograph in Volume II, page 127. The analysis response data associated with the final shot indicated approximately 0.2 inches permanent deformation. The maximum recorded strain associated with the final shot was approximately 18,500 micro-inches per inch (average of three gauges). For this condition, the analysis predicted 18,360 micro-inches per inch.

8.3.5 Test Specimen Number 5

Specimen 5 was a single layer homogeneous flat panel with all four sides fixed as described in Tables I and II. Tests and analyses were conducted for this specimen using shock/structure incidence angles of 90° , 60° , and 30° . The primary objective of testing at angles other than 90° , i.e., "head-on", was to generate data regarding shock enhancement as a function of incidence angle and shock strength.

Analysis results and test results are shown in Figures 70 - 75 which indicate maximum stress at the center of a clamped edge and maximum displacement at the center of the panel as expected. The stress data represents an average of gauges at the centers of three edges of the panel. The NOVA-2 analysis results were obtained by utilizing a 7 by 7 (MG = MB = 7) modal matrix and retaining 25 modal combinations, as was done in the static analysis.

TEST SPECIMEN NO. 4
REFLECTION FACTOR DATA

- TEST DATA ($\theta = 90^\circ$)
- TEST DATA ($\theta = 60^\circ$)
- △ TEST DATA ($\theta = 30^\circ$)

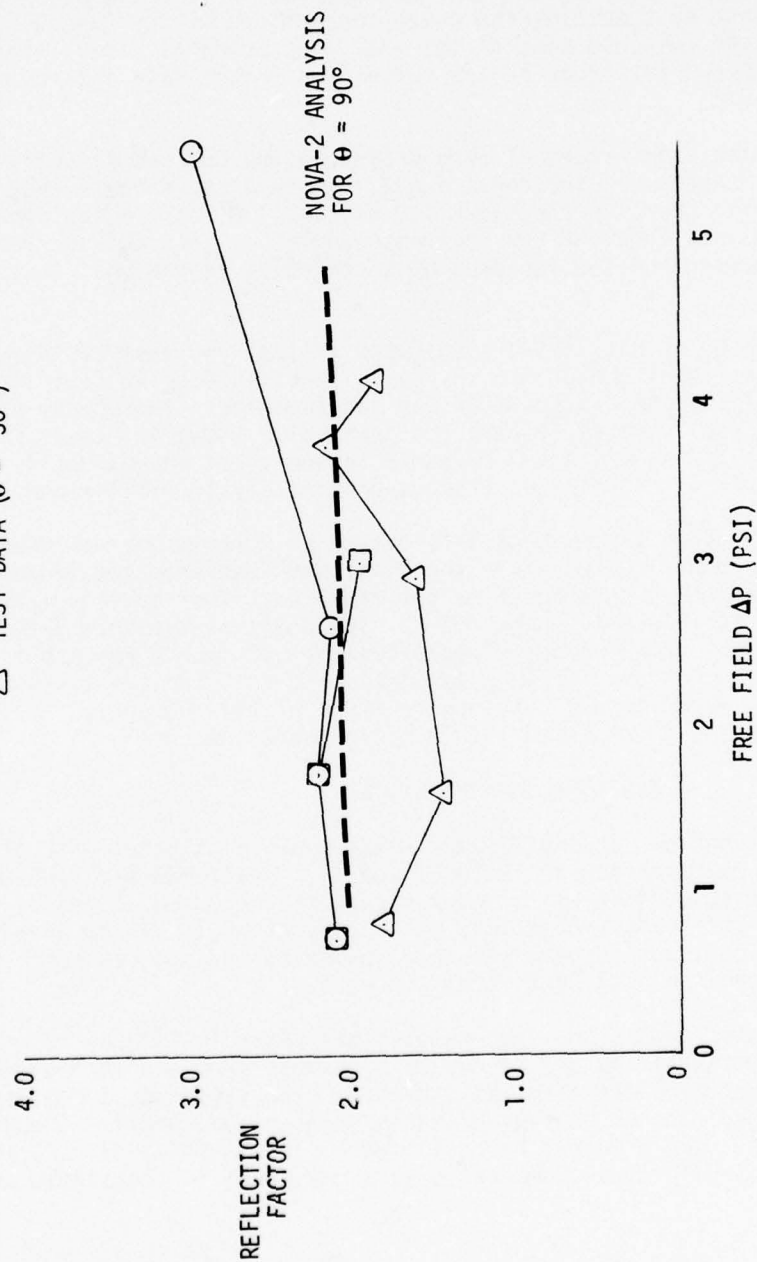


FIGURE 67. SHOCK REFLECTION FACTOR VS. FREE FIELD OVERPRESSURE - SPECIMEN 4

TEST SPECIMEN NO. 4
MEASURED PRESSURE DATA

- $\Delta P_{FF} = 1.0 \text{ PSI}$
 □ $\Delta P_{FF} = 2.0 \text{ PSI}$
 △ $\Delta P_{FF} = 3.0 \text{ PSI}$

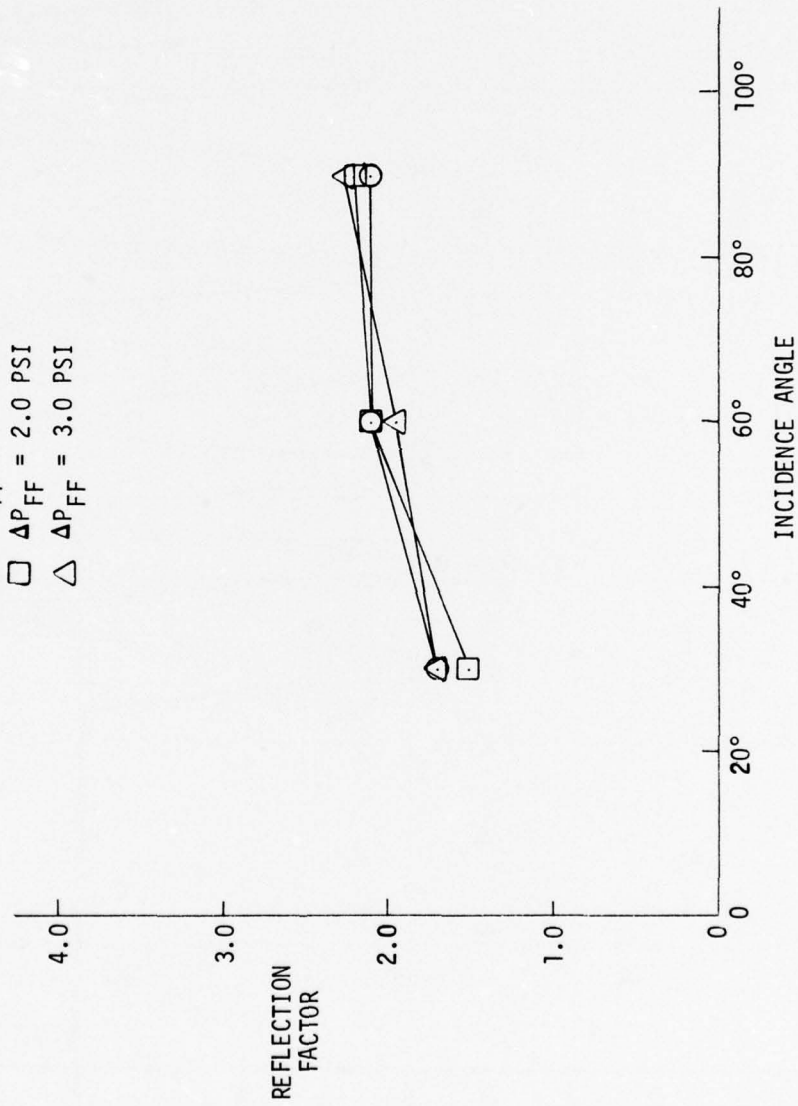


FIGURE 68. SHOCK REFLECTION FACTOR VS. INCIDENCE ANGLE - SPECIMEN 4

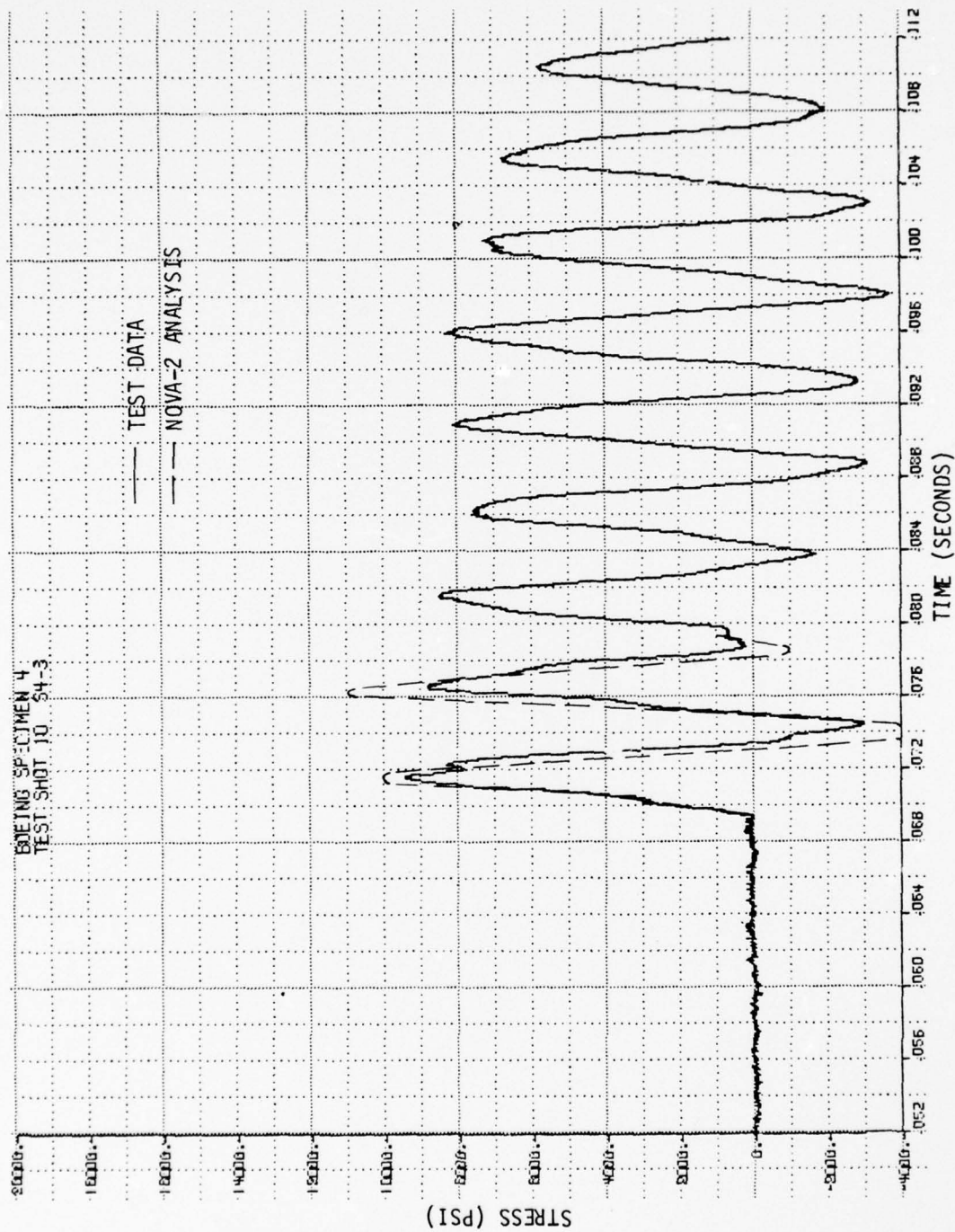


FIGURE 69. STRESS TIME HISTORY - SPECIMEN 4

TEST SPECIMEN NO. 5
STRESS AT CENTER OF EDGE
INCIDENCE ANGLE = 90°
(GAUGES S5-3, 4, 5)

○ TEST DATA

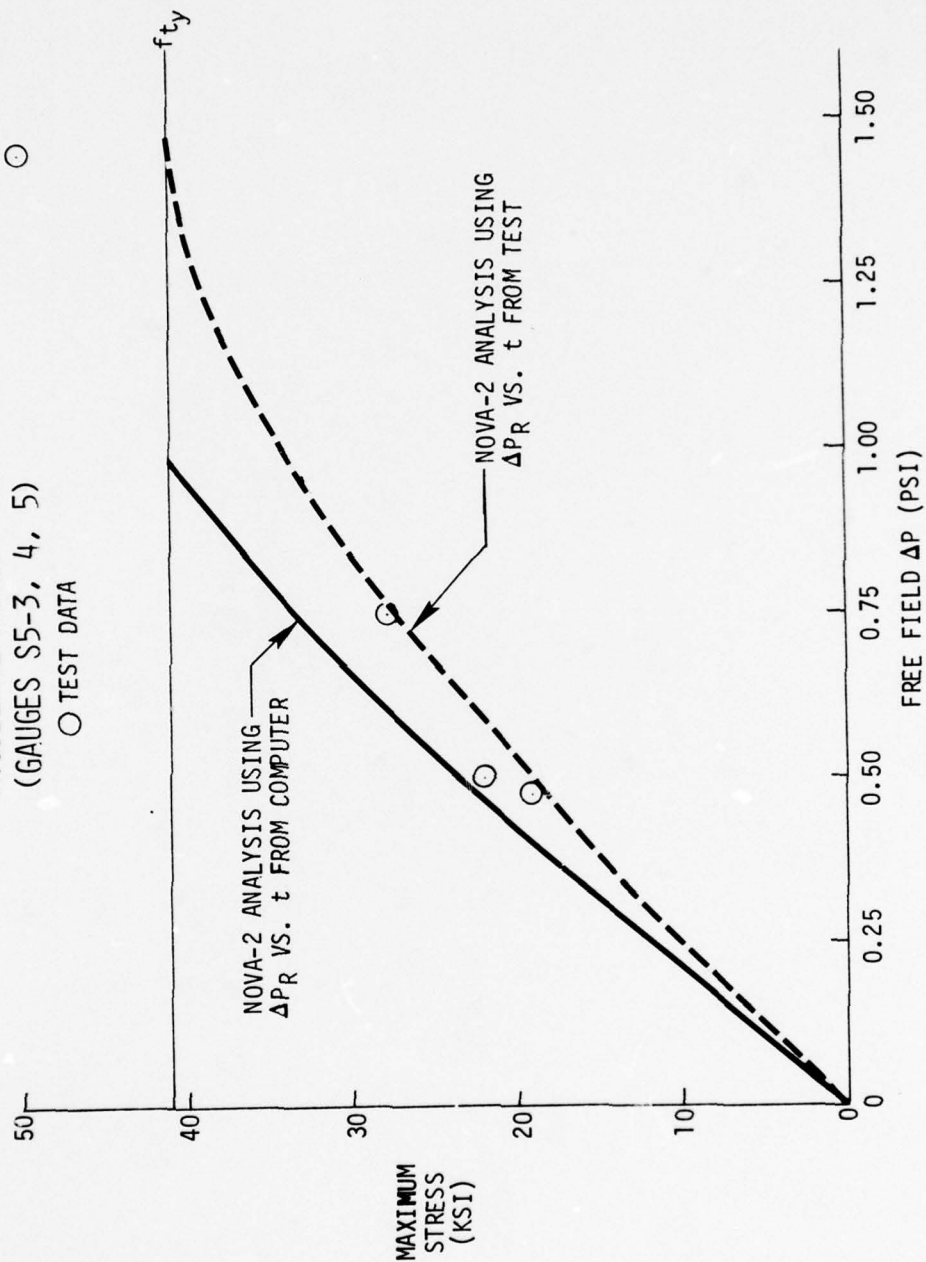


FIGURE 70. STRESS VS. FREE FIELD OVERPRESSURE - SPECIMEN 5

TEST SPECIMEN NO. 5
 STRESS AT CENTER OF EDGE
 INCIDENCE ANGLE = 60°
 (GAUGES S5-3, 4, 5)

○ TEST DATA

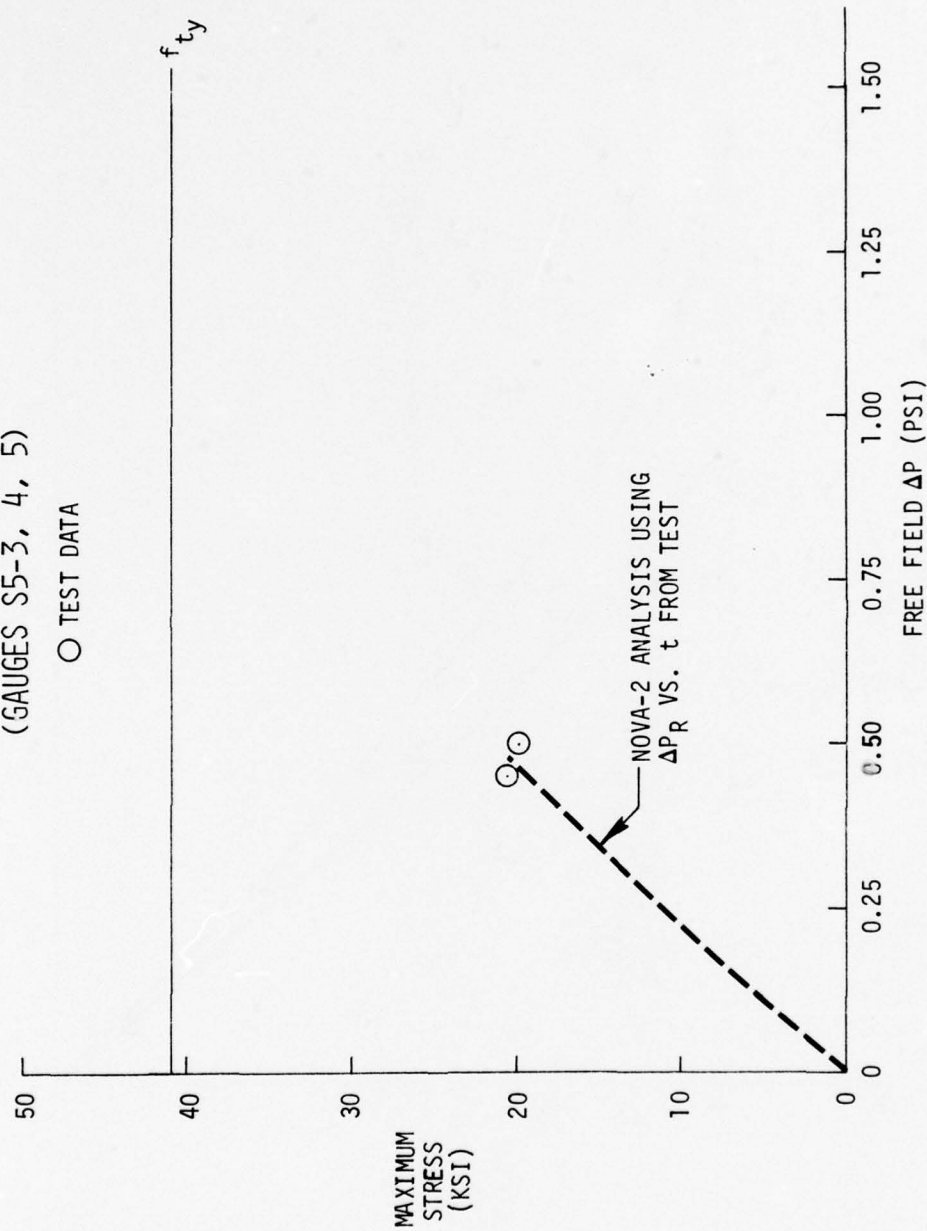


FIGURE 71. STRESS VS. FREE FIELD OVERPRESSURE - SPECIMEN 5

TEST SPECIMEN NO. 5
 STRESS AT CENTER OF EDGE
 INCIDENCE ANGLE = 30°
 (GAUGES S5-3, 4, 5)
 O TEST DATA

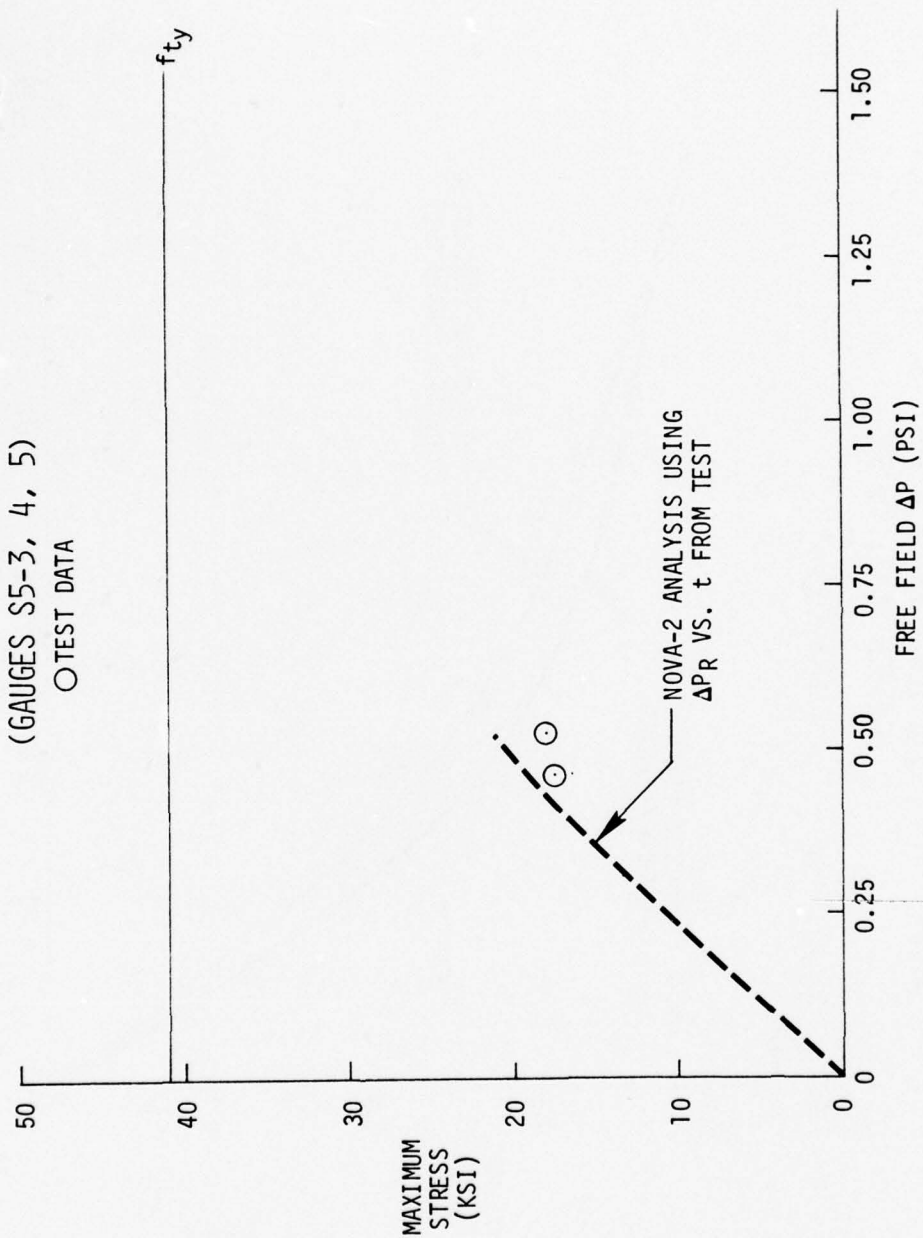


FIGURE 72. STRESS VS. FREE FIELD OVERPRESSURE - SPECIMEN 5

TEST SPECIMEN NO. 5
 DISPLACEMENT AT PANEL CENTER
 INCIDENCE ANGLE = 90°
 (GAUGES S5-3, 4, 5)

○ TEST DATA

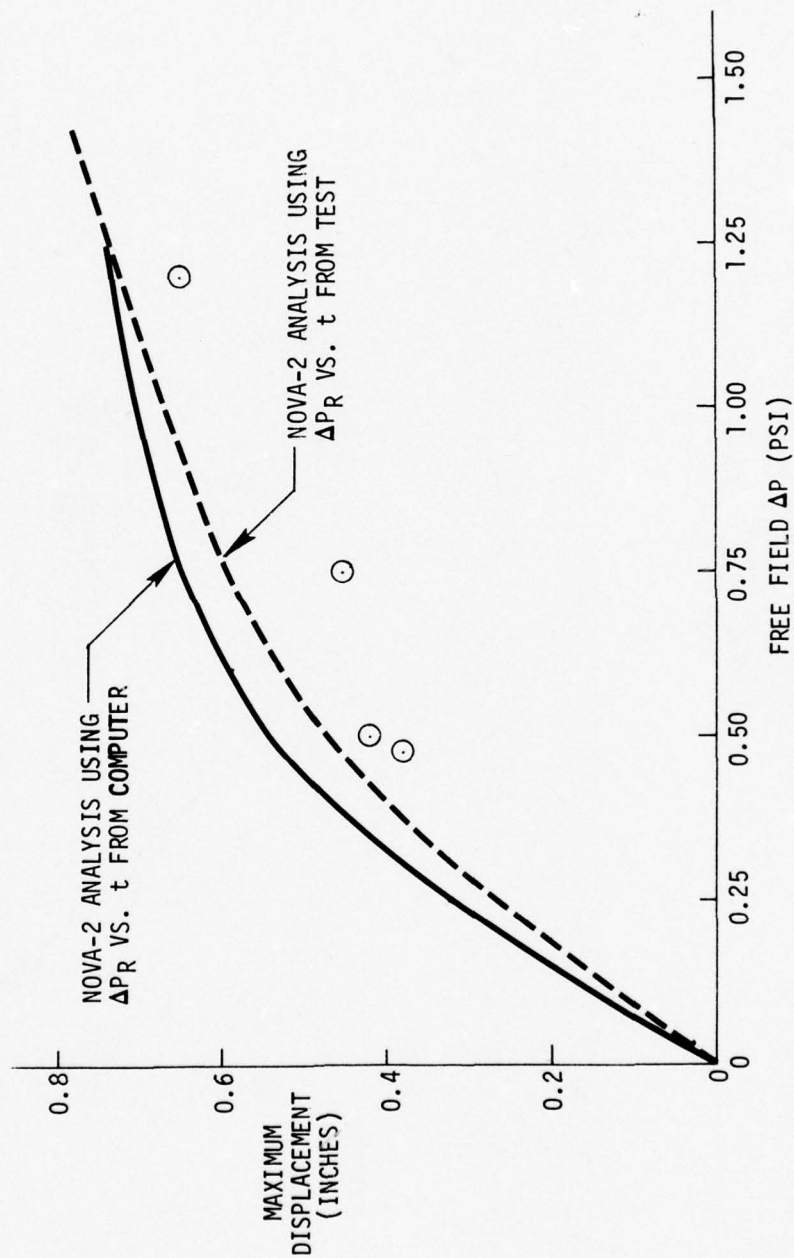


FIGURE 73. DISPLACEMENT VS. FREE FIELD OVERPRESSURE - SPECIMEN 5

TEST SPECIMEN NO. 5
DISPLACEMENT AT CENTER OF PANEL
INCIDENCE ANGLE = 60°
(GAUGE D5-10)

○ TEST DATA

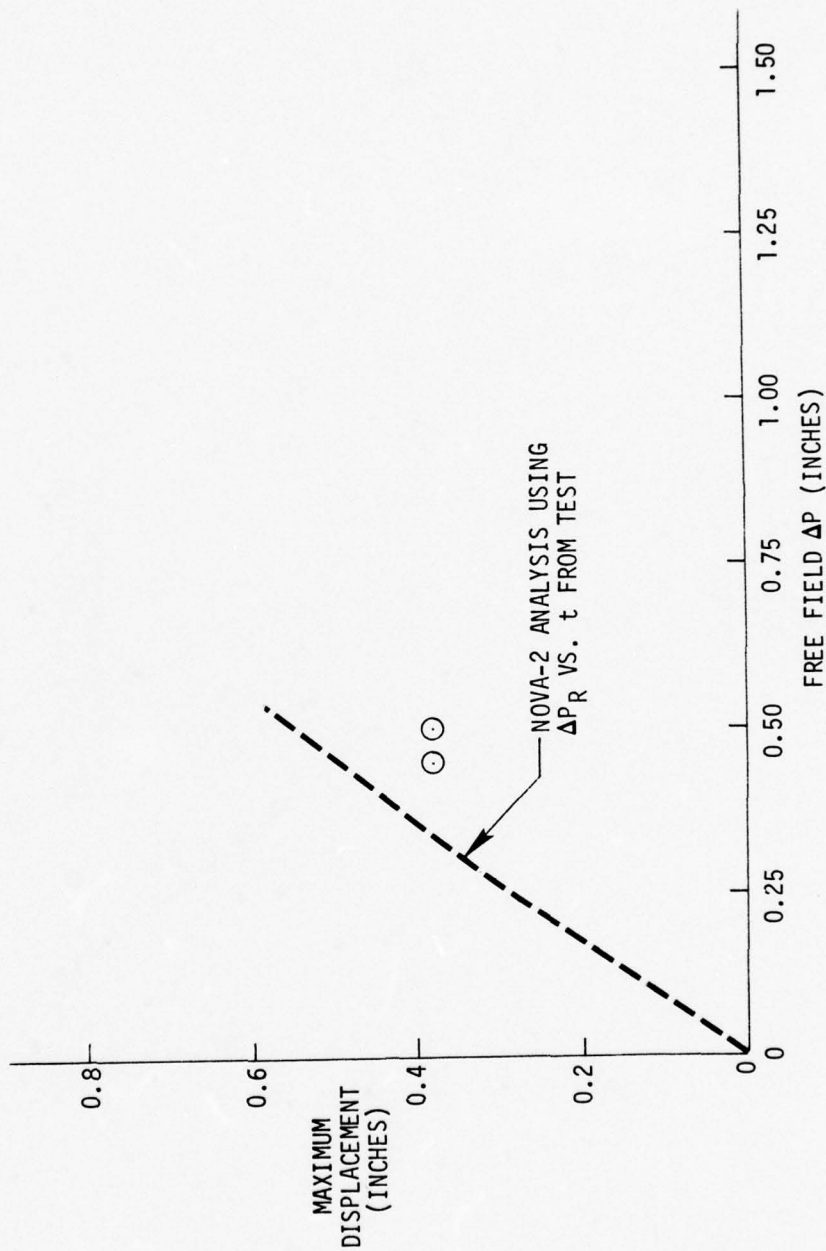


FIGURE 74. DISPLACEMENT VS. FREE FIELD OVERPRESSURE - SPECIMEN 5

TEST SPECIMEN NO. 5
 DISPLACEMENT AT CENTER OF PANEL
 INCIDENCE ANGLE = 30°
 (GAUGE D5-10)

○ TEST DATA

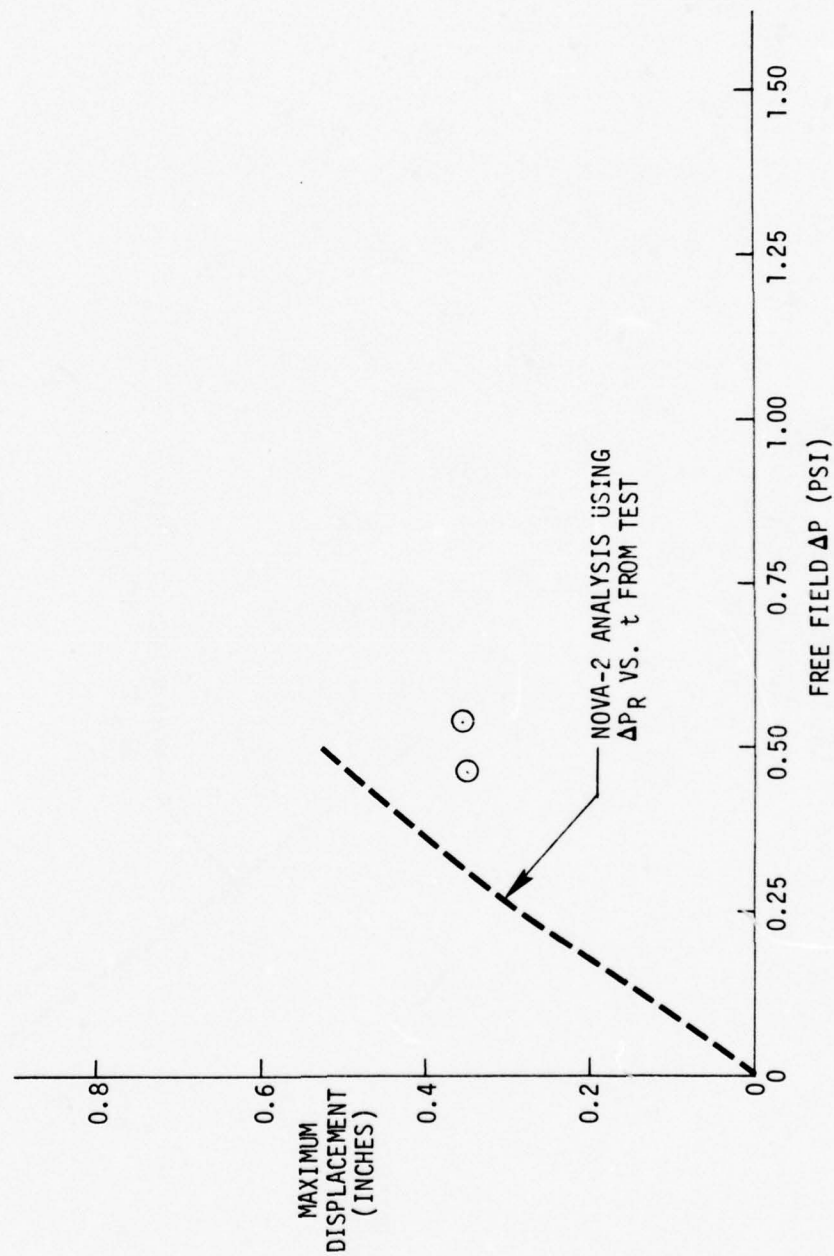


FIGURE 75. DISPLACEMENT VS. FREE FIELD OVERPRESSURE - SPECIMEN 5

Reasonably good agreement between test and analysis stress data is indicated for all three orientations. As shown in Figures 73 - 75, analysis results predict displacements at the center of the panel that are consistently higher than that measured.

Figure 76 illustrates a comparison of test and analysis stress time history for test shot number nine involving specimen 5. The test stress data shown is at one of the three edges that was instrumented. Therefore, the peak value shown does not agree identically with the peak value shown in Figure 70. Test data indicate a response frequency of approximately 140 cps, whereas analysis results exhibit a response frequency of approximately 160 cps. The analysis was terminated after approximately 10 milliseconds.

Since the peak free field shock strengths for the shots at 30° and 60° incidence angles were all essentially identical, no plots of reflection factors are shown. However, the data indicates essentially the same amount of amplification due to reflection (reflection factor of approximately 1.8) for incidence angles of 30°, 60°, and 90°. This was for peak free field shock intensities of approximately 0.5 psi. Substantial scatter was seen in the data at this low pressure intensity.

In addition, a permanent deformation of 0.92 inches was measured manually at the panel center after the final shot for this specimen. The condition of specimen 5 subsequent to the final test shot is illustrated in the photograph in Volume II, page 223. The analysis response data associated with the final shot indicated approximately 1.25 inches permanent deformation. The maximum recorded strain associated with the final shot was approximately 13,600 micro-inches per inch (average of three gauges). For this condition, the analysis predicted 19,200 micro-inches per inch.

8.3.6 Test Specimen Number 6

Specimen 6 was a single layer homogeneous curved panel with all four edges clamped as described in Tables I and II. All analyses and tests for specimen 6 were conducted for a blast/structure incidence angle of 90°, i.e., the shock propagation vector was perpendicular to the tangent plane at the center of the panel.

Specimen six was analyzed as a curved panel without initial imperfection and as a unit width curved beam for blast environments generated by the NOVA-2 computer program. These analysis results are compared to the test results for several panel locations in Figures 77 - 82. These analysis results were obtained by utilizing 25 modes in the NOVA-2 panel model from a 7 x 7 modal matrix and by assuming no initial imperfections. Also shown are the analysis results associated with a unit width curved beam representing a strip removed from the center of the panel.

Specimen 6 was also analyzed by utilizing the reflected pressure time histories that were measured during the shock tests. Included in this analysis model were initial radial imperfections as shown. These initial imperfections are consistent with those discussed in section 8.2.6. As discussed in section 8.2.6, no measurements of initial imperfections were made prior to shock load

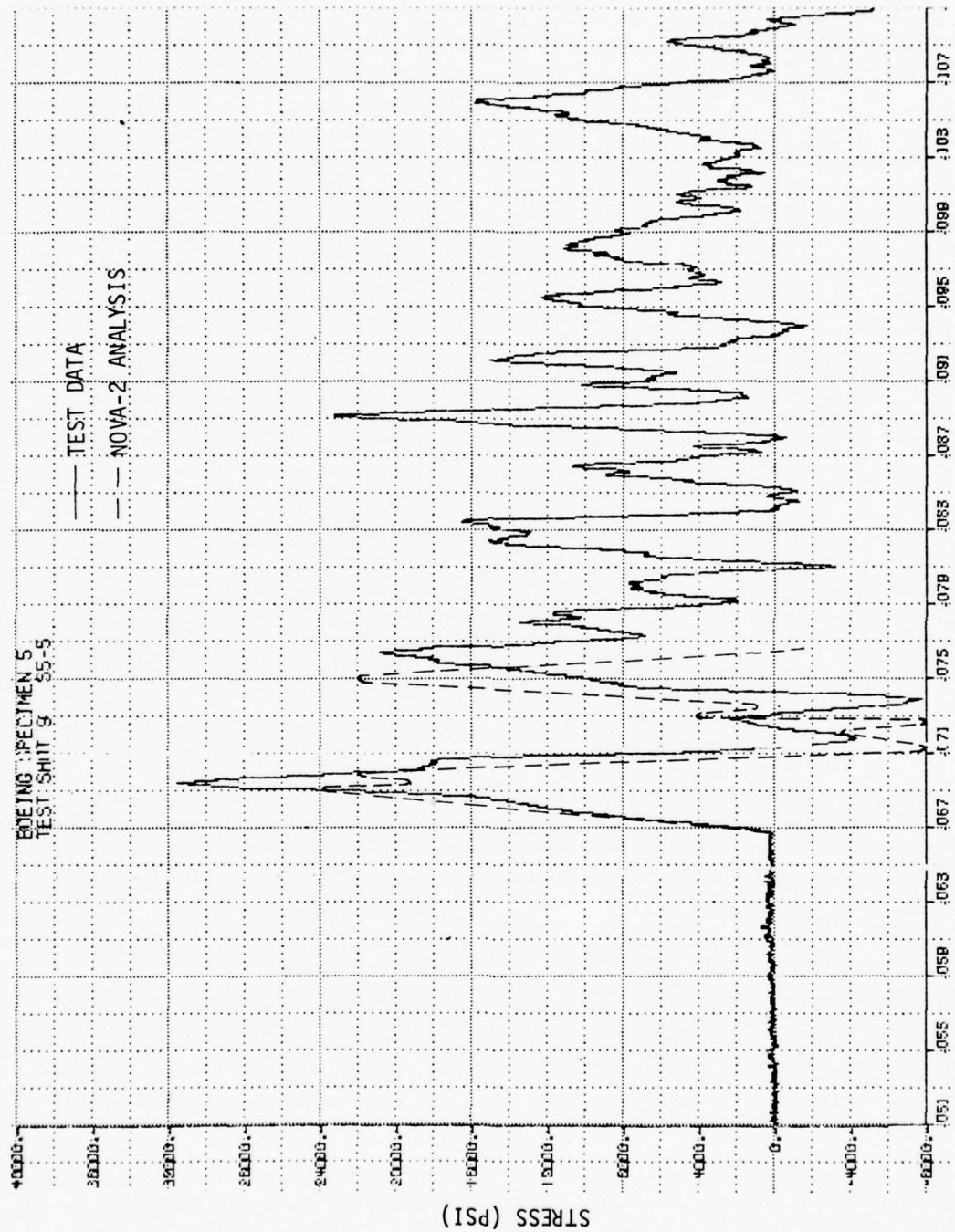


FIGURE 76. STRESS TIME HISTORY - SPECIMEN 5

TEST SPECIMEN NO. 6
STRESS AT PANEL CENTER (OUTSIDE)
(GAUGE S6-1)

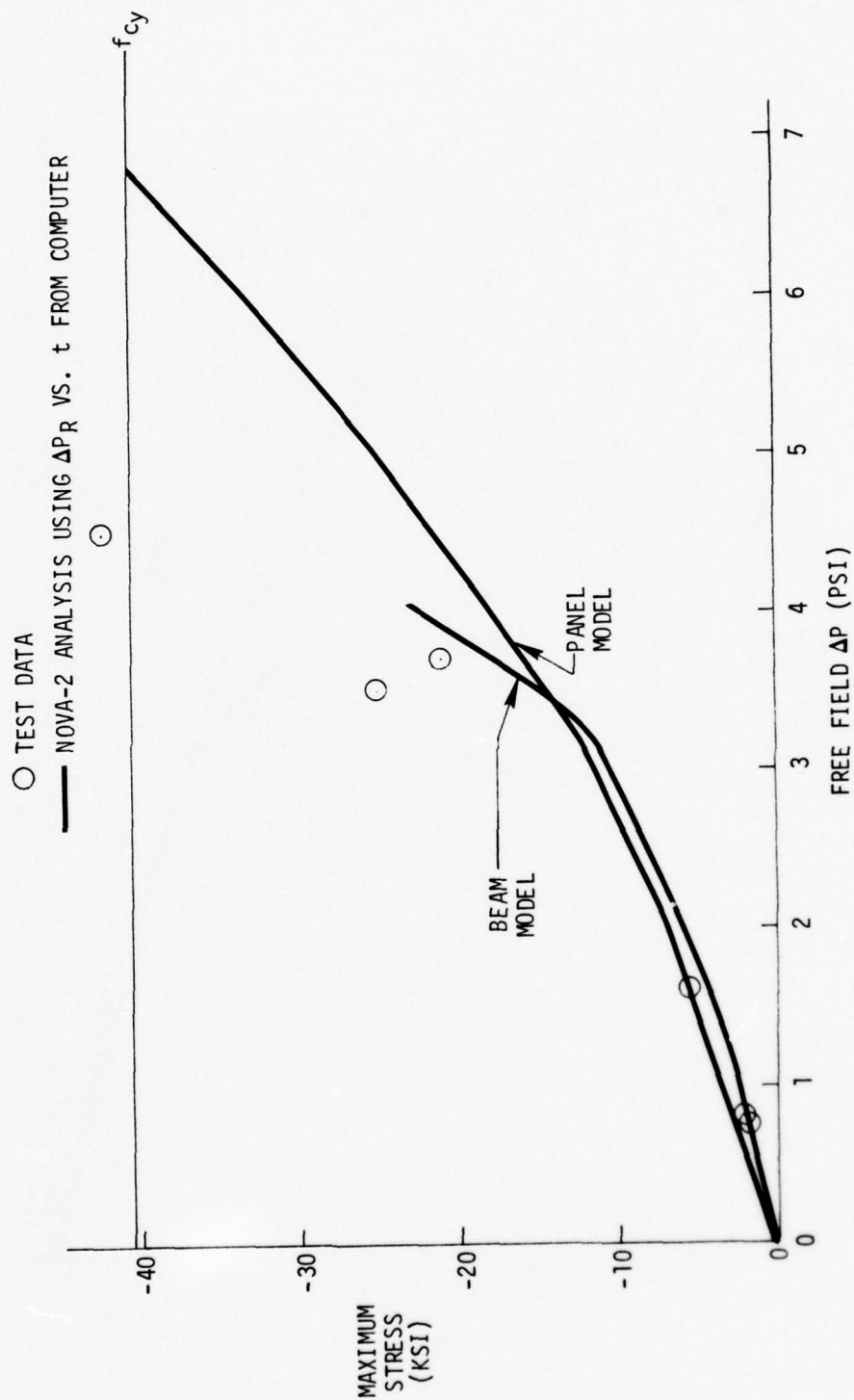


FIGURE 77. STRESS VS. FREE FIELD OVERPRESSURE - SPECIMEN 6

TEST SPECIMEN NO. 6
STRESS AT PANEL CENTER (INSIDE)
(GAUGE S6-2)

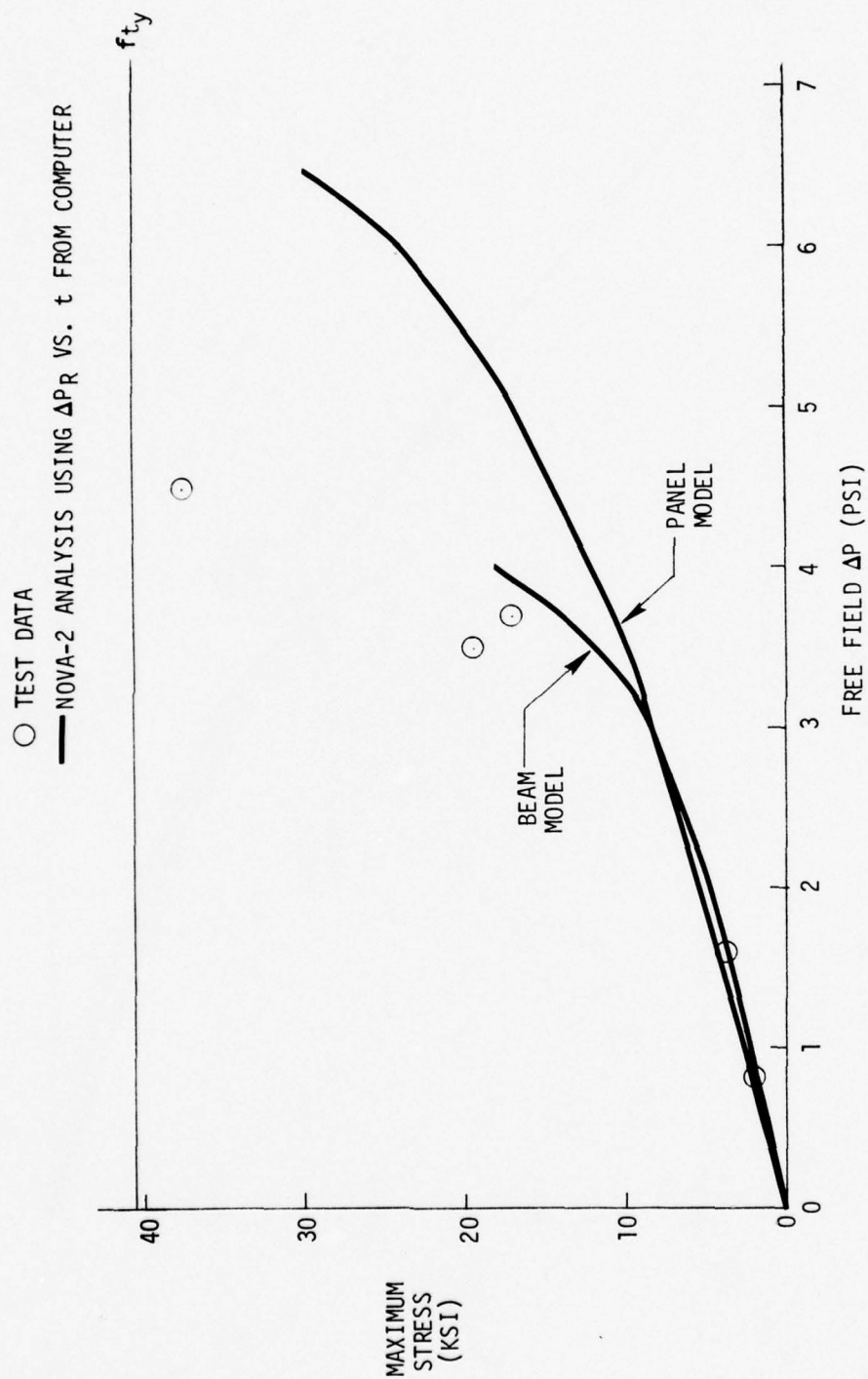


FIGURE 78. STRESS VS. FREE FIELD OVERPRESSURE - SPECIMEN 6

TEST SPECIMEN NO. 6
STRESS AT CENTER OF LONG EDGE (OUTSIDE)
(GAUGE S6-3)

○ TEST DATA
— NOVA-2 ANALYSIS USING ΔP_R VS t FROM COMPUTER

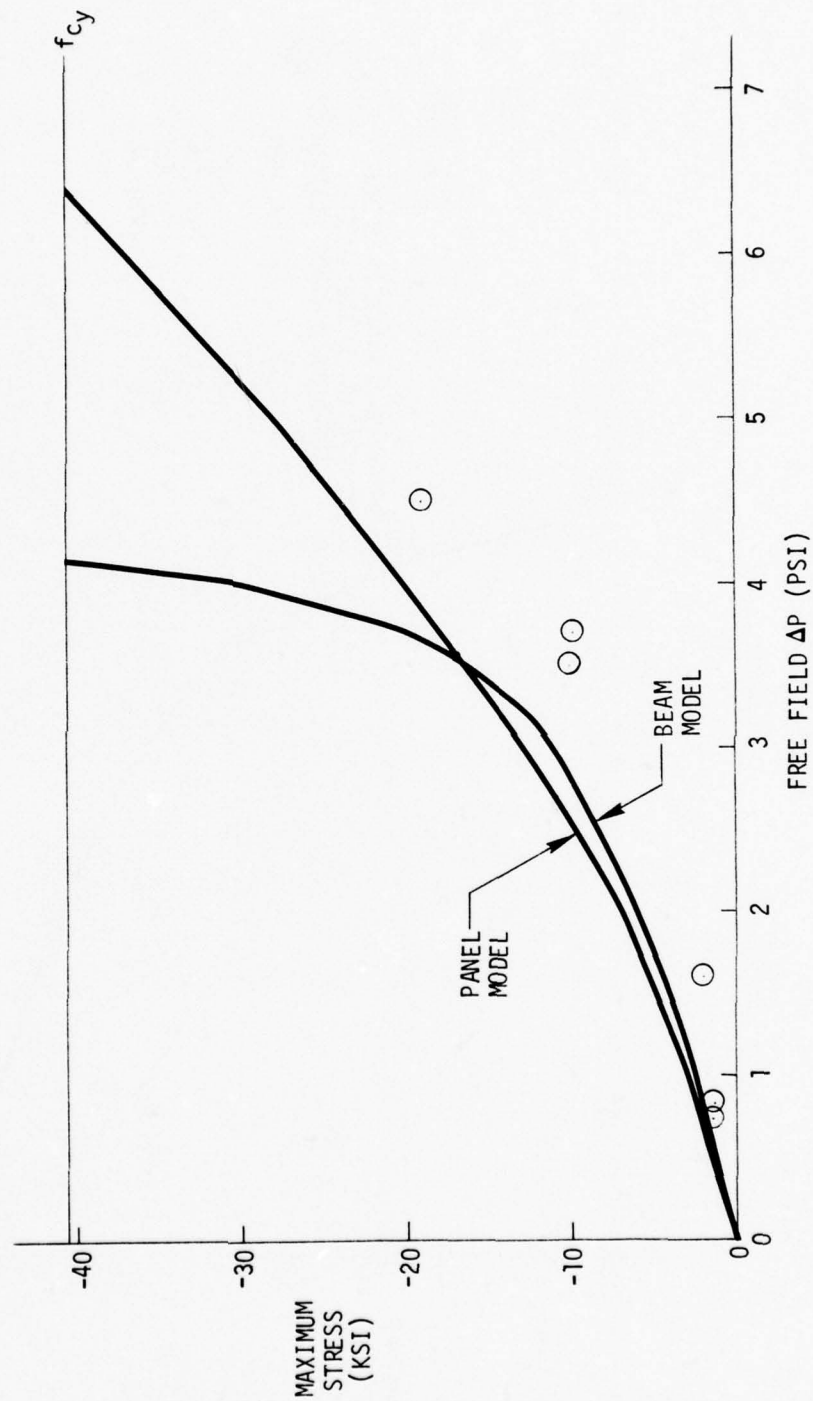


FIGURE 79. STRESS VS. FREE FIELD OVERPRESSURE - SPECIMEN 6

TEST SPECIMEN NO. 6
STRESS AT PANEL CENTER (INSIDE)
(GAUGE S6-2)

○ TEST DATA

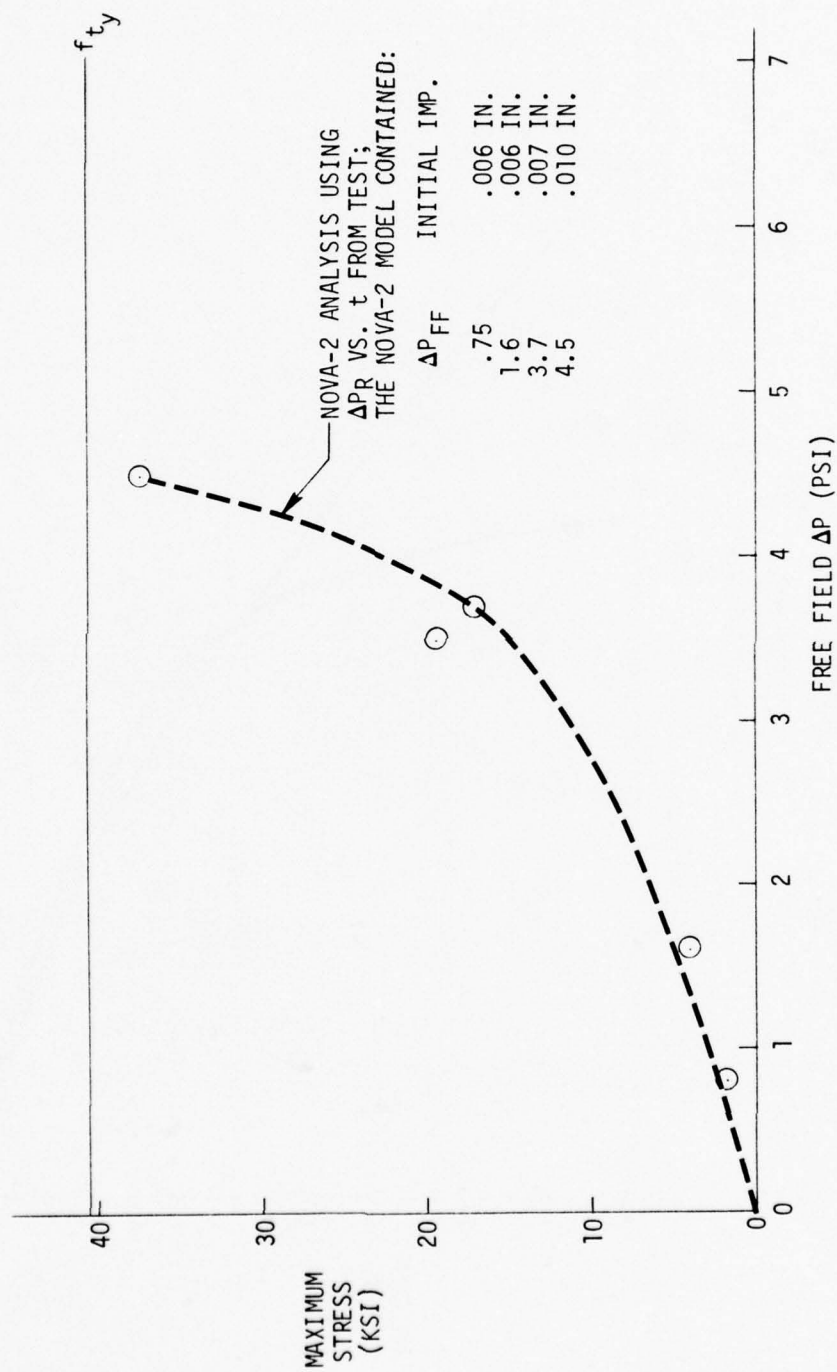


FIGURE 80. STRESS VS. FREE FIELD OVERPRESSURE - SPECIMEN 6

TEST SPECIMEN NO. 6
STRESS AT PANEL CENTER (OUTSIDE)
(GAUGE S6-1)

○ TEST DATA

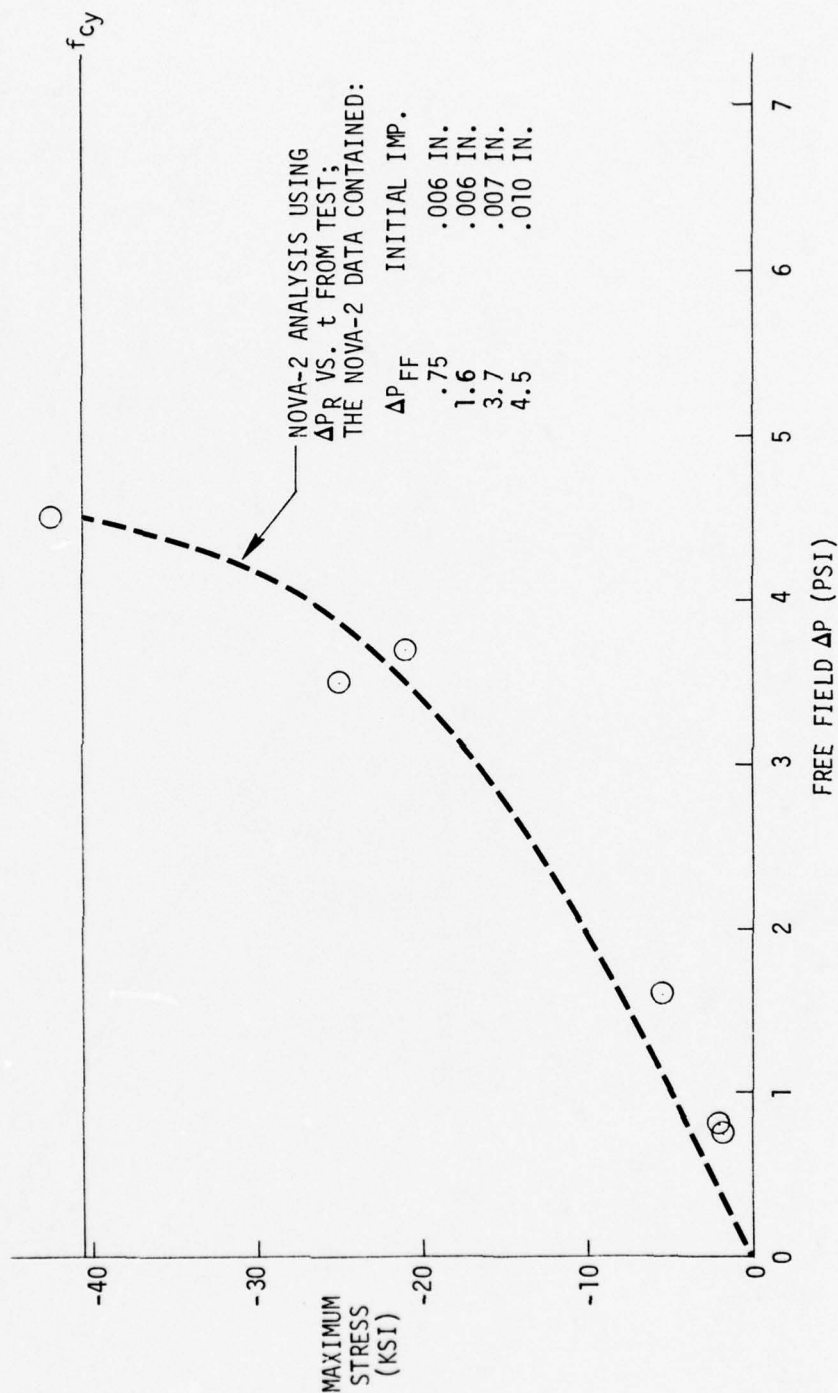


FIGURE 81. STRESS VS. FREE FIELD OVERPRESSURE - SPECIMEN 6

TEST SPECIMEN NO. 6
STRESS AT CENTER OF LONG EDGE (OUTSIDE)
(GAUGE S6-3)

○ TEST DATA

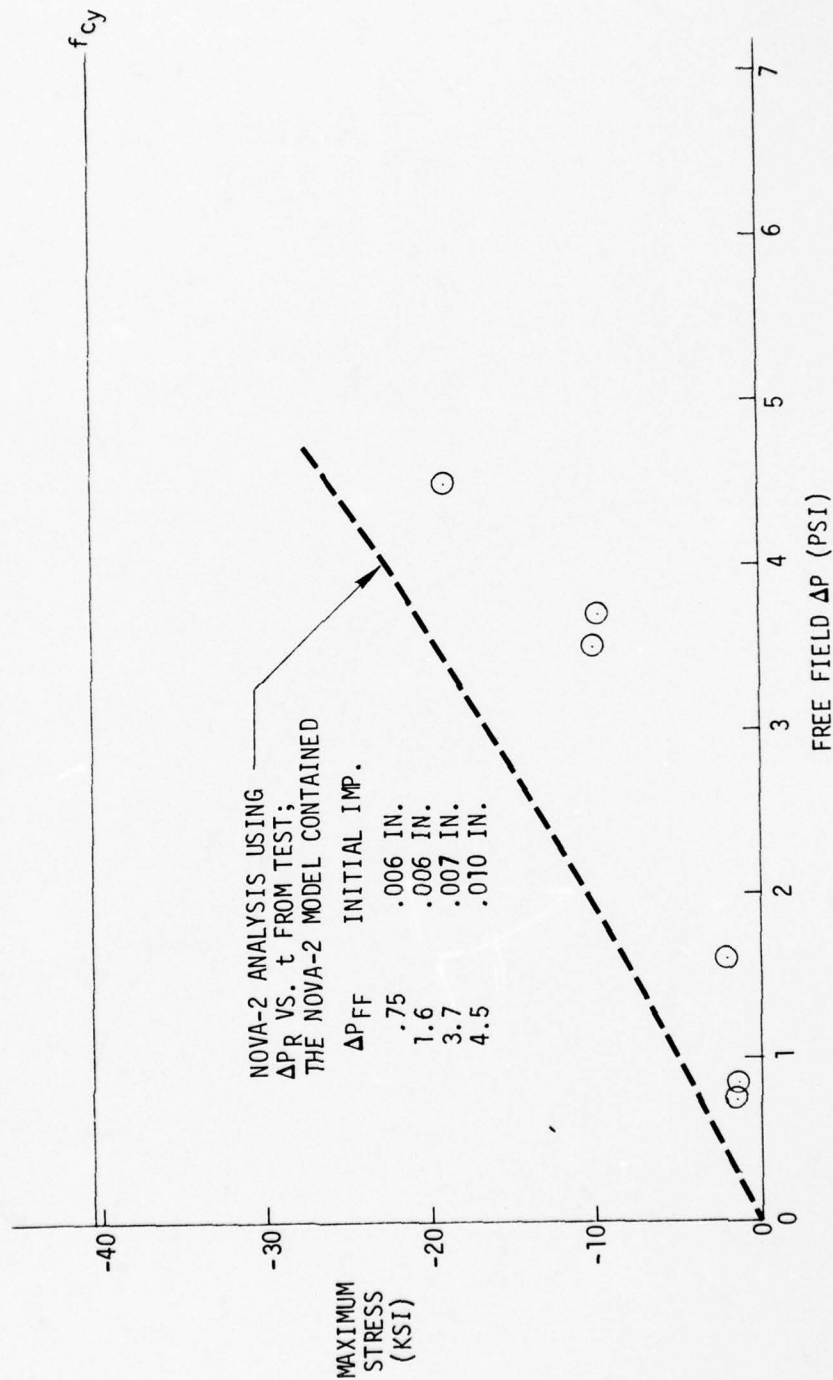


FIGURE 82. STRESS VS. FREE FIELD OVERPRESSURE - SPECIMEN 6

testing. Therefore, it is difficult to determine whether the initial imperfections included in the analysis accurately define the actual geometry of specimen 6.

A comparison of the test and analysis stress time history at the panel center for a selected test shot is shown in Figure 83. The test data indicates a fundamental response mode of approximately 100 cps with a secondary mode of approximately 600 cps superimposed on it. The analysis data indicates a fundamental frequency response mode of approximately 160 cps with a secondary mode of approximately 1500 cps superimposed on it.

No visible damage was done to specimen 6 as a result of the test shots as is evidenced in the photograph in Volume II, page 297.

The reader is cautioned that the analysis results shown for this specimen are in error due to the reasons discussed in Section 8.3. The magnitude of the error is unknown. To make a more meaningful comparison between test and analysis stress results, additional modifications must be made to NOVA-2 to allow for use of a shock loading environment that more nearly matches that which was measured.

8.3.7 Test Specimen Number 7

Specimen 7 was an aluminum honeycomb flat panel with all four edges pinned as described in Tables I and II. All analyses and tests for specimen 7 were conducted for a blast/structure incidence angle of 90°.

Analysis results and test results are shown in Figures 84 and 85 which indicate maximum stress and displacement at the center of the panel as expected. Figure 84 indicates excellent agreement between test and analysis stress data. As shown in Figure 85, the analysis consistently predicted greater displacement at the panel center than was measured.

A comparison of test and analysis stress time history for shot 2 is illustrated in Figure 86. The location is the center of the panel. Both test and analysis results indicate a response frequency of approximately 190 cps.

In addition, a permanent deformation of 0.2 inches was measured manually at the panel center after the final shot for this specimen. The condition of specimen 7 subsequent to the final test shot is illustrated in the photograph in Volume II, page 365. The analysis response data associated with the final shot indicated approximately 0.45 inches permanent deformation. The maximum recorded strain associated with the final shot was approximately 3900 micro-inches per inch in the "a" leg, 4600 micro-inches per inch in the "b" leg, and 4000 micro-inches per inch in the "c" leg of the shear rosette gauge. For this condition, the analysis predicted approximately 5400 micro-inches per inch in the "a" leg and "c" leg directions.

8.3.8 Test Specimen Number 8

Specimen 8 was an aluminum honeycomb flat panel with all four edges pinned as described in Tables I and II. Except for core cell size, this specimen was essentially identical to specimen 7. All analyses and tests for specimen 8 were conducted for a blast/structure incidence angle of 90°.

TEST SPECIMEN NO. 6
 TEST SHOT NO. 5
 STRESS AT PANEL CENTER (OUTSIDE)
 (GAUGE S6-1)

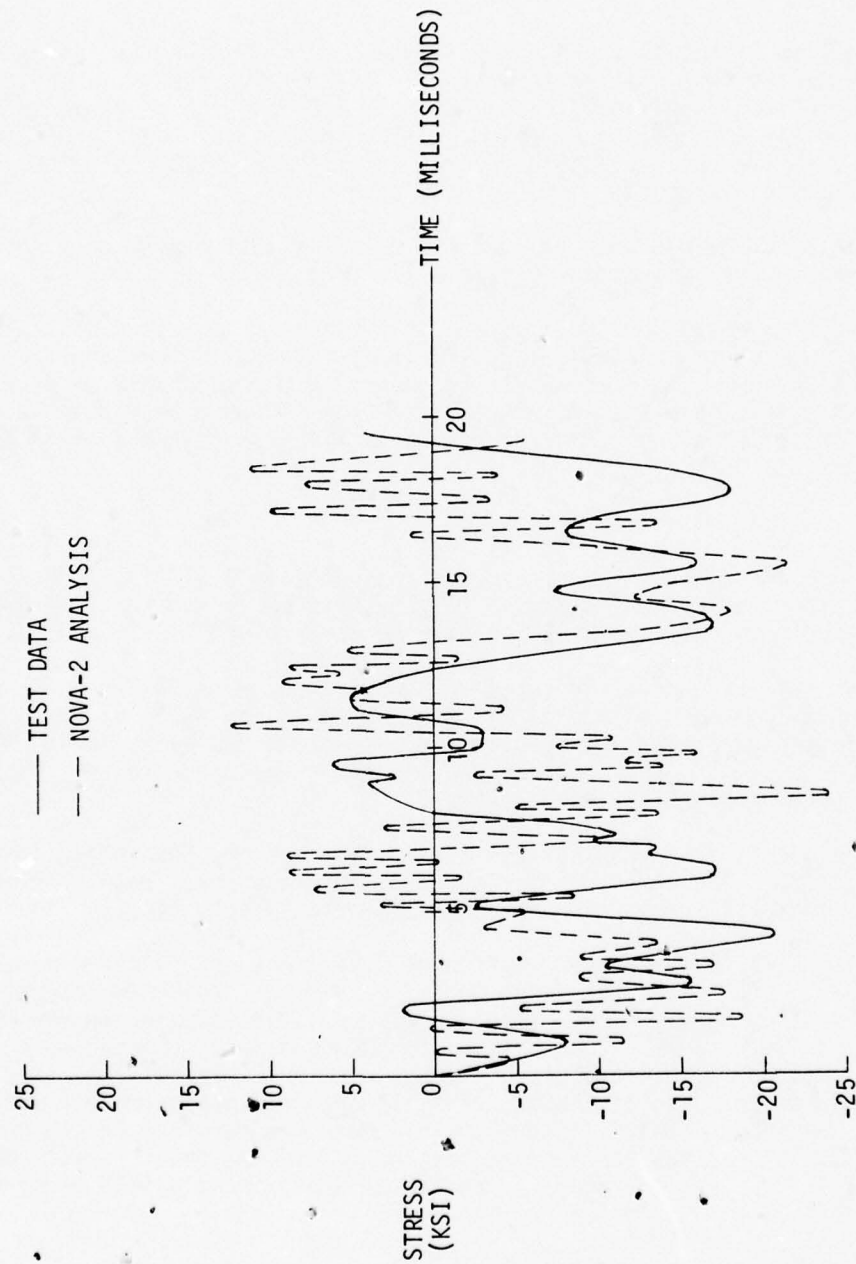


FIGURE 83. STRESS TIME HISTORY - SPECIMEN 6

TEST SPECIMEN NO. 7
STRESS AT CENTER OF PANEL (INSIDE)
(GAUGE S7-2)

○ TEST DATA

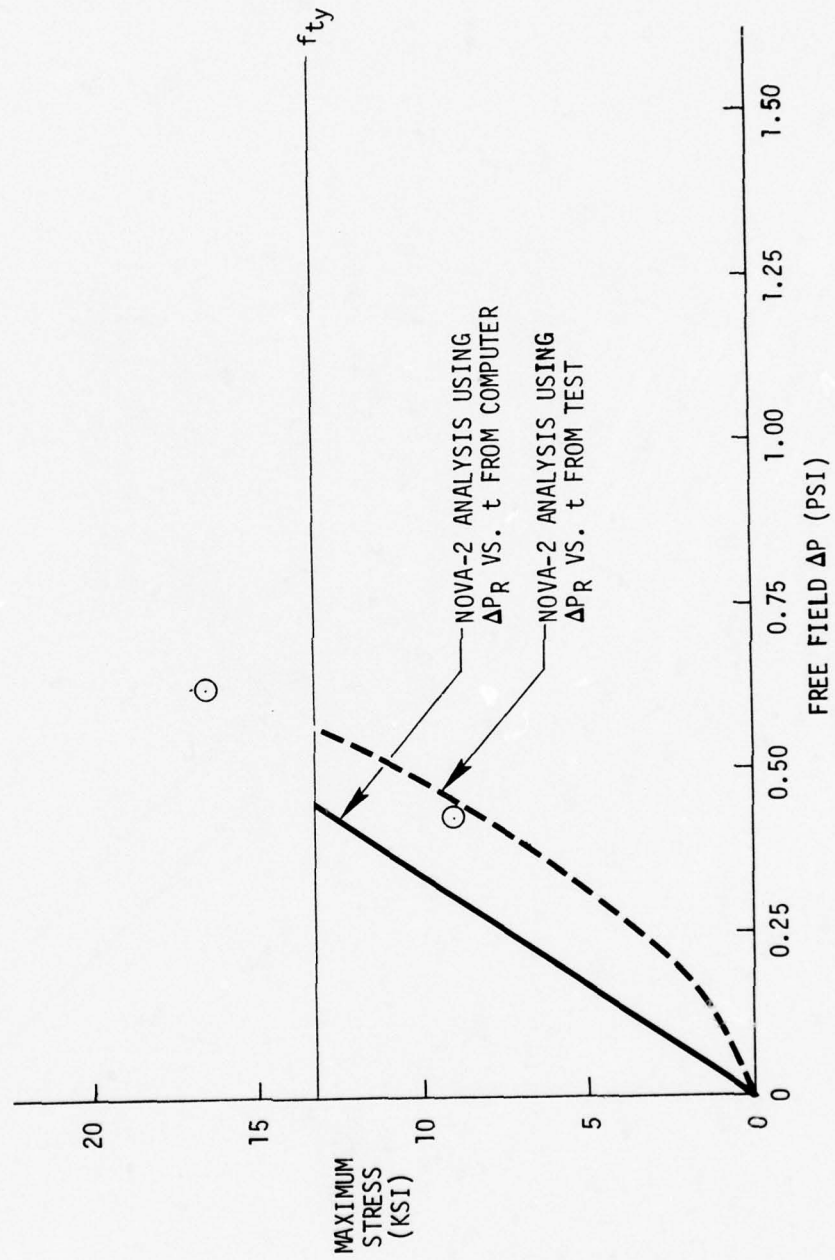


FIGURE 84. STRESS VS. FREE FIELD OVERPRESSURE - SPECIMEN 7

TEST SPECIMEN NO. 7
DISPLACEMENT AT PANEL CENTER
(GAUGE D7-9)

○ TEST DATA

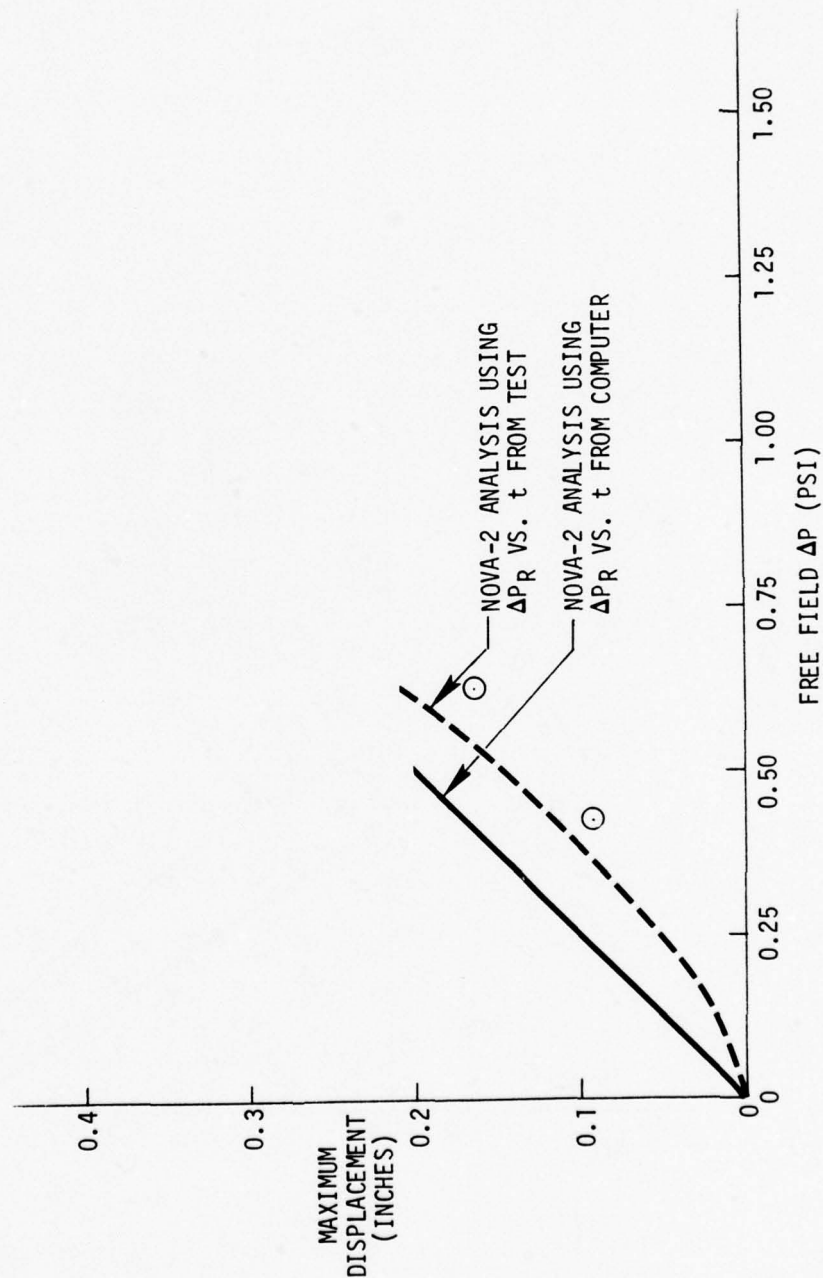


FIGURE 85. DISPLACEMENT VS. FREE FIELD OVERPRESSURE - SPECIMEN 7

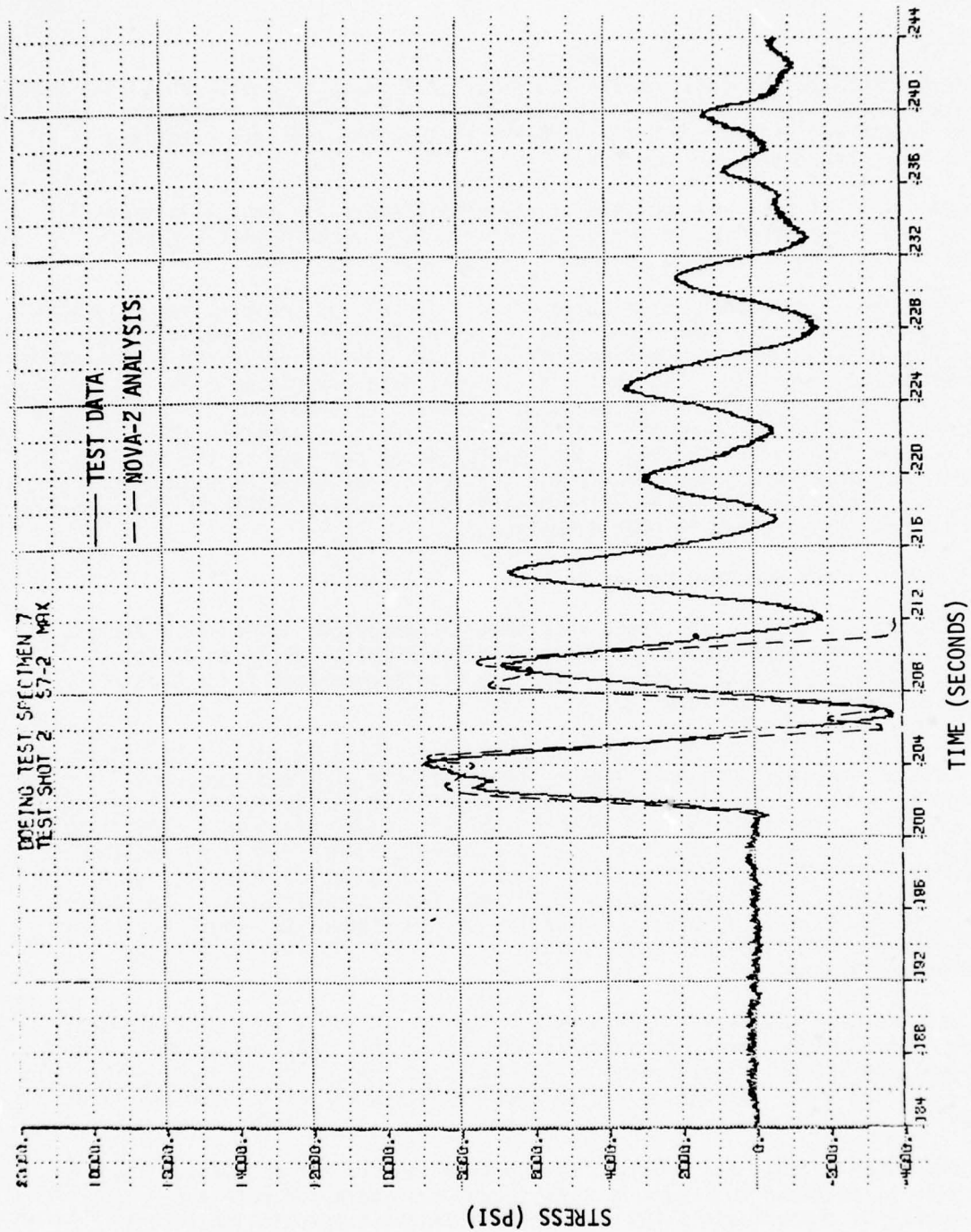


FIGURE 86. STRESS TIME HISTORY - SPECIMEN 7

Analysis results and test results are shown in Figures 87 and 88 which indicate maximum stress and displacement at the center of the panel as expected. For both stress and displacement at the panel center, the analysis predicted greater response than was measured.

A comparison of test and analysis stress time history for shot 2 is shown in Figure 89. The location is the center of the panel. Both test and analysis results indicate a response frequency of approximately 190 cps.

In addition, a permanent deformation of 0.75 inches was measured manually at the panel center after the final shot for this specimen. The condition of specimen 8 subsequent to the final test shot is illustrated in the photograph in Volume II, page 367. The analysis response data associated with the final shot indicated approximately 1.5 inches permanent deformation. The maximum recorded strain associated with the final shot was approximately 12300 micro-inches per inch in the "a" leg, 13800 micro-inches per inch in the "b" leg, and 13000 micro-inches per inch in the "c" leg of the shear rosette gauge. For this condition, the analysis predicted approximately 19200 micro-inches per inch in the "a" leg and "c" leg directions.

8.3.9 Test Specimen Number 9

Specimen 9 was a flat, stiffened skin panel as described in Tables I and II. The element of interest was the center stiffener which was fixed at both ends. All analyses and tests for specimen 9 were conducted for a blast/structure incidence angle of 90°.

Analysis results and test results are shown in Figures 90 and 91 which indicate maximum stress in the inner flange of the stiffener at the clamp point (compressive stress) and maximum displacement at the center of the stiffener as expected. Results from the initial analysis, which utilized a calculated blast environment, predicted essentially linear response data, whereas use of the measured reflected pressure time histories resulted in nonlinear peak response behavior as a function of peak free field overpressure. The latter analysis results agreed with test results at the higher pressure loads while the former analysis agreed extremely well with test results at the lower overpressure levels.

As was the case with other flat panels discussed earlier, test displacements were significantly larger than predicted. Since this specimen was 36 inches square, any lateral displacement of the walls of the holding fixture would be amplified when considering the vertical displacement of the center of the panel.

A comparison of test and analysis stress time history for a selected test shot is illustrated in Figure 92. As shown, test data indicate a response frequency of approximately 160 cps, whereas analysis results indicate a response frequency that is approximately twice the test value.

TEST SPECIMEN NO. 8
STRESS AT CENTER OF PANEL (INSIDE)
(GAUGE S8-2)

○ TEST DATA

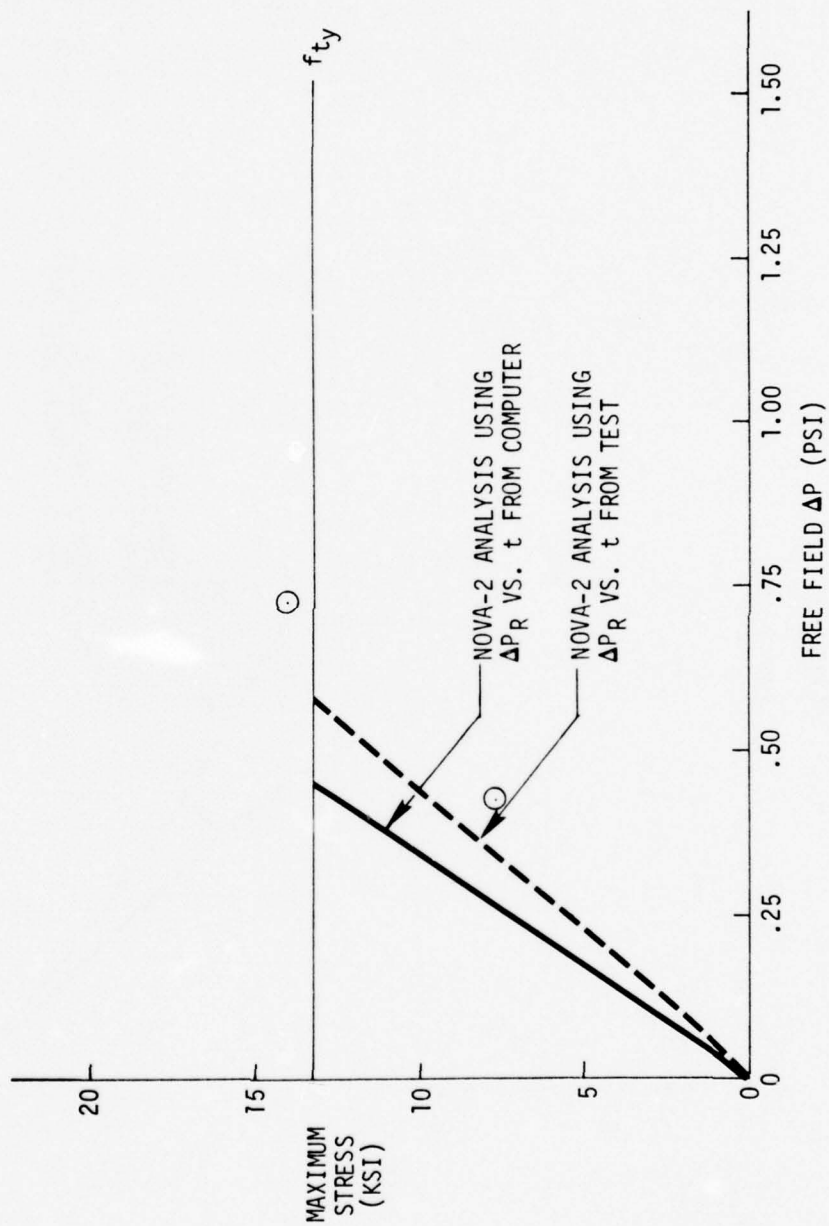


FIGURE 87. STRESS VS. FREE FIELD OVERPRESSURE - SPECIMEN 8

TEST SPECIMEN NO. 8
DISPLACEMENT AT PANEL CENTER
(GAUGE D8-9)

○ TEST DATA

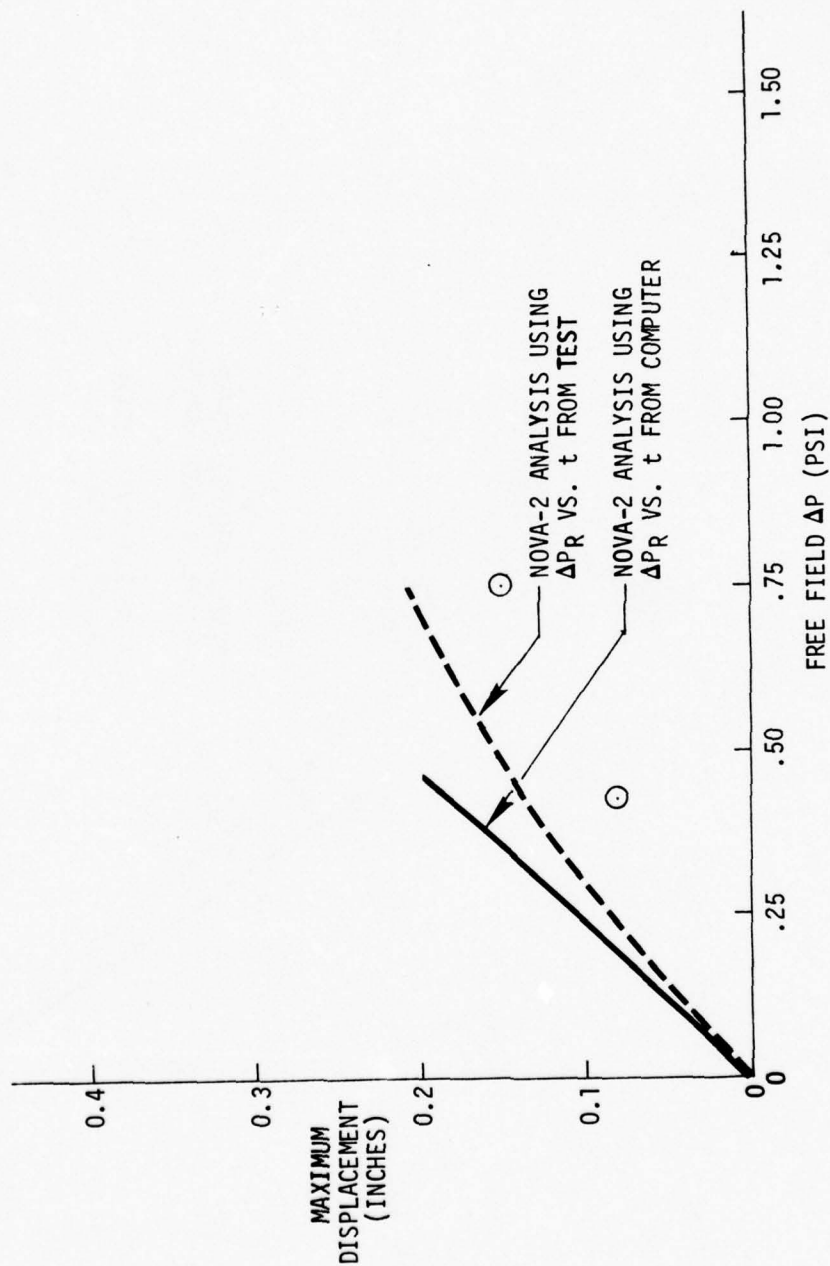


FIGURE 88. DISPLACEMENT VS. FREE FIELD OVERPRESSURE - SPECIMEN 8

TEST SPECIMEN NO. 8
TEST SHOT 2
(GAUGE S8-2)

— TEST DATA
-- NOVA-2 ANALYSIS

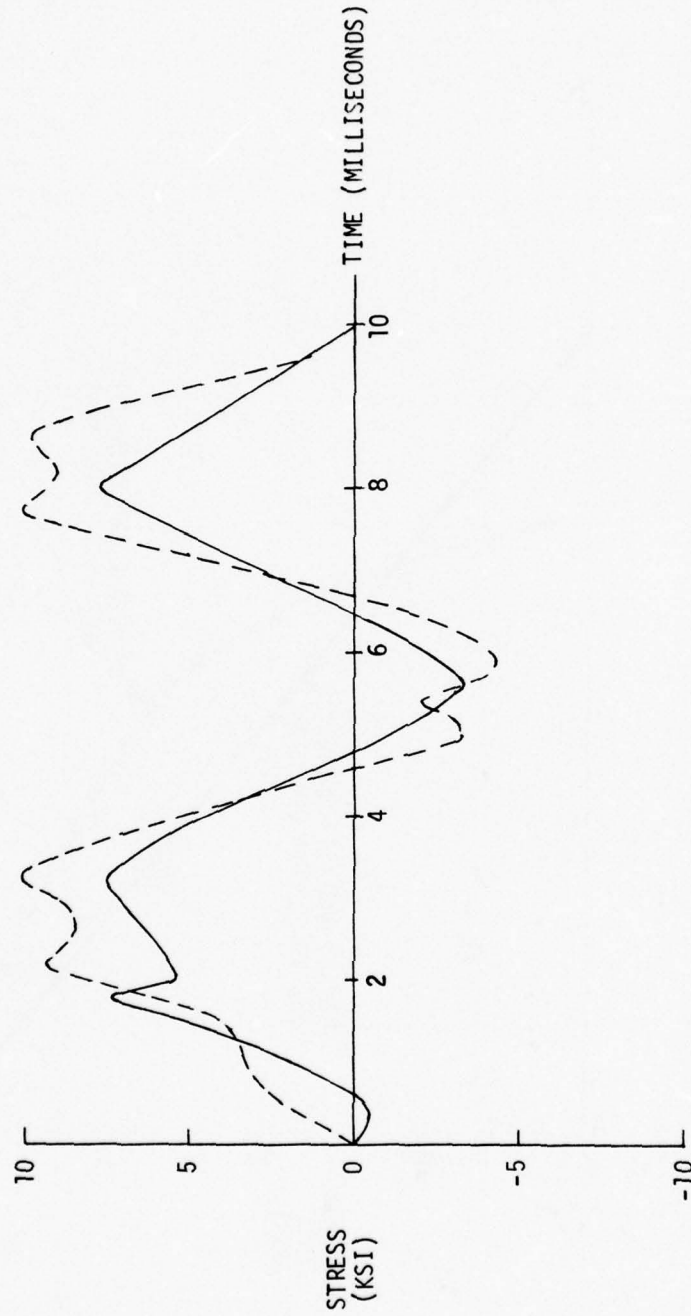


FIGURE 89. STRESS TIME HISTORY - SPECIMEN 8

TEST SPECIMEN NO. 9
STRESS IN INNER FLANGE AT CLAMP POINT
(GAUGE S9-5)

○ TEST DATA

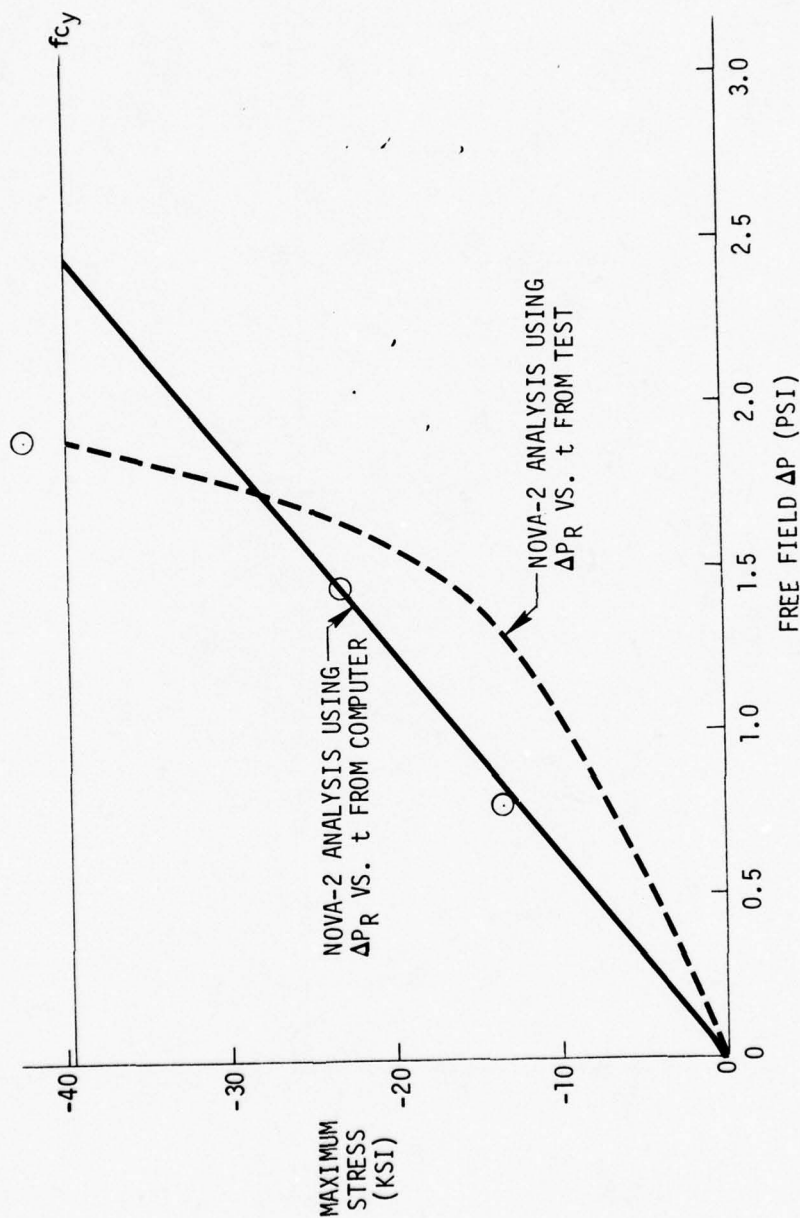


FIGURE 90. STRESS VS. FREE FIELD OVERPRESSURE - SPECIMEN 9

TEST SPECIMEN NO. 9
DISPLACEMENT AT BEAM CENTER
(GAUGE D9-4)

○ TEST DATA

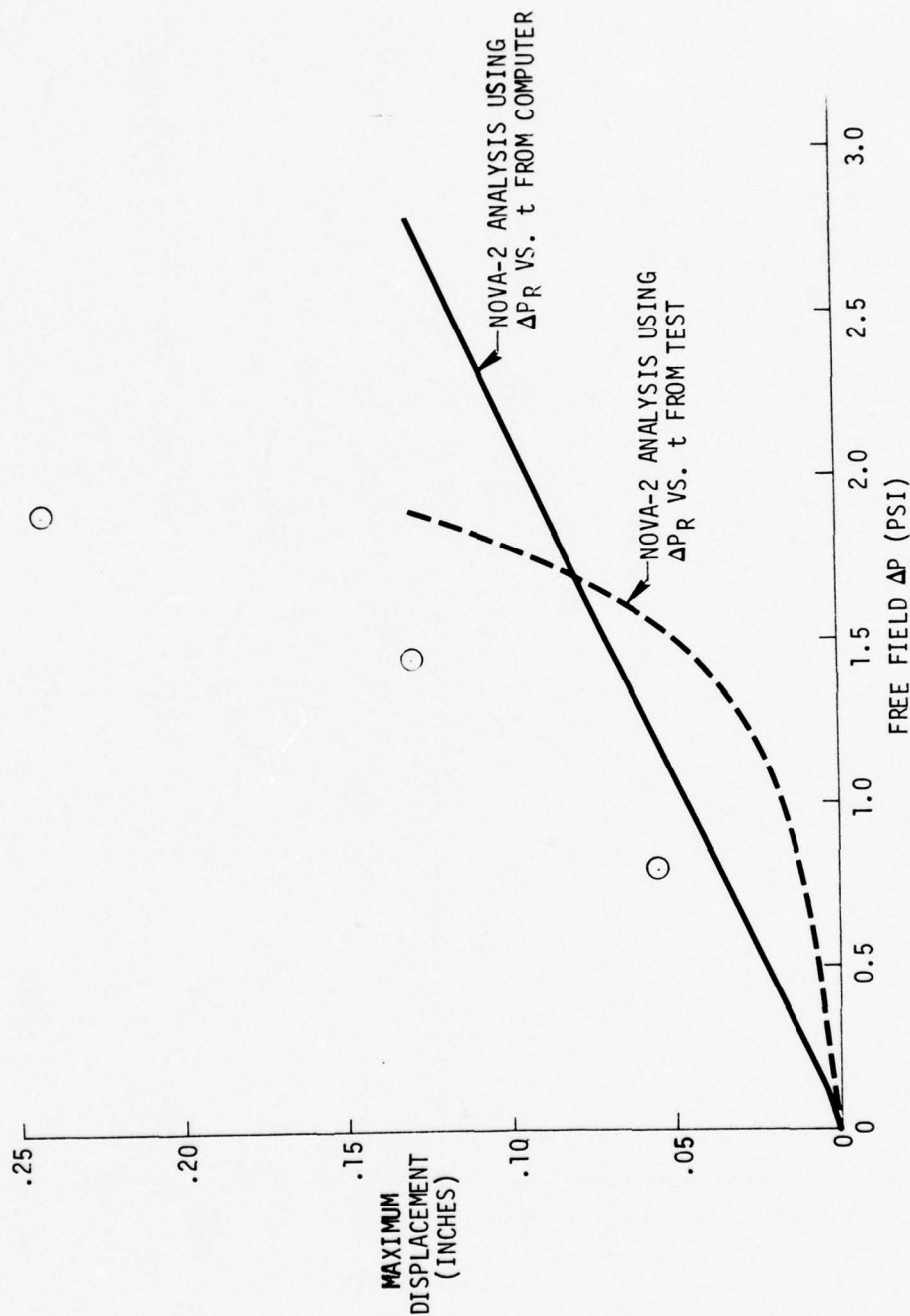


FIGURE 91. DISPLACEMENT VS. FREE FIELD OVERPRESSURE - SPECIMEN 9

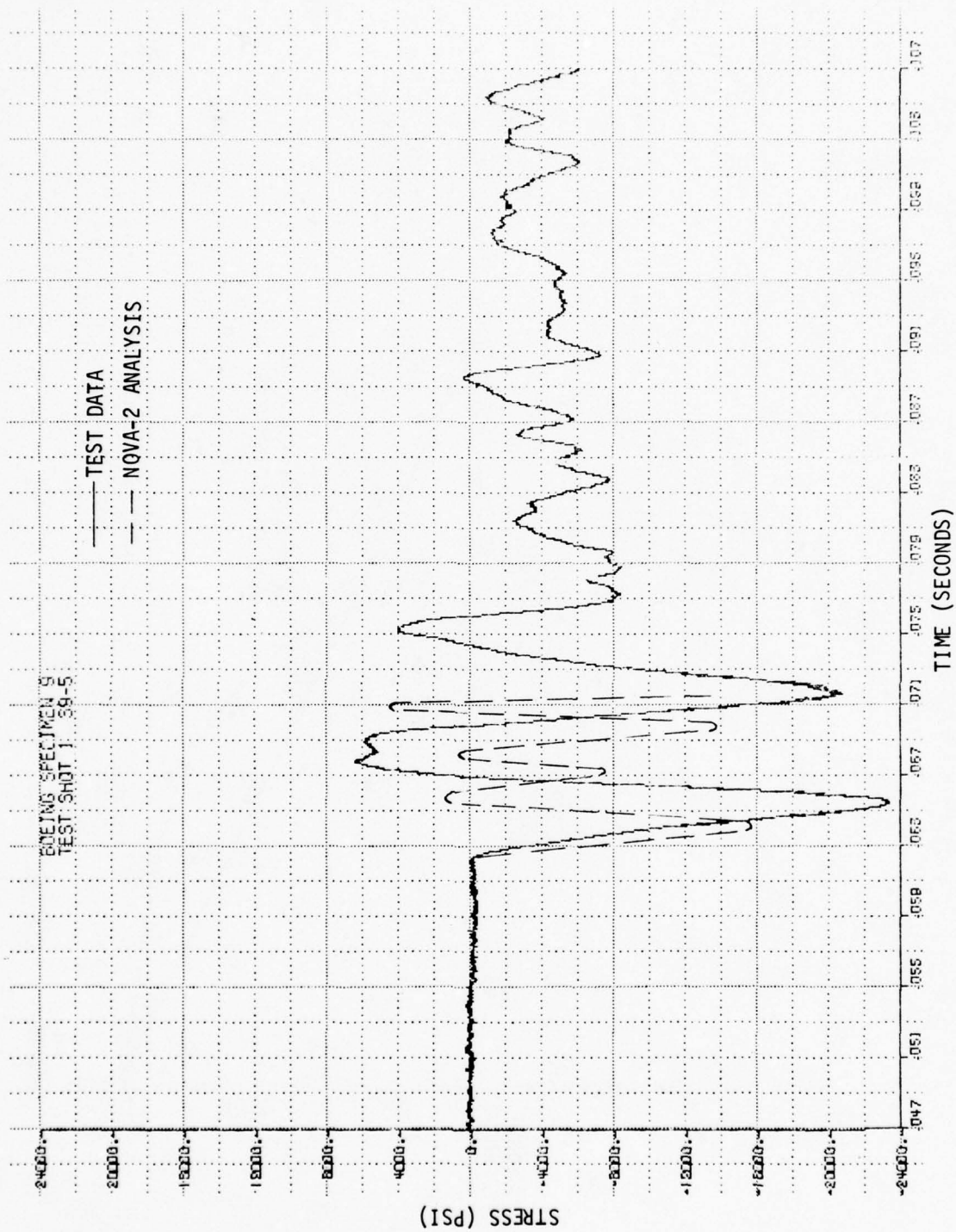


FIGURE 92. STRESS TIME HISTORY - SPECIMEN 9

In addition, a permanent deformation of approximately 0.05 inches was measured manually at the center of the stiffener after the final shot for this specimen. The condition of specimen 9 subsequent to the final test shot is illustrated in the photograph in Volume II, page 435. The analysis response data associated with the final shot indicated less than 0.2 inches permanent deformation. The maximum recorded strain associated with the final shot was approximately 19,200 micro-inches per inch. For this condition, the analysis predicted 12,480 micro-inches per inch.

The analysis that utilized measured reflected pressure time history data made use of reflected pressure time history data recorded on the external surface of the specimen as well as pressure time histories inside the specimen/fixture cavities. These latter pressures resulted from deflection of the specimen which compressed the volume of air in the cavity. An example of the internal pressure is shown in Figure 93. The pressure time history that was utilized in the analysis, therefore, was the reflected pressure time history measured on the external face of the specimen minus the pressure time history inside the cavity.

8.3.10 Test Specimen Number 10

Specimen 10 was a flat, stiffened skin panel as described in Tables I and II. This specimen was essentially identical to specimen 9 except that the ends of the stiffeners were pinned. As with specimen 9, the element of interest in this specimen was the center stiffener. All analyses and tests for specimen 10 were conducted for a blast/structure incidence angle of 90°.

Analysis results and test results are shown in Figures 94 and 95 which indicate maximum stress in the inner flange of the stiffener at the center (tensile stress) and maximum displacement at the center of the stiffener as expected. Results from the initial analysis which utilized a calculated blast environment predicted essentially linear peak response data, whereas use of the measured reflected pressure time histories resulted in nonlinear peak response behavior as a function of peak free field overpressure. However, both sets of analysis results agree very well with the test data regarding maximum stress and maximum displacement.

A comparison of test and analysis stress time history for a selected test shot is illustrated in Figure 96. Test data indicates a frequency response of approximately 140 cps, whereas the NOVA-2 analysis predicts a frequency of approximately 185 cps.

In addition, a permanent deformation of approximately 0.60 inches was measured manually at the center of the stiffener after the final shot for this specimen. The condition of specimen 10 subsequent to the final test shot is illustrated in the photograph in Volume II, page 440. The analysis response data associated with the final shot indicated less than 0.40 inches permanent deformation. The maximum recorded strain at the center of the stiffener associated with the final shot saturated the sensor, therefore, no comparison can be made with the analysis results.

TEST SPECIMEN NO. 9
TEST SHOT NO. 3
(GAUGE P9-10)

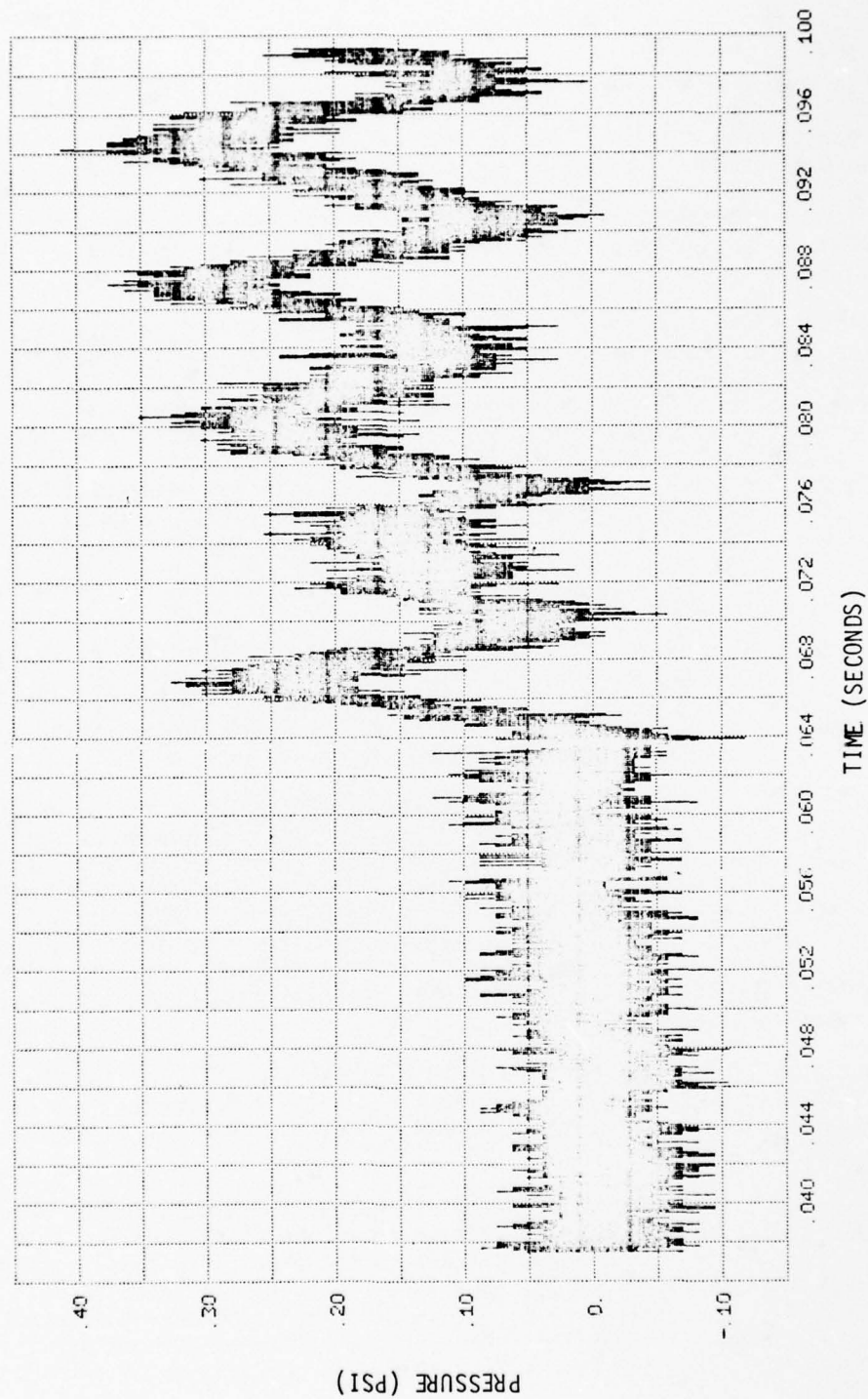


FIGURE 93. PRESSURE TIME HISTORY INSIDE THE SPECIMEN 9/HOLDING FIXTURE CAVITY

TEST SPECIMEN NO. 10
STRESS IN INNER FLANGE AT CENTER OF STIFFENER
(GAUGE S10-6)

○ TEST DATA

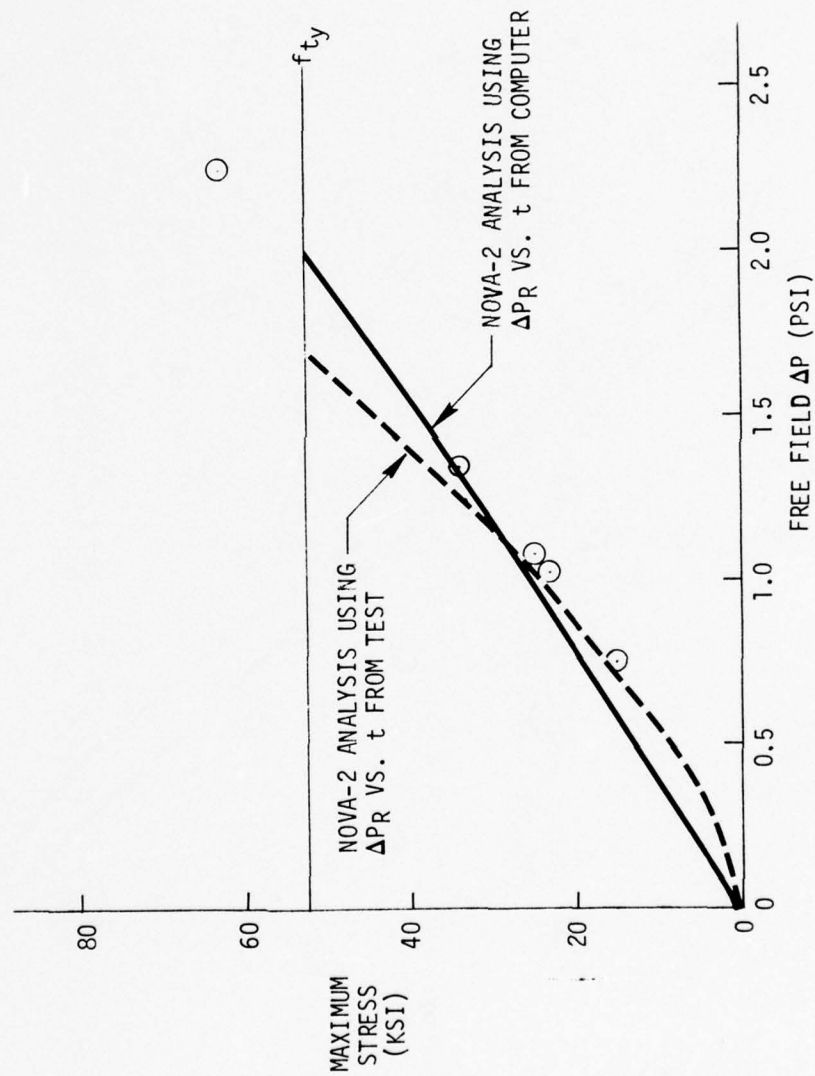


FIGURE 94. STRESS VS. FREE FIELD OVERPRESSURE - SPECIMEN 10

TEST SPECIMEN NO. 10
DISPLACEMENT AT CENTER OF STIFFENER
(GAUGE D10-7)

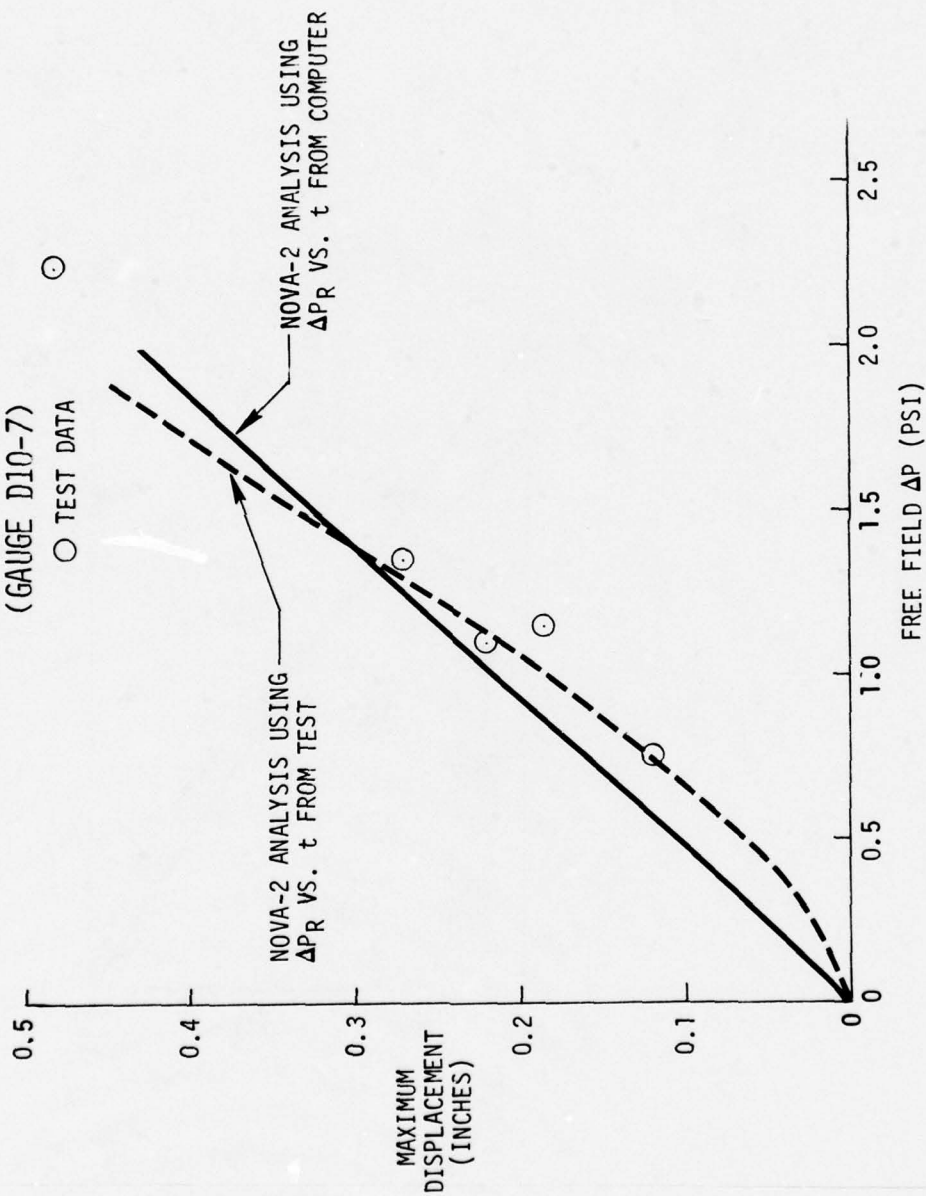


FIGURE 95. DISPLACEMENT VS. FREE FIELD OVERPRESSURE - SPECIMEN 10

TEST SPECIMEN NO. 10
TEST SHOT NO. 4
GAUGE S17-6

— TEST DATA
-- NOVA-2 ANALYSIS

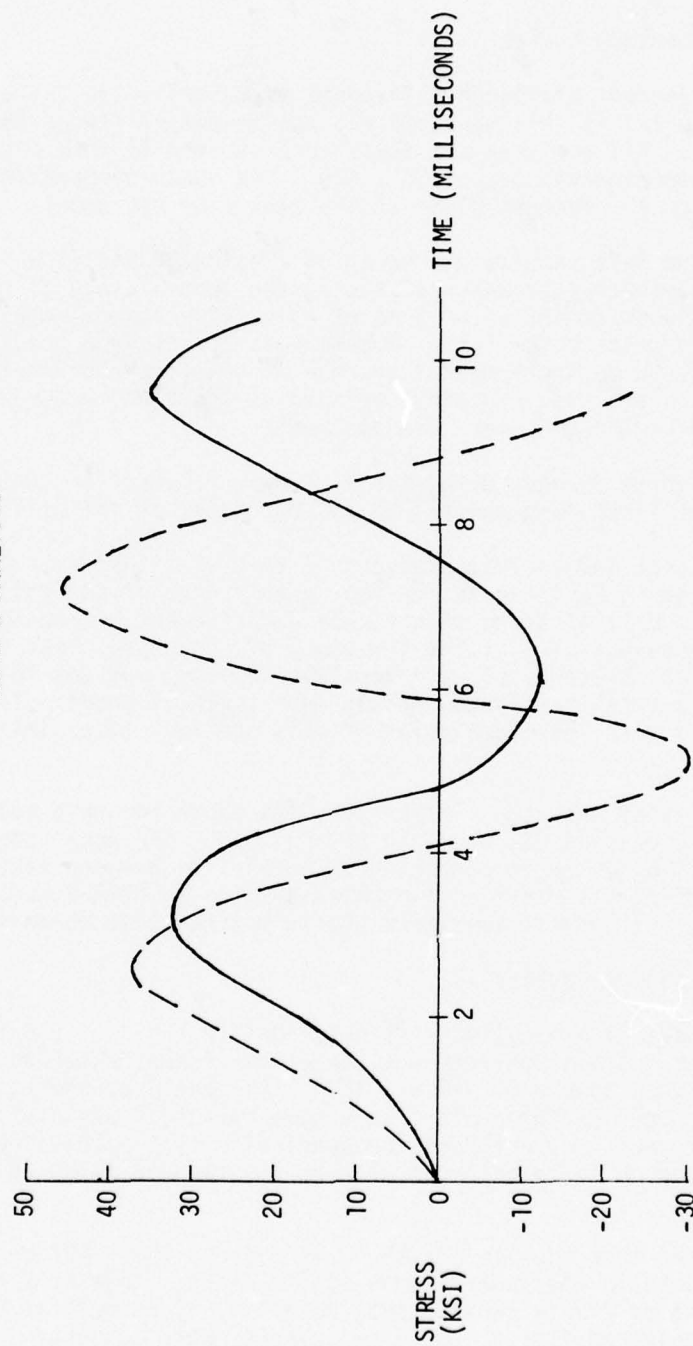


FIGURE 96. STRESS TIME HISTORY - SPECIMEN 10

8.3.11 Test Specimen Number 11

Specimen 11 was a curved, stiffened skin panel as described in Tables I and II. The element of interest in this specimen was the center stiffener that is fixed at both ends. All analyses and tests for specimen 11 were conducted for a blast/structure incidence angle of 90° , i.e., the shock propagation vector was perpendicular to the tangent plane at the center of the panel.

Analysis results and test results are shown in Figures 97 and 98 which illustrate comparisons between test and analysis in the inner flange of the stiffener at the center of the stiffener as well as at a location approximately 2.2° away from the clamp point. The latter location is the closest point to the clamp point that could be instrumented because of geometry consideration and it essentially coincides with the first mass point location in the NOVA-2 model. No displacements were measured for this specimen.

As indicated in Figures 97 and 98, better agreement between test and analysis was obtained at the first mass point than at the center of the stiffener.

The comparison of test and analysis results is further illustrated in Figure 99 which shows stress time histories in the inner flange of the stiffener as its center. Not only is there significant disagreement between peak magnitudes of stress, but also in the frequency of response. Test data indicates a response frequency of approximately 440 cps, whereas the NOVA-2 analysis predicts a frequency approximately four times as great. Time history comparisons near the clamp point of this specimen give similar results.

The reader is cautioned that the analysis results shown for this specimen are in error due to the reasons discussed in Section 8.3. The magnitude of the error is unknown. To make a more meaningful comparison between test and analysis stress results, additional modifications must be made to NOVA-2 to allow for use of a shock loading environment that more nearly matches that which was measured.

8.3.12 Test Specimen Number 12

Specimen 12 was a skin/frame cylinder as described in Tables I and II. The element of interest in this specimen was the center frame, which was fixed to a simulated floor beam at $\theta = 0^\circ$ and $\theta = 180^\circ$. All analyses and tests for specimen 12 were conducted for a blast/structure incidence angle of 90° , i.e., the shock propagation vector was perpendicular to the longitudinal axis of the cylinder and also perpendicular to the tangent plane at the mid-span of the frame.

Analysis results and test results are shown in Figures 100 - 107 and illustrate stress response in the inner flange of the center frame at approximately 5.5° from the point of fixity (NOVA-2 mass point No. 1) as well as 30° , 60° , and 90° from the point of fixity. No displacements were measured for this specimen.

TEST SPECIMEN NO. 11
STRESS IN INNER FLANGE AT
2.2° FROM CLAMP POINT
(GAUGE S11-5)

○ TEST DATA

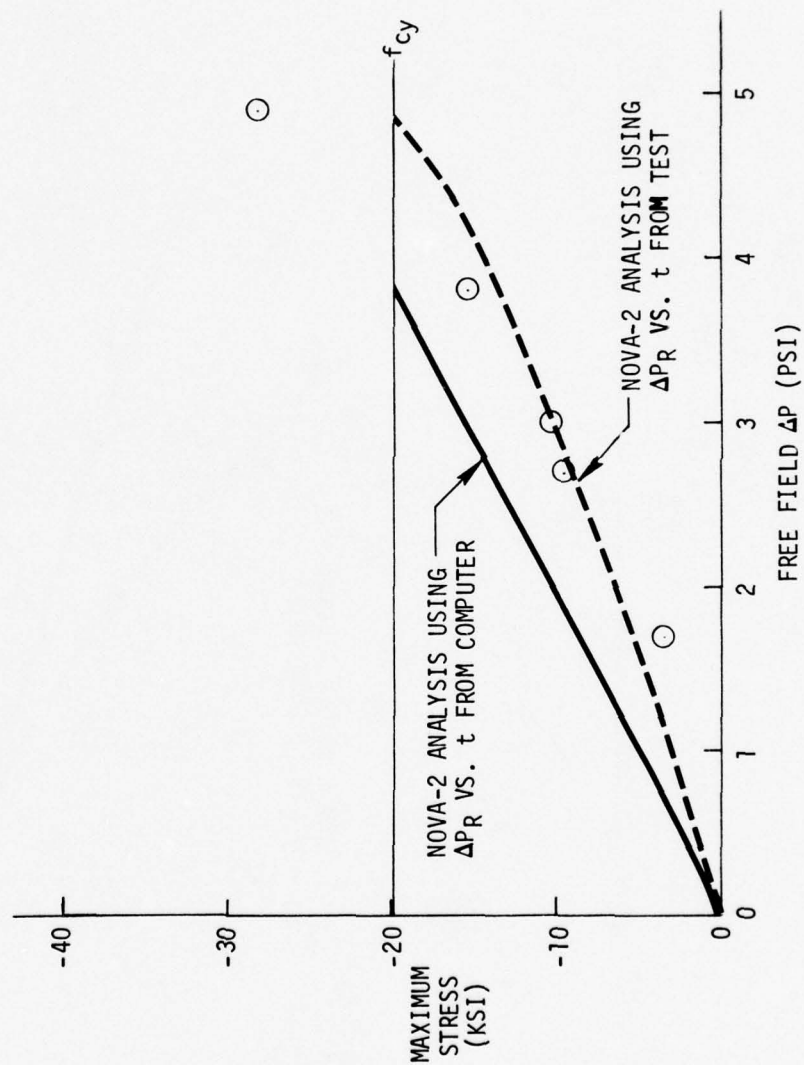


FIGURE 97. STRESS VS. FREE FIELD OVERPRESSURE - SPECIMEN 11

TEST SPECIMEN NO. 11
STRESS IN INNER FLANGE AT
CENTER OF STIFFENER
(GAUGE S11-3)

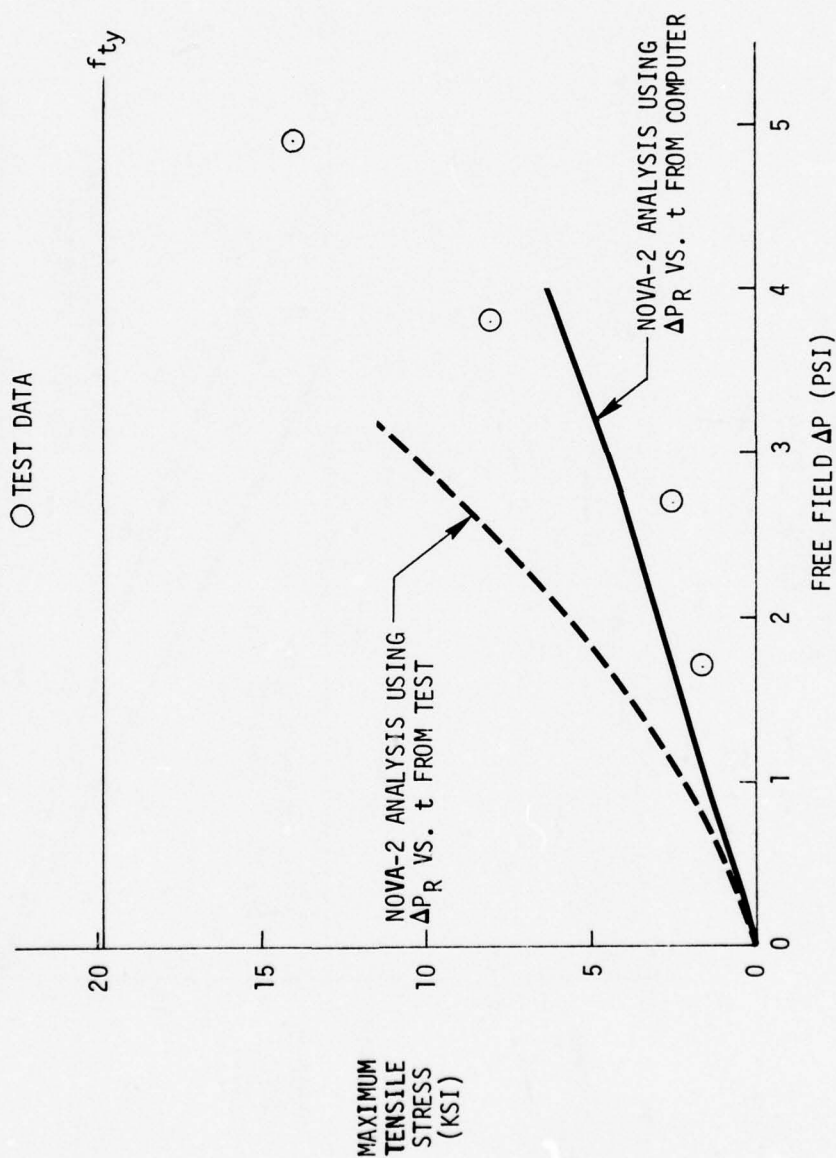


FIGURE 98. STRESS VS. FREE FIELD OVERPRESSURE - SPECIMEN 11

TEST SPECIMEN NO. 11
TEST SHOT NO. 2
(GAUGE S11-3)

— TEST DATA

-- NOVA-2 ANALYSIS

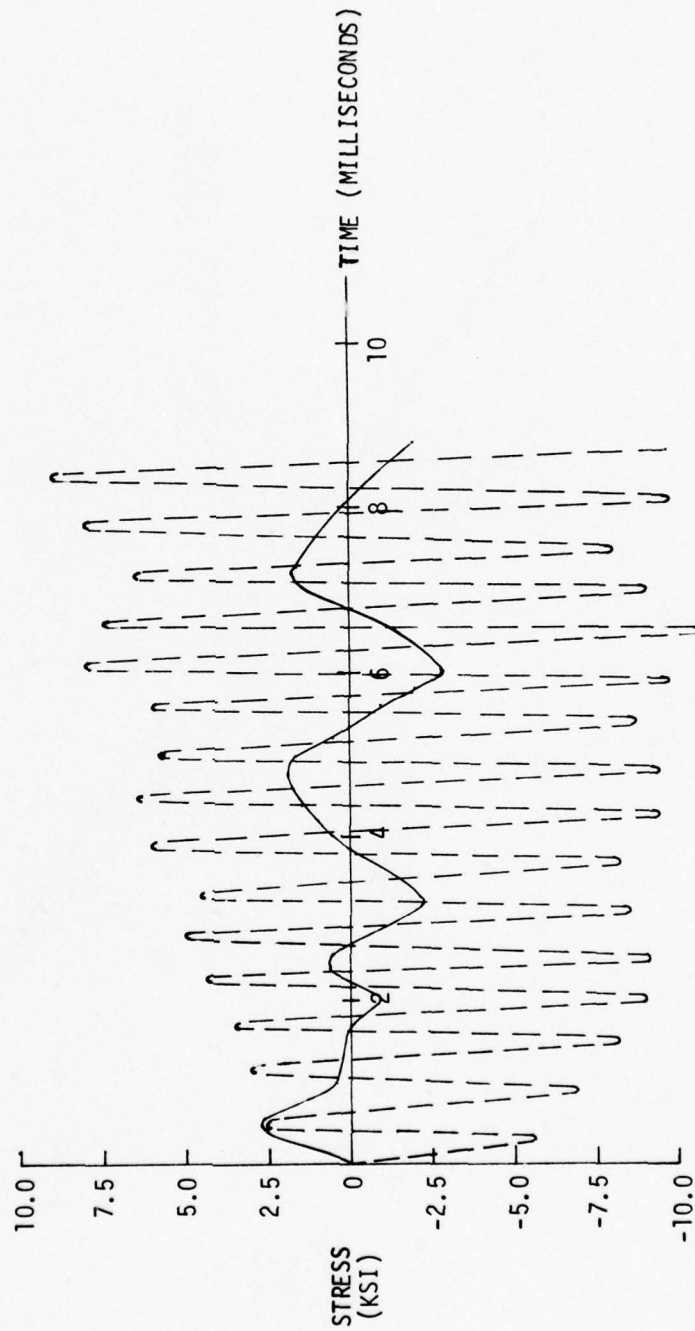


FIGURE 99. STRESS TIME HISTORY - SPECIMEN 11

TEST SPECIMEN NO. 12
 COMPRESSIVE STRESS IN INNER FLANGE AT 5.5°
 FROM CLAMP POINT
 (GAUGE S12-14)

○ TEST DATA

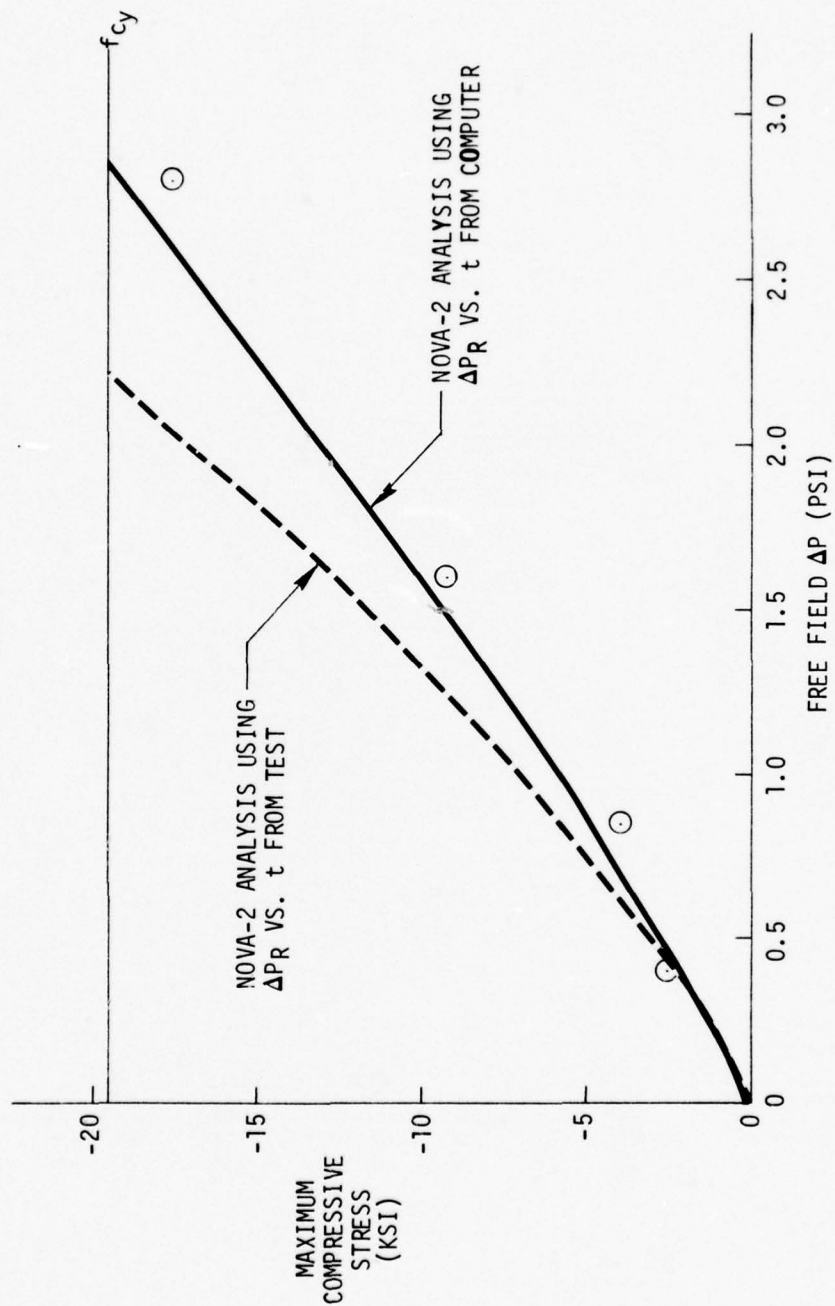


FIGURE 100. COMPRESSIVE STRESS VS. FREE FIELD OVERPRESSURE - SPECIMEN 12

TEST SPECIMEN NO. 12
TENSILE STRESS IN INNER FLANGE AT
5.5° FROM CLAMP POINT
(GAUGE S12-14)

○ TEST DATA

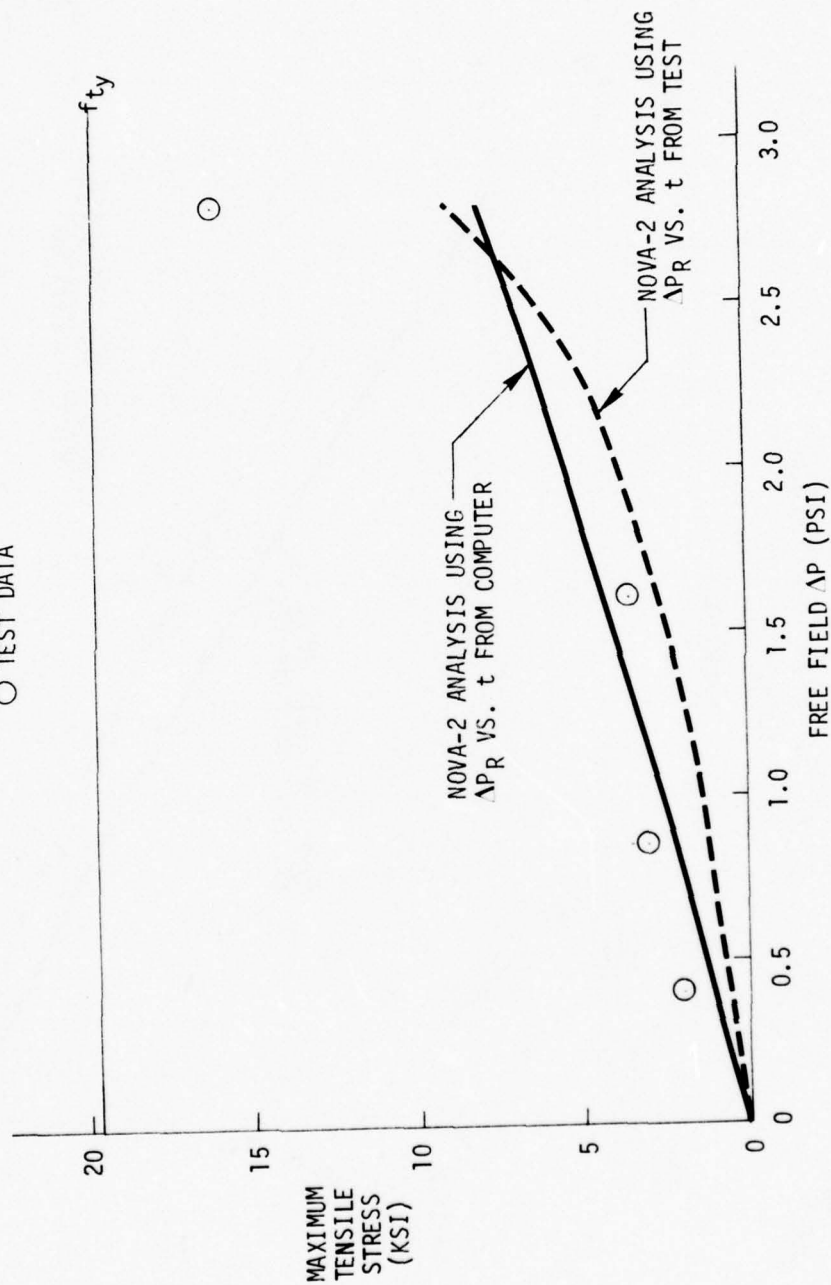


FIGURE 101. TENSILE STRESS VS. FREE FIELD OVERPRESSURE - SPECIMEN 12

TEST SPECIMEN NO. 12
 COMPRESSIVE STRESS IN INNER FLANGE
 AT 30° FROM CLAMP POINT
 (GAUGE S12-10)

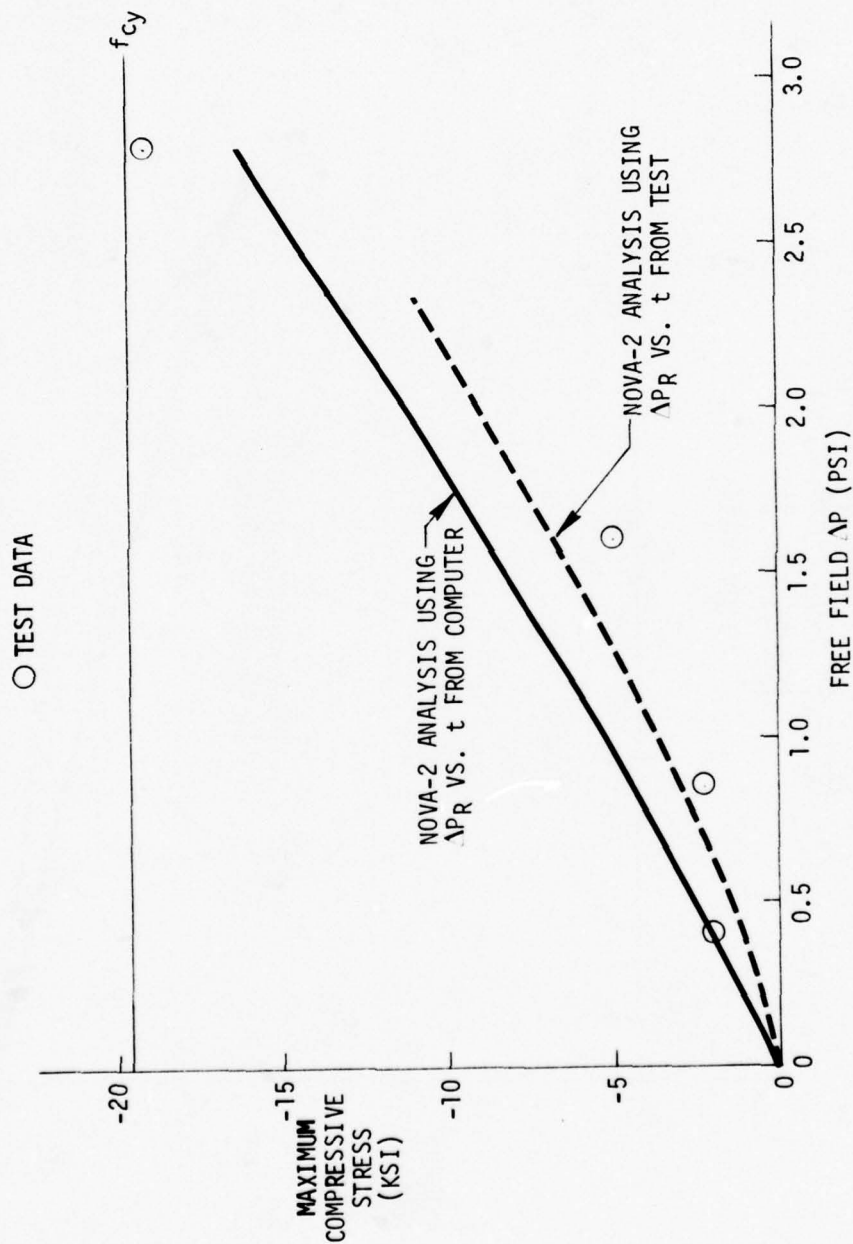


FIGURE 102. COMPRESSIVE STRESS VS. FREE FIELD OVERPRESSURE - SPECIMEN 12

TEST SPECIMEN NO. 12
TENSILE STRESS IN INNER FLANGE AT
30° FROM CLAMP POINT
(GAUGE S12-10)

○ TEST DATA

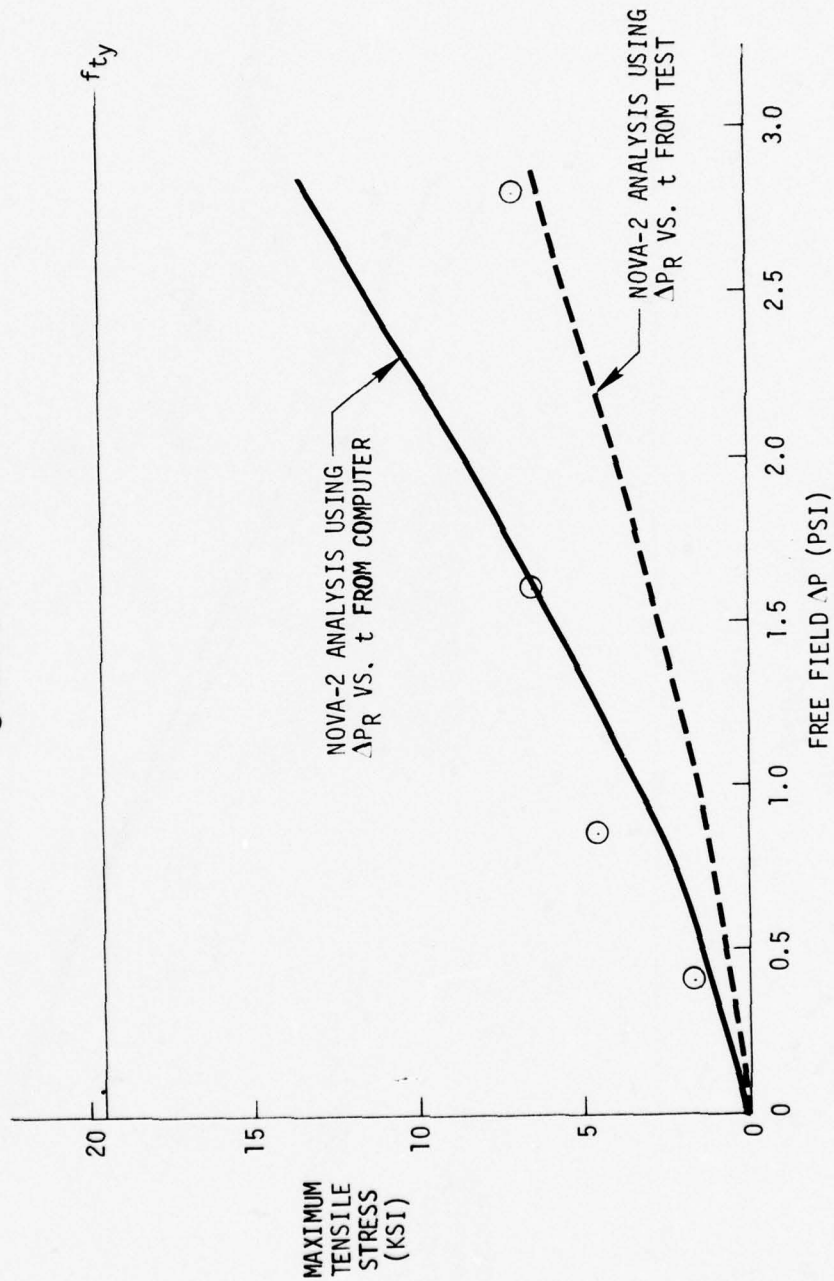


FIGURE 103. TENSILE STRESS VS. FREE FIELD OVERPRESSURE - SPECIMEN 12

TEST SPECIMEN NO. 12
 COMPRESSIVE STRESS IN INNER FLANGE AT
 60° FROM CLAMP POINT
 (GAUGE S12-7)

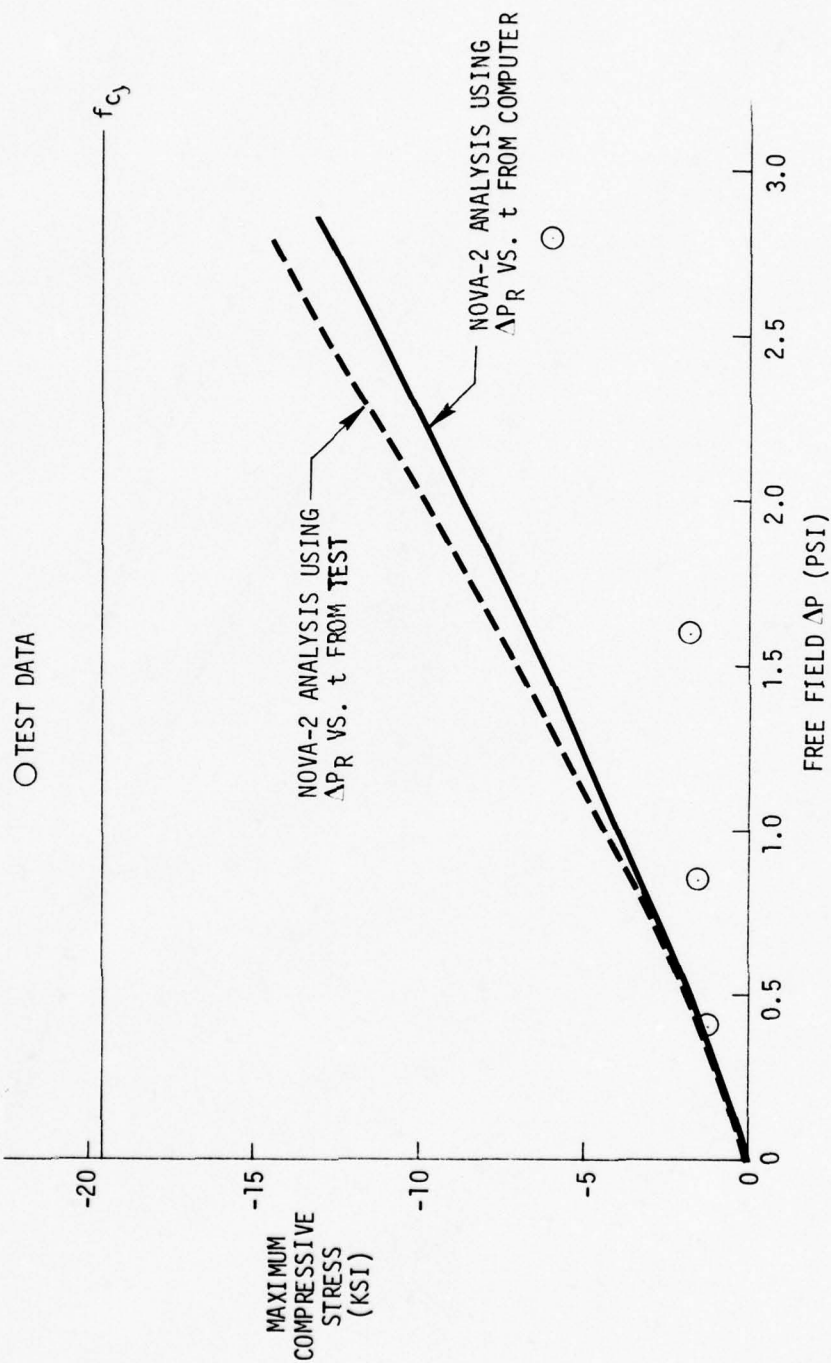


FIGURE 104. COMPRESSIVE STRESS VS. FREE FIELD OVERPRESSURE - SPECIMEN 12

TEST SPECIMEN NO. 12
TENSILE STRESS IN INNER FLANGE
AT 60° FROM CLAMP POINT
(GAUGE S12-7)

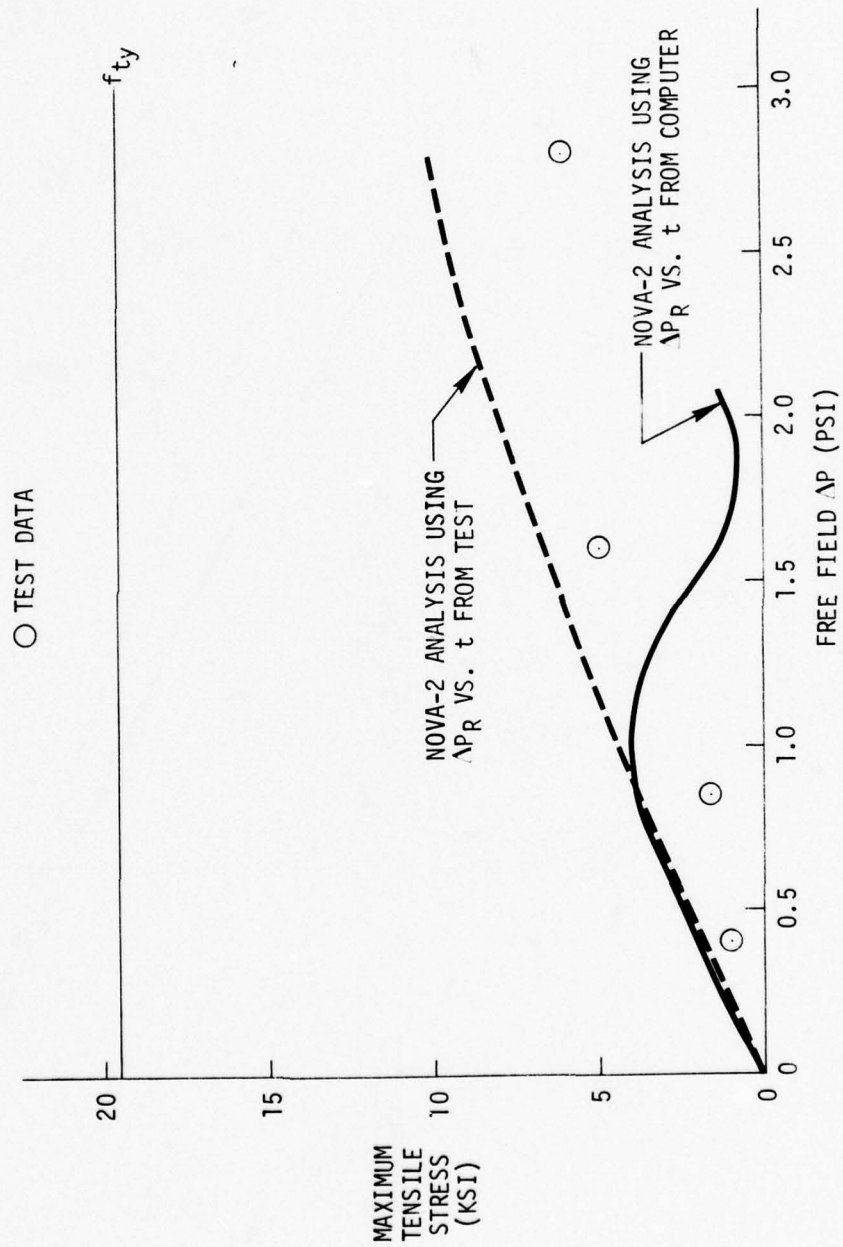


FIGURE 105. TENSILE STRESS VS. FREE FIELD OVERPRESSURE - SPECIMEN 12

TEST SPECIMEN NO. 12
STRESS IN INNER FLANGE AT
90° FROM CLAMP POINT
(GAUGE S12-3)

○ TEST DATA

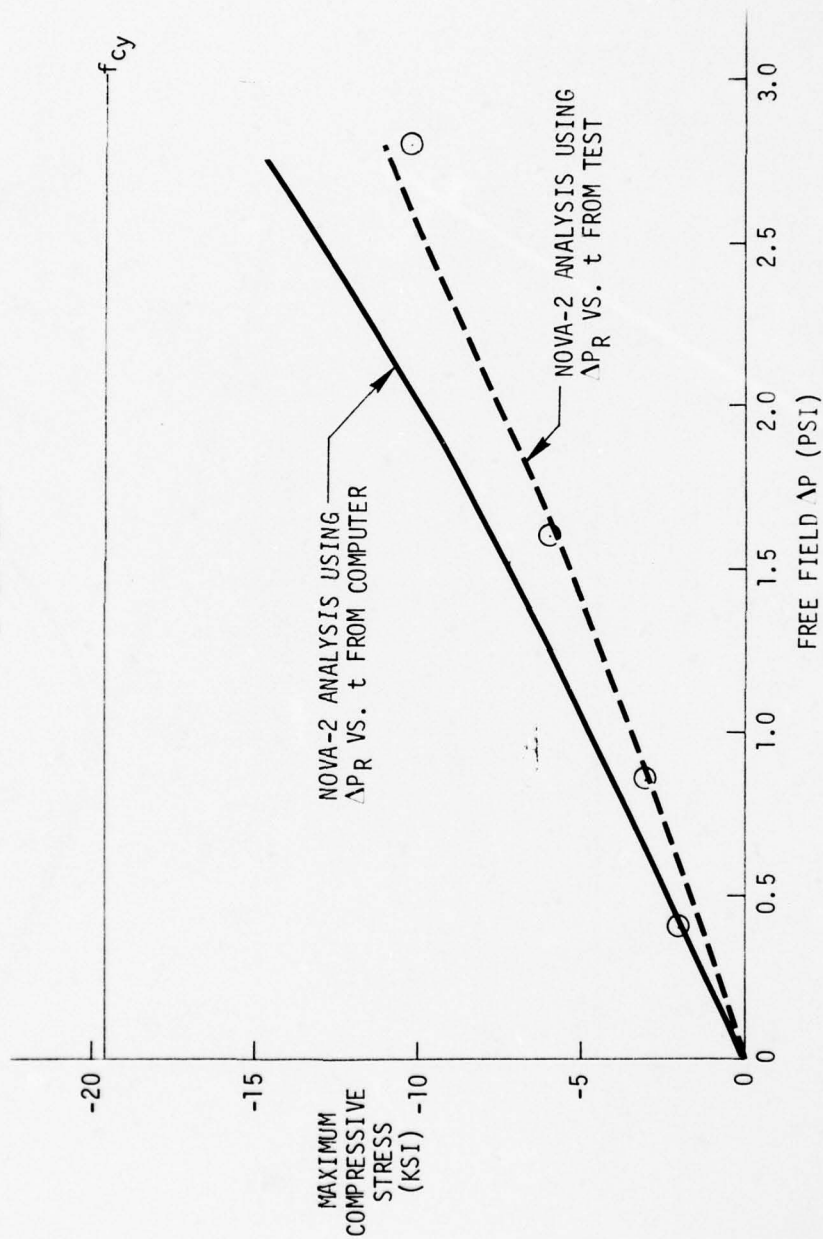


FIGURE 106. COMPRESSIVE STRESS VS. FREE FIELD OVERPRESSURE - SPECIMEN 12

TEST SPECIMEN NO. 12
 TENSILE STRESS IN INNER FLANGE
 AT 90° FROM CLAMP POINT
 (GAUGE S12-3)
 ○ TEST DATA

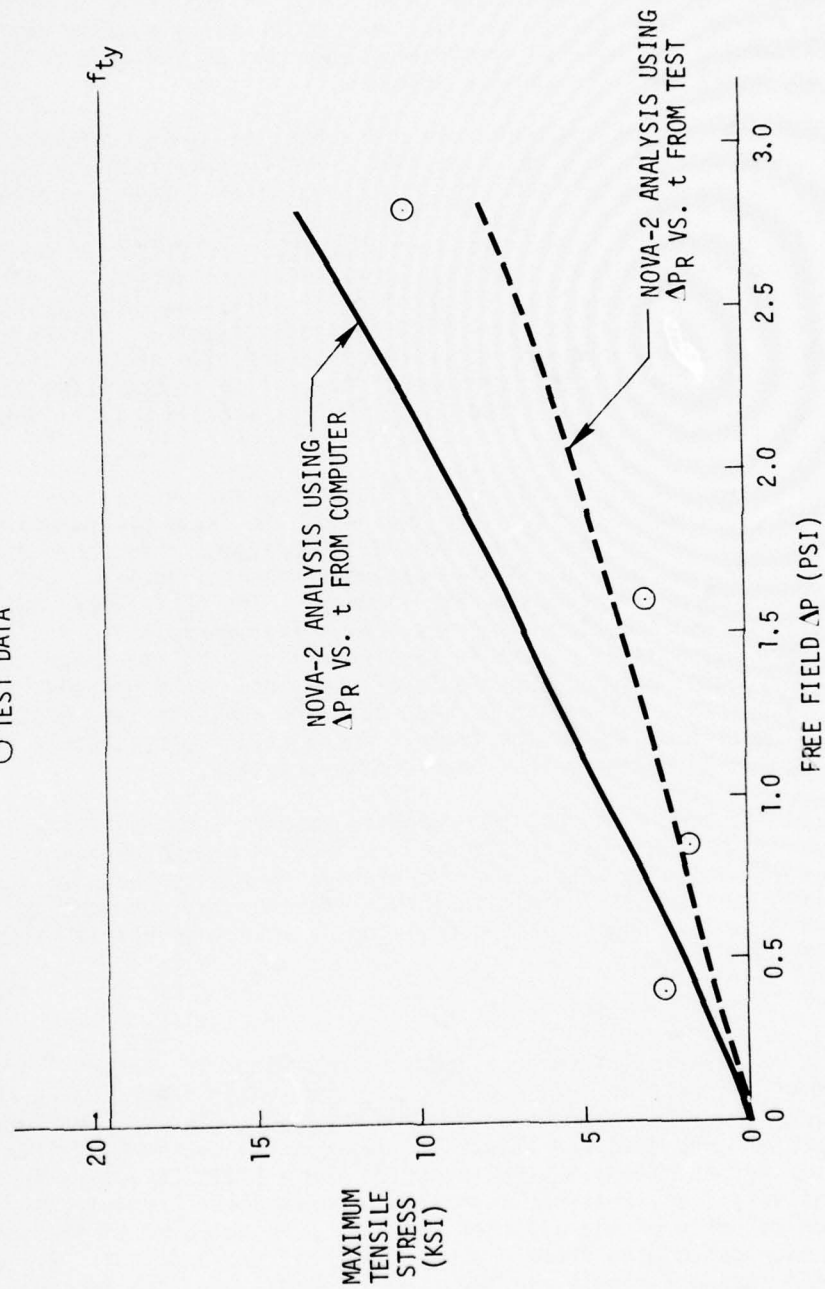


FIGURE 107. TENSILE STRESS VS. FREE FIELD OVERPRESSURE - SPECIMEN 12

As shown in Figures 100 - 107, the test results are similar, in general, to that of the analysis results. Analysis results predicted that the critical location of those instrumented would be in the inner flange at 5.5° from the clamp point. Test data indicated that points on the frame in the inner flange at 5.5° and 30° from the clamp point were essentially equally critical. Both test and analysis predicted compressive stresses at the critical location would be larger than the tensile stresses.

The frame experienced approximately 0.2 inches permanent deformation in a radial sense due to the final test shot. This deformation was measured manually at approximately 90° from the clamp point. The condition of specimen 12 subsequent to the final test shot is illustrated in the photograph in Volume II, page 556. The transducer that measured reflected pressure on the specimen at the "head-on" location became saturated during the final test shot. Therefore, an analysis of specimen 12 utilizing measured reflected pressure data for the final test shot was not performed. An analysis of this specimen utilizing a computer generated pressure time history for this condition, however, indicated a permanent deformation of approximately 0.1 inches. The strain gauge measuring strain at 5.5° from the clamp point was saturated as a result of this shot.

Figure 108 illustrates a comparison of test and analysis stress response time histories for a point on the inner flange of the frame at approximately 5.5° from the clamp point. As shown, test data indicates a response frequency of approximately 125 cps. The NOVA-2 analysis results, however, indicate a response frequency of approximately 1400 cps. The differences between test and analysis response time histories are further exemplified in Figure 109. This figure illustrates stress in the inner flange of the frame at 90° from the clamp point, that is, the middle of the span. As indicated, there is also a significant difference between test and analysis time history characteristics at this location on the frame. The analysis consistently predicts higher response frequency than recorded in the test.

The reader is cautioned that the analysis results shown for this specimen are in error due to the reasons discussed in Section 8.3. The magnitude of the error is unknown. To make a more meaningful comparison between test and analysis stress results, additional modifications must be made to NOVA-2 to allow for use of a shock loading environment that more nearly matches that which was measured.

8.3.13 Test Specimen Number 13

Specimen 13 was a skin/frame cylinder as described in Tables I and II. The element of interest in this specimen was the center frame, which was fixed to a simulated floor beam at $\theta = 0^\circ$ and $\theta = 180^\circ$. The only difference between this specimen and specimen 12 was the frame cross section. Initial analyses and tests for specimen 13 were conducted for a blast/structure incidence angle of 90° , i.e., the shock propagation vector was perpendicular to the longitudinal axis of the cylinder and also perpendicular to the tangent plane at the mid-span of the frame. Subsequent analyses and tests were accomplished for a 45° incidence angle and for several conditions that included internal

TEST SPECIMEN NO. 12
TEST SHOT NO. 4
GAUGE S12-3

— TEST DATA

-- NOVA-2 ANALYSIS

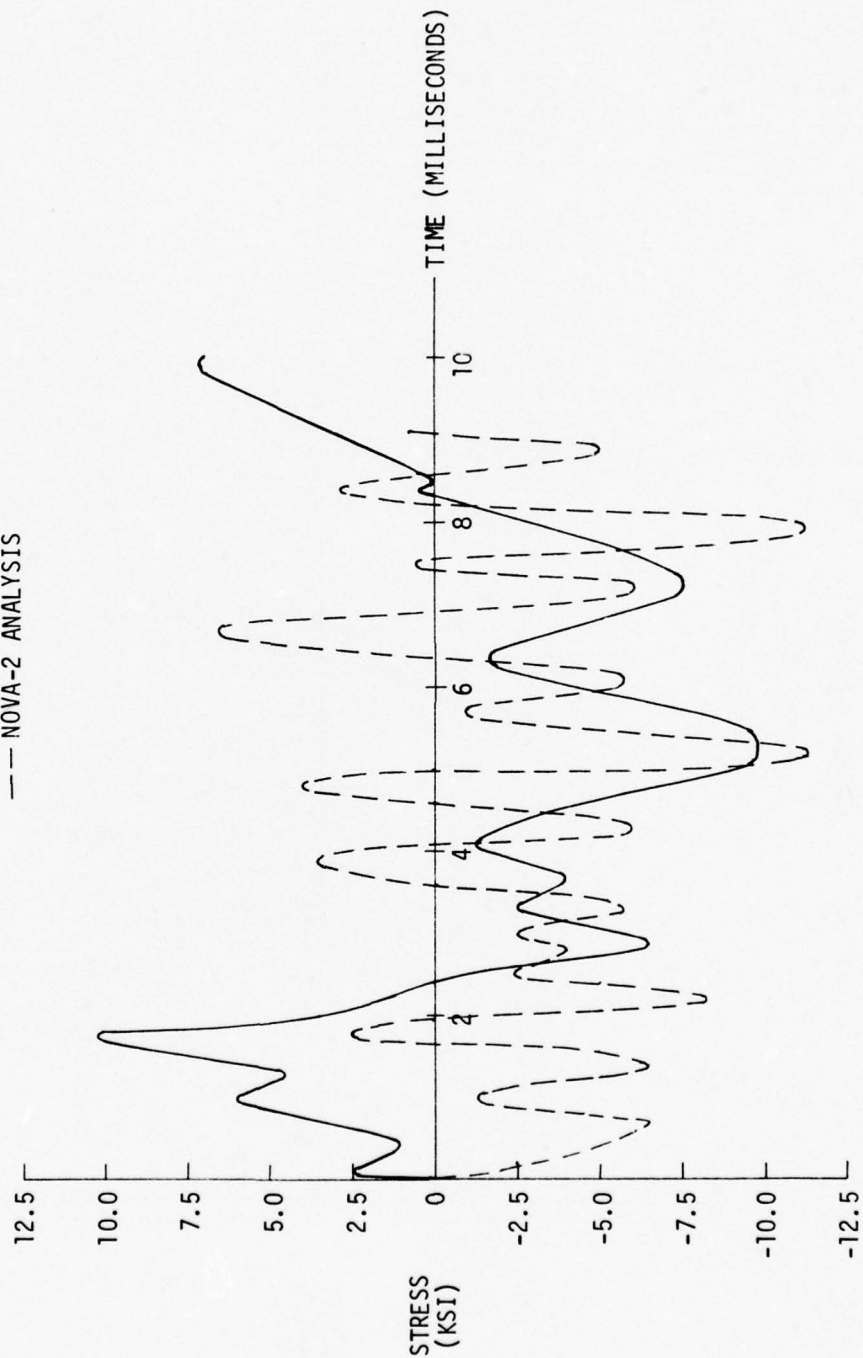


FIGURE 108. STRESS TIME HISTORY - SPECIMEN 12

TEST SPECIMEN NO. 12
TEST SHOT NO. 4
GAUGE S12-14

— TEST DATA
-- NOVA-2 ANALYSIS

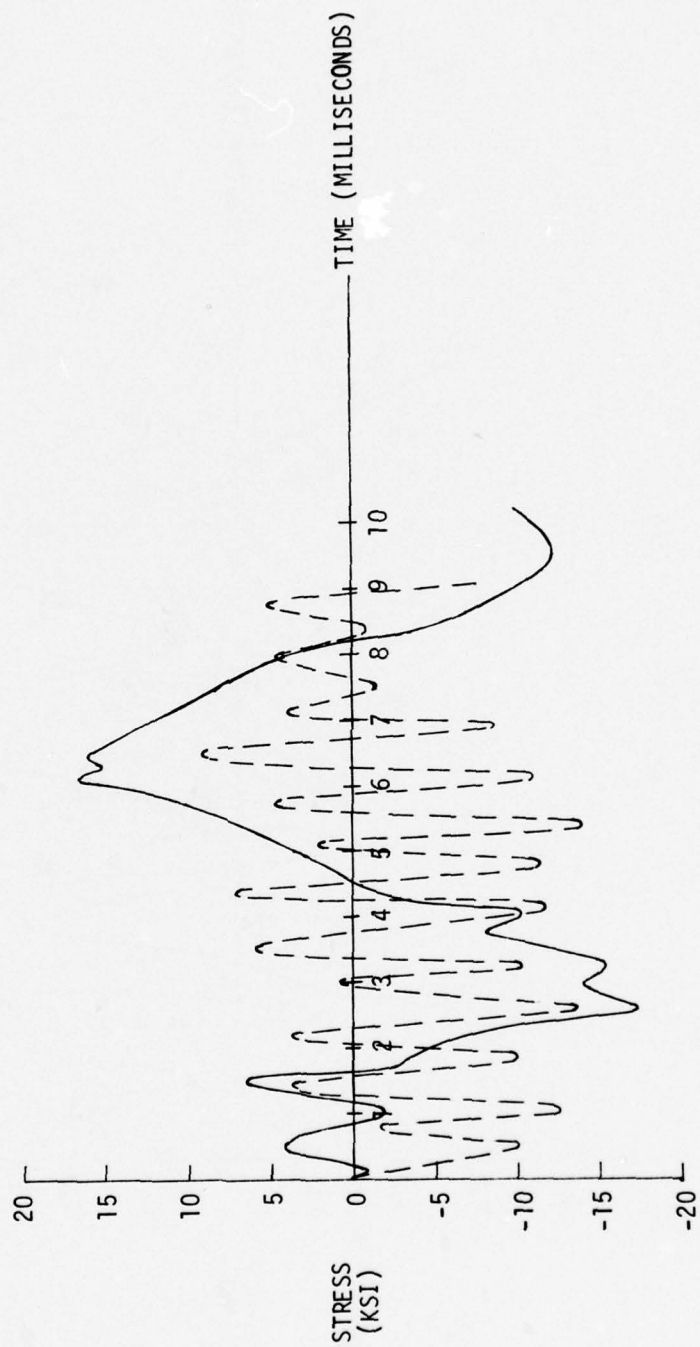


FIGURE 109. STRESS TIME HISTORY - SPECIMEN 12

pressurization of the specimen. The complete set of conditions for specimen 13 is illustrated in Table XII.

Analysis results and test results associated with test shots 3-5 are shown in Figures 110 - 117 and illustrate stress response in the inner flange of the center frame at approximately 5.5° from the point of fixity (NOVA-2 mass point No. 1), as well as 30° , 60° , and 90° from the point of fixity. No displacements were measured for this specimen. Test results indicate that the critical locations on specimen 13 were in the inner flange at approximately 5.5° and 90° from the clamp point (tension). The tension strain data for the inner flange at 90° from the clamp point for the final test shot saturated the signal and is, therefore, not plotted. Analysis results indicated that the critical location on the frame is in the inner flange at 30° from the clamp point (compression).

A comparison of stress time histories is shown in Figure 118 for specimen 13 for a selected test shot. The test data indicates a response frequency of approximately 1100 cps; however, the measured data shown in Volume II, page 616, indicates that this high frequency response is actually superimposed on a fundamental response frequency of approximately 120 cps. The analysis results indicate a response frequency of approximately 1200 cps; however, there is no apparent indication that this is superimposed on a lower frequency response mode.

The test results associated with test shots 3-9 are shown in Figures 119-124. These results illustrate the effect of shock incidence and preblast internal pressure on the response of the frame. Figure 119 indicates that shock incidence angles of 90° and 45° result in approximately the same response, and internal pressurization is beneficial for both orientation angles when considering maximum compressive stress at approximately 5.5° from the clamp point. The above results also hold true, in general, when examining the maximum tensile stress at this location. Figures 121 and 122 indicate that incidence angle and internal pressure have negligible effect on the response in the inner flange at a point approximately 30° from the clamp point. Figure 123 shows that an incidence angle of 45° as well as internal pressure provide beneficial effects regarding the maximum compressive response in the inner flange at a point approximately 60° from the clamp point. As shown in Figure 124, internal pressure increases the tensile response of the inner flange at a point approximately 60° from the clamp point, whereas a 45° incidence angle does not appear to increase the response over that resulting from a 90° incidence angle. No data was recorded at 90° from the clamp point for test shots 6-9.

The reader is cautioned that the analysis results shown for this specimen are in error due to the reasons discussed in Section 8.3. The magnitude of the error is unknown. To make a more meaningful comparison between test and analysis stress results, additional modifications must be made to NOVA-2 to allow for use of a shock loading environment that more nearly matches that which was measured.

TABLE XII
SPECIMEN 13 SHOCK LOAD TEST CONDITIONS

Test Shot No.	θ_1	θ_2	ΔP_{ff}	ΔP_{int}
1	90°	90°	Low	0.0
2	90°	90°	Low	0.0
3	90°	90°	0.55	0.0
4	90°	90°	1.10	0.0
5	90°	90°	2.0	0.0
6	90°	90°	1.2	3.0
7	90°	45°	1.2	0.0
8	90°	45°	0.92	3.0
9	90°	90°	7.5	0.0

θ_1 = Angle between shock propagation vector and longitudinal axis of the cylinder test specimen.

θ_2 = Angle between shock propagation vector and a plane that is tangent to the midspan of the frame.

ΔP_{ff} = Measured incident (free field) overpressure, psi.

ΔP_{int} = Uniform preblast overpressure inside the specimen, psi.

TEST SPECIMEN NO. 13
 COMPRESSIVE STRESS IN INNER FLANGE
 AT $\sim 5.5^\circ$ FROM CLAMP POINT
 (GAUGE S13-14)

○ TEST DATA

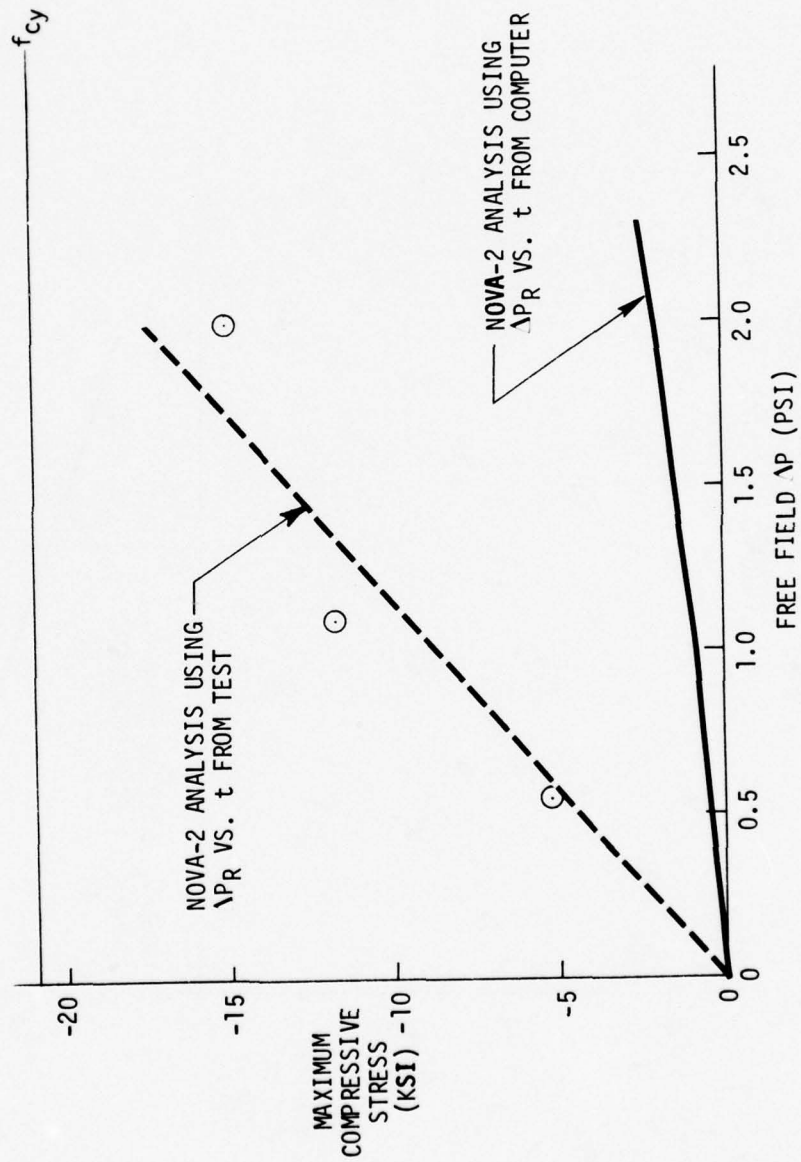


FIGURE 110. COMPRESSIVE STRESS VS. FREE FIELD OVERPRESSURE - SPECIMEN 13

TEST SPECIMEN NO. 13
TENSILE STRESS IN INNER FLANGE
AT ~5.5° FROM CLAMP POINT
(GAUGE S13-14)

○ TEST DATA

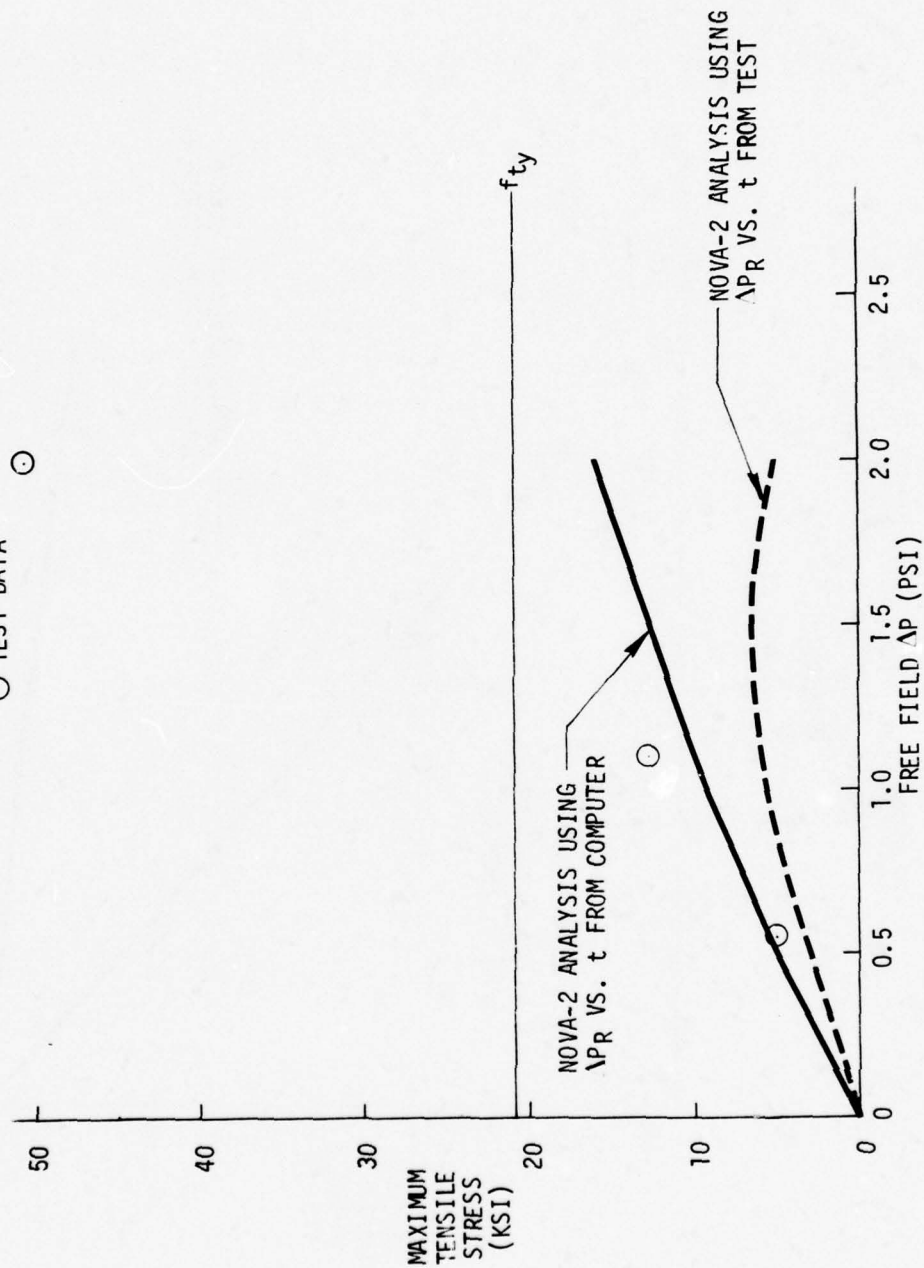


FIGURE 111. TENSILE STRESS VS. FREE FIELD OVERPRESSURE - SPECIMEN 13

TEST SPECIMEN NO. 13
 COMPRESSIVE STRESS IN INNER FLANGE
 AT $\sim 30^\circ$ FROM CLAMP POINT
 (GAUGE S13-10)

○ TEST DATA

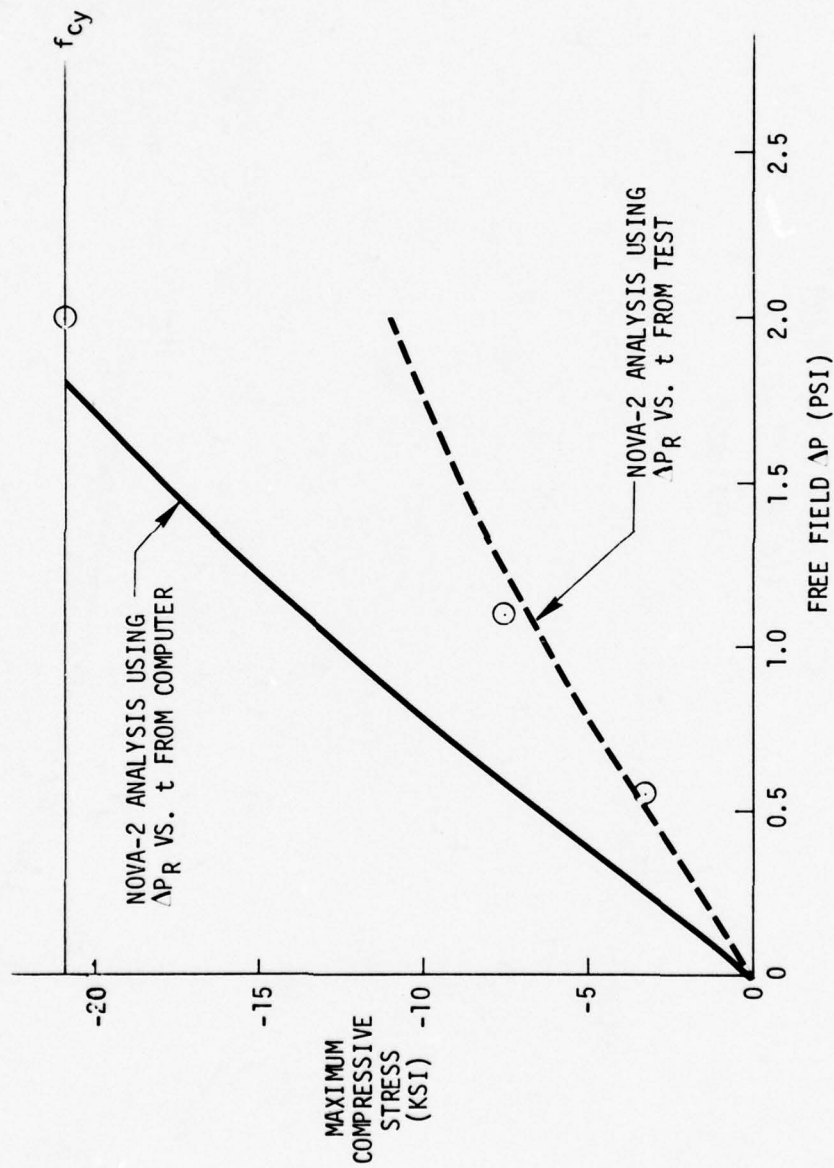


FIGURE 112. COMPRESSIVE STRESS VS. FREE FIELD OVERPRESSURE - SPECIMEN 13

TEST SPECIMEN NO. 13
TENSILE STRESS IN INNER FLANGE
AT $\sim 30^\circ$ FROM CLAMP POINT
(GAUGE S13-10)

○ TEST DATA

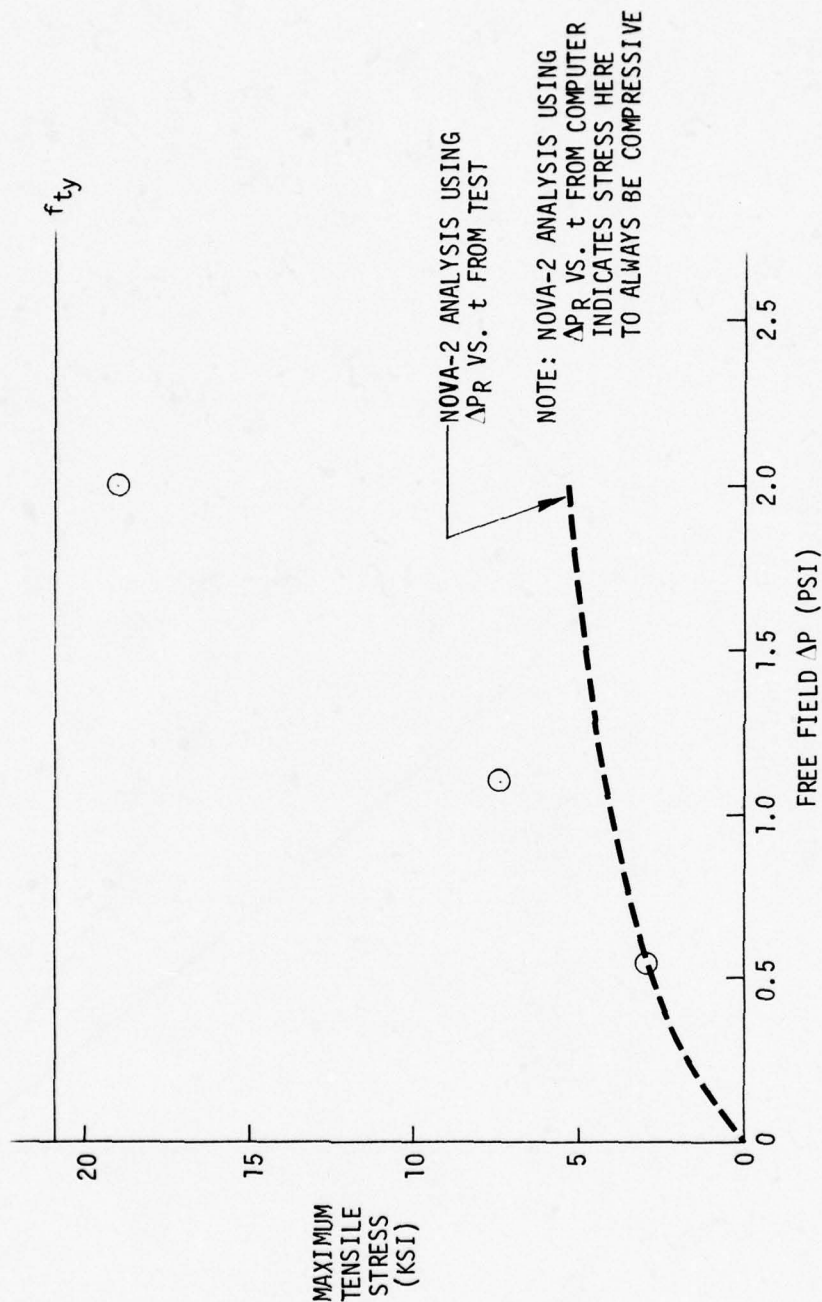


FIGURE 113. TENSILE STRESS VS. FREE FIELD OVERPRESSURE - SPECIMEN 13

TEST SPECIMEN NO. 13
 COMPRESSIVE STRESS IN INNER FLANGE
 AT $\sim 60^\circ$ FROM CLAMP POINT
 (GAUGE S13-7)

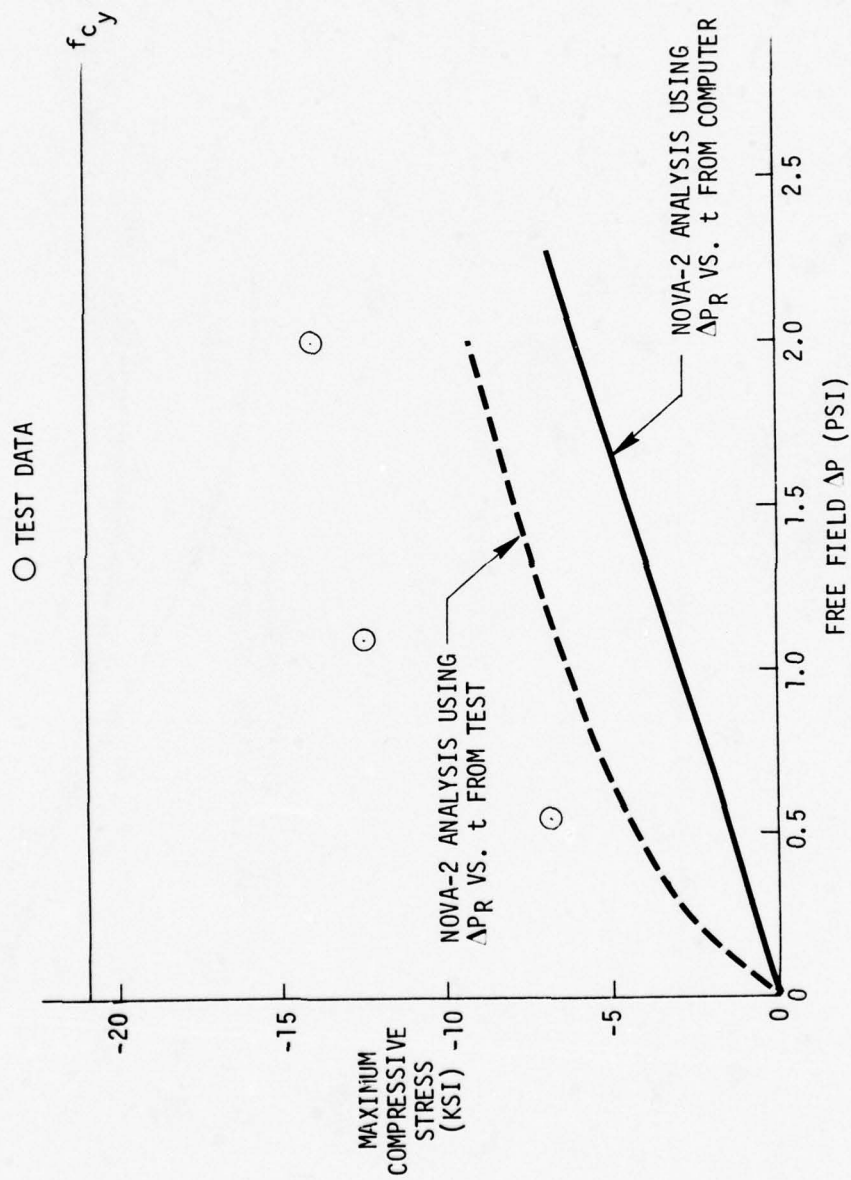


FIGURE 114. COMPRESSIVE STRESS VS. FREE FIELD OVERPRESSURE - SPECIMEN 13

TEST SPECIMEN NO. 13
TENSILE STRESS IN INNER FLANGE
AT ~60° FROM CLAMP POINT
(GAUGE S13-7)

○ TEST DATA

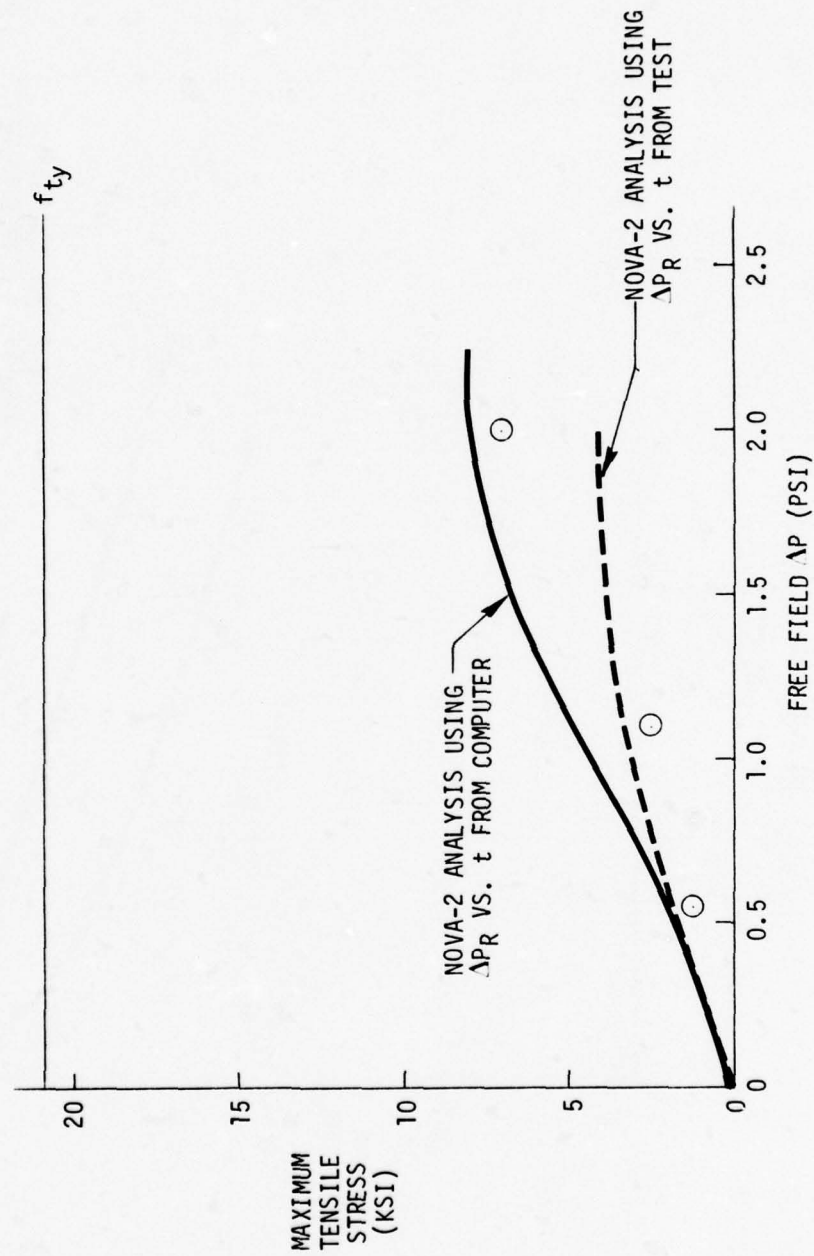


FIGURE 115. TENSILE STRESS VS. FREE FIELD OVERPRESSURE - SPECIMEN 13

TEST SPECIMEN NO. 13
 COMPRESSIVE STRESS IN INNER FLANGE
 AT 90° FROM CLAMP POINT
 (GAUGE S13-3)
 O TEST DATA

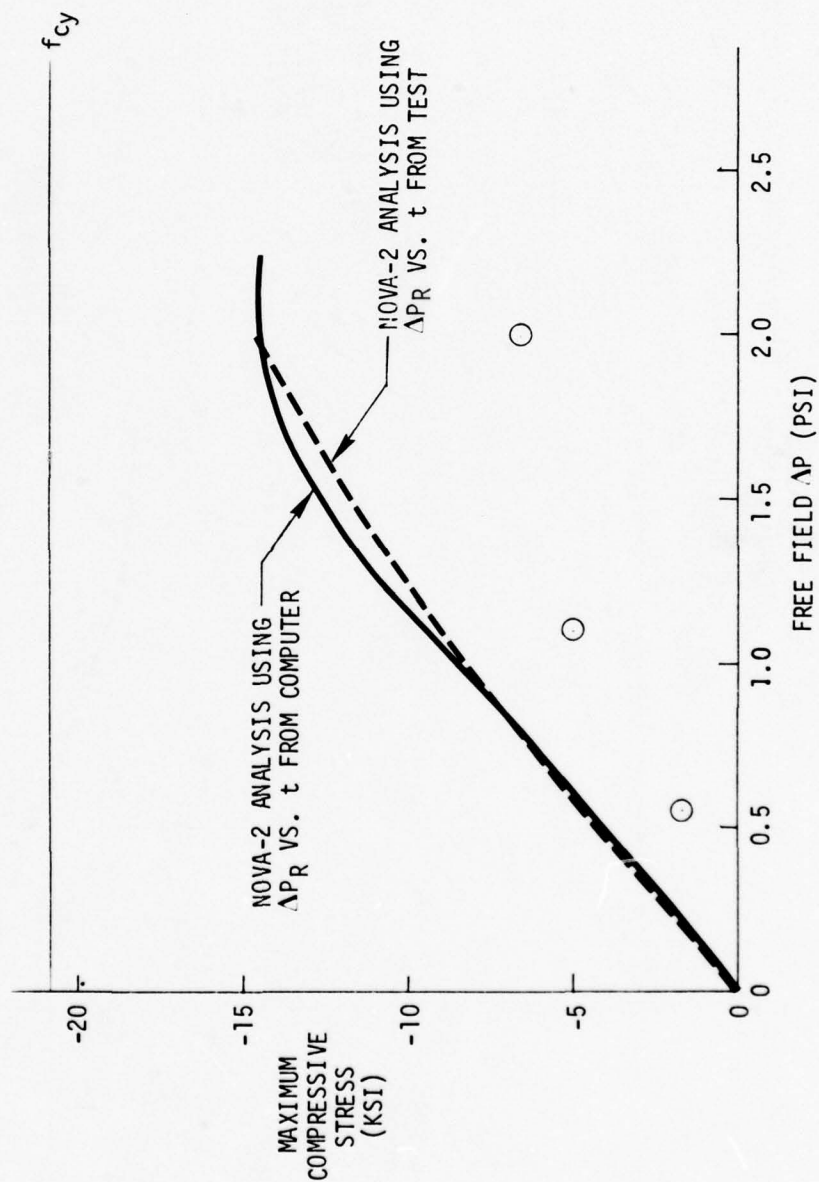
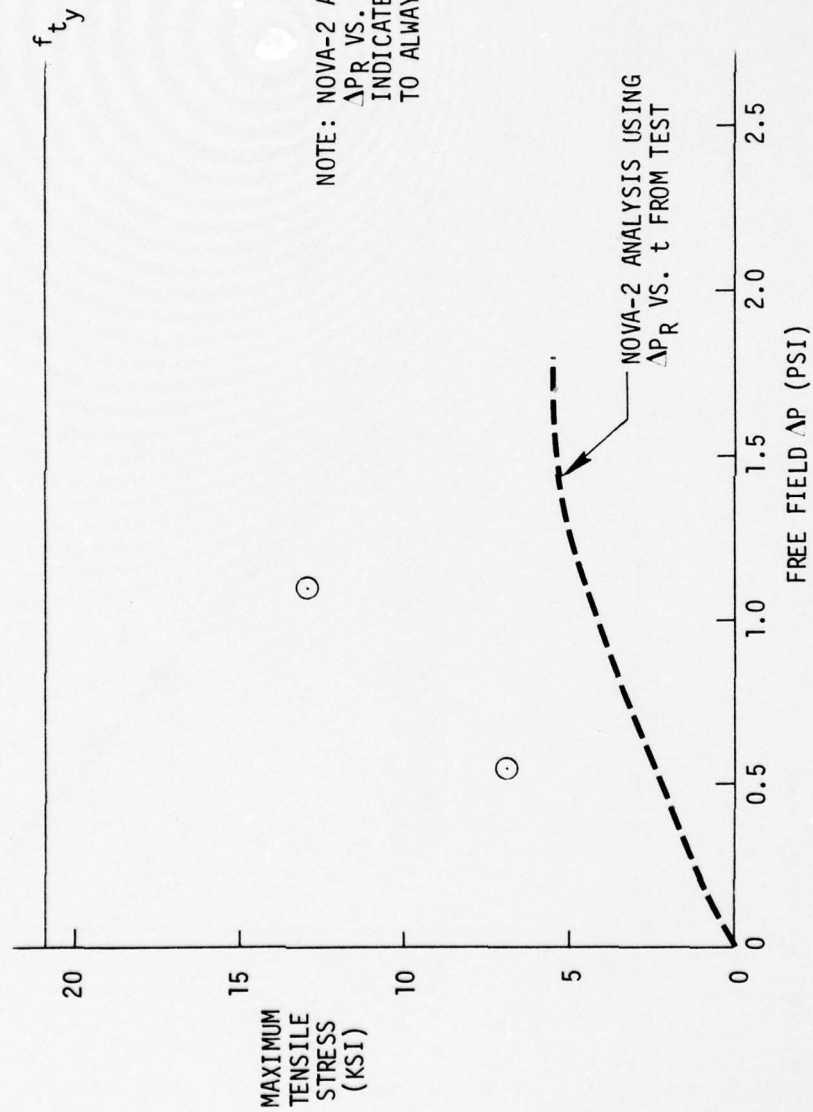


FIGURE 116. COMPRESSIVE STRESS VS. FREE FIELD OVERPRESSURE - SPECIMEN 13

TEST SPECIMEN NO. 13
TENSILE STRESS IN INNER FLANGE
AT 90° FROM CLAMP POINT
(GAUGE S13-3)

○ TEST DATA



NOTE: NOVA-2 ANALYSIS USING ΔP_R VS. t USING COMPUTER INDICATES STRESS HERE TO ALWAYS BE COMPRESSIVE

FIGURE 117. TENSILE STRESS VS. FREE FIELD OVERPRESSURE - SPECIMEN 13

TEST SPECIMEN NO. 13
 TEST SHOT NO. 4
 (GAUGE S13-3)
 ——— TEST DATA
 --- NOVA-2 ANALYSIS

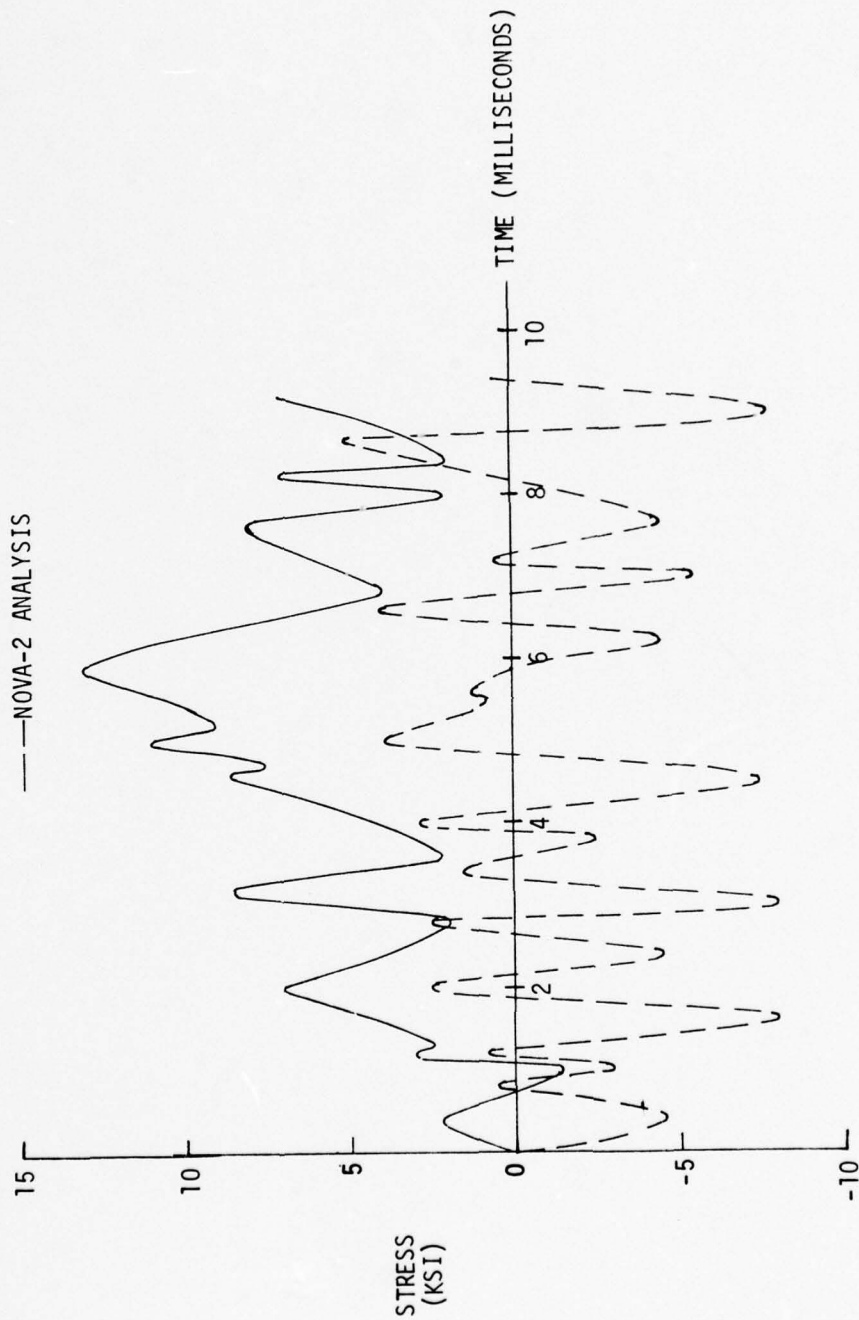


FIGURE 118. STRESS TIME HISTORY - SPECIMEN 13

TEST SPECIMEN NO. 13
 COMPRESSIVE STRESS IN INNER FLANGE
 AT 5.5° FROM CLAMP POINT

(GAUGE S13-14)

- $\Delta P_{INT} = 0.0$ ($\theta = 90^\circ$)
- $\Delta P_{INT} = 3.0$ ($\theta = 90^\circ$)
- △ $\Delta P_{INT} = 0.0$ ($\theta = 45^\circ$)
- ◇ $\Delta P_{INT} = 3.0$ ($\theta = 45^\circ$)

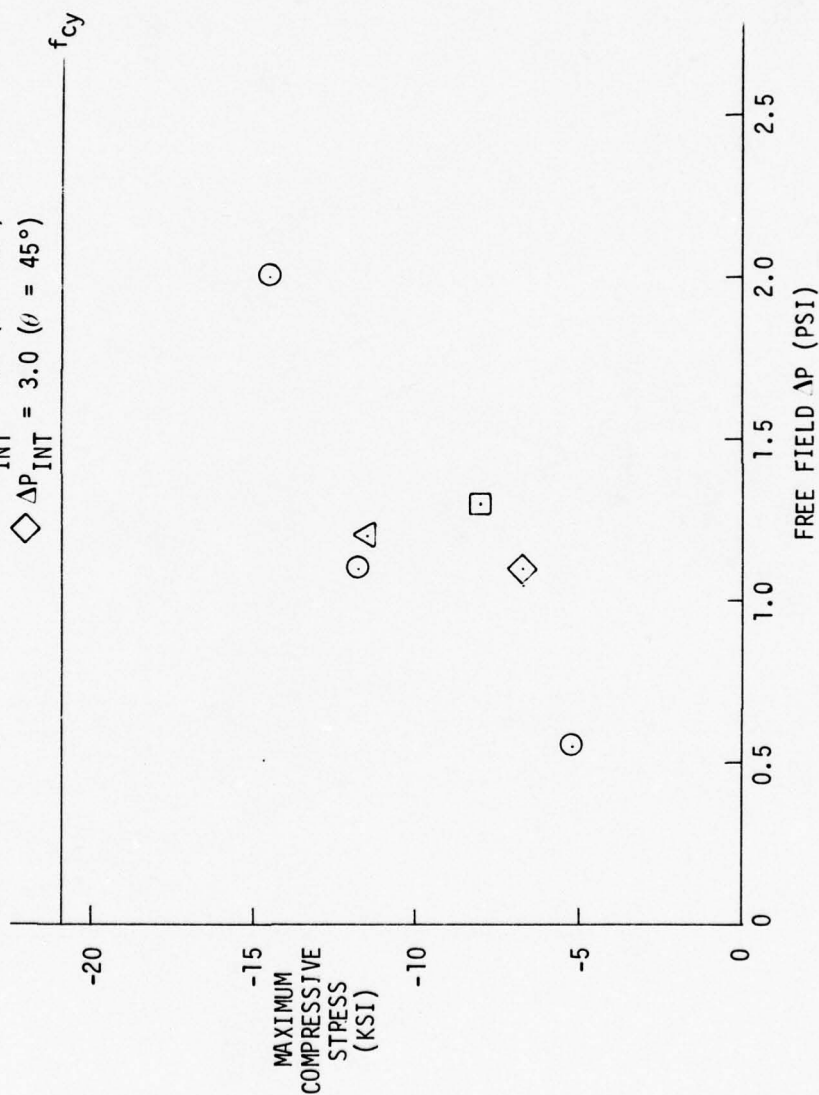


FIGURE 119. THE EFFECT OF INTERNAL PRESSURE AND SHOCK INCIDENCE ANGLE ON RESPONSE OF SPECIMEN 13

TEST SPECIMEN NO. 13
TENSILE STRESS IN INNER FLANGE
AT $\sim 5.5^\circ$ FROM CLAMP POINT
(GAUGE S13-14)

- $\Delta P_{INT} = 0.0$ ($\theta = 90^\circ$)
- $\Delta P_{INT} = 3.0$ ($\theta = 90^\circ$)
- △ $\Delta P_{INT} = 0.0$ ($\theta = 45^\circ$)
- ◇ $\Delta P_{INT} = 3.0$ ($\theta = 45^\circ$)

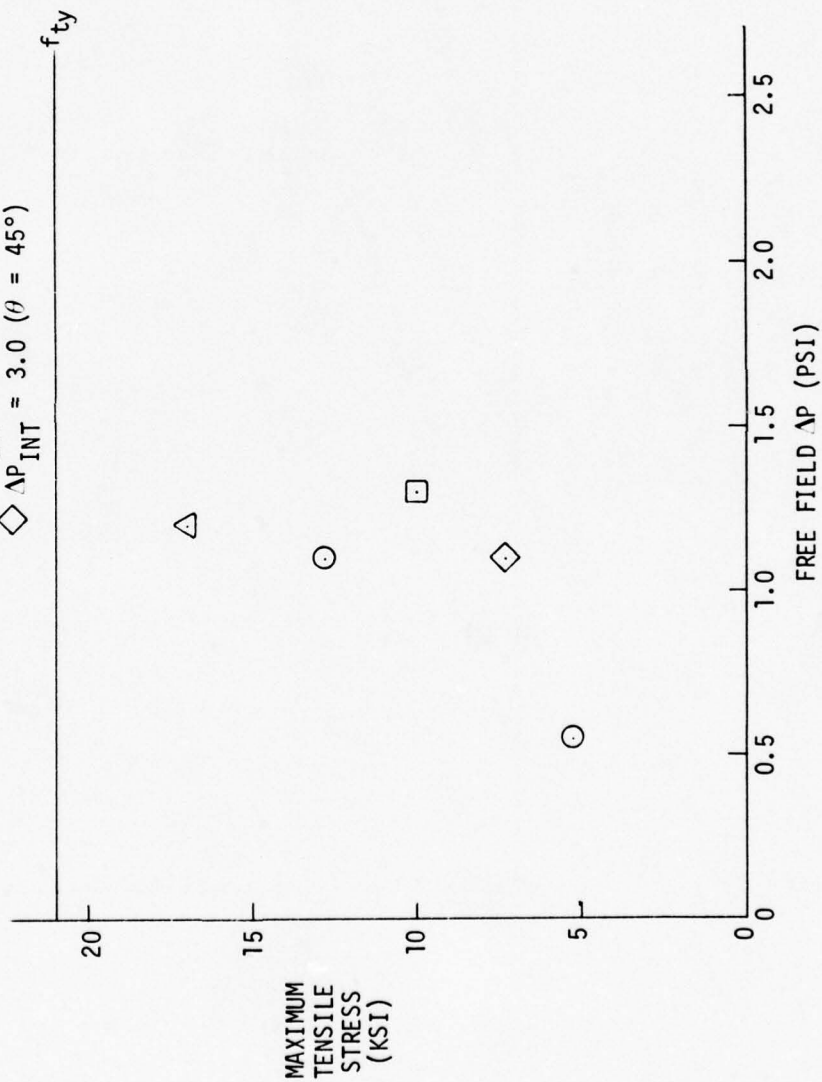


FIGURE 120. THE EFFECT OF INTERNAL PRESSURE AND SHOCK INCIDENCE ANGLE ON RESPONSE OF SPECIMEN 13

TEST SPECIMEN NO. 13
 COMPRESSIVE STRESS IN INNER FLANGE
 AT 30° FROM CLAMP POINT
 (GAUGE S13-10)

- $\Delta P_{INT} = 0.0$ ($\theta = 90^\circ$)
- $\Delta P_{INT} = 3.0$ ($\theta = 90^\circ$)
- △ $\Delta P_{INT} = 0.0$ ($\theta = 45^\circ$)
- ◇ $\Delta P_{INT} = 3.0$ ($\theta = 45^\circ$)

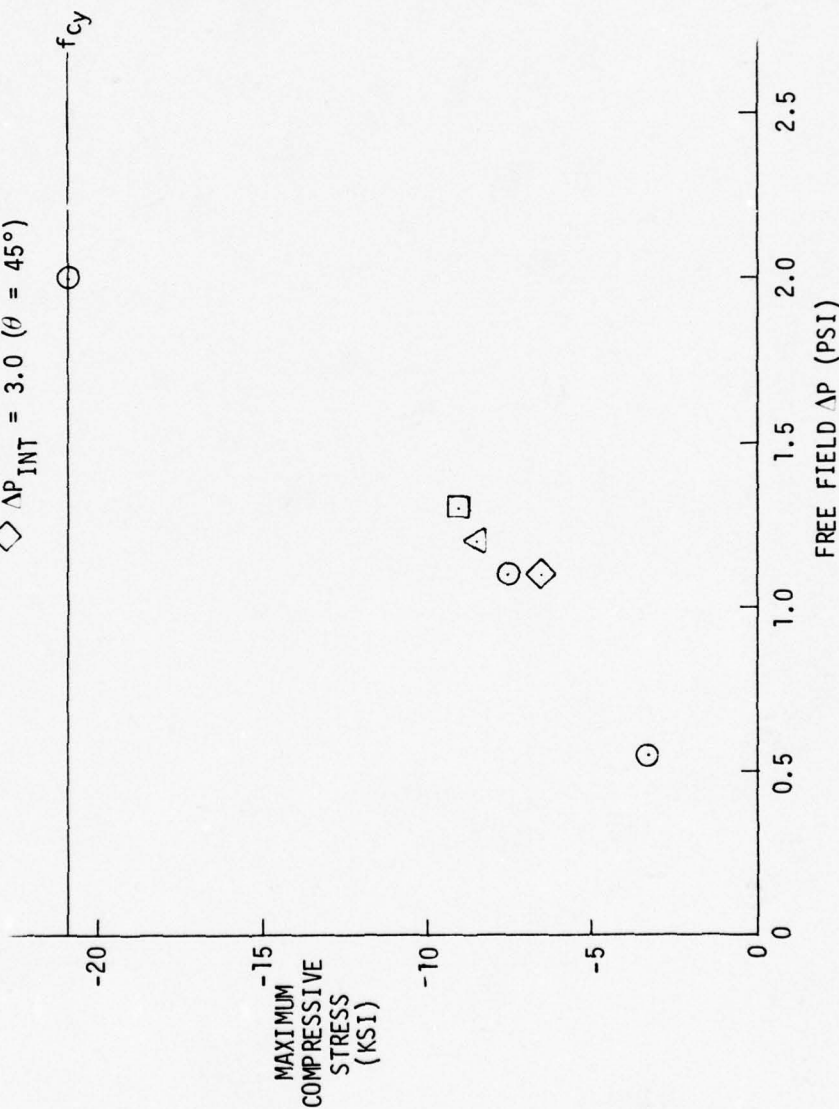


FIGURE 121. THE EFFECT OF INTERNAL PRESSURE AND SHOCK INCIDENCE ANGLE ON RESPONSE OF SPECIMEN 13

TEST SPECIMEN NO. 13
TENSILE STRESS IN INNER FLANGE
AT 30° FROM CLAMP POINT
(GAUGE S13-10)

- $\Delta P_{INT} = 0.0$ ($\theta = 90^\circ$)
- $\Delta P_{INT} = 3.0$ ($\theta = 90^\circ$)
- △ $\Delta P_{INT} = 0.0$ ($\theta = 45^\circ$)
- ◇ $\Delta P_{INT} = 3.0$ ($\theta = 45^\circ$)

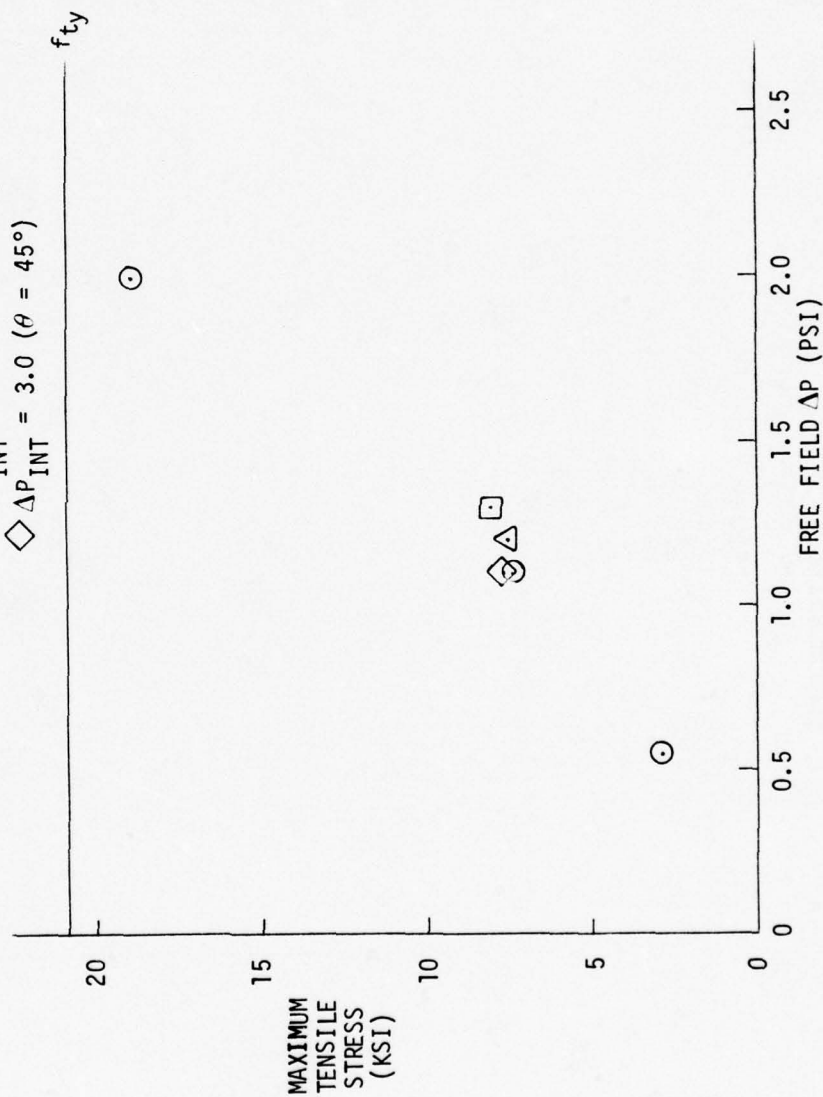


FIGURE 122. THE EFFECT OF INTERNAL PRESSURE AND SHOCK INCIDENCE ANGLE ON RESPONSE OF SPECIMEN 13

TEST SPECIMEN NO. 13
 COMPRESSIVE STRESS IN INNER FLANGE
 AT 60° FROM CLAMP POINT
 (GAUGE S13-7)

- $\Delta P_{INT} = 0.0$ ($\theta = 90^\circ$)
- $\Delta P_{INT} = 3.0$ ($\theta = 90^\circ$)
- △ $\Delta P_{INT} = 0.0$ ($\theta = 45^\circ$)
- ◇ $\Delta P_{INT} = 3.0$ ($\theta = 45^\circ$)

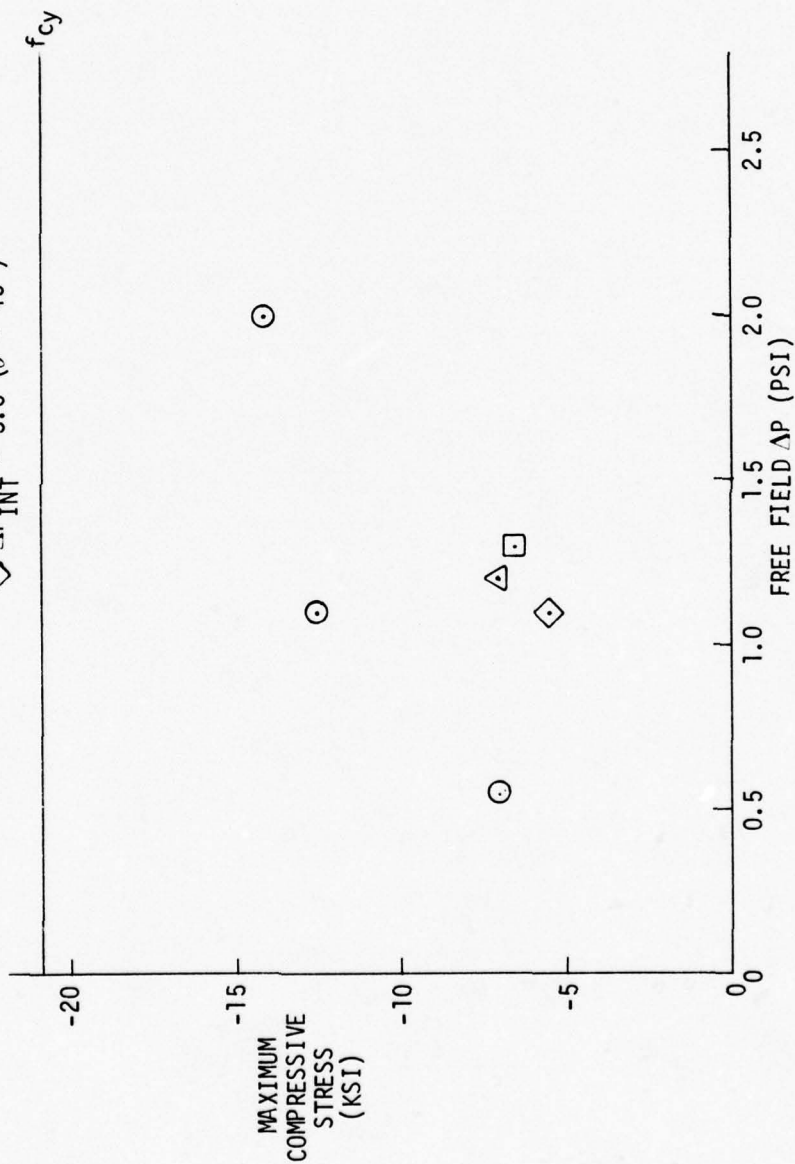


FIGURE 123. THE EFFECT OF INTERNAL PRESSURE AND SHOCK INCIDENCE ANGLE ON RESPONSE OF SPECIMEN 13

TEST SPECIMEN NO. 13
TENSILE STRESS IN INNER FLANGE
AT 60° FROM CLAMP POINT
(GAUGE S13-7)

- $\Delta P_{INT} = 0.0$ ($\theta = 90^\circ$)
- $\Delta P_{INT} = 3.0$ ($\theta = 90^\circ$)
- △ $\Delta P_{INT} = 0.0$ ($\theta = 45^\circ$)
- ◇ $\Delta P_{INT} = 3.0$ ($\theta = 45^\circ$)

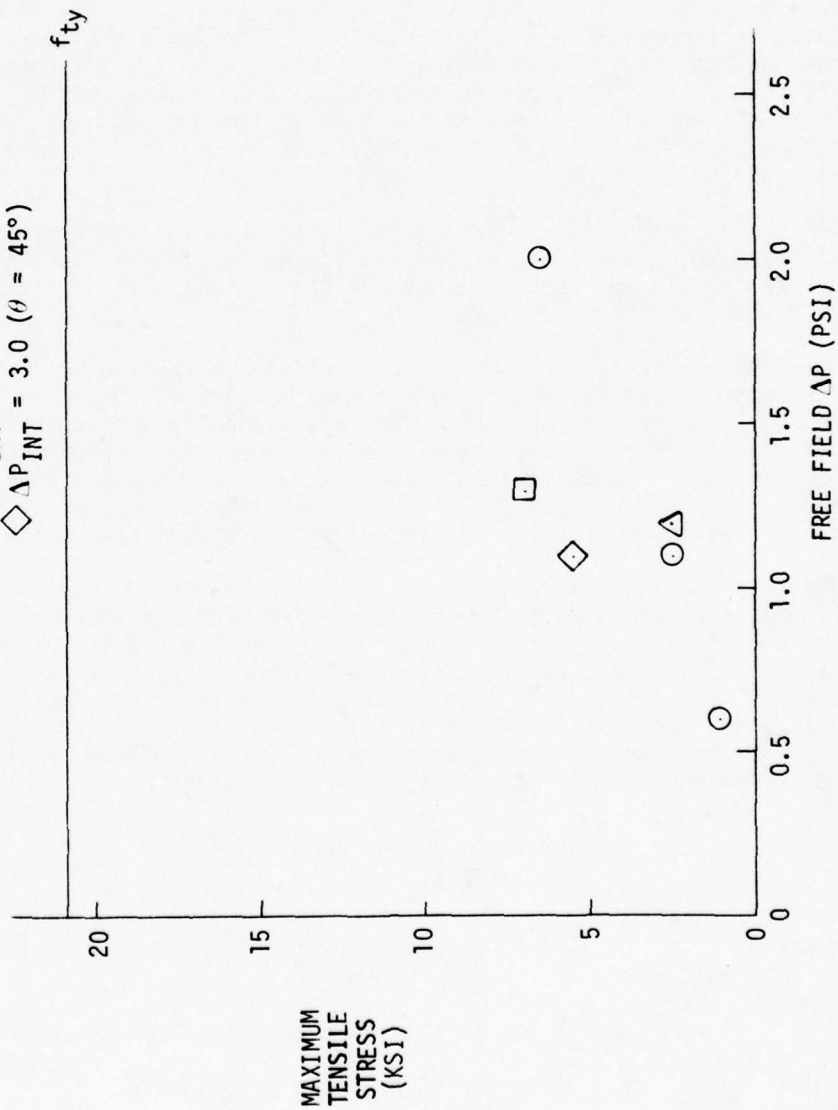


FIGURE 124. THE EFFECT OF INTERNAL PRESSURE AND SHOCK INCIDENCE ANGLE ON RESPONSE OF SPECIMEN 13

8.3.14 Test Specimen No. 14-17

Test specimens 14-17 are four essentially identical columns as described in Tables I and II and Section 8.2.14. As stated earlier in this report, the only significant difference between these specimens was the amount of initial lateral imperfection at the column centers. These initial lateral imperfections were $<.01$, $.01$, $<.01$, and $.03$ inches for specimens 14, 15, 16 and 17, respectively.

During the shock load testing of specimens 14-17, the box holding fixture shown in Figure 125 was utilized. The columns were positioned inside the box holding fixture with one end fixed to prohibit displacement and one end attached to a loading piston permitting axial displacement. Figure 125 shows the position of the four pistons in the box holding fixture. The attachment of the piston to the column is illustrated in more detail in Figure 126.

The box holding fixture was oriented such that the shock propagation vector was perpendicular to the piston faces. As the piston faces were loaded by the shock wave, they displaced in the cylinder and, in turn, provided axial load to the columns.

The NOVA-2 computer program is not designed to analyze this structural configuration directly, and therefore modification of NOVA-2 by AFWL was required. Furthermore, no provisions are available within NOVA-2 for including friction forces which may have existed between the pistons and the cylinders. However, with the exception of one test data point where the piston obviously bound up in the cylinder, the lack of substantial scatter in the response data indicates that friction effects were probably negligible.

The test and analysis results are shown in Figure 127. As indicated in this figure, the stress data are well clustered with the exception of specimen 17 for the final test shot. Three of the columns yielded at approximately 15.2 psi free field overpressure. Also shown are analysis results for columns with $.01$ and $.03$ inches initial imperfection. These imperfections define the preblast condition of the column at its center. In the NOVA-2 computer program the remainder of the column is defined to exhibit initial imperfections as described in the following equation:

$$\Delta w = \frac{\delta}{2} \left[1 - \cos \left(\frac{2\pi x}{L} \right) \right]$$

where

Δw = Initial imperfection at an axial location x on the column.

δ = Initial imperfection at center of column.

x = Axial position on column

L = Column length

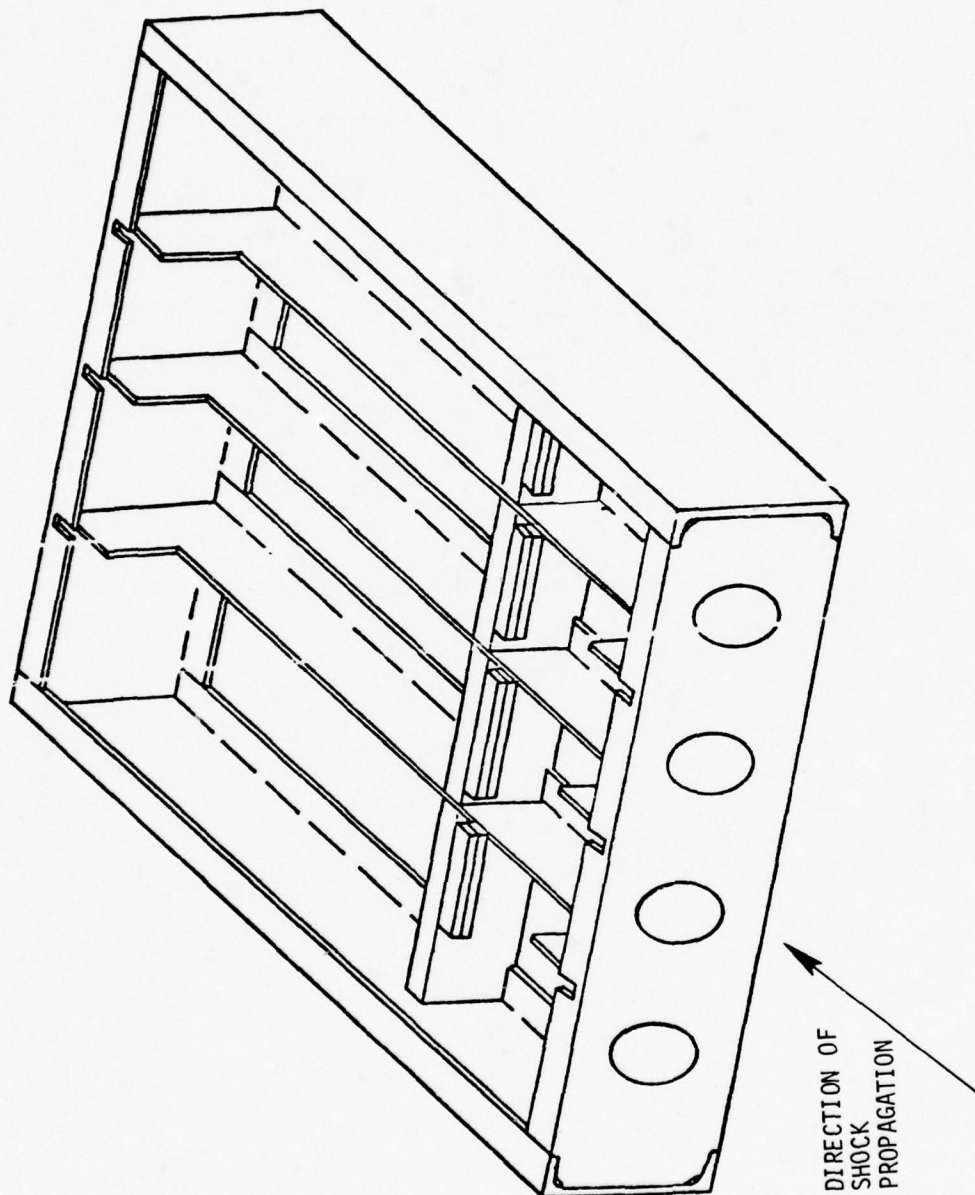


FIGURE 125. BOX HOLDING FIXTURE

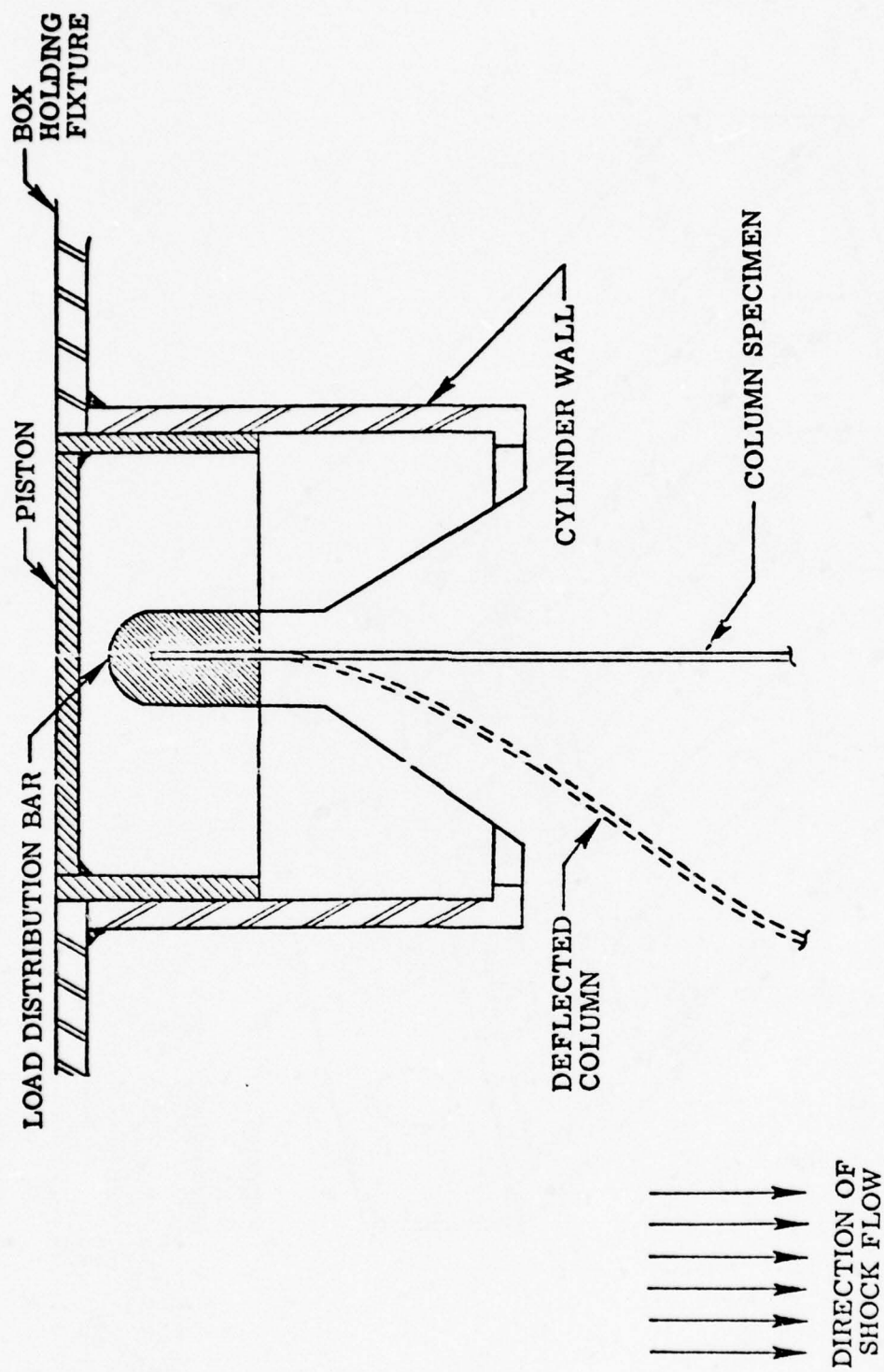


FIGURE 126. COLUMN LOADING DEVICE

TEST SPECIMENS 14 - 17
STRESS AT CENTER OF COLUMNS
(GAUGES S14-1, S15-2, S16-2, S17-2)

- SPECIMEN 14, INITIAL IMP < .01
- SPECIMEN 15, INITIAL IMP = .01
- △ SPECIMEN 16, INITIAL IMP < .01
- ◇ SPECIMEN 17, INITIAL IMP = .03

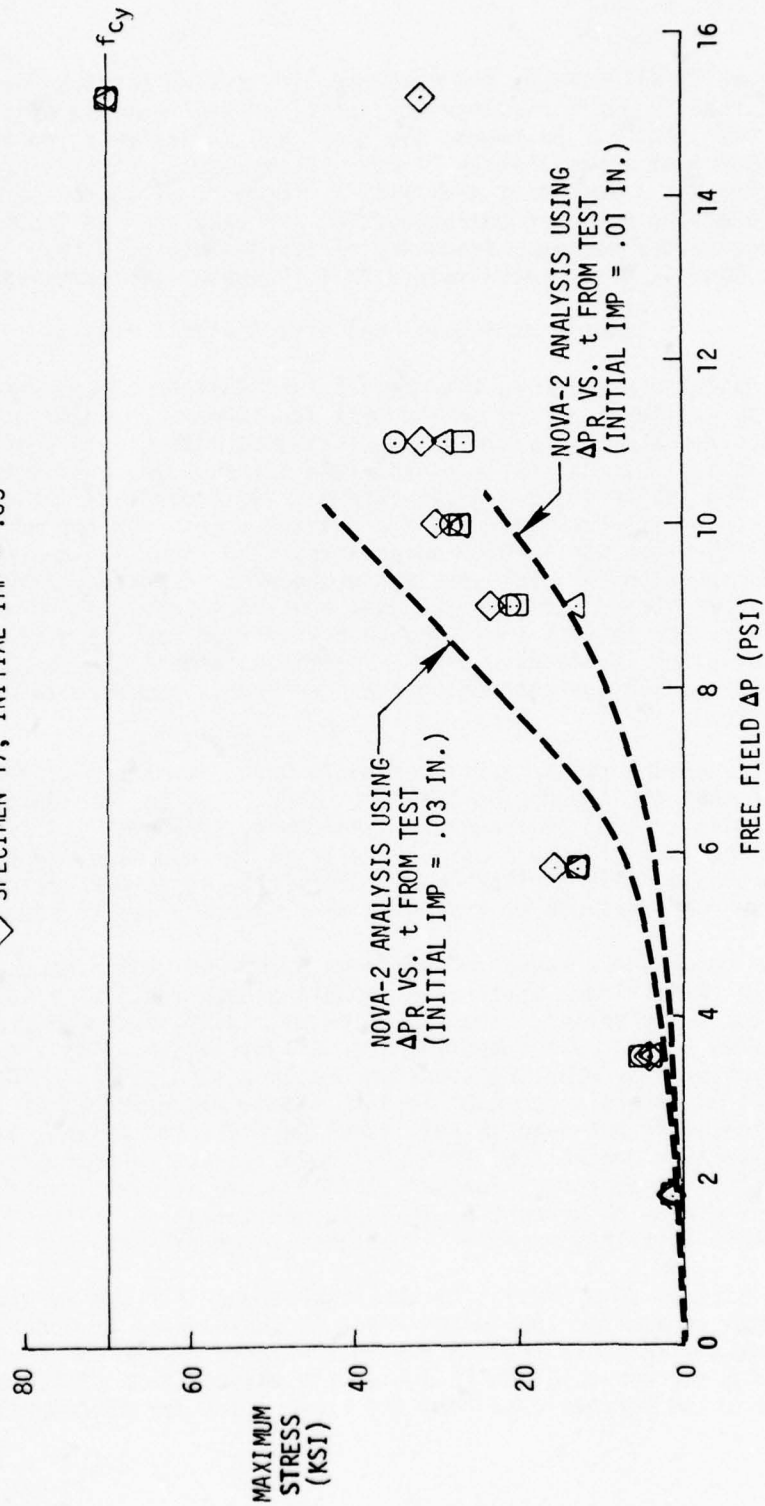


FIGURE 127. STRESS VS. FREE FIELD OVERPRESSURE - SPECIMENS 14 - 17

Figure 128 illustrates the measured stress time history for specimen 16 for test shot 5. This response is typical of the response of all four columns for test shot 5. As shown, the test data indicates a fundamental response frequency of approximately 11 cps. Superimposed on this mode of response, however, is a secondary mode with a frequency of approximately 1400 cps. The analysis data for this condition are tabulated in Table XIII and indicate a fundamental response frequency of approximately 10 cps. Superimposed on this mode is a secondary mode with a frequency of approximately 1250 cps.

8.4 Summary of Static Load Test/Analysis Results

As indicated earlier in this report, all test specimens were static tested, but not to failure. Since the test specimens were purposely not tested up to their respective yield point, it is not possible to compare static test and analysis loads resulting in yield stress without significantly extrapolating test results. As an alternative, Figure 129 illustrates a comparison of measured stress and predicted stress for the maximum static load condition that was imposed on each test specimen. In general, the maximum load condition for each specimen produced a stress equal to 50-75 percent of the yield stress. Figure 129 does provide valuable trend information; however, the results would change for certain specimens if the static test had resulted in yielding of the specimens, and if the comparison had been made regarding the respective pressure levels required to cause this yielding.

As discussed earlier, test specimen 5 was a homogeneous, flat, unstiffened panel that was clamped on all four edges. Due to its geometry (length/thickness = 1100) and boundary conditions, stress at the center of the edge and in a direction perpendicular to the edge was found to increase dramatically with applied load. Difficulty was experienced in predicting the proper magnitude of stress at this location due to convergence problems.

Three results are shown for specimen 6 (curved unstiffened panel). The first result (PANEL*) was obtained by modeling specimen 6 as a curved panel without initial imperfection. The second result (BEAM) was obtained by modeling specimen 6 as a curved beam or arch of unit width. The third result (PANEL**) was achieved by modeling specimen 6 as a curved panel including an initial radial imperfection of 0.01 inches. Since measurements of initial imperfections were not made on this specimen prior to testing, it is not possible to determine whether the (PANEL**) model is a true representation of the actual test specimen. However, this assumed initial imperfection is only approximately 10 percent of the specimen thickness. Therefore, it is possible that this model is a reasonable representation of specimen 6.

In addition, some difficulty was experienced in properly predicting the maximum stress for specimens 12 and 13 (skin/frame cylinders). Maximum measured stress occurred in the inner flange of the center frame near the clamp point for specimen 12 and at the extreme inner fiber of the center frame at 30 degrees away from the clamp point for specimen 13.

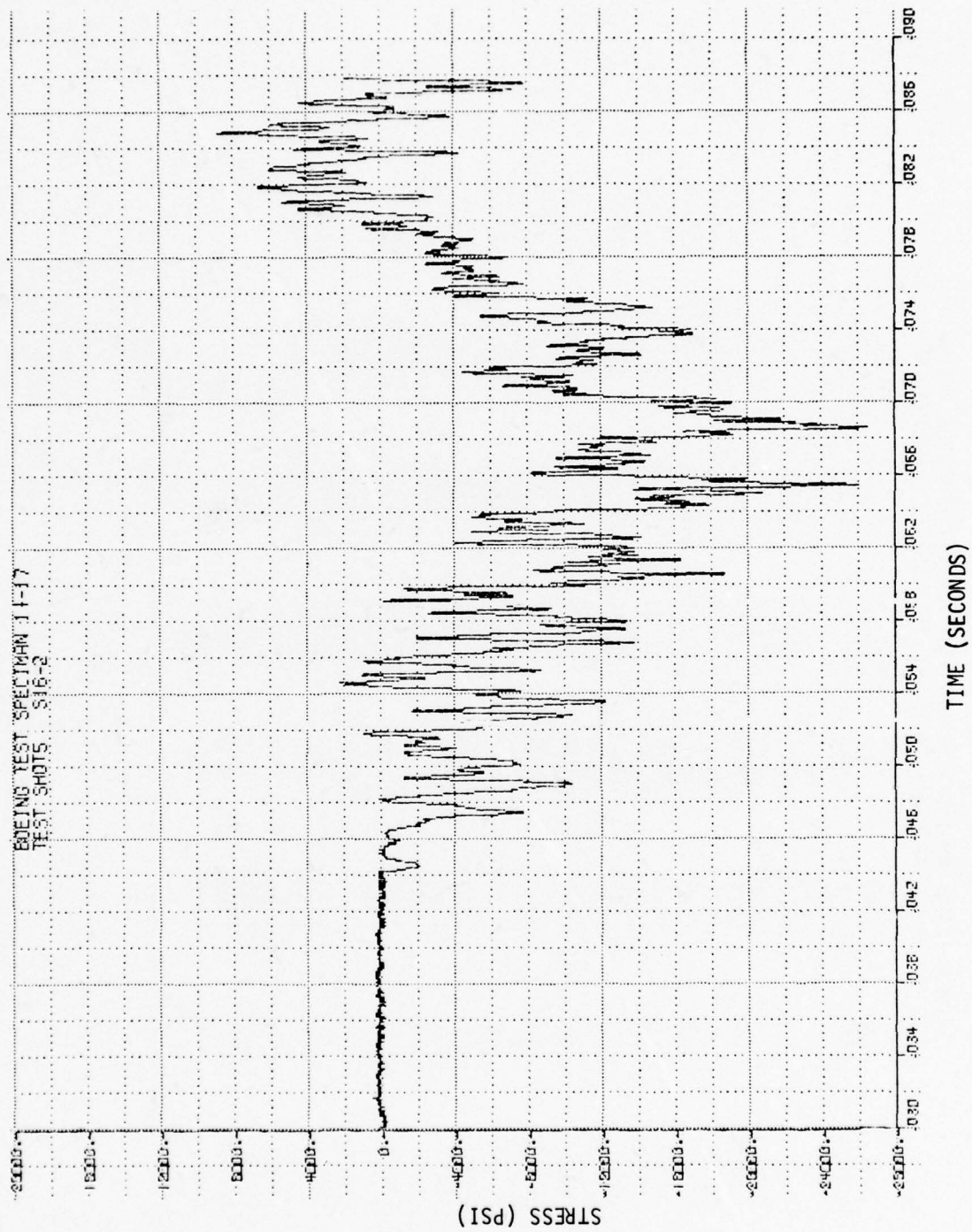


FIGURE 128. STRESS TIME HISTORY - SPECIMEN 16

TABLE XIII - ANALYSIS STRESS TIME HISTORY DATA FOR CENTER OF SPECIMEN 14-17 FOR TEST SHOT 5 (INITIAL IMP = 0.01")

Time (Seconds)	σ (PSI)	Time (Seconds)	σ (PSI)	Time (Seconds)	σ (PSI)		
0.0	0.0	.01052	-7150.	.02012	-14904.	.02578	-20744.
.000472	-2125.	.01090	-3676.	.02039	-17925.	.02592	-19334.
.000899	+3091.	.01133	-8358.	.02048	-17320.	.02616	-21348.
.00135	-2276.	.01169	-5035.	.02063	-18529.	.02637	-17421.
.00178	0.0	.01207	-9264.	.02140	-14904.	.02652	-20644.
.00220	-2014.	.01245	-5790.	.02165	-19637.	.02670	-18630.
.00258	+114.	.01286	-10574.	.02187	-16112.	.02691	-21147.
.00301	-2518.	.01324	-6848.	.02201	-18630.	.02711	-17623.
.00348	+352.	.01367	-11077.	.02216	-17522.	.02767	-20140.
.00389	-2397.	.01400	-7653.	.02237	-19032.	.02785	-16313.
.00432	-25.	.01443	-12487.	.02266	-15709.	.02805	-19133.
.00477	-3222.	.01479	-8761.	.02288	-18932.	.02823	-16716.
.00517	-298.	.01517	-12285.	.02313	-20039.	.02843	-19237.
.00562	-3384.	.01553	-9063.	.02338	-15911.	.02861	-16011.
.00602	-886.	.01594	-14098.	.02351	-19133.	.02881	-18529.
.00645	-3736.	.01632	-9869.	.02369	-17723.	.02897	-16212.
.00683	-1208.	.01681	-14400.	.02389	-19838.	.02918	-18630.
.00728	-4572.	.01708	-11379.	.02414	-16414.	.02940	-14904.
.00767	-1813.	.01749	-15709.	.02443	-19637.	.02956	-18327.
.00811	-5095.	.01785	-12084.	.02466	-21046.	.02976	-16112.
.00847	-2387.	.01832	-16817.	.02486	-16918.	.02999	-18730.
.00892	-6183.	.01859	-13695.	.02502	-20140.		
.00930	-2669.	.01893	-17119.	.02520	-18327.		
.00973	-6465.	.01935	-13695.	.02540	-20845.		
.01012	-2971.	.01985	-19032.	.02563	-17723.		

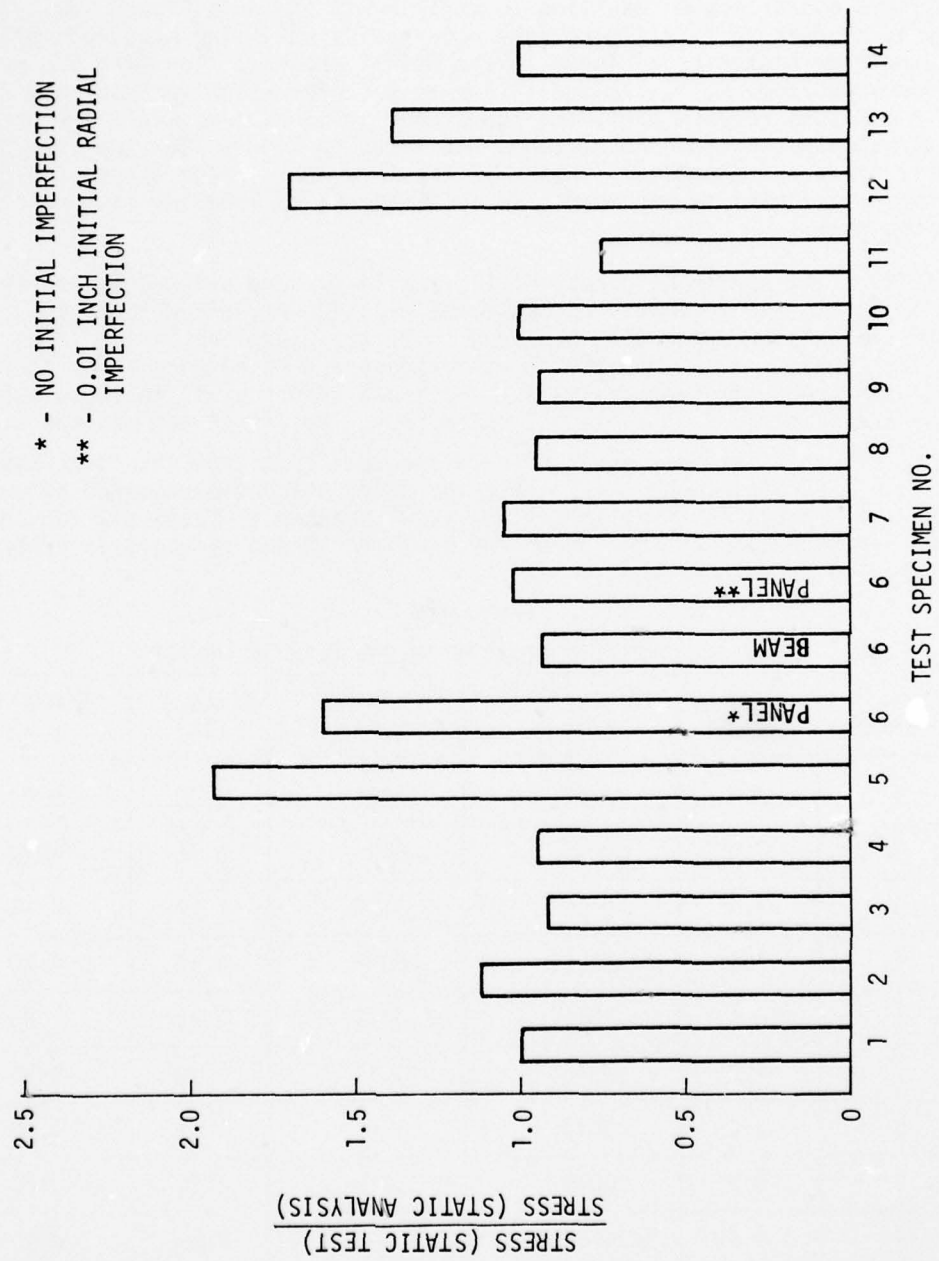


FIGURE 129. STATIC TEST AND ANALYSIS RATIO VS. SPECIMEN NO.

8.5

Summary of Shock Load Test/Analysis Results

As discussed earlier, all test specimens were exposed to a series of simulated nuclear overpressure environments resulting in stresses up to yield and beyond. The specimens were analyzed by utilizing the measured reflected pressure time histories as well as computer generated pressure time histories. A comparison of the test peak free field overpressure and the analysis peak free field overpressure resulting in yielding is shown in Figure 130. The analysis results in this figure were obtained by utilizing measured reflected pressure time histories as input to the NOVA-2 program. Ignoring the results for test specimens 6, 11, 12 and 13 due to the discussion in Section 8.3, the NOVA-2 analysis results predicted the proper critical free field overpressure for all specimens within 20 percent. As noted in Figure 130, the analysis results for specimens 6, 11, 12 and 13 are in error. Since the degree of error for these specimens is not known, it is difficult to make any firm conclusions from the data.

In addition all specimens except 6, 11, and 14-17 were exposed to one test shot of sufficient intensity to cause measurable permanent deformation. All of these conditions were also analyzed, with the exception of the final test shot for specimen 13 (since pressure transducers were removed prior to this shot). The comparison of analysis results and test results in the plastic region are summarized in Table XIV below. ϵ_{\max} refers to the maximum strain and δ refers to the permanent deformation resulting from the final test shot. Subsequent to completion of the analysis, Kaman Avidyne discovered an error in the NOVA-2 program that may impact the results shown in Table XIV for specimen 9. Analysis results are not shown for specimen 12 due to analysis errors described in Section 8.3.

TABLE XIV
TEST AND ANALYSIS RESULTS IN THE PLASTIC REGION

Test Specimen	ΔP_{ff} (PSI)	$\epsilon_{\max}^{(Test)}$ (in/in)	$\epsilon_{\max}^{(Anal)}$ (in/in)	$\delta^{(Test)}$ (in)	$\delta^{(Anal)}$ (in)
1	6.5	.0127	.0084	0.06	0.0
2	7.5	.0049	.0032	0.78	0.20
3	7.3	.0120	.0109	0.14	0.13
4	11.5	.0019	.0018	0.16	0.20
5	3.5	.0014	.0019	0.92	1.25
7	1.7	.0040	.0054	0.20	0.45
8	3.4	.0013	.0019	0.75	1.50
9	5.2	.0019	.0013	0.50	0.20
10	4.4	Saturated Signal	-	0.60	0.40
12	7.2	Saturated Signal	-	0.20	

NOTE: ΔP IS THAT LEVEL OF FREE
FIELD OVERPRESSURE RESULTING
IN THRESHOLD OF DAMAGE

* - 0.01 INCH INITIAL RADIAL
IMPERFECTION

+ - ANALYSIS IS IN ERROR,
SEE SECTION 8.3

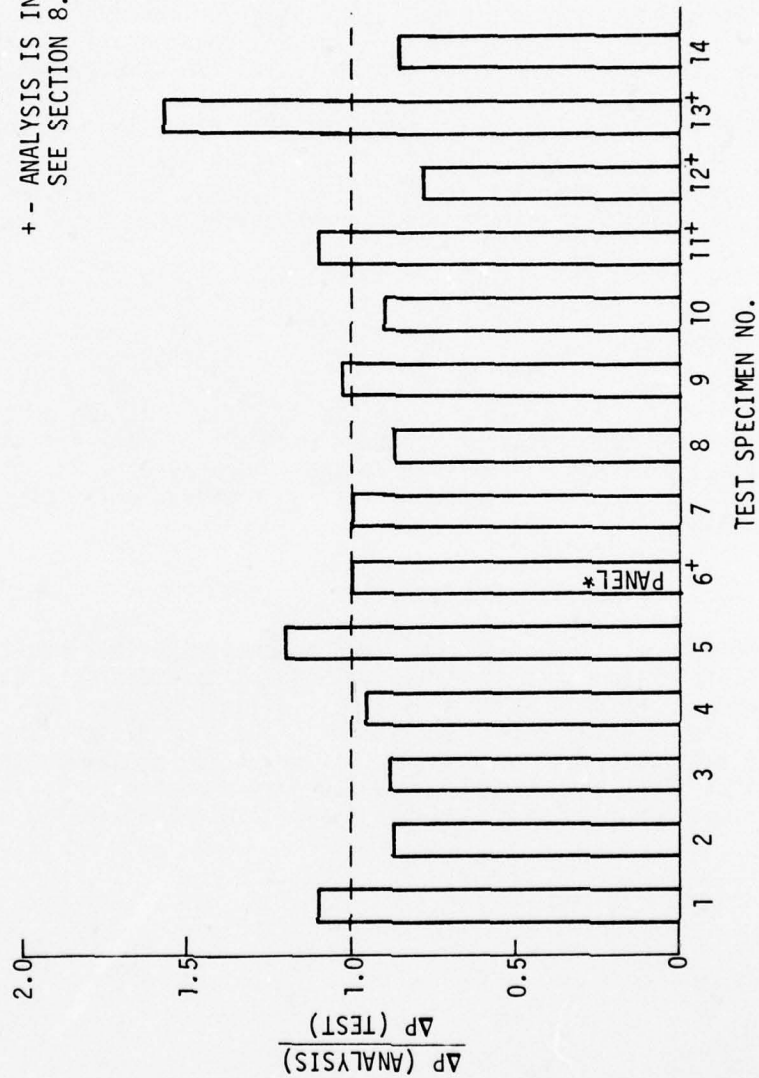


FIGURE 130. SHOCK LOAD ANALYSIS AND TEST RATIO VS. SPECIMEN NO.

Structural response due to a shock load environment can be significantly greater than that resulting from exposure to a static overpressure environment even though the peak pressure intensities of the two environments are identical. This phenomenon occurs because: (1) the free field (incident) overpressure is enhanced due to reflection and (2) magnification of the response results from the dynamic nature of the loading. In other words, a specific structural response in a particular test specimen will be caused by exposure to a simulated nuclear overpressure pulse whose peak free field intensity is, in general, considerably less than the magnitude of static overpressure which causes the same structural response. This is shown in Figure 131 for specimens 1-14. Specifically, this figure compares the peak free field overpressure intensity (ΔP_{ff}) resulting in a specific structural response to the static overpressure (ΔP_s) resulting in the same structural response. The response for each test specimen is the maximum stress that it experienced during the static test.

With the exception of test specimen 14-17, Figure 131 indicates that the structural response resulting from exposure to a given static load can also be obtained from exposure to a simulated nuclear overpressure load with a peak free field intensity 20-35 percent of the static overpressure level. It is anticipated that results similar to this would also be observed at load levels necessary to cause yielding of the specimens. The data for test specimen 14 are an average of data for four essentially identical buckling - sensitive columns. The results for these columns indicate essentially the same stress/load characteristics for both types of loading.

A limited analysis was accomplished to determine the sensitivity of structural response to selected structural parameters. Length, width, thickness, and modulus of elasticity variations were analyzed for a square flat panel clamped on all four edges. The nominal specimen was considered to be test specimen No. 1. In addition, beam length variations were analyzed for a straight beam with clamped boundary conditions, i.e., variations to test specimen 9. These variations are illustrated in Table XV below.

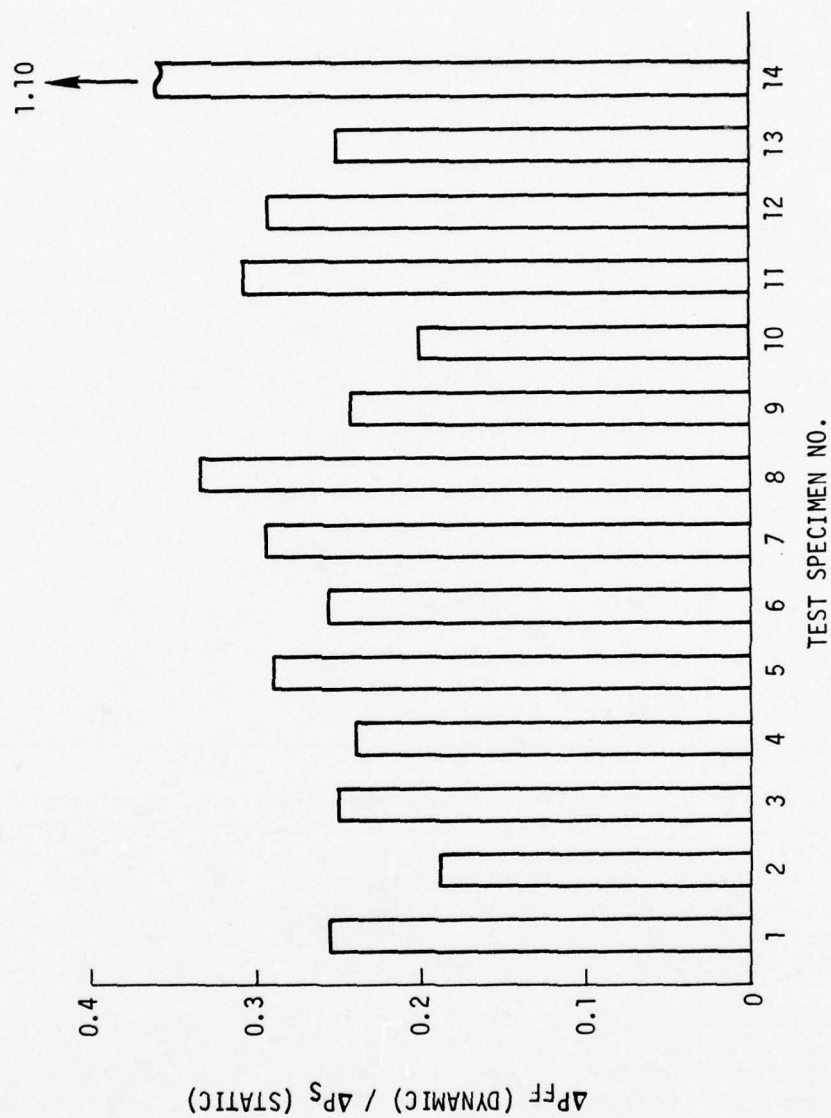


FIGURE 131. COMPARISON OF ΔP_{FF} AND ΔP_S FROM TEST RESULTING IN THE SAME STRUCTURAL RESPONSE VS. SPECIMEN NO.

TABLE XV
SENSITIVITY STUDY VARIATIONS

TEST SPECIMEN NO.	LENGTH (IN)	WIDTH(IN)	THICKNESS(IN)	MODULUS OF ELASTICITY (PSI)
1	22.0	22.0	0.191	11.0×10^6
1a	22.0	22.0	0.05	11.0×10^6
1b	22.0	22.0	0.10	11.0×10^6
1c	22.0	22.0	0.30	11.0×10^6
1d	11.0	11.0	0.191	11.0×10^6
1e	33.0	33.0	0.191	11.0×10^6
1f	16.5	16.5	0.191	11.0×10^6
1g	22.0	22.0	0.191	8.8×10^6
1h	22.0	22.0	0.191	13.2×10^6
9	36.0	NOM	NOM	NOM
9a	18.0	NOM	NOM	NOM
9b	54.0	NOM	NOM	NOM

The results of the sensitivity study are illustrated in Figures 132 through 135. Figure 132 shows the predicted free field pressure associated with the threshold of permanent damage as a function of panel thickness. The length and width of these specimens was 22.0 inches. These results indicate the pronounced nonlinear behavior of a flat, square, clamped panel as the thickness varies through the membrane region into the thin plate region and eventually into the thick plate region.

Figure 133 illustrates the effect of panel length and width on the response of a square flat panel fixed on all four edges. The thickness of these specimens was 0.191 inches. As would be expected, for a fixed panel thickness, the strength increases as the size of the panel decreases. The 11 inch square panel falls into the thick plate category, the 22 inch square panel falls into the thin plate category, whereas the 33 inch square panel is reasonably close to the membrane category.

SENSITIVITY STUDY RESULTS
 SQUARE FLAT PANEL WITH ALL SIDES CLAMPED
 LENGTH = WIDTH = 22.0 INCHES

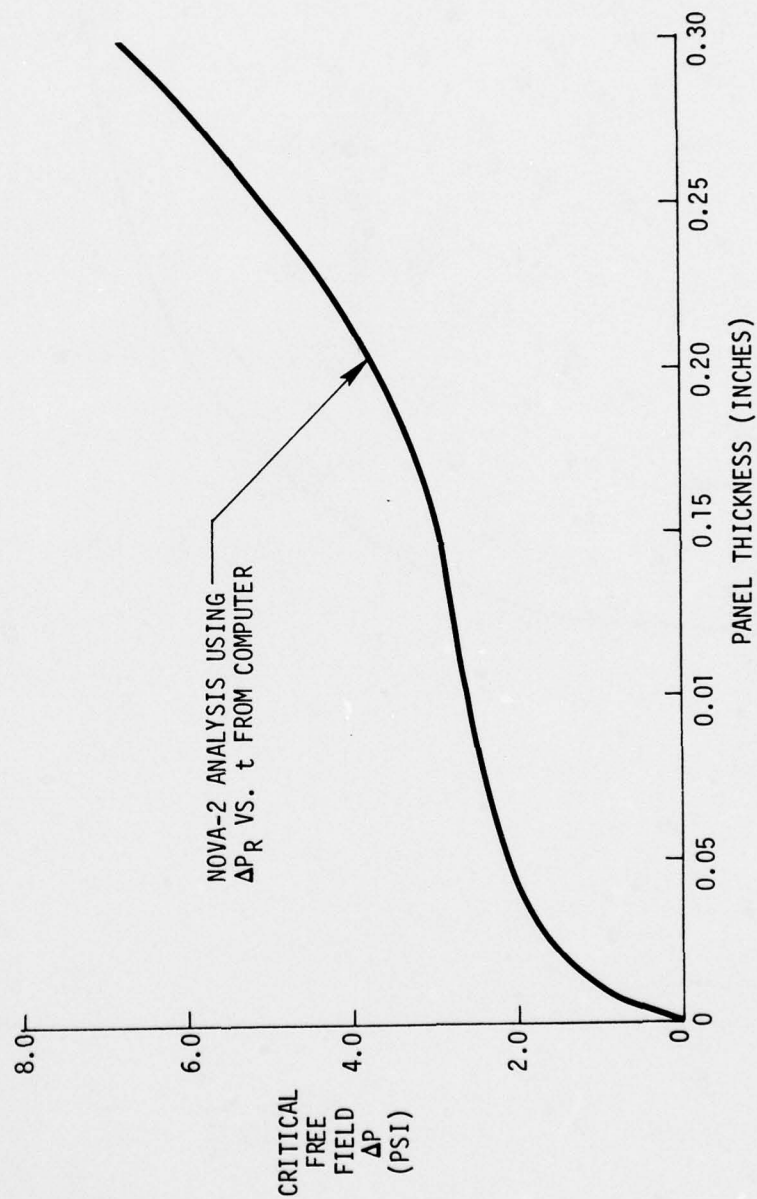


FIGURE 132. EFFECT OF PANEL THICKNESS ON ΔP_{FF} (CRITICAL)

SENSITIVITY STUDY RESULTS
 SQUARE FLAT PANEL WITH ALL SIDES CLAMPED
 PANEL THICKNESS = 0.1915 INCHES

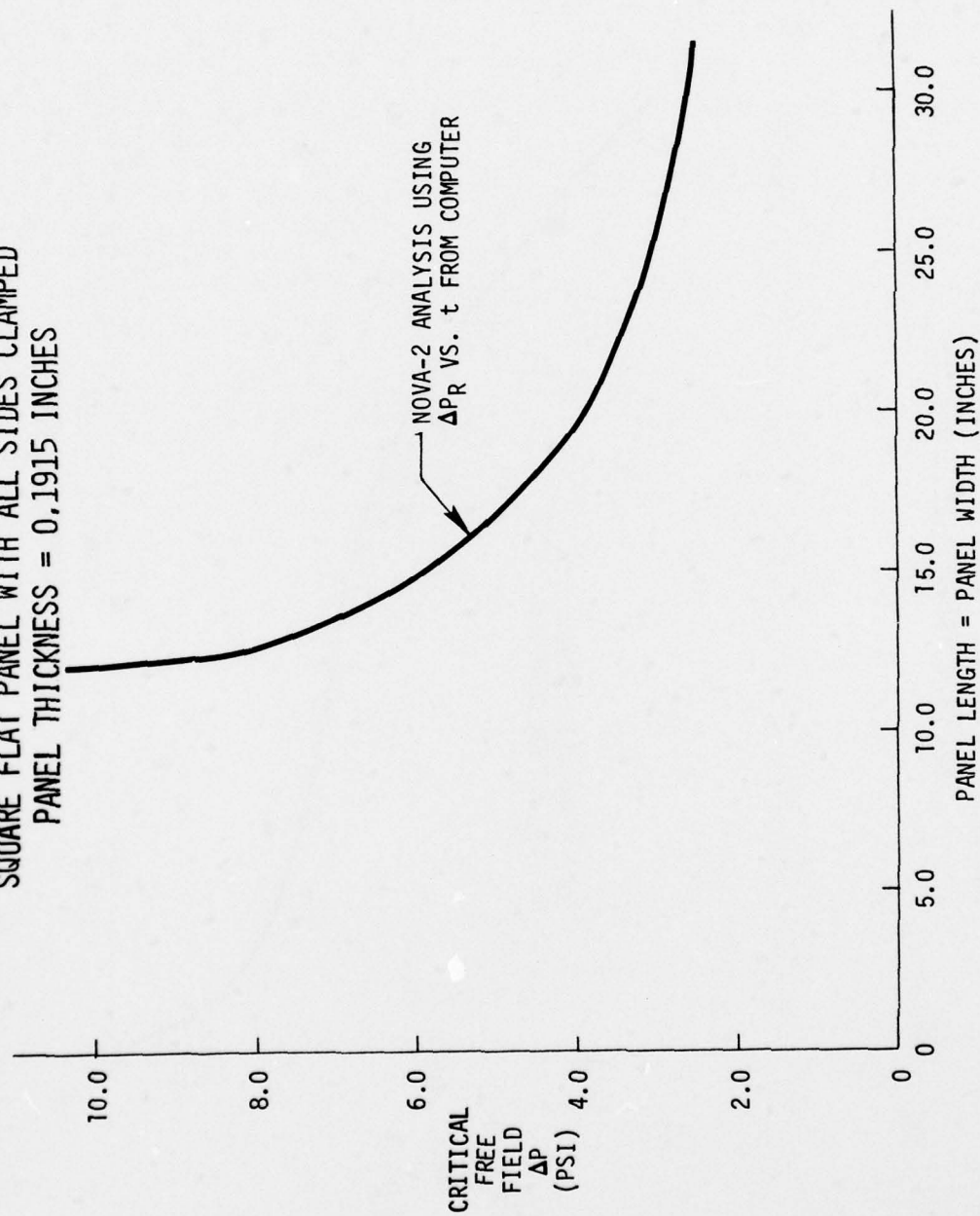


FIGURE 133. EFFECT OF PANEL LENGTH (WIDTH) ON ΔP_{FF} (CRITICAL)

Figure 134 illustrates the effect of modulus of elasticity on the response of a square flat panel fixed on all four edges. The length and width of these specimens was 22.0 inches, and the thickness was 0.191 inches. These data illustrate the linear relationship between panel response and modulus of elasticity.

Figure 135 shows the effect of beam length on the response of a straight beam that is fixed at both ends. These data indicate the nonlinear relationship between beam response and beam length. For uniform static loading, classical strength analysis techniques indicate that stress would be inversely proportional to the square of the beam length. The analysis results shown in Figure 135 illustrate that the relationship between beam length and stress due to spatially uniform dynamic load is approximately an inverse square relationship, also. The exact inverse square relationship is apparently modified somewhat by frequency effects.

SENSITIVITY STUDY RESULTS
 SQUARE FLAT PANEL WITH ALL SIDES CLAMPED
 PANEL THICKNESS = 0.1915 INCHES
 LENGTH = WIDTH = 22.0 INCHES

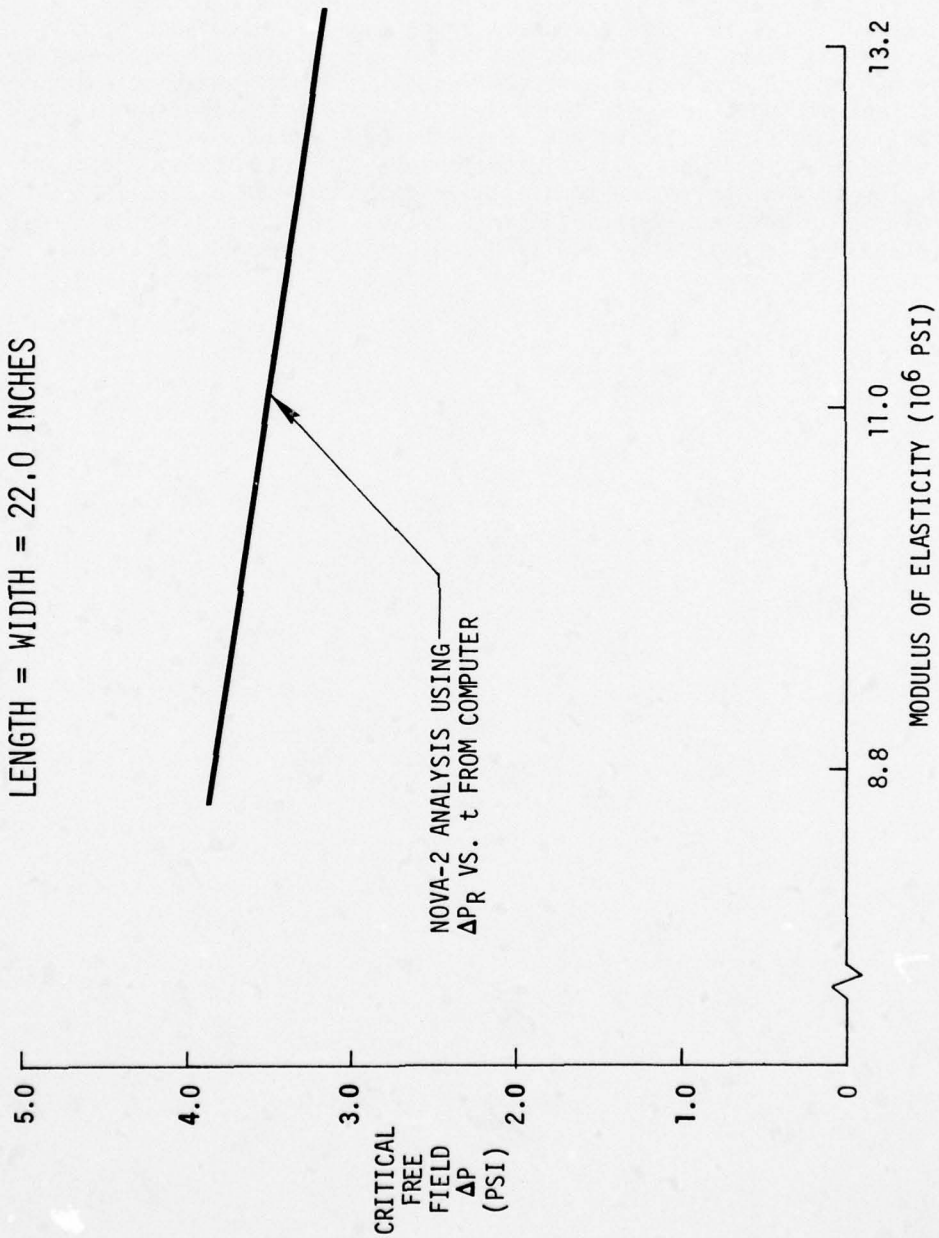


FIGURE 134. EFFECT OF MODULUS OF ELASTICITY ON ΔP_{FF} (CRITICAL)

SENSITIVITY STUDY RESULTS
STRAIGHT BEAM WITH BOTH ENDS CLAMPED

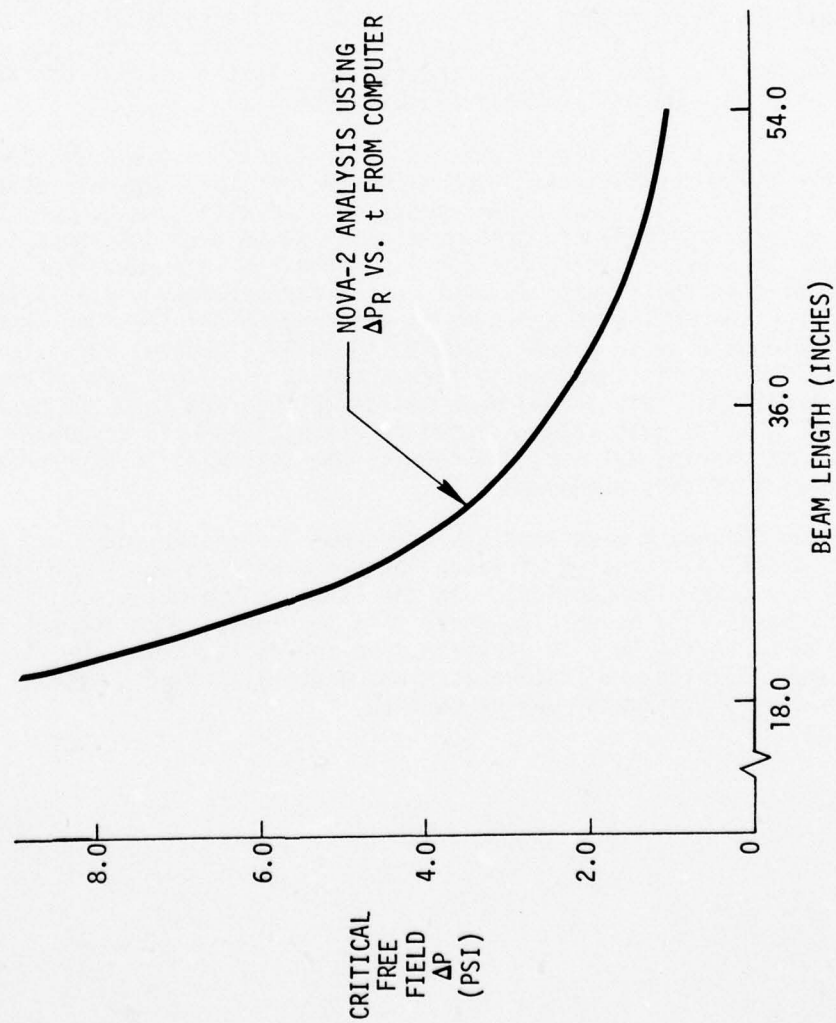


FIGURE 135. EFFECT OF BEAM LENGTH ON ΔP_{FF} (CRITICAL)

Results obtained from the static test, shock load test, and analysis have led to the following observations and conclusions:

(a) As discussed in Section 8.3, the versions of NOVA-2 currently available are not designed to properly analyze the curved specimens (6, 11, 12, and 13) for their respective shock load test conditions. As a result, the shock load analysis results for test specimens 6, 11, 12 and 13 are in error.

(b) The THUNDERPIPE shock tube is a useful blast simulation facility for tests of the nature described in this report. However, use of long strings of primacord to obtain the desired pulse positive phase duration results in a series of small detonations and produces a pressure pulse that is more ragged than that desired. Improvements in the quality of the pressure pulse will be a priority item in future testing.

(c) Significant enhancement of the free field (incident) over-pressure pulse due to interaction with the test specimens was observed throughout the test. This shock enhancement, coupled with dynamic application of the load, caused significantly greater stress in the test specimens (except the columns) than was observed for corresponding static loads. For a significant number of test shots, such as test shot 3 for specimen 6 (see Volume II, page 317) the reflected pressure as measured on the specimen experienced an instantaneous rise to a peak value followed by a general decay for approximately 1.5 milliseconds followed by an instantaneous rise to a second peak value. For many conditions, this second peak was often observed to be 50 percent greater than the initial peak value. Based on discussions with personnel from R&D Associates, Marina del Rey, California, the following is offered as a possible explanation of this phenomenon:

The large secondary peak loadings measured on the structures may have been due to geometric focusing of waves reflected off the shock tube walls (particularly the diverging section). In the acoustic approximation, the amplitudes of such waves vary as $r^{-1/2}$, where r is the radius from the tube's centerline, and show no variation with distance down the centerline. The repetitive nature of the pressure fluctuations was probably caused by radial reverberations in the six-foot diameter driver section.

(d) With the exception of test specimens 5, 12, and 13, the NOVA-2 static stress analysis results agree very well with static test results. This assumes, of course, that the panel model of specimen 6 with initial imperfections is a reasonable representation of the actual structure. As stated earlier in this report, the NOVA-2 program available for use in this program is not designed to perform a static analysis of buckling sensitive columns. Therefore, the static analysis results shown in this report were obtained by use of classical Euler buckling techniques. However, Kaman Avidyne personnel recently modified NOVA-2 to allow for analysis of column buckling under static load. Limited analysis results that were made available to the authors of this report indicate good agreement with test results. With regard to test specimen 5 (thin flat panel clamped on all four edges), a significant amount of analysis was performed utilizing various mesh sizes and modal retention sets to study convergence of the analysis solution. Inclusion of mesh sizes and modal retention sets well above the current limitations of the NOVA-2 program still resulted in analysis stresses at the panel edge that were significantly less than measured stresses. For test specimens 12 and 13 (skin/frame cylinders) measured stresses were observed to be substantially greater than predicted. It is anticipated that the complex wrinkling pattern experienced by the skin caused the frame to experience bending in a higher order mode than was anticipated, thereby resulting in higher stresses than predicted.

Less favorable agreement is observed when comparing predicted displacement to measured displacement of the test specimens. Displacements resulting from the static loads were measured for all stiffened and unstiffened flat panels, specimens 1-5 and 7-10. For test specimens 1, 3, and 4, the test data indicated displacements at the center of the specimens that were 10-16 percent greater than predicted. It is anticipated that some relaxation of the supports occurred in a lateral direction allowing a magnification of the displacement perpendicular to the plane of the specimen. Specimen two displacement was 70 percent greater than predicted. Much of this disagreement is attributed to the effect of the offset hinge as described in Section 8.2.2. Much better agreement between predicted and measured displacements was observed for specimens 5 and 7-10.

(e) Ignoring the analysis results for test specimens 6, 11, 12, and 13 due to reasons outlined in Section 8.3, the NOVA-2 analysis results predicted the proper critical free field overpressure for all test specimens within 20 percent. However, significant differences between predicted and measured response frequencies were observed for specific test specimens. Again ignoring the analysis results for specimens 6, 11, 12 and 13, the predicted fundamental response frequencies were higher than those measured for both beam-type specimens, whereas favorable comparison was observed for all flat panel specimens as shown in Table XVI.

TABLE XVI
TEST AND ANALYSIS STRUCTURAL RESPONSE FREQUENCIES

TEST SPECIMEN	FUNDAMENTAL RESPONSE FREQUENCY (CPS)	
	TEST	ANALYSIS
1	150.	154.
2	115.	128.
3	135.	159.
4	205.	210.
5	140.	160.
6+	100/600*	160/1500*
7	185.	180.
8	185.	185.
9	160.	380.
10	140.	185.
11+	440.	1770.
12+	125.	1400.
13+	120/1100*	1200.
14-17	11/1400*	10/1250*

* Secondary Response Frequency

+ Analysis Results are in error, see Section 8.3

(f) With the exception of the column specimens (14-17), significant amplification of the response of the test specimens was observed by comparing shock load response data to static load response data. As stated earlier, the range of this amplification is approximately 3 to 5. That is, for the load environments described earlier in this report, the test specimens were able to withstand a simulated nuclear overpressure pulse with a peak free field intensity that is 3 to 5 times the magnitude of the static overpressure load and still exhibit essentially the same peak response that occurred in the static test. Essentially no amplification was observed in the response of the columns. This was probably due to the inertia effects of the piston and the loading block and their relieving effect on the dynamic response of the columns. That is, if the piston and loading block had been massless, the response of the columns during the shock load test would have increased. This would have decreased the amplitude of the bar for specimen 14 in Figure 131. The effect of a massless piston and load block will be investigated analytically in the follow-on program which will involve additional column specimens.

(g) From Table XIV, which compares test and analysis results in the plastic response region, it is observed that the quality of NOVA-2 results varies significantly from specimen to specimen. It is possible that a more complex mathematical model, e.g., finer mesh size, more modes, more mass points, is required for certain test specimens compared to that which is utilized in elastic analyses.

(h) For all test specimens, it was observed that measurable permanent set was not apparent even though the critical ΔP_{ff} was slightly exceeded. Only after exposure to a free field overpressure pulse significantly greater than that defining the threshold of damage was measurable permanent set apparent. In other words, there appears to be a significant range in pressure between that defining the threshold of damage (sure-safe) and that causing enough damage to be significant in determining "mission completion" nuclear hardness of a system. This is illustrated in Table XVII for those specimens that experienced measurable permanent deformation.

(i) From the limited testing of specimen 13 with and without internal pressure, it was observed that internal pressure, in general, was beneficial. That is, preblast internal pressurization offered additional nuclear hardness to the specimen.

(j) As a result of this program, several conclusions have been reached regarding NOVA-2 mathematical modeling techniques.

Table XVIII describes data associated with the mathematical models of the homogeneous flat panels. MG, MB, and modes deleted indicate that 15 modal combinations were retained from a set of 25 modal combinations. MBAR and NBAR refer to the number of spatial integration points utilized in the solution process. The reader is referred to Reference 1 for a more detailed discussion of these parameters and to Volume II of this report for a complete listing of NOVA-2 models for all test specimens.

TABLE XVII
SUMMARY OF ELASTIC/PLASTIC TEST RESULTS

TEST SPECIMEN	ΔP_1 (PSI)	ΔP_2 (PSI)	δ (IN)
1	3.0	6.5	.06
2	2.3	7.5	.78
3	2.7	7.3	.14
4	2.8	11.5	.16
5	1.2	3.5	.92
7	0.55	1.7	.20
8	0.70	3.4	.75
9	1.85	5.2	.50
10	1.95	4.4	.60
12	2.85	7.0	.20

ΔP_1 = Free Field Overpressure Associated with the Threshold of Permanent Damage

ΔP_2 = Maximum Free Field Overpressure Imposed on a Test Specimen

δ = Maximum Permanent Deformation Measured After the Final Test Shot for Each Specimen

TABLE XVIII
MATHEMATICAL MODEL DATA FOR HOMOGENEOUS FLAT PANELS

TEST SPECIMEN	LENGTH ÷ THICKNESS	BOUNDARY CONDITIONS	MG	MB	MODES DELETED	MBAR	NBAR
1	115	4 Sides Clamped	7	7	24	11	11
2	115	4 Sides Pinned	7	7	24	11	11
3	114	2 Sides Clamped 2 Sides Pinned	7	7	24	11	11
4	70	4 Sides Clamped	7	7	24	11	11
5	1100	4 Sides Clamped	8	8	32	19	19
6		4 Sides Clamped	8	8	32	19	19
7		4 Sides Clamped	8	8	32	19	19
8		4 Sides Clamped	8	8	32	19	19

The conclusion derived from these data and the response results discussed earlier is that for flat homogeneous panels that fall into a thin plate or thick plate category based on length/thickness ratio as described in Reference 9, the modal combinations and integration points described in Table XVIII result in an excellent mathematical representation of the actual test specimen. As the length/thickness ratio increases to the point where the panel falls into the membrane category, such as specimen 5, more modal combinations and integration points must be included in the model to more closely approach the proper solution. Even with the combination of parameters shown for specimen 5, analysis results differed from test results by approximately 20 percent. The follow-on program will include two additional homogeneous flat panels with length/thickness between 115 and 1100 to provide additional data on the response of thin flat panels.

A listing of the mathematical models of specimens 9 and 10, flat stiffened panels, are shown in Volume II of this report. Table XIX gives a description of selected model parameters associated with the stiffeners. As described in Reference 1, N is the number of mass points in the model (18 for half the beam span in specimen 9 and 35 for the full span of specimen 10) and NX is the maximum number of flanges per layer in the beam cross section. Inclusion of these data in the mathematical models gives rise to analysis results that compare very favorably with test results.

TABLE XIX
MATHEMATICAL MODEL DATA FOR STRAIGHT BEAMS

TEST SPECIMEN	BEAM LENGTH (IN)	BOUNDARY CONDITIONS	N	NX
9	36.0	Clamped	18	4
10	36.0	Pinned	35	4

With regard to the column specimens (14-17), initial imperfections were measured prior to testing at the center of the span. Analysis results that were obtained by use of these imperfections agreed quite well with test results. Test results for specimens 14-17 indicate that initial imperfection is an important parameter in defining response of the column up to and including the point at which the column buckles. Since three of four columns yielded at essentially the same load level, it appears that

the load level at which a column yields is not strongly a function of the initial imperfection. Conversely, the NOVA-2 results are a function of the initial imperfection right up to the yield point. Additional testing of buckling sensitive columns is planned in the follow-on program to provide more information on this subject.

Due to the reasons outlined in Section 8.3, it is difficult to comment on modeling techniques for the curved specimens (6, 11, 12, and 13). However, it appears that curved panels will require larger modal retention sets than comparable flat panels. In addition, curved panel solutions require much larger values of TSTOP (See Reference 1). Once the NOVA-2 computer program is modified to properly analyze these test specimens for their respective test conditions, conclusions regarding modeling techniques will be available.

10.0 APPLICATION OF TEST/ANALYSIS RESULTS

10.1 General Discussion

As stated earlier in this report, the primary objective of this program was to generate experimental data describing the response of a variety of basic structural elements to a series of simulated nuclear overpressure environments. This objective was accomplished. Another objective was to utilize the test data to evaluate the structural response capabilities of the NOVA-2 computer program. Due to the inability of the current versions of the NOVA-2 program to provide reflected pressure time histories for curved specimens (see discussions in Section 8.3) that are a satisfactory representation of those which were measured, the current evaluation of NOVA-2 is limited to the flat test specimens. By incorporating additional modifications to the NOVA-2 computer program, this evaluation can be extended to include all test specimens that were considered in this program.

In addition to the evaluation of NOVA-2, which is of current interest, the test data from this program are available for use in the evaluation of other current and future structural response programs.

10.2 Impact on Future Nuclear Hardness Studies

Results of this program will impact future nuclear hardness studies in various ways, including:

(a) NOVA-2 can be utilized with a high level of confidence in establishing the pressure levels associated with the threshold of damage of flat panels and stiffeners similar to the structural types included in this program. This statement may eventually be extended to include the curved specimens, once the NOVA-2 program is properly modified and the analysis is accomplished.

(b) NOVA-2 gives reasonable results regarding elastic-plastic deformation and permanent set. If the models of the test specimens had been made more complex in terms of modal retention sets, integration points, etc., it is possible that the elastic-plastic analysis results would have agreed even better with the test results. Cost and schedule limitations did not permit an exhaustive study of this in the current program.

(c) As stated earlier, the difference between those pressure levels required to cause significant permanent deformation and those pressure levels resulting in the threshold of damage are significant. It is anticipated that this strength capability is typical of many types of structure found in aircraft.

(d) Extreme care must be exercised in constructing mathematical models of the actual weapon system hardware. Parameters such as modulus of elasticity and strength allowables can vary from established handbook values. Therefore, wherever possible, coupon tests should be accomplished on material from which the structure is constructed to establish material properties. For structure that is buckling sensitive, it is important that initial imperfections be properly represented. Therefore, measurements of these imperfections should be made. Since individual aircraft within a large fleet will exhibit measurable differences regarding a variety of structural properties, engineering judgement must be exercised judiciously in representing the actual structure by a series of mathematical models.

(e) The NOVA-2 program can be an expensive analysis tool. As is the case with most analysis techniques, a trade off between solution accuracy and solution cost must be considered in the conduct of an analysis. This is particularly true when conducting a detailed hardness evaluation of a complex weapon system which includes a large number of structural items. From this program, it was determined that panels require longer run times than beams, and the elastic-plastic solution requires more run time than the elastic solution. This is illustrated in more detail in Table XX for a variety of structural models on the CDC 7600 computer. As shown, the run time increased dramatically for those cases where the pressure time history was input on cards. The reason for this is that a larger modal retention set, a more dense mesh, and larger TSTOP values were utilized.

(f) To help minimize the computational costs associated with a comprehensive nuclear hardness evaluation of a complex weapon system, consideration needs to be given to evaluating overpressure nuclear hardness of certain structure by comparison with similar structure for which test results and/or analysis results already exist.

In conclusion, it must be reemphasized that this program was designed to include test specimens that are basic structural elements with well-defined boundary conditions and primary load paths. For a variety of reasons, many structural items in a typical airframe are more complex than these. Therefore, to more fully evaluate the capabilities of the NOVA-2 program, additional testing and analysis need to be accomplished on more complex structural assemblies. A program of this nature will be accomplished as a follow-on to the current program.

TABLE XX
TYPICAL NOVA-2 RUN TIMES ON CDC 7600 COMPUTER

TEST SPECIMEN	STRUCTURAL TYPE	SOLUTION OPTION		TSTOP (SEC)	CP TIME (SEC)
		ELASTIC	ELASTIC-PLASTIC		
1	Panel	X		.003	60.
1	Panel		X	.010	244.
2	Panel		X	.010	291.
3	Panel	X		.004	78.
3	Panel		X	.010	281.
4	Panel	X		.011	881.+
4	Panel	X		.010	467.
4	Panel		X	.011	1893.+
5	Panel		X	.010	2823.+
6	Panel	X		.015	1460.
9	Beam	X		.005	73.
10	Beam	X		.005	91.
11	Beam	X		.003	16.
12	Beam	X		.0036	98.
13	Beam	X		.0036	64.
14	Column	X		.020	137.

+ Pressure time history was input on cards.

REFERENCES

1. "NOVA-2 - A Digital Computer Program for Analyzing Nuclear Overpressure Effects on Aircraft," Kaman Avidyne, September 1975, & AFWL-TR-75-262, Parts 1 & 2, August 1976.
2. "Nuclear Blast and Shock Simulators," Panel N-2 Report N2: TR2-72, 28 December 1972.
3. Boeing Document D3-9788-4, "Structural Response to Simulated Nuclear Overpressure: Static and Shock Loads Test Procedures," 18 March 1976.
4. NASA SP221, "The NASTRAN Theoretical Manual".
5. NASA SP222, "The NASTRAN User's Manual".
6. NASA SP223, "The NASTRAN Programmer's Manual".
7. NASA SP224, "The NASTRAN Demonstration Problem Manual".
8. Formulas For Stress and Strain, R. J. Roark, McGraw-Hill Book Company, Inc., 1954.
9. Airplane Structural Analysis and Design, E. E. Sechler and L. G. Dunn, Dover Publications, Inc., 1963.
10. Mente, L. J., "The Dynamic, Elastic - Plastic, Large Displacement Response of Buckling Sensitive Cylindrical Shells to Blast - Type Loadings, -- Part I: Analytical Formulation", AMC-2-68-(T), Kaman Avidyne TR-53, Kaman Sciences Corporation, August 1968.
11. Mente, L. J., and Manzelli, J. C., "The Dynamic, Elastic - Plastic, Large Displacement Response of Buckling Sensitive Cylindrical Shells to Blast - Type Loadings, -- Part II: Applications and DEPICS User's Manual", AMC-11-71-(T), Kaman Avidyne TR-74, Kaman Sciences Corporation, April 1971.
12. Metallic Materials and Elements for Aerospace Vehicle Structures, MIL-HDBK-5B, September 1971.
13. Foundations of the Nonlinear Theory of Elasticity, Novozhilov, V.V., Graylock Press, Rochester, New York, 1953.
14. Leissa, A.W., "Vibration of Plates," NASA SP-160, 1969.
15. Leissa, A.W., "Vibration of Shells," NASA SP-288, 1973.

[illegible]

DISTRIBUTION LIST

DEPARTMENT OF DEFENSE

Director
Defense Advanced Rsch. Proj. Agency
ATTN: Strategic Tech. Office

Defense Documentation Center
12cy ATTN: TC

Director
Defense Nuclear Agency
ATTN: TISI, Archives
ATTN: DDST
3cy ATTN: TITL, Tech. Library
3cy ATTN: SPAS

Dir. of Defense Rsch. & Engineering
ATTN: S&SS (OS)

Commander
Field Command
Defense Nuclear Agency
ATTN: FCPR

Director
Joint Strat. Tgt. Planning Staff, JCS
ATTN: JPTM
ATTN: JLTW-2
ATTN: JPTP

Chief
Livermore Division, Field Command
Defense Nuclear Agency
ATTN: FCPRL

OJCS/J-3
ATTN: J-3, Operations

OJCS/J-5
ATTN: J-5, Plans & Policy Nuc. Div.

DEPARTMENT OF THE ARMY

Program Manager
BMD Program Office
ATTN: DACS-BMT, Clifford E. McLain
ATTN: DACS-BMT, John Shea

Dep. Chief of Staff for Rsch. Dev. & Acq.
ATTN: NCP Division

Commander
Harry Diamond Laboratories
ATTN: DRXDO-NP
ATTN: DRXDO-RBH, Paul A. Caldwell

Commander
U.S. Army Mat. & Mechanics Rsch. Ctr.
ATTN: DRXMR-HH, John F. Dignam

Commander
U.S. Army Materiel Dev. & Readiness Cmd.
ATTN: DRCDE-D, Lawrence Flynn

Commander
U.S. Army Nuclear Agency
ATTN: ATCA-NAW

DEPARTMENT OF THE ARMY (Continued)

Commander
U.S. Army Missile Command
ATTN: DRSMI-RRR, Bud Gibson
ATTN: DRSMI-XS, Chief Scientist

DEPARTMENT OF THE NAVY

Chief of Naval Material
ATTN: MAT 0323, Irving Jaffe

Chief of Naval Operations
ATTN: OP 622
ATTN: OP 62

Chief of Naval Research
ATTN: Code 464, Thomas P. Quinn

Director
Naval Research Laboratory
ATTN: Code 5180, Mario A. Pershechino

Officer-in-Charge
Naval Surface Weapons Center
ATTN: Code WA501, Navy Nuc. Prgms. Off.
ATTN: Code WA07, Carson Lyons
ATTN: Code 2302, Leo F. Gowen

Director
Strategic Systems Project Office
ATTN: NSP-272, CDR Leslie Stoessl
ATTN: NSP-273

Commanding Officer
Naval Weapons Evaluation Facility
ATTN: Lary Oliver

DEPARTMENT OF THE AIR FORCE

AF Materials Laboratory, AFSC
ATTN: T. Nicholas
ATTN: MBC, Donald L. Schmidt
ATTN: MAS

AF Weapons Laboratory, AFSC
ATTN: SR
ATTN: SRR
ATTN: SUL
ATTN: Dr. Minge
ATTN: DYV/Al Sharp

HQ USAF/RD
ATTN: RDQ
ATTN: RDQSM
ATTN: RDPM

SAMSO/DY
ATTN: DYS

SAMSO/MN
ATTN: MNNR

SAMSO/RS
ATTN: RSS
ATTN: RSSE

DEPARTMENT OF THE AIR FORCE (Continued)

Commander in Chief
Strategic Air Command
ATTN: XPFS
ATTN: DOXT

Commander
ASD
ATTN: ENFTV, Dudley Ward

DEPARTMENT OF ENERGY

University of California
Lawrence Livermore Laboratory
ATTN: G. Staihle, L-24

Los Alamos Scientific Laboratory
ATTN: Doc. Control for R. Olwin
ATTN: Doc. Control for J. W. Taylor

Sandia Laboratories
ATTN: Doc. Control for T. Gold
ATTN: Doc. Control for Larry Baaken

Sandia Laboratories
ATTN: Doc. Control for Charles Winter

DEPARTMENT OF DEFENSE CONTRACTORS

Aeronautical Rsch. Assoc. of Princeton, Inc.
ATTN: Coleman Donaldson

Aerospace Corporation
ATTN: J. McClelland

Avco Research & Systems Group
ATTN: C. K. Mullen
ATTN: John E. Stevens, J100
ATTN: Doc. Control

Battelle Memorial Institute
ATTN: Richard Castle

Boeing Wichita Company
ATTN: Roger P. Syring
ATTN: W. Dale Pierson

General Electric Company
TEMPO-Center for Advanced Studies
ATTN: DASIAC

DEPARTMENT OF DEFENSE CONTRACTORS (Continued)

Kaman Sciences Corporation
ATTN: Thomas Meagher
ATTN: Frank H. Shelton

Lockheed Missiles and Space Co., Inc.
ATTN: Raymond R. Capioux

McDonnell Douglas Corporation
ATTN: J. F. Garibotti
ATTN: R. J. Reck

National Academy of Sciences
ATTN: National Materials Advisory Board for
Donald G. Groves

Physics International Company
ATTN: Doc. Control for Allen Klein

R & D Associates
ATTN: Albert L. Latter
ATTN: Arlen Field

SRI International
ATTN: Herbert E. Lindberg
ATTN: George R. Abrahamson

Systems, Science and Software, Inc.
ATTN: Kedar D. Pyatt

TRW Defense & Space Sys. Group
2cy ATTN: I. E. Alber, R1-1008
2cy ATTN: W. H. Baer, R1-2136

TRW Defense & Space Sys. Group
ATTN: E. Y. Wong, 527/712
ATTN: Earl W. Allen, 520/141

Kaman Avidyne
Division of Kaman Sciences Corporation
ATTN: Norman Hobbs

Institute for Defense Analyses
ATTN: IDA Librarian, Ruth S. Smith
ATTN: Joel Bengston